LIFE ON THE FRINGE:
SURVEYING THE ECOPHYSIOLOGICAL TENACITY OF METHANOGENS AND ANAEROBIC METHANOTROPHS IN THE OLIGOTROPHIC DEEP SUBSURFACE BIOSPHERE

Rachel Lee Harris

A DISSERTATION

PRESENTED TO THE FACULTY

OF PRINCETON UNIVERSITY

IN CANDIDACY FOR THE DEGREE

OF DOCTOR OF PHILOSOPHY

RECOMMENDED FOR ACCEPTANCE

BY THE DEPARTMENT OF

GEOSCIENCES

Advisor: Professor Tullis C. Onstott

June 2020

ABSTRACT

Methanogenesis coupled to the Wood-Ljungdahl pathway and its reversal, the anaerobic oxidation of methane, AOM, are believed to be among the most ancient metabolisms known to life on Earth. Recent advances in cultivation-independent techniques utilizing high-throughput sequencing, cellular imaging, geochemical modeling and experimentation, and bioinformatics are rapidly altering the ways in which we investigate complex microbial communities in the environment. In particular, the application of these methods to the exploration of the deep biosphere has ignited a renaissance in the study of methane biogeochemistry, as mining efforts into these environments – both literally and computationally – continue to reveal that methanogens and anaerobic methanotrophs (ANMEs) are more diverse, pervasive, and resilient than ever previously thought.

In the spirit of continuing to "move the goalposts" that define the extent of microbial methane metabolisms, this dissertation explores the ecophysiologies of methanogens and ANMEs surviving under extreme conditions which characterize the deep biosphere of Earth and Mars. We develop a novel fluorescent *in situ* hybridization method, FISH-TAMB, to visualize mRNA in living methanogens and ANMEs, discussing its potential to characterize microbial dark matter and identify horizontal gene transfer based on metabolic function. We then investigate oligotrophic continental fracture fluid from South Africa, characterizing the potential of AOM in a novel species of phylum *Candidatus* "Bathyarchaeota". We then explore the high-pressure, high-temperature sub-seafloor sediments of the Nankai Trough, employing high-pressure cultivation, stable isotope probing, 16S rDNA sequencing, and metagenomics to hunt for

the first experimental evidence of thermo-piezotolerant AOM. Finally, we subject axenic cultures of the methanogen *Methanosarcina barkeri* to controlled incubations simulating freezing and highly oxidizing conditions of a perchlorate-riddled Mars Special Region, utilizing transcriptomics to better understand the potential of biological methanogenesis on the Red Planet. Collectively, these results demonstrate the remarkable tenacity of methanogens and ANMEs to survive on the biotic fringe.

ACKNOWLEDGEMENTS

In the past 5 years I have often been reminded of the proverb “it takes a village to raise a child”, only in this case, it took an international network of experts, both scientific and otherwise, to raise my Ph.D.

I have some very vague memories being a small child in Florida and being fascinated by the natural world outside my house. Awed by the labyrinth that was my dad’s towering vegetable garden, I was inspired to have a garden of my own just like his. To my parents’ chagrin, 3 year-old me decided that the best place to break ground (and subsequently overwater) was right outside the back patio door. It’s taken a while and a lot of practice, but eventually I developed a green thumb in my own right. Fortunately, some of this skill also transferred into anaerobic cultivation. Maybe I was onto something way back when I inadvertently installed an artificial wetland in the backyard.

I don’t remember exactly when the obsession began, but by the time I was 5 I was spending recess brushing dirt away from buried rocks I was absolutely convinced were dinosaur fossils (they were not). I must have regaled my parents with stories, as two years later my dad and I went on a father-daughter vacation to the Wyoming Dinosaur Center in Thermopolis, Wyoming, where we spent a week digging into the middle-Jurassic beds of the Morrison Formation. Though I ended up in the field of microbial ecology, I still want to be a paleontologist when I grow up (Figure I); just ask TC about my interests in obtaining “dinosaur microbiomes” from coprolites.

Speaking of TC, I am exceptionally grateful for his seemingly infinite knowledge and willingness to trailblaze. I arrived to Princeton never having as much as taken a GEO

course in undergrad, and yet as I finish my degree here, I realize I am confidently both a microbial ecologist and a biogeochemist, and that is thanks to TC's enthusiasm to approach complex problems using every available tool he can get his hands on.

I am also so thankful to have been introduced to so many wonderful and ingenious collaborators. During my first field campaign to South Africa, Tom Kieft spent an afternoon by my side as we sampled dissolved gases from hot springs in the Limpopo Province, offering many tips and tricks on how to cultivate methanogens anaerobically without working in a glove bag. Tom, thank you for saving me so much time. To Esta van Heerden, thank you for keeping such an immaculate lab and for flawlessly coordinating every trip underground. To Errol Cason and Jan-G Vermeulen, I am fondly reminded of your "biovial" rap every time I work with serum vials. Thank you for your humor and good spirits which saved us all down in the mines. To Barbara Sherwood-Lollar and Ed Young, thank you for giving my crazy theories about clumped isotopes a second pass. To my second reader, Doug Bartlett, thank you so much for hosting me in your lab at Scripps for the duration of my Deep Life cultivation internship. From day 1 your lab welcomed me as one of your own and I will always look back fondly at my growth as a scientist and as a person while under your charge.

Maggie Lau was instrumental throughout our overlapping time at Princeton in discussing the details of complex experiments or bioinformatic pipelines. I would not be anywhere near as well-rounded a scientist if it were not for her gentle and supportive guidance. I also remind Zack Garvin every chance I get how happy I am to have him as a lab mate. I am forever grateful for his perspective and the many venting sessions we have shared to combat the daily grind of graduate life.

There are so many people who have made the GEO department feel like family, and it is because of them I am sad to come to terms with the reality that I must soon graduate. Sheryl Robas and Nora Zelizer, thank you for indulging us with Tea Time, Guyot Prom, jerseys for intramural ice hockey, and your unwavering support of the Coprolites. One of my proudest achievements from graduate school is earning back-to-back championships in the summer softball league. Dawn Reading, your collection of dog biscuits had Freyja and me both trained to take regular breaks. Eva Groves, I am always so touched when you order an extra apple for lab meeting on Friday. Danielle Schmitt, Sirus Han, Katja Luxem, thank you for always checking in and always being down for adventure. And to Danielle Schlesinger, thank you for helping me stay accountable and agreeing to "quarantine dissertation bootcamp" as we try to wrap up this crazy time in our lives.

To Rabbi Bentzi and Chaya Brook, I am so thankful for your warmth, delicious meals, and wonderful humor. Chabad provided me with an escape from my daily circuit and you have helped me learn so much. I promise I have time now for Hebrew lessons! To Blake and Elise Chambers, thank you for rooting for me for all these years. As I sit here and write this in the bleak hours of the night, you are (virtually) by my side ordering me post-dissertation-submission breakfast in bed. Thank you for being my best friends. To Ilona Harris, I cannot sufficiently put into words how instrumental you have been in helping me get to this point. I wouldn't have made it out of here in one piece without you.

And finally, thank you to Freyja for making every day better than the last. I promise we'll go on a really long walk today.

Figure I. A fossilized track of an unidentified therapod dinosaur from the 167 million year-old Sundance Formation in Big Horn County, Wyoming. 7 year-old Rachel for scale.

Dedicated to my family,
even though they probably won't read far past this point.

"The history of evolution is that life escapes all barriers. Life breaks free. Life expands to new territories. Painfully, perhaps even dangerously. But life finds a way."

– Dr. Ian Malcolm, *Jurassic Park* (1990), by Michael Crichton

TABLE OF CONTENTS

LIST OF TABLES

LIST OF FIGURES

CHAPTER 1

Introduction

1.1 PREFACE

The Earth's habitable deep subsurface is a geochemically heterogeneous landscape that plays host to one of the largest and most diverse reservoirs of microbial biomass on the planet (Onstott et al., 2009; Kallmeyer et al., 2012; Bar-On et al., 2018; Magnabosco et al., 2018; Orsi, 2018). Though we have explored less than 0.01% of the deep biosphere's expected habitable volume (Cario et al., 2019), we have found microbial life 5.3 km below land surface (Szewzyk et al., 1994) and 2.5 km below the seafloor (10.5 km below sea level) (Inagaki et al., 2015). Relative to most surface environments, many sites in the deep biosphere are characterized by extreme temperatures, pH, salinities, pressures, energy limitation, nutrient limitation, or combinations thereof. The transition zone where conditions become too inhospitable for even the most extreme organisms to survive is known as the biotic fringe (Shock, 2014), and its study is of great interest to astrobiological investigations aiming to explore the potential of subsurface life on extraterrestrial bodies (e.g., Jones et al., 2018; Onstott et al., 2019).

Despite extreme conditions, the deep biosphere is estimated to account for 15% of the Earth's total biomass and perhaps up to 90% of all *Bacteria* and *Archaea* (Bar-On et al., 2018). The vast majority of these organisms are microbial dark matter; that is, they are only known from environmental sequencing have not been obtained in pure culture (Marcy et al., 2007; Rinke et al., 2013). To infer their ecophysiological potentials, we can rely on high-throughput sequencing of molecular marker genes (amplicon sequencing) or environmental DNA (metagenomics). To appreciate their contributions to global

biogeochemical cycles, however, we must elucidate their metabolic activities. In this dissertation we accomplish this by combining the aforementioned methodologies with fluorescent *in situ* hybridization (FISH) of messenger RNA and stable isotope probing (SIP).

While research into the geochemistry and microbial ecology of the deep oligotrophic biosphere can help inform us in the search for life beyond this planet, we can also learn about the limits of life from model organisms. Armed with extensive descriptions of cellular physiologies, environmental distributions, and fully sequenced genomes, we can comb the literature and hand pick microorganisms of interest to poke, prod, and push under controlled extreme conditions. By employing techniques such RNA-Seq to monitor global shifts in gene expression, we can thoroughly characterize metabolic responses of cells to the conditions to which we expose them. The insights we gain from this work helps construct an interpretive framework to ultimately quantify biological and biosignature potential in extreme environments on Earth and beyond.

1.2 THE DEEP BIOSPHERE'S CONNECTION TO THE METHANE CYCLE

Methane (CH_4) is the second most abundant greenhouse gas behind carbon dioxide (CO_2) in Earth's atmosphere, contributing an estimated 20% of total radiative forcing by greenhouse gases since pre-industrial times (Kirschke et al., 2013). A relatively long-lived greenhouse gas with an atmospheric residence time of ~200 years, CH_4 is 85 times more potent than CO_2 in the first 20 years of residence, and 20 times more potent after a century (Jackson et al., 2019). Nearly 70% of CH_4 is biogenic in

origin, produced by methanogenic *Archaea* living in anaerobic environments (Conrad, 2009).

Our understanding of the global CH_4 budget is in a constant state of flux. Unlike CO_2, which has steadily risen in concentration in the atmosphere since monthly measurements began at the Mauna Loa Observatory in 1958 (NOAA, 2018), CH_4 build up in the atmosphere appeared to stabilize to 1773 ± 3 ppb at the beginning of the 21st century after nearly tripling from pre-industrial times (Figure 1.1A,B; Kirschke et al., 2013). Atmospheric CH_4 growth resumed again by 2007 and has continued since (Rigby et al., 2008; Turner et al., 2019). At the time of this writing, global CH_4 levels are 1877 ± 3 ppb (NOAA; Figure 1.1C).

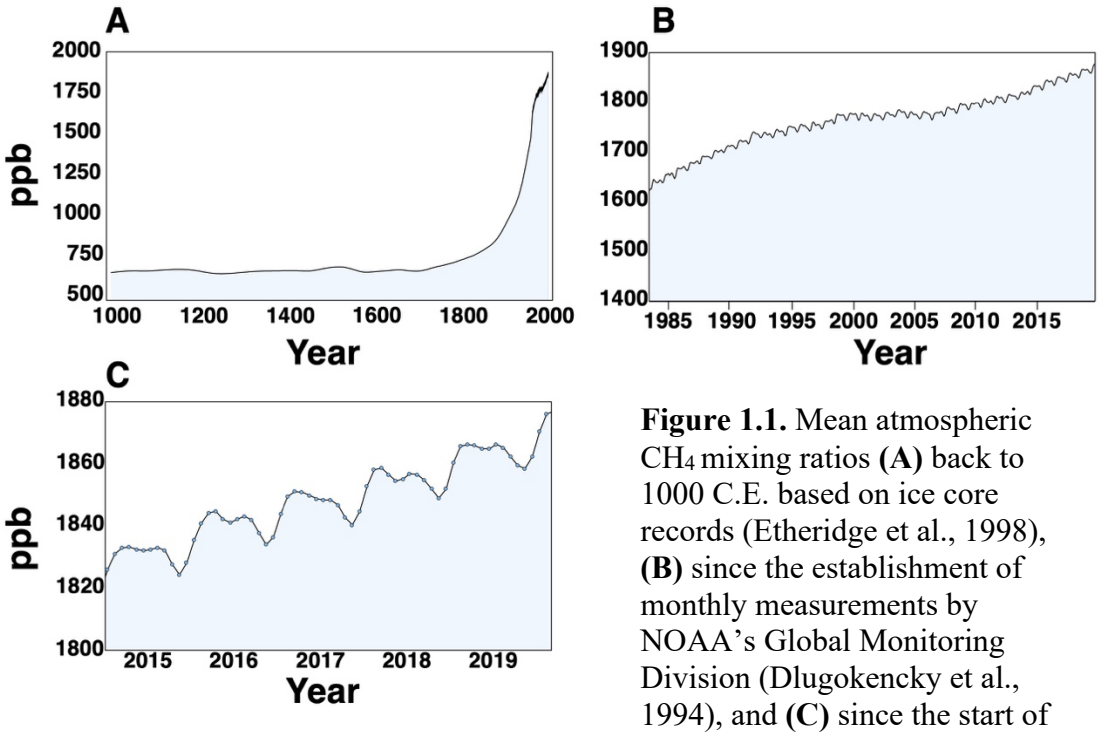

Figure 1.1. Mean atmospheric CH_4 mixing ratios **(A)** back to 1000 C.E. based on ice core records (Etheridge et al., 1998), **(B)** since the establishment of monthly measurements by NOAA's Global Monitoring Division (Dlugokencky et al., 1994), and **(C)** since the start of the author's Ph.D.

Top-down inversions of the global CH_4 budget (Figure 1.2) estimate annual emissions in the range of about 500-600 Tg yr^{-1} and sinks between 514 – 560 Tg CH_4 yr^{-1}

(Conrad, 2009; Dlugokencky et al., 2011; Kirschke et al., 2013; Saunois et al., 2016). While these global fluxes are reasonably well constrained, estimates for individual sectors of sources and sinks can vary significantly. For example, predicted global rates of the anaerobic oxidation of methane (AOM) range between 45 Tg yr^{-1} (Egger et al., 2018) and 304 Tg yr^{-1} (Hinrichs and Boetius, 2002). Such large discrepancies are due to a combination of limited sampling of the continental deep biosphere and oligotrophic sub-seafloor sediments, as well as coarse extrapolations of data from productive continental shelves over large areas.

Sulfate-dependent AOM, which couples the reduction of sulfate with methane oxidation, is considered to be the dominant AOM sink due to its predominance in continental margin sediments (Valentine and Reeburgh, 2000). However, recent discoveries of additional electron acceptors beside sulfate (e.g., Raghoebarsing et al., 2006; Beal et al., 2009; Ettwig et al., 2010; Ettwig et al., 2016; Cai et al., 2018; Leu et al., 2020), coupled to an observed global mean sulfate:methane net flux ratio of 1.4:1 (Egger et al., 2018) demonstrate that sulfate-methane transition zones, or SMTZs, are not the only significant AOM sinks. By one bottom-up estimation for the 2000s, a stoichiometric imbalance of almost 50 Tg yr^{-1} was calculated between mean global emissions and sinks, significantly larger than the observed growth rate of 6 Tg CH_4 yr^{-1} (Kirschke et al., 2013). "Cryptic" CH_4 cycling – where AOM and methanogenesis proceed concurrently along small and geochemically near-indiscernible temporospatial scales (Beulig et al., 2019) is difficult to quantify and generally ignored by these models (Egger et al., 2018). To be certain, continued exploration of AOM in the deep biosphere is essential filling these gaps in our understanding.

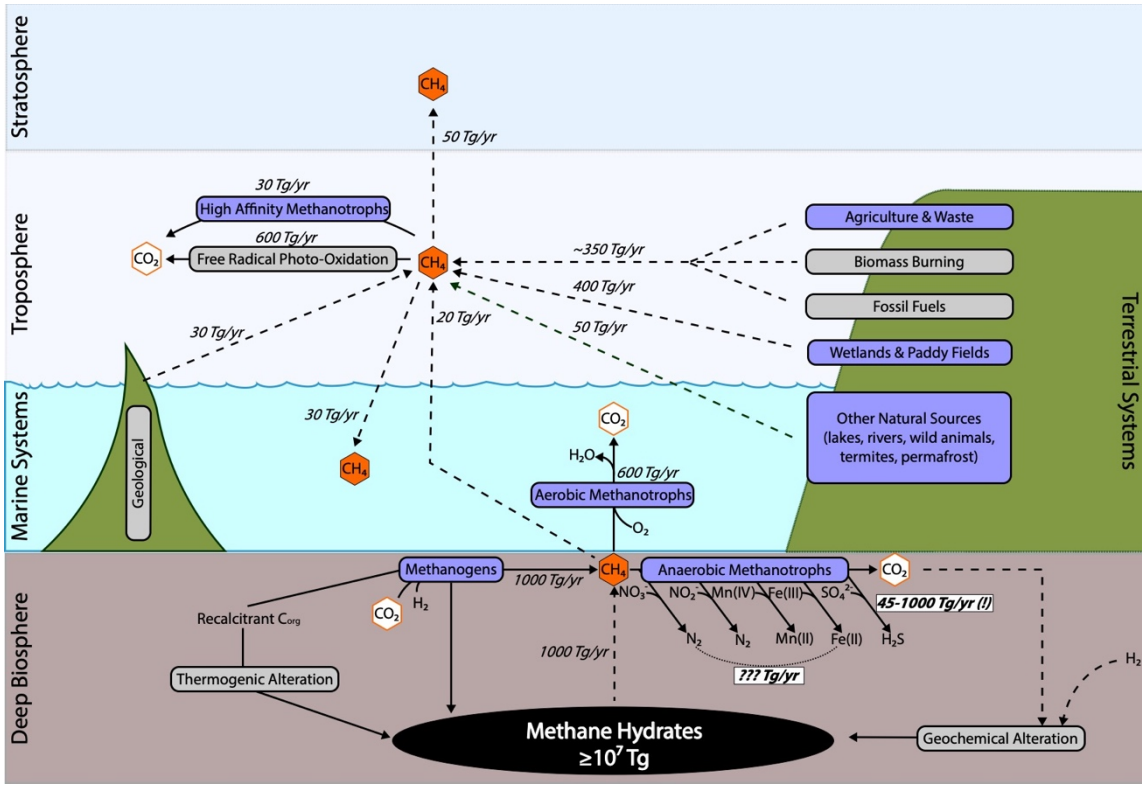

Figure 1.2. Global methane sources, sinks, and fluxes. Modified from Thauer et al. (2008) with additional inputs from Conrad (2009), Dlugokencky et al. (2011), Kirschke et al. (2013), and Egger et al. (2018).

1.3 STUDY SITES

1.3.1 ***BE326 BH2 borehole, Beatrix Gold Mine, South Africa***. BE326 BH2 is a horizontal borehole located 1.34 km below land surface (kmbls) in South Africa's Beatrix Gold Mine (S 28.235º, E 26.795º). Beatrix Mine is situated in the southwestern range of the 2.81± 0.2 Ga Witwatersrand Supergroup, a 5-7 km-thick intracratonic sedimentary basin that hosts the world's largest gold reserve and some of its deepest mines (Frimmel and Minter, 2002; Onstott et al., 2006) (Figure 1.3). BE326 BH2 has been the subject of numerous biogeochemical and molecular studies since it was first drilled in 2007.

Through a combination of gene amplicon surveys (Magnabosco et al., 2014), metagenomics (Lau et al., 2014), metatranscriptomics (Lau et al., 2016), metaproteomics (Lau et al., 2016), and isotopic analyses of dissolved gases and bacterial phospholipid fatty acids (PLFAs) (Simkus et al., 2016), BE326 BH2 has been characterized as a Subsurface Lithoautotrophic Microbial Ecosystem (SLiME) (Stevens and McKinley, 1995) with a CH_4-based carbon cycle mediated by low-abundance methanogens and anaerobic methanotrophs (ANMEs) existing in close metabolic syntrophy with sulfate reducing bacteria and denitrifying sulfur oxidizers (Figure 1.4).

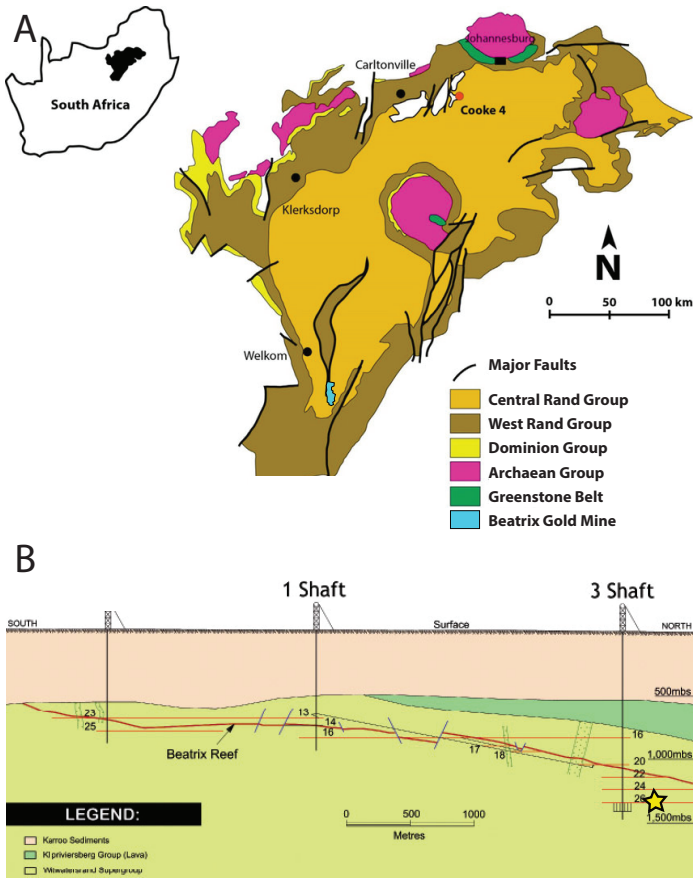

Figure 1.3. Geologic setting of Beatrix Mine **(A)** within the Witwatersrand Basin and **(B)** local stratigraphy of the Beatrix Reef orebody. Approximate location of the BE326 BH2 borehole is indicated by gold star. Modified from figures obtained from Mngadi et al. (2019) and Gold Fields, Ltd. (Johannesburg, South Africa).

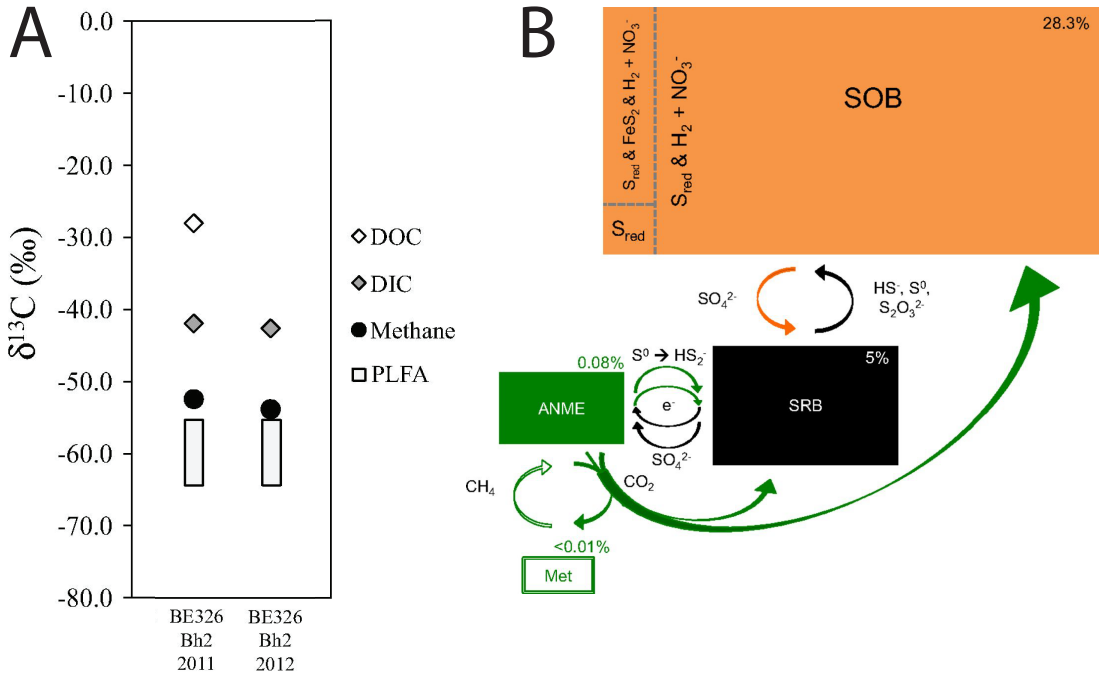

Figure 1.4. Isotopic and metatranscriptomic support for a CH_4-supported SLiME at BE326 BH2. **(A)** $\delta^{13}C$ values for dissolved organic carbon (DOC), dissolved inorganic carbon (DIC), CH_4, and PLFAs (modified from Simkus et al., 2016 with permission of the lead author). **(B)** C1 carbon flow map at BE326 BH2 based on transcriptional activity of methanogens (Met), anaerobic methanotrophs (ANME), sulfate reducing bacteria (SRB), and sulfur oxidizing bacteria (SRB). Arrows indicate direction of metabolite flow. Percent abundance (upper right-hand corner of boxes) inferred from relative abundance of ribosomal proteins in metatranscriptome. Figure taken from Lau et al. (2016) with lead author's permission.

1.3.2 ***IODP 370 site C0023A, Nankai Trough accretionary complex.*** International Ocean Discovery Program (IODP) Expedition 370 established drilling site C0023A on 17 September 2016 at the protothrust zone of the Nankai Trough, approximately 180 km offshore Cape Muroto, Japan (N 32.367˚, E 134.978˚). Site C0023A lies within the Muroto Transect within the vicinity of other Ocean Drilling Program (ODP) sites 1173, 1174, and 808 (Moore et al., 2001; Moore et al., 2005). Starting at the ocean floor at a water depth of 4776 m, site C0023A continues an additional 1180 m into sub-seafloor

sediment, crossing the décollement zone of the Eurasian and Philippine Sea plate boundary and spanning a temperature gradient of ~2˚C to ~130˚C (Figure 1.5; Heuer et al., 2017). Because of this gradual temperature increase, a primary objective of Expedition 370 was to identify biotic-abiotic transition zones and examine the factors that control the biomass, activity, and diversity of microbial communities inhabiting so-called "biotic fringe" environments (Hinrichs et al., 2016).

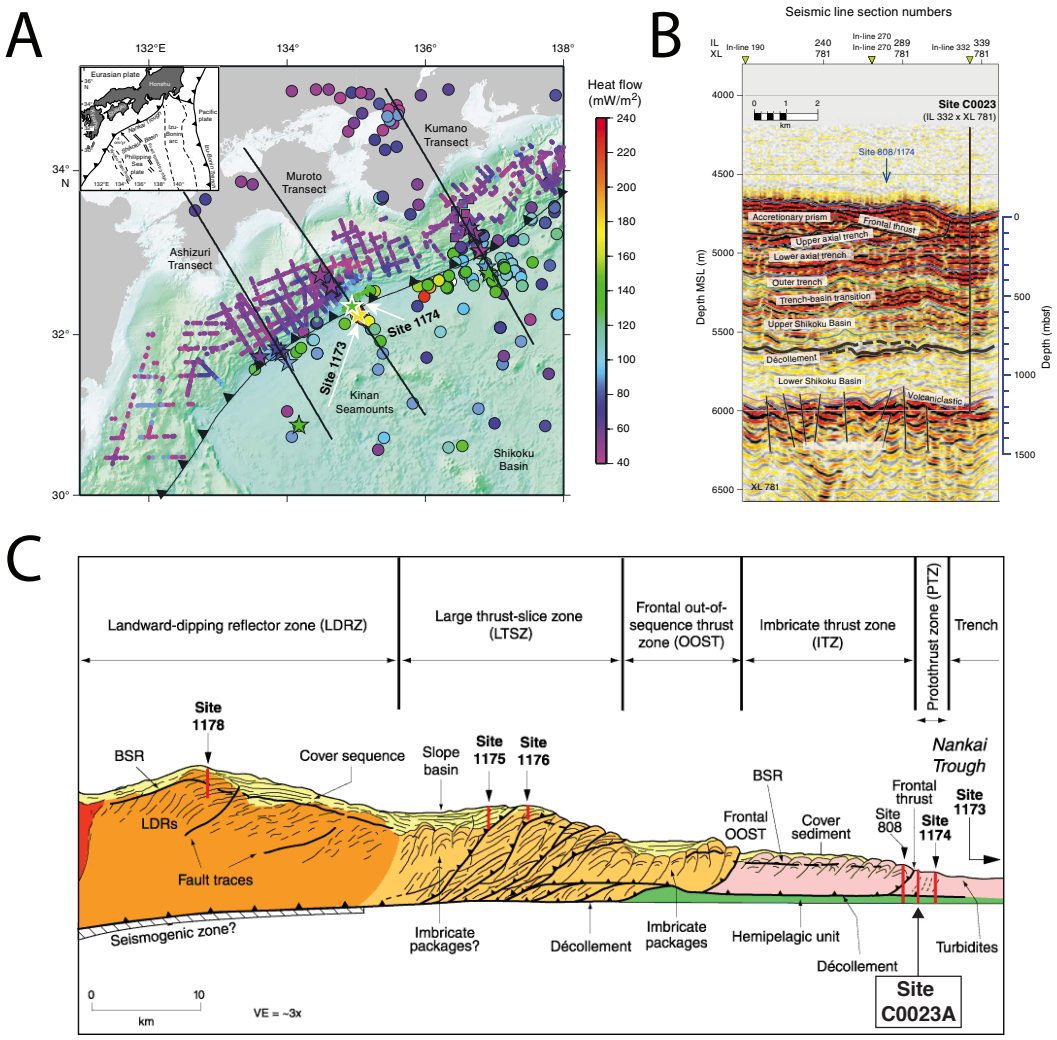

Figure 1.5. Regional context of site C0023A and the greater Muroto Transect. **(A)** Heat flow map generated from data collected by marine probes (large circles), bottom-simulating reflectors (small circles), and boreholes (stars). Circles on land reflect heat flow values collected from boreholes. **(B)** Depth-covered pre-stack time migration seismic section of site C0023A overlain with geological interpretation. **(C)** Schematic interpretation of the Muroto Transect showing tectonic regions and drill sites of ODP Leg 190 and IODP 370 for reference. Modified from Moore et al. (2001) and Heuer et al. (2017) with permission. Abbreviations: MSL, meters below sea level; MBSL, meters below seafloor; BSL, bottom-simulating radar.

1.4 OUTLINE OF DISSERTATION

Chapter 2 focuses on the development and application of fluorescent *in situ* hybridization of transcript-annealing molecular beacons (FISH-TAMB), a novel

molecular technique capable of fluorescently labeling messenger RNA (mRNA) of target genes in living cells. The idea of FISH-TAMB was inspired by a growing urgency in the field of microbial ecology to identify metabolically active microorganisms in complex communities without biasing against 16S rRNA gene phylogeny and without killing biomass via cellular fixation. In this chapter we first describe the synthesis of FISH-TAMB probes from constituent molecular beacon sequences (Goel et al., 2005) and cell-penetrating peptides (Patel et al., 2007). We then demonstrate the co-application of FISH-TAMB with confocal microscopy, flow cytometry, and traditional 16S rRNA FISH (e.g., DeLong et al., 1989; Amann et al., 1990) to identify mRNA transcribed from methyl coenzyme M reductase A (*Mcr*A) in a pure culture of the methanogen *Methanosarcina barkeri* strain Schnellen (*M. barkeri*), as well as ANME-2 enriched from BE326 BH2. To assess the potential of FISH-TAMB to identify mRNA from functional genes obtained via horizontal gene transfer, we combined FISH-TAMB with flow cytometry to identify *Mcr*A transformed onto an inducible operon in *Escherichia coli* str JM109 (*E. coli* mcrA^{+}) from *M. barkeri*. Finally, we measure growth curves of FISH-TAMB-treated *M. barkeri* and *E. coli* and compare them with those of untreated populations to assess how FISH-TAMB may impact cellular viability for continued study post-analysis.

In Chapter 3 we parse metagenomic sequence data generated from BE326 BH2 DNA to assemble and characterize a nearly complete genome belonging to a novel species – *Candidatus* (*Ca.*) "Bathyarchaeota" BE326-BA-RLH (Harris et al., 2018). The *Ca.* "Bathyarchaeota" are known as a microbial dark matter phylum; that is, they are only known from environmental sequencing data and do not possess any lineages that have been successfully isolated in pure culture (Marcy et al., 2007). In this chapter we utilize

bioinformatics to describe the phylogeny and metabolic potential of the metagenome-assembled genome (MAG) belonging to *Ca.* "Bathyarchaeota" BE326-BA-RLH. We employ maximum likelihood analysis to characterize the 16S rRNA gene phylogeny of the *Ca.* BE326-BA-RLH within the *Ca.* Bathyarchaeota, particularly in relation to putatively described methanogenic taxa (Evans et al., 2015). Using both sequence- and structure-based homology searches, we characterize protein-encoding genes specific to pathways for methanogenesis and dissimilatory nitrate reduction to ammonia (DNRA), assessing the potential of *Ca.* BE326-BA-RLH to perform AOM. This includes a description of a divergent *Mcr*A sequence from the BE326 BH2 metagenome that deeply roots the *Ca.* "Bathyarchaeota" phylum based on maximum likelihood phylogenetic analysis.

The discovery of novel CH_4-metabolizing microorganisms plainly illustrates the infancy of our understanding of deep biosphere biogeochemical cycling and the diversity and distribution of the functional groups that mediate it. Pursuant to this issue, in Chapter 4 we aim to provide evidence of a "missing niche" in biological CH_4 cycling: thermophilic, piezophilic ANMEs. To accomplish this, we switch gears from the deep continental subsurface of South Africa to the deep sub-seafloor of the Nankai Trough, applying a suite of methodologies of methodologies, corroborating the data with those collected by other Expedition 370 scientists, to assess for evidence of AOM in the deep, hot biosphere. We first perform geochemical modeling to assess the thermodynamic favorability of AOM metabolisms for 9 unique depths, each constrained by their *in situ* physical properties and geochemistry. We then employ SIP in combination with high-pressure cultivation to trace the oxidation of $^{13}CH_4$ under simulated *in situ* pressure and

temperature conditions. Grappling with noisy, inconclusive data tied to low *in situ* cell counts, we attempt FISH-TAMB and 16S rRNA FISH to directly visualize active ANMEs in our enrichments. We compare these results with genomic evidence for ANMEs based on a 16S rRNA gene survey of fresh core sediment as well as metagenomes from parallel incubations enriched with natural abundance CH_4 at ambient atmospheric pressure.

Looking beyond Earth, in Chapter 5 we take our inspiration from nearly two decades of research into Martian methane to investigate how methanogens may survive under simulated subsurface conditions of Mars, specifically under freezing temperatures and in the presence of chaotropic perchlorate salts. We tracked CH_4 production and changes in global gene expression patterns via transcriptomics in *Methanosarcina barkeri* strain MS following prolonged enrichment at 30˚C or 0˚C, with and without high concentrations (10 mM) of dissolved sodium-, magnesium, or calcium perchlorate. We discuss the potential of abiotic interactions of perchlorate anions with media components and supplied H_2 gas. We assess our findings in the context of previously published observations to speculate how catalytic nickel and H_2 may contribute to the reduction of perchlorate in methanogenic cultures. We conclude the chapter by discussing how these insights from transcriptomics can help us contextualize biology as a potential source of CH_4 observed on Mars.

Chapter 6 reviews the advances generated by this dissertation as well as the questions whose answers remain at large. We then look to the next generation of powerful up-and-coming molecular, geochemical, and computational tools and speculate

how a rapidly advancing state of the art will help us resolve the story of microbial methane cycling on Earth – and how it can inform us in the search for life beyond.

1.5 REFERENCES

Amann R. I., Krumholz L. and Stahl D. A. (1990) Fluorescent-oligonucleotide probing of whole cells for determinative, phylogenetic, and environmental studies in microbiology. *J. Bacteriol.* **172**, 762–770. Available at: http://jb.asm.org/lookup/doi/10.1128/jb.172.2.762-770.1990.

Bar-On Y. M., Phillips R. and Milo R. (2018) The biomass distribution on Earth. *Proc. Natl. Acad. Sci.* **115**, 6506–6511. Available at: http://www.pnas.org/lookup/doi/10.1073/pnas.1711842115.

Beal E. J., House C. H. and Orphan V. J. (2009) Manganese- and Iron-Dependent Marine Methane Oxidation. *Science (80-.).* **325**, 184–187. Available at: https://www.sciencemag.org/lookup/doi/10.1126/science.1169984.

Beulig F., Røy H., McGlynn S. E. and Jørgensen B. B. (2019) Cryptic CH4 cycling in the sulfate–methane transition of marine sediments apparently mediated by ANME-1 archaea. *ISME J.* **13**, 250–262. Available at: http://www.nature.com/articles/s41396-018-0273-z.

Cai C., Leu A. O., Xie G.-J., Guo J., Feng Y., Zhao J.-X., Tyson G. W., Yuan Z. and Hu S. (2018) A methanotrophic archaeon couples anaerobic oxidation of methane to Fe(III) reduction. *ISME J.* **12**, 1929–1939. Available at: http://www.nature.com/articles/s41396-018-0109-x.

Cario A., Oliver G. C. and Rogers K. L. (2019) Exploring the Deep Marine Biosphere:

Challenges, Innovations, and Opportunities. *Front. Earth Sci.* **7**. Available at: https://www.frontiersin.org/article/10.3389/feart.2019.00225/full.

Conrad R. (2009) The global methane cycle: recent advances in understanding the microbial processes involved. *Environ. Microbiol. Rep.* **1**, 285–292. Available at: http://doi.wiley.com/10.1111/j.1758-2229.2009.00038.x.

DeLong E., Wickham G. and Pace N. (1989) Phylogenetic stains: ribosomal RNA-based probes for the identification of single cells. *Science (80-.).* **243**, 1360–1363. Available at: http://www.sciencemag.org/content/243/4896/1360.abstract.

Dlugokencky E. J., Nisbet E. G., Fisher R. and Lowry D. (2011) Global atmospheric methane: budget, changes and dangers. *Philos. Trans. R. Soc. A Math. Phys. Eng. Sci.* **369**, 2058–2072. Available at: https://royalsocietypublishing.org/doi/10.1098/rsta.2010.0341.

Egger M., Riedinger N., Mogollón J. M. and Jørgensen B. B. (2018) Global diffusive fluxes of methane in marine sediments. *Nat. Geosci.* **11**, 421–425. Available at: http://www.nature.com/articles/s41561-018-0122-8.

Ettwig K. F., Butler M. K., Le Paslier D., Pelletier E., Mangenot S., Kuypers M. M. M., Schreiber F., Dutilh B. E., Zedelius J., de Beer D., Gloerich J., Wessels H. J. C. T., van Alen T., Luesken F., Wu M. L., van de Pas-Schoonen K. T., Op den Camp H. J. M., Janssen-Megens E. M., Francoijs K.-J., Stunnenberg H., Weissenbach J., Jetten M. S. M. and Strous M. (2010) Nitrite-driven anaerobic methane oxidation by oxygenic bacteria. *Nature* **464**, 543–548. Available at: http://dx.doi.org/10.1038/nature08883.

Ettwig K. F., Zhu B., Speth D., Keltjens J. T., Jetten M. S. M. and Kartal B. (2016)

Archaea catalyze iron-dependent anaerobic oxidation of methane. *Proc. Natl. Acad. Sci.* **113**, 12792–12796. Available at: http://www.pnas.org/lookup/doi/10.1073/pnas.1609534113.

Evans P. N., Parks D. H., Chadwick G. L., Robbins S. J., Orphan V. J., Golding S. D. and Tyson G. W. (2015) Methane metabolism in the archaeal phylum Bathyarchaeota revealed by genome-centric metagenomics. *Science* **350**, 434–8. Available at: http://www.sciencemag.org/content/350/6259/434.short.

Frimmel H. E. and Minter W. E. L. (2002) Recent Developments Concerning the Geological History and Genesis of the Witwatersrand Gold Deposits, South Africa. In *Integrated Methods for Discovery: Global Exploration in the Twenty-First Century* Society of Economic Geologists. Available at: https://pubs.geoscienceworld.org/books/book/1883/chapter/107029423.

Goel G., Kumar A., Puniya A. K., Chen W. and Singh K. (2005) Molecular beacon: a multitask probe. *J. Appl. Microbiol.* **99**, 435–442. Available at: http://doi.wiley.com/10.1111/j.1365-2672.2005.02663.x.

Harris R. L., Lau M. C. Y., Cadar A., Bartlett D. H., Cason E., van Heerden E. and Onstott T. C. (2018) Draft Genome Sequence of "Candidatus Bathyarchaeota" Archaeon BE326-BA-RLH, an Uncultured Denitrifier and Putative Anaerobic Methanotroph from South Africa's Deep Continental Biosphere ed. J. C. Dunning Hotopp. *Microbiol. Resour. Announc.* **7**. Available at: http://mra.asm.org/content/7/20/e01295-18.abstract.

Heuer V. B., Inagaki F., Morono Y., Kubo Y., Maeda L. and Scientists and the I. E. 370 (2017) Expedition 370 Preliminary Report: Temperature Limit of the Deep

Biosphere off Muroto. *Int. Ocean Discov. Progr.* Available at: http://dx.doi.org/10.14379/iodp.pr.370.2017.

Hinrichs K.-U. and Boetius A. (2002) The Anaerobic Oxidation of Methane: New Insights in Microbial Ecology and Biogeochemistry. In *Ocean Margin Systems* Springer Berlin Heidelberg, Berlin, Heidelberg. pp. 457–477. Available at: http://link.springer.com/10.1007/978-3-662-05127-6_28.

Hinrichs K.-U., Inagaki F., Heuer V. B., Kinoshita M., Morono Y. and Kubo Y. (2016) Expedition 370 Scientific Prospectus T-Limit of the Deep Biosphere off Muroto (T-Limit) Deciphering factors that constrain the extent of the deep. *Int. Ocean Discov. Progr.*

Inagaki F., Hinrichs K. U., Kubo Y., Bowles M. W., Heuer V. B., Hong W. L., Hoshino T., Ijiri A., Imachi H., Ito M., Kaneko M., Lever M. A., Lin Y. S., Methe B. A., Morita S., Morono Y., Tanikawa W., Bihan M., Bowden S. A., Elvert M., Glombitza C., Gross D., Harrington G. J., Hori T., Li K., Limmer D., Liu C. H., Murayama M., Ohkouchi N., Ono S., Park Y. S., Phillips S. C., Prieto-Mollar X., Purkey M., Riedinger N., Sanada Y., Sauvage J., Snyder G., Susilawati R., Takano Y., Tasumi E., Terada T., Tomaru H., Trembath-Reichert E., Wang D. T. and Yamada Y. (2015) Exploring deep microbial life in coal-bearing sediment down to 2.5 km below the ocean floor. *Science (80-.).* **349**, 420–424. Available at: https://www.sciencemag.org/lookup/doi/10.1126/science.aaa6882.

Jackson R. B., Solomon E. I., Canadell J. G., Cargnello M. and Field C. B. (2019) Methane removal and atmospheric restoration. *Nat. Sustain.* **2**, 436–438. Available at: http://www.nature.com/articles/s41893-019-0299-x.

Jones R. M., Goordial J. M. and Orcutt B. N. (2018) Low Energy Subsurface Environments as Extraterrestrial Analogs. *Front. Microbiol.* **9**. Available at: https://www.frontiersin.org/article/10.3389/fmicb.2018.01605/full.

Kallmeyer J., Pockalny R., Adhikari R. R., Smith D. C. and D'Hondt S. (2012) Global distribution of microbial abundance and biomass in subseafloor sediment. *Proc. Natl. Acad. Sci.* **109**, 16213–16216. Available at: http://www.pnas.org/cgi/doi/10.1073/pnas.1203849109.

Kirschke S., Bousquet P., Ciais P., Saunois M., Canadell J. G., Dlugokencky E. J., Bergamaschi P., Bergmann D., Blake D. R., Bruhwiler L., Cameron-Smith P., Castaldi S., Chevallier F., Feng L., Fraser A., Heimann M., Hodson E. L., Houweling S., Josse B., Fraser P. J., Krummel P. B., Lamarque J.-F., Langenfelds R. L., Le Quéré C., Naik V., O'Doherty S., Palmer P. I., Pison I., Plummer D., Poulter B., Prinn R. G., Rigby M., Ringeval B., Santini M., Schmidt M., Shindell D. T., Simpson I. J., Spahni R., Steele L. P., Strode S. A., Sudo K., Szopa S., van der Werf G. R., Voulgarakis A., van Weele M., Weiss R. F., Williams J. E. and Zeng G. (2013) Three decades of global methane sources and sinks. *Nat. Geosci.* **6**, 813–823. Available at: http://www.nature.com/articles/ngeo1955.

Lau M. C. Y., Cameron C., Magnabosco C., Brown C. T., Schilkey F., Grim S., Hendrickson S., Pullin M., Sherwood Lollar B., van Heerden E., Kieft T. L. and Onstott T. C. (2014) Phylogeny and phylogeography of functional genes shared among seven terrestrial subsurface metagenomes reveal N-cycling and microbial evolutionary relationships. *Front. Microbiol.* **5**, 531. Available at: http://journal.frontiersin.org/article/10.3389/fmicb.2014.00531/abstract.

Lau M. C. Y., Kieft T. L., Kuloyo O., Linage-Alvarez B., van Heerden E., Lindsay M. R., Magnabosco C., Wang W., Wiggins J. B., Guo L., Perlman D. H., Kyin S., Shwe H. H., Harris R. L., Oh Y., Yi M. J., Purtschert R., Slater G. F., Ono S., Wei S., Li L., Sherwood Lollar B. and Onstott T. C. (2016) An oligotrophic deep-subsurface community dependent on syntrophy is dominated by sulfur-driven autotrophic denitrifiers. *Proc. Natl. Acad. Sci.* **113**, E7927–E7936. Available at: http://www.pnas.org/lookup/doi/10.1073/pnas.1612244113.

Leu A. O., Cai C., McIlroy S. J., Southam G., Orphan V. J., Yuan Z., Hu S. and Tyson G. W. (2020) Anaerobic methane oxidation coupled to manganese reduction by members of the Methanoperedenaceae. *ISME J.* **14**, 1030–1041. Available at: http://www.nature.com/articles/s41396-020-0590-x.

Lin L. H., Hall J., Onstott T. C., Gihring T., Lollar B. S., Boice E., Pratt L., Lippmann-Pipke J. and Bellamy R. E. S. (2006) Planktonic microbial communities associated with fracture-derived groundwater in a deep gold mine of South Africa. *Geomicrobiol. J.* **23**, 475–497.

Magnabosco C., Lin L.-H., Dong H., Bomberg M., Ghiorse W., Stan-Lotter H., Pedersen K., Kieft T. L., van Heerden E. and Onstott T. C. (2018) The biomass and biodiversity of the continental subsurface. *Nat. Geosci.* **11**, 707–717. Available at: http://www.nature.com/articles/s41561-018-0221-6.

Magnabosco C., Tekere M., Lau M. C. Y., Linage B., Kuloyo O., Erasmus M., Cason E., van Heerden E., Borgonie G., Kieft T. L., Olivier J. and Onstott T. C. (2014) Comparisons of the composition and biogeographic distribution of the bacterial communities occupying South African thermal springs with those inhabiting deep

subsurface fracture water. *Front. Microbiol.* **5**, 679. Available at: http://journal.frontiersin.org/article/10.3389/fmicb.2014.00679/abstract.

Marcy Y., Ouverney C., Bik E. M., Losekann T., Ivanova N., Martin H. G., Szeto E., Platt D., Hugenholtz P., Relman D. A. and Quake S. R. (2007) Dissecting biological "dark matter" with single-cell genetic analysis of rare and uncultivated TM7 microbes from the human mouth. *Proc. Natl. Acad. Sci.* **104**, 11889–11894. Available at: http://www.pnas.org/cgi/doi/10.1073/pnas.0704662104.

Mngadi S. B., Durrheim R. J., Manzi M. S. D., Ogasawara H., Yabe Y., Yilmaz H., Wechsler N., Van Aswegen G., Roberts D., Ward A. K., Naoi M., Moriya H., Nakatani M., Ishida A., SATREPS Team and ICDP DSeis Team (2019) Integration of underground mapping, petrology, and high-resolution microseismicity analysis to characterise weak geotechnical zones in deep South African gold mines. *Int. J. Rock Mech. Min. Sci.* **114**, 79–91. Available at: https://linkinghub.elsevier.com/retrieve/pii/S1365160918301436.

Moore G. F., Mikada H., Moore J. C., Becker K. and Taira A. (2005) Legs 190 and 196 Synthesis: Deformation and Fluid Flow Processes in the Nankai Trough Accretionary Prism. In *Proceedings of the Ocean Drilling Program, 190/196 Scientific Results* Ocean Drilling Program. Available at: http://www-odp.tamu.edu/publications/190196SR/synth/synth.htm.

Moore G. F., Taira A., Bangs N. L., Kuramoto S., Shipley T. H., Alex C. M., Gulick S. S., Hills D. J., Ike T., Ito S., Leslie S. C., McCutcheon A. J., Mochizuki K., Morita S., Nakamura Y., Park J.-O., Taylor B. L., Toyama G., Yagi H. and Zhao Z. (2001) Leg 190 Summary. In *Proceedings of the Ocean Drilling Program, 190 Initial*

Reports

NOAA (2018) Monthly Mean Atmospheric Carbon Dioxide at Mauna Loa Observatory, Hawaii. *Natl. Ocean. Atmos. Adm.*

Onstott T. C., Colwell F. S., Kieft T. L., Murdoch L. and Phelps T. J. (2009) New Horizons for Deep Subsurface Microbiology. *Microbe* **4**, 499–505.

Onstott T. C., Ehlmann B. L., Sapers H., Coleman M., Ivarsson M., Marlow J. J., Neubeck A. and Niles P. (2018) Paleo-Rock-Hosted Life on Earth and the Search on Mars: a Review and Strategy for Exploration. *Astrobiology*. Available at: http://arxiv.org/abs/1809.08266.

Onstott T. C., Lin L.-H., Davidson M., Mislowack B., Borcsik M., Hall J., Slater G., Ward J., Sherwood Lollar B., Lippmann-Pipke J., Boice E., Pratt L. M., Pfiffner S., Moser D., Gihring T., Kieft T. L., Phelps T. J., Vanheerden E., Litthaur D., Deflaun M., Rothmel R., Wanger G. and Southam G. (2006) The origin and age of biogeochemical trends in deep fracture water of the Witwatersrand Basin, South Africa. *Geomicrobiol. J.* **23**, 369–414.

Orsi W. D. (2018) Ecology and evolution of seafloor and subseafloor microbial communities. *Nat. Rev. Microbiol.* **16**, 671–683. Available at: http://www.nature.com/articles/s41579-018-0046-8.

Patel L. N., Zaro J. L. and Shen W. C. (2007) Cell penetrating peptides: Intracellular pathways and pharmaceutical perspectives. *Pharm. Res.* **24**, 1977–1992.

Raghoebarsing A. A., Pol A., van de Pas-Schoonen K. T., Smolders A. J. P. P., Ettwig K. F., Rijpstra W. I. C., Schouten S., Sinninghe Damsté J. S., Op Den Camp H. J. M. M., Jetten M. S. M. M., Strous M., Damsté J. S. S., Op Den Camp H. J. M. M.,

Jetten M. S. M. M. and Strous M. (2006) A microbial consortium couples anaerobic methane oxidation to denitrification. *Nature* **440**, 918–21. Available at: http://www.ncbi.nlm.nih.gov/pubmed/16612380.

Rigby M., Prinn R. G., Fraser P. J., Simmonds P. G., Langenfelds R. L., Huang J., Cunnold D. M., Steele L. P., Krummel P. B., Weiss R. F., O'Doherty S., Salameh P. K., Wang H. J., Harth C. M., Mühle J. and Porter L. W. (2008) Renewed growth of atmospheric methane. *Geophys. Res. Lett.* **35**, L22805. Available at: http://doi.wiley.com/10.1029/2008GL036037.

Rinke C., Schwientek P., Sczyrba A., Ivanova N. N., Anderson I. J., Cheng J.-F., Darling A. E., Malfatti S., Swan B. K., Gies E. a, Dodsworth J. A., Hedlund B. P., Tsiamis G., Sievert S. M., Liu W.-T., Eisen J. A., Hallam S. J., Kyrpides N. C., Stepanauskas R., Rubin E. M., Hugenholtz P. and Woyke T. (2013) Insights into the phylogeny and coding potential of microbial dark matter. *Nature* **499**, 431–437. Available at: http://www.ncbi.nlm.nih.gov/pubmed/23851394.

Saunois M., Bousquet P., Poulter B., Peregon A., Ciais P., Canadell J. G., Dlugokencky E. J., Etiope G., Bastviken D., Houweling S., Janssens-Maenhout G., Tubiello F. N., Castaldi S., Jackson R. B., Alexe M., Arora V. K., Beerling D. J., Bergamaschi P., Blake D. R., Brailsford G., Brovkin V., Bruhwiler L., Crevoisier C., Crill P., Covey K., Curry C., Frankenberg C., Gedney N., Höglund-Isaksson L., Ishizawa M., Ito A., Joos F., Kim H.-S., Kleinen T., Krummel P., Lamarque J.-F., Langenfelds R., Locatelli R., Machida T., Maksyutov S., McDonald K. C., Marshall J., Melton J. R., Morino I., Naik V., O'Doherty S., Parmentier F.-J. W., Patra P. K., Peng C., Peng S., Peters G. P., Pison I., Prigent C., Prinn R., Ramonet M., Riley W. J.,

Saito M., Santini M., Schroeder R., Simpson I. J., Spahni R., Steele P., Takizawa A., Thornton B. F., Tian H., Tohjima Y., Viovy N., Voulgarakis A., van Weele M., van der Werf G. R., Weiss R., Wiedinmyer C., Wilton D. J., Wiltshire A., Worthy D., Wunch D., Xu X., Yoshida Y., Zhang B., Zhang Z. and Zhu Q. (2016) The global methane budget 2000–2012. *Earth Syst. Sci. Data* **8**, 697–751. Available at: https://www.earth-syst-sci-data.net/8/697/2016/.

Shock E. (2014) Finding the Biotic Fringe. In *AGU Fall Meeting Abstracts* pp. B23G-01.

Simkus D. N., Slater G. F., Sherwood Lollar B., Wilkie K., Kieft T. L., Magnabosco C., Lau M. C. Y., Pullin M. J., Hendrickson S. B., Wommack K. E., Sakowski E. G., van Heerden E., Kuloyo O., Linage B., Borgonie G. and Onstott T. C. (2016) Variations in microbial carbon sources and cycling in the deep continental subsurface. *Geochim. Cosmochim. Acta.* **173**, 264–283.

Stevens T. O. and McKinley J. P. (1995) Lithoautotrophic Microbial Ecosystems in Deep Basalt Aquifers. *Science (80-.).* **270**, 450–455. Available at: https://www.sciencemag.org/lookup/doi/10.1126/science.270.5235.450.

Szewzyk U., Szewzyk R. and Stenstrom T. A. (1994) Thermophilic, anaerobic bacteria isolated from a deep borehole in granite in Sweden. *Proc. Natl. Acad. Sci.* **91**, 1810–1813. Available at: http://www.pnas.org/cgi/doi/10.1073/pnas.91.5.1810.

Thauer R. K., Kaster A.-K., Seedorf H., Buckel W. and Hedderich R. (2008) Methanogenic archaea: ecologically relevant differences in energy conservation. *Nat. Rev. Microbiol.* **6**, 579–591. Available at: http://www.nature.com/articles/nrmicro1931.

Turner A. J., Frankenberg C. and Kort E. A. (2019) Interpreting contemporary trends in

atmospheric methane. *Proc. Natl. Acad. Sci.* **116**, 2805–2813. Available at: http://www.pnas.org/lookup/doi/10.1073/pnas.1814297116.

Valentine D. L. and Reeburgh W. S. (2000) New perspectives on anaerobic methane oxidation. *Env. Microbiol* **2**, 477–484.

CHAPTER 2

Using FISH-TAMB, a fixation-free mRNA fluorescent labeling technique, to reveal active minority methane-cycling lineages

Keywords: molecular beacons, cell-penetrating peptides, fluorescence *in situ* hybridization, live cell imaging, methanogens, anaerobic methanotrophs, deep biosphere

2.1 ABSTRACT

We report on the development of fluorescent *in situ* hybridization of transcript-annealing molecular beacons (FISH-TAMB) to label messenger RNA (mRNA) of methyl-coenzyme M reductase A (*mcr*A) in living methanogens and anaerobic methanotrophic archaea (ANMEs). FISH-TAMB utilizes polyarginine cell-penetrating peptides to deliver molecular beacons (MBs) across prokaryotic cell walls and membranes, fluorescently labeling cells when MBs hybridize to target mRNA sequences. FISH-TAMB's target specificity and sensitivity was demonstrated by labeling *mcr*A mRNA expressed in *Methanosarcina barkeri,* ANME-2, and *Escherichia coli* containing a plasmid with a partial *M. barkeri mcr*A gene (*E. coli* mcrA^{+}). Growth curve analysis supported sustained cellular viability following FISH-TAMB treatment. FISH-TAMB is capable of labeling single planktonic cells and cells in microbial aggregates in real time, supporting its application in investigating syntrophically activated metabolisms between physically associated microorganisms. FISH-TAMB can be applied to target mRNA of any functional gene of interest and does not require prior knowledge of 16S ribosomal RNA-based taxonomy. Nonetheless, we demonstrated that FISH-TAMB is compatible with 16S rRNA FISH, enabling simultaneous metabolic and taxonomic identification of microbes active in biogeochemical cycling. Our results demonstrate FISH-TAMB as a versatile addition to the molecular ecologist's toolkit, with potential widespread application in the field of environmental microbiology.

2.2 INTRODUCTION

The studies of ribosomal RNA (rRNA) and, more recently, shotgun sequencing of genomic DNA have vastly expanded our knowledge of microbial diversity and metabolic potential in natural communities, including uncultivated microbial species of the rare biosphere and microbial dark matter (MDM) (Sogin et al., 2006; Rinke et al., 2013; Spang et al., 2015; Vanwonterghem et al., 2016; Seitz et al., 2016; Zaremba-Niedzwiedzka et al., 2017; Lazar et al., 2017). Shotgun sequencing of mRNA from environmental samples, metatranscriptomics, has revealed the *in situ* metabolic activity of microbial ecosystems (Poretsky et al., 2005; Poretsky et al., 2009; He et al., 2010; Gifford et al., 2011; Hollibaugh et al., 2011; He et al., 2012; Lau et al., 2016; Lau et al., 2018). Despite these advances or because of them, the need to enrich, isolate and characterize the physiology of rare biosphere and MDM species has increased. While high-throughput sequencing is an excellent means to identify novel lineages with divergent functional genes (Evans et al., 2015; Harris et al., 2018; Borrel et al., 2019; McKay et al., 2019; Wang et al., 2019; Evans et al., 2019; Boyd et al., 2019), enrichments and labeling experiments on living biomass are ultimately necessary to assess physiological characteristics – such as substrate affinity (Möller and van Heerden, 2006; Laso-Pérez et al., 2016; Pratscher et al., 2018; Chen et al., 2019) and enzymatic directionality (Fuseler, 1996; Thorup et al., 2017) – which cannot be inferred from -omics efforts alone.

Visualization and sorting of these species can be performed through fluorescence *in situ* hybridization (FISH), which involves the use of fluorescent oligonucleotide linear probes targeting the 16S rRNA gene (DeLong et al., 1989; Amann et al., 1990) or

messenger RNA (mRNA) (Pernthaler and Amann, 2004; Kalyuzhnaya et al., 2006; Jen et al., 2007; Mota et al., 2012; Rosenthal et al., 2013; Nikolakakis et al., 2015; Choi et al., 2016; DePas et al., 2016). These approaches, however, typically require fixed (i.e. dead) cells, rendering impossible the capture of labeled rare taxa for cultivation-based research. Fixation-free 16S rRNA FISH has been applied on environmental samples for subsequent enrichment (Yilmaz et al., 2010), but to our knowledge a fixation-free FISH protocol targeting mRNA has not yet been reported. Imaging and sorting of translationally active cells from environmental samples has been achieved through the use of bioorthogonal noncanonical amino acid tagging (BONCAT) (Hatzenpichler et al., 2016) but this approach has to be combined with fixation-free techniques to target specific taxonomic or functional clades for enrichment. It would be advantageous, therefore, to use a fixation-free fluorescent labeling technique that identifies metabolically active cells based on the transcription of target functional genes to enable subsequent sorting and enrichment.

We describe here the development of fluorescent *in situ* hybridization of transcript-annealing molecular beacons (FISH-TAMB) to label mRNA of a targeted functional gene in living, transcriptionally active prokaryotic cells without the need for cellular fixation. Molecular beacons (MBs), with a hairpin oligonucleotide sequence outfitted with a fluorophore and a fluorescence quencher (Tyagi and Kramer, 1996) were selected to target the mRNA of bacteria and archaea, as they result in a higher signal-to-background noise ratio than linear probes and have also been successfully applied to detect intracellular mRNA of living eukaryotic cells (Sokol et al., 1998; Nitin et al., 2004; Santangelo et al., 2006; Bao et al., 2009; Larsson et al., 2012). In the unbound state, complementary bases on the 5’ and 3’ ends of MBs self-anneal to form a stem structure,

which results in fluorescence quenching. Recognition of a target sequence results in MB linearization for subsequent hybridization (Figure 2.1). Thus, the fluorophore is no longer in physical proximity to the quencher, resulting in emission of a known wavelength at a level differentiable from the background fluorescence due to autofluorescence and unbound MBs (Goel et al., 2005). In order to deliver the MBs into prokaryotic cells without causing cell death, cell-penetrating peptides are used as the cargo-delivering vehicle, as they have been shown to successfully deliver DNA and nanoparticles into living cyanobacteria with negligible toxicity (Liu et al., 2013a; Liu et al., 2013b), though the mechanism by which cellular uptake occurs is presently not fully understood.

In this study, we demonstrate the usage of FISH-TAMB by applying the methodology to visualize *in vivo* intracellular mRNA expressed by the alpha subunit of methyl-coenzyme M reductase (*mcr*A), a marker gene of methanogens (Lueders et al., 2001; Luton et al., 2002; Evans et al., 2015; Vanwonterghem et al., 2016) and the uncultivated anaerobic methanotrophic archaea (ANMEs) (Hinrichs et al., 1999; Boetius et al., 2000; Orphan et al., 2001; Orphan et al., 2002; Hallam et al., 2003). Following the formation of FISH-TAMBs via non-covalent hybridization of MBs to R9 cell-penetrating peptides, we applied the FISH-TAMB methodology to target *mcr*A mRNA in cells from three scenarios: (i) a methanogen grown in pure culture (*Methanosarcina barkeri*), (ii) ANMEs enriched from Precambrian shield subsurface fracture fluid (BE326 BH2-Conc) (Lau et al., 2016; Simkus et al., 2016; Magnabosco et al., 2018), and (iii) *Escherichia coli* transformed with partial *mcr*A gene derived from *M. barkeri* (*E. coli* mcrA^{+}), which is used as a proxy for potential inter-domain horizontal gene transfer. Cells were visualized and enumerated using spinning disk confocal microscopy and flow cytometry (FC). To

fluorescently identify active ANMEs, we followed FISH-TAMB treatment of BE326 BH2-Conc with standard 16S rRNA FISH protocol, and observed microbial consortia were compared with taxonomic information obtained from the associated metagenome. Ability of pure cultures to grow post FISH-TAMB treatment was assessed by growth curve analysis.

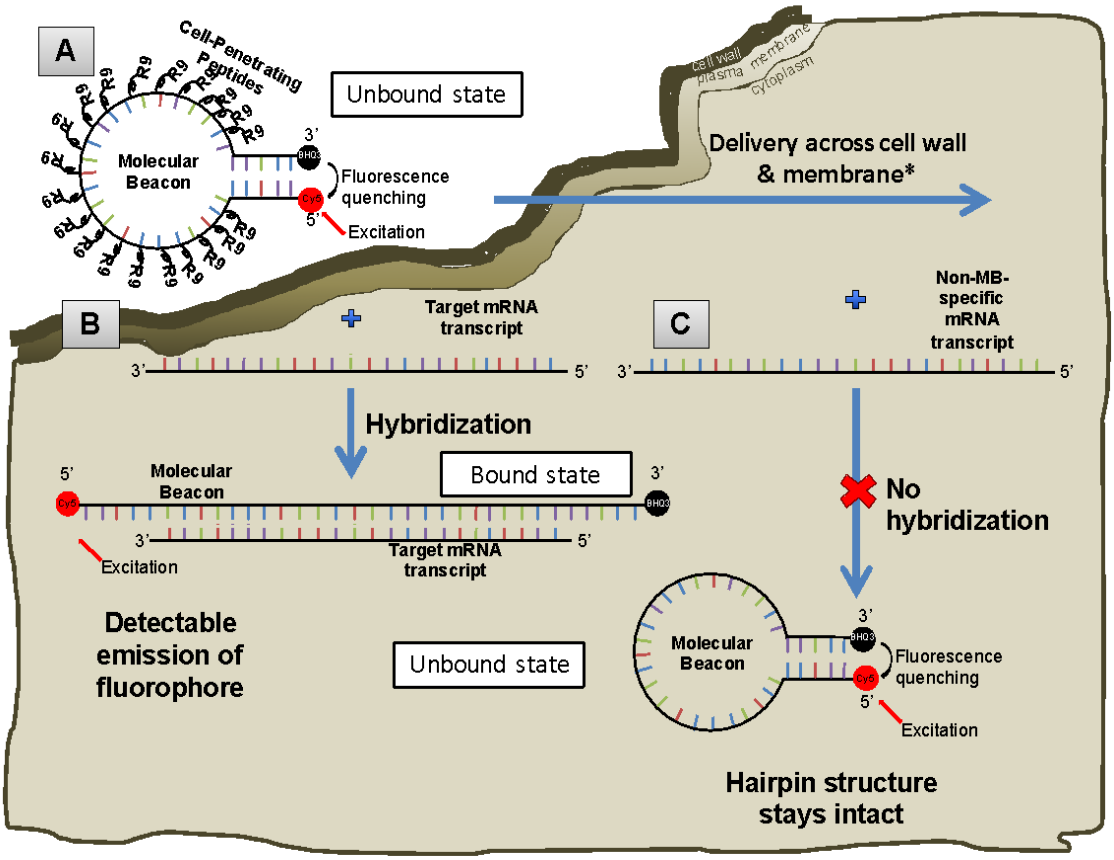

Figure 2.1. FISH-TAMB conformation and hybridization to encountered messenger RNAs. **(A)** An oligomer comprised of a 24 base-long complementary *mcr*A mRNA sequence is flanked by 5 reverse complement nucleotides to form a molecular beacon (MB) loop and stem structure. Cell-penetrating peptides (CPPs) comprising 9 arginine sequences (R9) are non-covalently bound to the MB sequence and are responsible for its delivery across the cell wall and plasma membrane. **(B)** Fluorescence of Cy5 fluorophore covalently bound to the 5' end of the MB sequence remains quenched by BHQ3 bound to the 3' terminus until the MB hybridizes to a target transcript sequence. Hybridization results in the linearization of the MB, subsequently unquenching Cy5 from BHQ3, allowing the fluorophore's emission upon excitation by a source in the red bandwidth of the visible light spectrum. **(C)** If the MB encounters an mRNA transcript that is not its intended target, it will retain its hairpin conformation and fluorescence of Cy5 will remain quenched by BHQ3. Images not to scale. Mechanism of CPP delivery across the cell wall and plasma membrane remains under debate. Intracellular fate of R9 is unknown.

2.3 MATERIALS AND METHODS

2.3.1 ***Microbial sampling of borehole BE326 BH2***. Fracture fluid was collected in June 2016 following established sampling procedures (Lau et al., 2014; Magnabosco et al., 2014) from a horizontal borehole located 1.34 km below land surface on the 26th level of shaft 3 of the Beatrix Gold Mine in South Africa (BE326 BH2) (S 28.235º, E 26.795º). Due to a low *in situ* cell concentration (Simkus et al., 2016) of 10^3 to 10^4 cells ml^{-1}, the fracture fluid was first filtered using a 0.2 µm hollow fiber MediaKap®-10 filter (Spectrum Labs, New Brunswick, NJ USA) and then back-flushed with fracture fluid into sterile, N_2-sparged 160-ml borosilicate serum vials to obtain a final concentration of ~10^7 cells ml^{-1}. Dissolved gas samples were collected along with field measurements of certain environmental parameters (SI Materials & Methods, results in Table 2S.1).

2.3.2 ***Enrichments of methanogens and anaerobic methanotrophs (ANMEs)***. Axenic *Methanosarcina barkeri* str. Schnellen cultures (ATCC® 43569™) were enriched for hydrogenotrophic methanogenesis using modified DSMZ medium 120a (Bryant and Boone, 1987). The medium was titrated with anaerobic 1 M NaOH to pH 7.2. Growth at 37˚C was monitored via optical density measurements taken at 550 nm [OD_{550}] (Anderson et al., 2012) using a Hach DR/2010 Spectrophotometer (Hach Company, Loveland, CO USA. Methane production was observed using a gas chromatograph equipped with a flame ionization detector (FID) (Peak Performer 1 series, Peak Laboratories, Mountain View, CA USA).

The anaerobic oxidation of methane coupled to sulfate reduction (S-AOM) was enriched in BE326 BH2-Conc samples by inoculating fracture fluid into a modified

anaerobic artificial seawater medium containing SO_4^{2-} as the sole electron acceptor (Widdel and Bak, 1992; Holler et al., 2011). The medium was pH-adjusted to pH 8.2 and contained 10 mM SO_4^{2-} to reflect the *in-situ* conditions observed at BE326 BH2 (Table 2S.1). AOM activity was determined via stable isotopic monitoring of $^{13}CH_4$ tracer oxidized to $^{13}CO_2$ using a Picarro G2101-*I* cavity ringdown spectrometer (Picarro, Inc. Santa Clara, CA USA). Sulfate reduction to sulfide was monitored using a Dionex IC25 ion chromatograph coupled to an MSQ-quadruple mass spectrometer (Thermo Scientific, Waltham, MA USA). Media recipes and details of enrichment maintenance are described in SI Materials & Methods.

Total DNA isolation was performed on the BE326 BH2-Conc AOM enrichment for metagenomic sequencing using a Qiagen DNeasy PowerSoil Kit following the manufacturer's protocol (QIAGEN, Hilden, Germany). Isolated DNA was quantified using a Qubit high sensitivity dsDNA assay kit and a Qubit 2.0 analyzer according to the manufacturer's instructions (ThermoFisher Scientific, Waltham, MA USA), and DNA was kept frozen at -20˚C for further processing. Metagenomic libraries were prepared using a PrepX DNA library kit and an automated Apollo 324 system (WaferGen Biosystems, Inc., Fremont CA USA). Paired end (2 x 100 nt) DNA sequencing was performed on a HiSeq 2000 platform (Illumina, Inc., San Diego, CA USA) located at the Marine Biological Laboratory in Woods Hole, MA USA. Quality filtering of sequenced reads and subsequent metagenome assembly and annotation was performed as previously described (Harris et al., 2018). A total of 35,669,635 raw paired end reads were processed using fastp v.0.12.6 (Chen et al., 2018) to remove reads matching the Illumina universal adapter sequence, that were shorter than 50 nt, had Phred quality scores < 30, and

contained Ns as bases. The resulting 32,139,898 quality-filtered paired end reads were assembled using SPAdes v.3.11.0 (-meta option) (Bankevich et al., 2012). Taxonomic diversity of the assembled metagenome was assessed using Kaiju v.1.6.2 (Menzel et al., 2016) against the nr_euk database using greedy mode (-a greedy), allowing 5 mismatches (-e 5) and a maximum e-value threshold of 5×10^{-5} (-E 0.00005). Gene predictions were made from assembled scaffolds of length > 200 bp using Prodigal v2.6.3 (-p meta option) (Hyatt et al., 2010). Resulting open reading frames (ORFs) were annotated using BLASTp against the nr database (-max_target_seqs 10). The consensus protein identity was determined as the most common assignment amongst the top 10 collected hits with an e-value < 10^{-10}.

2.3.3 *E. coli* expression clones. *E. coli* JM109 expression clones were grown at 37˚C on an orbital shaker at 150 rpm in a suspension of Luria broth containing 0.05 mg ml^{-1} ampicillin. Growth was monitored via optical density at 600 nm [OD_{600}] using a Beckman DU® 530 Life Science UV/Vis Spectrophotometer (Beckman Coulter®, Indianapolis, IN USA). Transcription of the *lac* operon containing either target *lacZα* or *mcr*A genes was induced at OD_{600} ~ 0.6 by adding 1 mM Isopropyl β-D-1-thiogalactopyranoside (IPTG). IPTG-induced cultures were incubated at 37˚C and 150 rpm for 4 hours prior to treatment with FISH-TAMB.

E. coli $mcrA^+$ was periodically monitored for gene loss by plating liquid culture aliquots onto Luria broth cloning plates with 0.05 mg ml^{-1} ampicillin, 0.05 mg ml^{-1} IPTG, and 0.08 mg X-gal (LB/AIX) for blue/white screening (SI Materials & Methods). If *mcr*A was absent from the plasmid, the cloning procedure was repeated.

Details of transformation procedures, including isolation and purification of *M. barkeri mcr*A, can be found in SI Materials and Methods.

2.3.4 ***Molecular beacon (MB) design***. The MBs in this study each comprised a GC-rich 5-base pair stem and 24-mer nucleotide probe sequence. The MB targeting *lac*Zα mRNA was designed to overlap the insertion site sequence of the pGEM®-T Easy Vector and have a similar melting temperature and GC content as the MB targeting *mcr*A mRNA. The *mcr*A MB sequence was modified from the *mcr*A-rev reverse primer (5'-CGTTCATBGCGTAGTTVGGRTAGT-3') commonly used in diversity studies of methanogens and ANMEs belonging to phylum *Euryarchaeota* (Steinberg and Regan, 2009). Both *lac*Zα and *mcr*A MBs were flanked on the 5' end by a covalently bound Cy5 fluorophore (excitation peak at 640 nm, and emission peak at 665 nm) and on the 3' end by a BHQ3 Black Hole Quencher® (MilliporeSigma, St. Louis, MO USA). MB sequences can be found in Table 2S.2.

As the additional bases on the stem structure (as indicated by small letters in the MB sequences) may affect the specificity of the MB to target transcripts, the similarity between MB sequences and their respective targets was assessed *in silico* using BLAST (https://blast.ncbi.nlm.nih.gov/Blast.cgi) against the nucleotide database. *In vitro* hybridization was done to assess potential non-specific hybridization fluorescence and melting curve analysis was done to determine the optimal incubation temperature for positive MB-target hybridization (SI Materials & Methods, SI Results & Discussion).

2.3.5 ***Formation of FISH-TAMB probes***. A cell-penetrating peptide comprised of nine arginine residues (R9) was selected as a carrier to deliver MBs across cell walls and plasma membranes, as it has been demonstrated to penetrate cyanobacterial walls and membranes without harmful effects (Liu et al., 2013a). R9 was mixed with MB in 1× Dulbecco's phosphate buffered saline solution (DPBS) (Corning Mediatech, Manassas, VA USA) in an FISH-TAMB molar ratio of 20:1. Reactions were incubated for 30 minutes at 37˚C in a C1000 Touch™ Thermal Cycler (Bio-Rad Laboratories, Inc., Irvine, CA USA) to allow for the complexation of all free-floating MBs in solution. FISH-TAMB probes were subsequently stored in the dark at -20˚C until use. Procedures and data determining optimal component ratios for FISH-TAMB probe formation are found in SI Materials & Methods, SI Results & Discussion, and Table 2S.3, respectively.

2.3.6 ***Growth assessment of FISH-TAMB treated cultures***. *E. coli* mcrA^{+}, *E. coli* lacZα^{+}, and *M. barkeri* (~10^{6} cells) were incubated with 1 μM FISH-TAMB probes as described and subsequently inoculated into Luria broth containing 0.05 mg ml^{-1} ampicillin (LB/A) (for *E. coli*) and DSMZ 120a media (for *M. barkeri*). Growth curves were obtained by measuring optical density at 600 nm for *E. coli* using a Beckman DU® 530 Life Science UV/Vis Spectrophotometer (Beckman Coulter®, Indianapolis, IN USA) and at 550 nm for *M. barkeri* using a Hach DR/2010 Spectrophotometer (Hach Company, Loveland, CO USA). Growth rates for FISH-TAMB treated cultures were compared to those obtained by control cultures (i.e. not treated with FISH-TAMB).

2.3.7 ***FISH-TAMB and 16S rRNA FISH***. All pure cultures and enrichments (~10^6 cells) were incubated in the dark for 15 minutes at 37˚C in 100-µl reactions containing 1 µM FISH-TAMB probes in 1× DPBS solution. Reactions for *M. barkeri* and BE326 BH2-Conc enrichments were prepared using degassed 1× DPBS in an anaerobic glove bag (Coy Laboratory Products, Grass Lake, MI USA) to maintain cell activity in the absence of atmospheric O_2. FISH-TAMB treated cells of known taxonomy (i.e. pure cultures) were immediately analyzed in downstream applications (e.g. spinning disk confocal microscopy, flow cytometry) to visualize labeled mRNA, while cells from BE326 BH2-Conc AOM enrichments were fixed for subsequent taxonomic identification via 16S rRNA FISH. Briefly, FISH-TAMB-treated cells from AOM enrichments were washed once in 1× PBS and centrifuged at 2,000 × g for 5 minutes. The supernatant was pipetted off and cells were resuspended in a 1:1 mixture of chilled absolute ethanol and 1× DPBS and stored overnight at -20˚C before being subsequently filtered onto 0.2 µm polycarbonate membrane filters (Whatman International Ltd., Maidstone, UK). Filters were washed twice with filter-sterilized distilled MilliQ water and chilled absolute ethanol then allowed to air dry before being stored at -20˚C until 16S rRNA FISH treatment.

Sequences belonging to ANME-2 methanotrophs previously identified by metatranscriptomics at BE326 BH2 (Lau et al., 2016) were targeted by 16S rRNA FISH in BE326 BH2-Conc AOM enrichments. For 16S rRNA FISH, fixed samples were hybridized with 50 ng μl^{-1} dual-labeled ANME-2-targeted oligonucleotide probes (Boetius et al., 2000; Orphan et al., 2001; Hatzenpichler et al., 2016) with Atto 565 fluorophores (Biomers.net, Ulmer, Germany; ATTO-TEC GmbH, Siegen, Germany).

Hybridizations were performed at 46˚C for 2 hours and subsequently washed at 48˚C for 15 minutes and counterstained with 1 μM 4,6-diaminidino-2-phynylindole (DAPI) following an established protocol (Glöckner et al., 1996). Hybridization stringency of probes to targets was verified using varied formamide concentrations (0%, 10%, 20%, 30%, and 40%) prior to application to BE326 BH2-Conc AOM enrichments. Each probe set was hybridized in a technical duplicate and compared to unfixed, FISH-TAMB-labeled and unfixed, unlabeled control samples. 16S rRNA FISH probe sequences can be found in Table 2S.2.

2.3.8 ***Spinning disk confocal microscopy***. *M. barkeri* and BE326 BH2-Conc cells were imaged using a Nikon Ti-E with Perfect Focus System (PFS) inverted microscope (Nikon Instruments, Melville, NY USA) equipped with a 100× Plan Apo NA 1.45 oil objective lens, Yokogawa CSU-21 spinning disk, Orca Flash camera (Hamamatsu, Bridgewater, NJ USA). The 405-nm laser channel was used to excite F420 autofluorescence in unfixed *M. barkeri*, *M. barkeri* and fixed BE326 BH2-Conc cells that were labeled with 1 μM DAPI. Unfixed *E. coli* mcrA^{+} and *E. coli* lacZα^{+} expression clones were stained with 1 μM Hoechst 33342 (Thermo Fisher Scientific, Waltham, MA USA), and fluorescent cells were detected on the 461-nm emission filter. Atto 565 coinciding with 16S rRNA FISH labeling of ANME-2 cells was excited at 561 nm and detected at 590 nm. Excitation and emission of the Cy5 fluorophore in FISH-TAMB probes were set to 647 nm and 670 nm, respectively. To minimize focus drift, samples were maintained inside a humidity controlled environmental chamber at 25˚C under a 100% CO_2 atmosphere during imaging. Unfixed FISH-TAMB labeled cells from the

BE326 BH2-Conc enrichment were imaged every minute for 14 hours to assess Cy5 fluorescence lifetime, with multiple positions recorded simultaneously using an MS-2000 motorized stage (Applied Scientific Instrumentation, Eugene, OR USA).

M. barkeri cells exposed to atmospheric O_2 prior to imaging were transferred in 1-ml aliquots (~10^8 cells) into sterile 1.5 ml Eppendorf tubes and incubated in a heat block at 37˚C overnight on an orbital shaker at 150 rpm. Exposure to O_2 was verified via media color change from clear (anaerobic) to bright pink (oxidized) as indicated by O_2 sensitive resazurin in solution. FISH-TAMB treatment and imaging parameters were as previously described.

Three-dimensional projections were generated from z-stacks to localize mRNA labeling in *E. coli* mcrA$^+$ and *E. coli* lacZα^+ expression clones. FISH-TAMB-treated cells were stained with 1 μM Hoechst 33342 and imaged using a Bruker Opterra II swept-field confocal microscope (Bruker Scientific Instruments, Billerica, MA USA) equipped with a multiphoton super-resolution Luxendo light-sheet (Luxendo GmbH, Heidelberg, Germany). Hoechst 33342 fluorescence was excited with a 405 nm laser line and emission was detected at 461 nm. Cy5 fluorescence from FISH-TAMBs was excited at 640 nm and detected at 665 nm.

Composite micrographs were generated from raw microscopy images using ImageJ v. 2.0.0-rc-69/1.52n. Images were enhanced to show contrast using Adobe Photoshop Elements 15 (Adobe Inc., San Jose, CA USA).

2.3.9 ***Flow cytometry***. For detection of unfixed FISH-TAMB labeled cells via flow cytometry, ~10^6 cells were incubated for 15 minutes at 37˚C in 100-μl reaction

mixtures containing 1 μM FISH-TAMBs, 1× DPBS solution. Following incubation, reaction mixtures were diluted in 0.9 ml 1× DPBS solution containing ~10^6 ml^{-1} Fluoresbrite™ plain red 0.5 μm microspheres (Polysciences, Inc., Warrington, PA USA). Flow cytometry was performed on a BD LSRII Multi-Laser Analyzer (BD Biosciences, San Jose, CA USA) at the Princeton University Flow Cytometry Resource Facility. Data were acquired for 120 seconds for each sample at 8 μl min^{-1} average flow rate using four independent laser channels at default wattage settings (355 nm at 30 mW, 405 nm at 50 mW, 488 nm at 20 mW, and 640 nm at 40 mW). Forward and side-scattered light were set to logarithmic scale and used to trigger events. The system was flushed with 10% (v/v) bleach solution for 1 minute before analysis and between samples to minimize the potential for cross-contamination.

Fluorescent microsphere counts were used to calculate the volume of fluids being analyzed to determine cell concentrations. For all samples, events gated as cell-sized objects and FISH-TAMB-labeled cells in 1× DPBS + FISH-TAMB probes + growth medium (see SI Materials & Methods for cell population gating parameters) were subtracted from final counts collected for each cell type. Statistical analysis of observed differences in FISH-TAMB labeling between samples and their respective controls was performed using a Student t-test (StatPlus:mac LE software, AnalystSoft, Inc., Walnut, CA USA).

2.4 RESULTS AND DISCUSSION

2.4.1 ***FISH-TAMB response to metabolic activity of methanogens***. Coupling FISH-TAMB with spinning disk confocal microscopy, we observed significant variability

in FISH-TAMB fluorescence level at different growth stages and after O_2 exposure (Figure 2.2). During exponential growth of *M. barkeri*, all observable cells detected from F420 autofluorescence were also co-labeled with the FISH-TAMB Cy5 fluorophore (Figure 2.2A), demonstrating successful delivery of MBs across archaeal cell walls and membranes as was observed for bacterial cell wall and membranes. (Figure 2.2A). By comparison, only ~20% of enumerable *M. barkeri* in stationary phase were also FISH-TAMB labeled, and on average appeared to show lower Cy5 fluorescence intensity relative to exponential phase cells (Figure 2.2B). Following overnight exposure to atmospheric O_2, fewer than 1% of observed cells showed FISH-TAMB-associated fluorescence (Figure 2.2C). Both the decrease in the number of labeled cells and observed drops in Cy5 fluorescence intensity are consistent with anticipated diminished methanogenesis rates typical of stationary phase (Hutten et al., 1980) or prolonged O_2 exposure (Fetzer et al., 1993). This suggests that FISH-TAMB counts and fluorescence intensity are affected by transcription rates, although further experiments will be necessary to test this hypothesis and quantify such relationships.

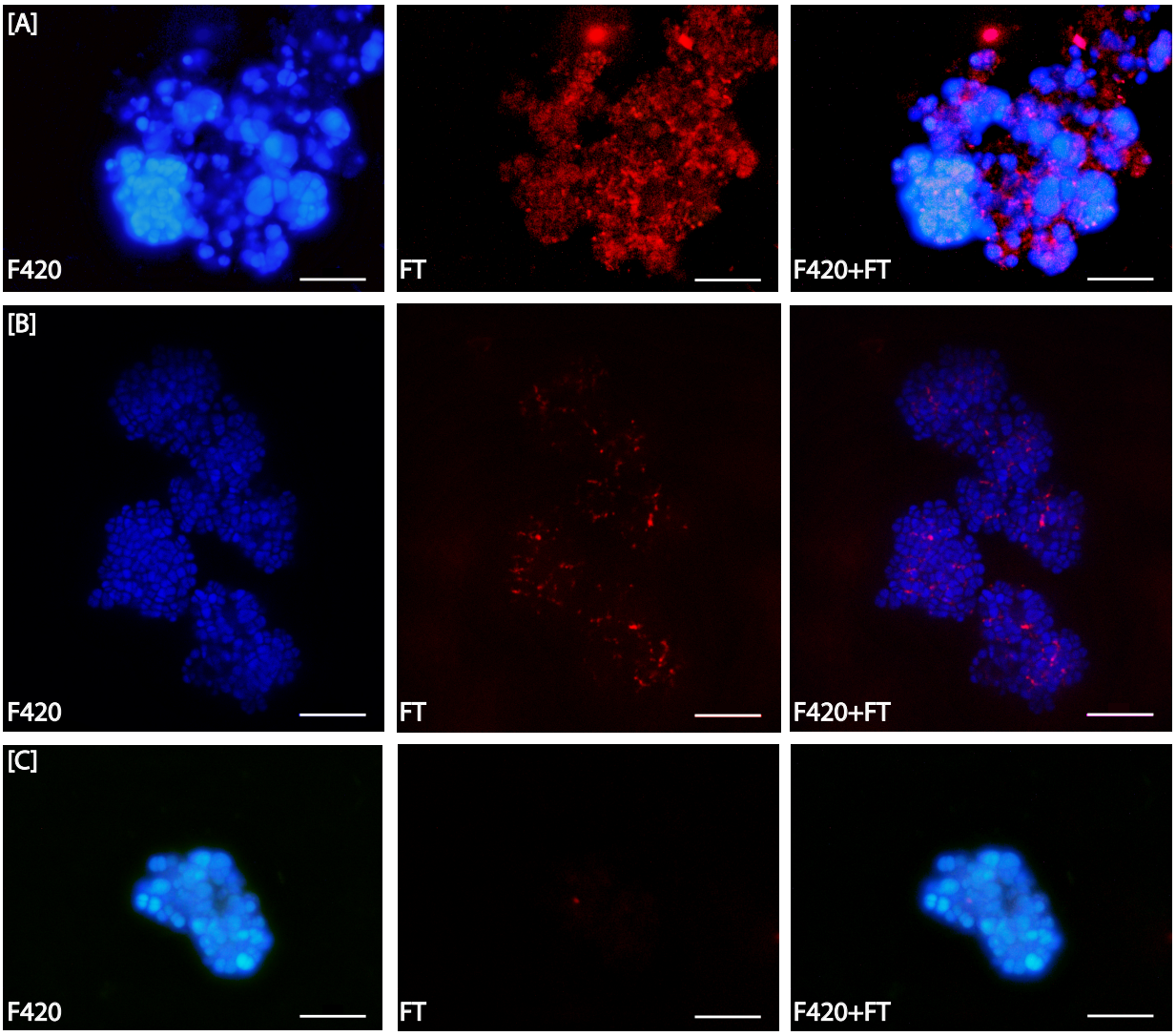

Figure 2.2. FISH-TAMB sensitivity to *mcr*A transcription in *Methanosarcina barkeri* during exponential phase **(A)**, stationary phase **(B)** and following overnight exposure to air **(C)**. F420: F420 autofluorescence (excitation 405 nm, emission 461 nm). FT: Cy5 fluorescence from FISH-TAMB labeling (excitation 647 nm, emission 670 nm). F420+FT: Composite image of F420 and FT micrographs. Scale bar 10 µm.

2.4.2 *FISH-TAMB identification of active ANMEs within microbial consortia*.

To establish the efficacy of FISH-TAMB as a method for tracking transcriptional activity of uncultivated lineages, we coupled it to 16S rRNA FISH and confocal microscopy to identify ANME-2 *Archaea* actively performing anaerobic oxidation of methane (AOM)

in microcosm incubations of a fracture water sample from a 1.34 km deep borehole in South Africa (BE326 BH2-Conc). Following a pre-incubation period of 50 days with $^{13}CH_4$ and SO_4^{2-}, microcosm aliquots were first treated with FISH-TAMB probes targeting *mcr*A mRNA to target cells actively oxidizing CH_4. The same samples were subsequently fixed with EtOH:PBS, labeled with 16S rRNA FISH probes targeting ANME-2, and counter-stained with DAPI. Under these conditions, we observed ANME-2-labeled cells were also co-labeled by FISH-TAMB. ANME-2 cells were situated in consortia with DAPI-only labeled cells (Figure 2.3), which were likely sulfate-reducing bacteria (SRB) living in metabolic syntrophy (Lau et al., 2016; Magnabosco et al., 2018).

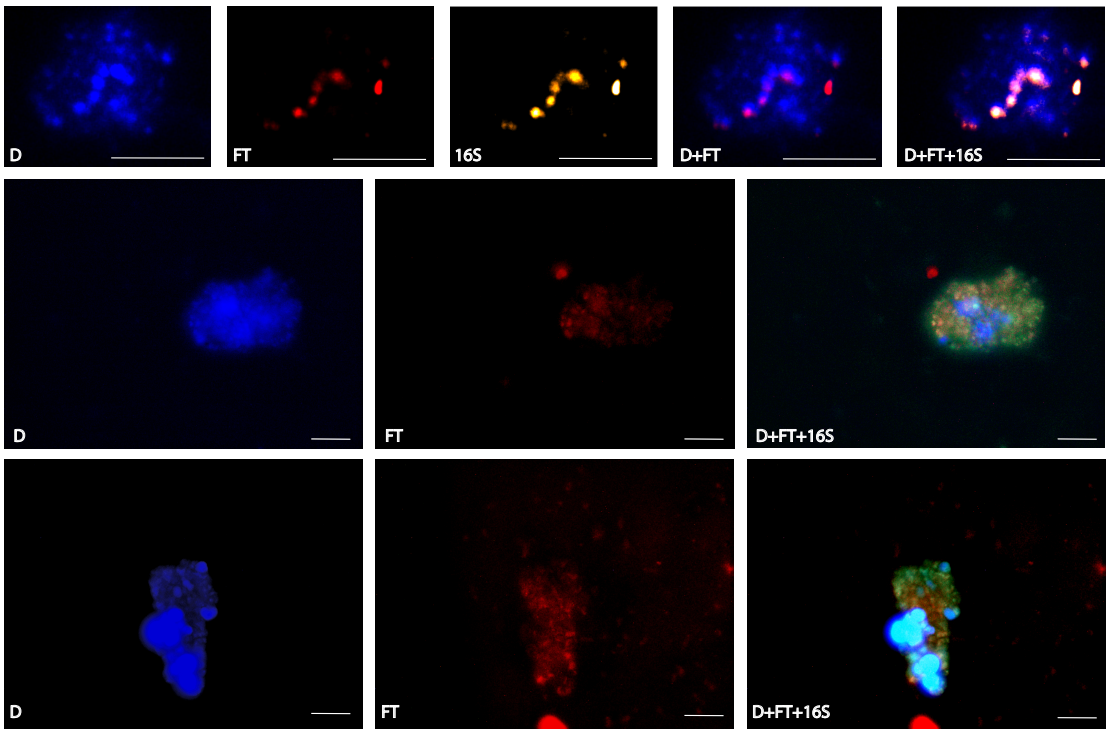

Figure 2.3. Co-labeling of active ANME-2 cells in microbial consortia by FISH-TAMB and 16S rRNA FISH. D: DAPI (excitation 405 nm, emission 461 nm). FT: Cy5 fluorescence from FISH-TAMB labeling (excitation 647 nm, emission 670 nm). 16S: Atto 565 fluorescence from 16S rRNA FISH labeling (excitation 561 nm, emission 590 nm). D+FT+16S: Composite of D, FT, and 16S micrographs. Scale bar 10 µm.

Using Kaiju for taxonomic classification, we confirmed the presence of two ANME-2d OTUs in the associated metagenome, collectively comprising 1% relative abundance amongst the *Archaea* and 0.03% abundance relative to the entire microbial community. Similarly, although we did not target ANME-2 SRB partners in our 16S rRNA FISH survey, we did identify sequences allied to the *Desulfosarcina/Desulfococcus* and *Desulfobulbus* clades (0.08% and 0.05% relative abundance, respectively). We also identified significant enrichment of *Desulfotomaculum* (1% relative abundance), which have been identified in ANME-2 anaerobic sludge enrichments (Li et al., 2019). Collectively, these results support the application of FISH-TAMB to identify low abundance microbial dark matter based on its transcriptional activity. Indeed, FISH-TAMB, when coupled to 16S rRNA FISH, demonstrated the first microscopic evidence of AOM microbial consortia from the continental deep biosphere.

2.4.3 *Temporal monitoring of FISH-TAMB labeled cells from BE326 BH2-Conc*

. Using spinning disk photomicroscopy, we monitored intensity and duration of Cy5 fluorescence in unfixed FISH-TAMB labeled cells from BE326 BH2-Conc. Various cell morphologies were observed over a 14-hour monitoring period, including single planktonic cells (Figure 2S.3A), paired cells (Figure 2S.3B-C), and cell aggregates (Figure 2S.3D). Fluorescence intensity of all cell morphologies was significantly reduced within 2 hours of hybridization. Interestingly, however, single planktonic cells maintained discernable fluorescence much longer than labeled cells in aggregates with extracellular polymeric substances (EPS) – up to 6 hours post-FISH-TAMB treatment (Figure 2S.3A). This observable difference is likely correlated to the phenomenon that

microorganisms living in aggregates exhibit markedly different patterns of gene expression compared to free-living cells (even those of the same species), focusing significant transcriptional effort in the repair and maintenance of the EPS matrix (Rumbo-Feal et al., 2013; Nakamura et al., 2016; Berlanga and Guerrero, 2016; Guilhen et al., 2016). We speculate that the gradual decrease in Cy5 fluorescence intensity observed in microbial aggregates reflects a regulatory switch typical of biofilm "group behavior" under stress (Kostakioti et al., 2013), though metatranscriptomics would be necessary to confirm this hypothesis.

Notably, at the beginning of the imaging experiment, we captured a duplet of cells in which one cell of the pair was brightly labeled and the other appeared unlabeled (Figure 2.4). Within 20 minutes, we were able to detect an increase in Cy5 fluorescence in the initially unlabeled cell (Figure 2.4B). Over the course of the next two hours it became unambiguously brighter and distinct from its fluorescent partner. Interestingly, the appearance of a labeled cell 20 minutes into observation coincides with the *mcr*A mRNA half-life of ~25 ± 8 minutes reported in *Methanosarcina acetivorans* (Peterson et al., 2016), suggesting labeling of an *mcr*A mRNA which was transcribed after the FISH-TAMB incubation took place. It is unlikely that focus drift artificially generated the fluorescence signal by bringing an out-of-focus cell into view because brightfield images taken simultaneously at each time point show the second cell in focus for the duration of the imaging experiment (Figure 2.4A), confirming the 300 nm positional accuracy of the stage (Stehbens et al., 2012). We therefore conclude that we likely captured *in vivo* FISH-TAMB hybridization to target transcripts.

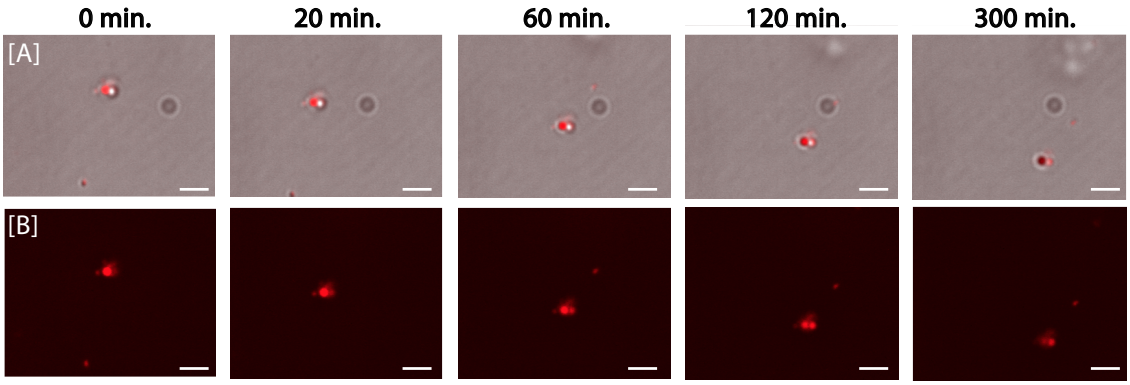

Figure 2.4. *In situ* monitoring of mRNA captures apparent real-time labeling by FISH-TAMB. BE326 BH2-PC enrichments were incubated anaerobically with 1 µM FISH-TAMBs targeting *mcr*A mRNA and subsequently imaged via spinning disk photomicroscopy. **(A)** Composite brightfield and Cy5 channel shows a cell duplet in focus over the duration of imaging. **(B)** Cy5 channel distinguishes a gradual increase in fluorescence intensity of an initially unlabeled cell ~20 minutes into imaging. Samples were analyzed at 100× magnification under a 100% CO_2 atmosphere and imaged every minute for 14 hours (647/670 nm excitation/emission). Micrographs show first 5 hours of imaging. Scale bar 5 µm.

2.4.4 *Target specificity in E. coli expression clones as a proxy for inter-domain horizontal gene transfer*

E. coli JM109 competent cells were transformed with pGEM®-T Easy Vectors with intact beta-galactosidase-encoding insertion sites (*E. coli* lacZα$^+$). To assess partial non-specific hybridization of *lac*Zα-targeting FISH-TAMBs, a second expression clone line was generated by ligating *mcr*A genes PCR-amplified directly from *M. barkeri* (*E. coli* mcrA$^+$). *E. coli* mcrA$^+$ was used to test FISH-TAMB's ability to permeate bacterial membranes and also functioned as a proxy for the hypothetical scenario of bacterial cells obtaining *mcr*A via horizontal gene transfer from archaea in the environment.

Responsiveness of FISH-TAMB to transcriptional activity was assessed by comparing *E. coli* mcrA$^+$ cultures whose mRNA expression was turned on and off when respectively grown in the presence or absence of *lac* operon inducer isopropyl β-D-1-

thiogalactopyranoside (IPTG). For IPTG-induced *E. coli* mcrA$^+$ populations, flow cytometry data showed 91.73 ± 6.03% of observed cells were labeled by FISH-TAMB (Figure 2.5D). By comparison, only 0.03 ± 0.06% of uninduced *E. coli* mcrA$^+$ cells were labeled by FISH-TAMB (Figure 2.5B), which was not statistically different from the FISH-TAMB-treated control containing untransformed *E. coli* JM109 (Student t-test, $t = 1.6$, $p = 0.25$). The addition of IPTG had no significant effect on Cy5 fluorescence in control incubations that were not treated with FISH-TAMB (Figure 2.5A, C). IPTG-induced *E. coli* mcrA$^+$ yielded insignificant labeling (0.05% ± 0.03%) when treated with FISH-TAMB targeting the *lacZα* insertion site (Figure 2.5E) (Student t-test, $t = 2.5$, $p = 0.24$). These results indicate that FISH-TAMB detects transcription of targeted cells in exponential phase.

The *E. coli* results also demonstrate that 1) R9 cell-penetrating peptides are as successful delivering MBs across Gram-negative bacteria cell walls and membranes, and 2) FISH-TAMB effectively detects transcription of artificially horizontally transferred genes. Provided that the FISH-TAMB targeting site is preserved after horizontal gene transfer events, it is reasonable to anticipate that FISH-TAMB would enable the detection of lateral gene transfer that happened across cells of different cell wall and membrane composition.

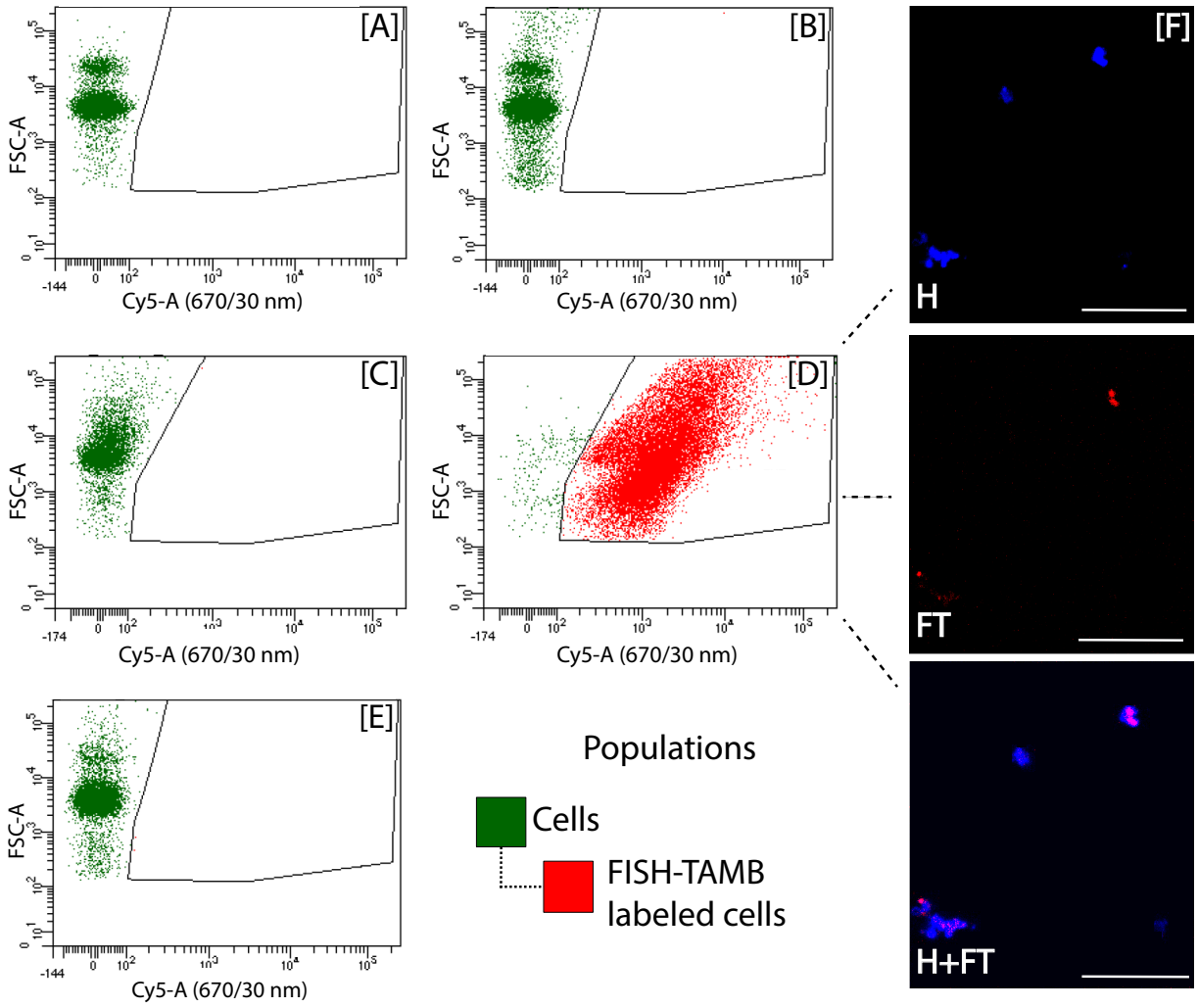

Figure 2.5. Flow cytometry data of FISH-TAMB targeting messenger RNA in *E. coli* grown in the presence (induced) or absence (uninduced) of IPTG - Isopropyl β-D-1-thiogalactopyranoside – which triggers the transcription of the lac operon containing this gene. FISH-TAMB targeting *mcr*A in induced *E. coli* mcrA$^+$ is indicated by the population gated in red. Cy5 was excited at 640 nm and emitted fluorescence collected via 670/30 nm bandpass filter. **(A)** Uninduced *E. coli mcr*A$^+$ control (no FISH-TAMB treatment). **(B)** FISH-TAMB targeting *mcr*A mRNA + Uninduced *E. coli* mcrA$^+$. **(C)** IPTG-induced *E. coli* mcrA$^+$ control (no FISH-TAMB treatment). **(D)** FISH-TAMB targeting *mcr*A mRNA+ IPTG-induced *E. coli* mcrA$^+$. **(E)** FISH-TAMB targeting *lac*Zα mRNA + IPTG-induced *E. coli* mcrA$^+$. **(F)** Fluorescence microscopy of IPTG-induced *E. coli* mcrA$^+$ treated with FISH-TAMB targeting *mcr*A mRNA. H: Hoechst-33342 (excitation 405 nm, emission 461 nm), FT: Cy5 fluorescence from FISH-TAMB labeling (excitation 640 nm, emission 670 nm). H+FT: composite of H and FT micrographs. Scale bar 10 µm.

2.5.5 ***Sustained growth of FISH-TAMB-treated cultures***. To illustrate if FISH-TAMB treated cells remained culturable, we monitored the growth of *E. coli* mcrA$^+$, *E.*

coli lacZα^+, and *M. barkeri* incubated with and without FISH-TAMBs. Results showed that the applied FISH-TAMB dosage (on average 6×10^{-6} pmol per cell) had no inhibitory effect on the growth rate of these pure cultures (Figure 2S.6). Both FISH-TAMB-treated and untreated *E. coli* exhibited similar growth rates: $\mu_{control}$ of *E. coli* mcrA$^+$ = 1.04 ± 0.16 h^{-1}, $\mu_{FISH\text{-}TAMB}$ = 0.83 ± 0.06 h^{-1}, whereas *E. coli* lacZα^+ grew at $\mu_{control}$ = 1.12 ± 0.25 h^{-1}, $\mu_{FISH\text{-}TAMB}$ = 1.00 ± 0.32 h^{-1}. (Figure 2S.6) Doubling times for both control and FISH-TAMB-treated *M. barkeri* were ~ 21 hours ($\mu_{control}$ = 0.03 ± 0.01 h^{-1} and $\mu_{FISH\text{-}TAMB}$ = 0.03 ± 0.01 h^{-1} (Figure 2S.6B), which are consistent with previous reports of hydrogenotrophic *M. barkeri* growth rates (Maestrojuan and Boone, 1991). Further investigations should be conducted to determine whether other microbial species have different tolerances to the per-cell concentration of FISH-TAMBs, i.e. different "optimal dosages" of FISH-TAMB.

2.5 CONCLUSIONS

2.5.1 ***Implications of FISH-TAMB for microbial ecology***. Cellular fixation with paraformaldehyde and/or ethanol is a traditional step in the FISH protocol that stabilizes cell integrity for efficient membrane permeabilization, but at the expense of DNA-protein crosslinking and potential downstream sequencing bias (Amann et al., 1995; Yilmaz et al., 2010). By targeting unfixed cells, FISH-TAMB can identify cells without nucleic acid modification. Coupled with established FISH techniques, we have demonstrated that FISH-TAMB can identify transcriptionally active cells from mixed microbial communities, including low abundance and slow growing populations, based on the expression of a targeted functional gene. The identification of *mcr*A transcription in

ANMEs within larger microbial consortia offers opportunities to further investigate *in situ* syntrophic interactions between target cells and their physically associated partners. ANME/SRB aggregates are taxonomically well described, but the mechanisms by which they exchange electrons remain under debate (Hoehler et al., 1994; Valentine and Reeburgh, 2000; Sørensen et al., 2001; Moran et al., 2008; Milucka et al., 2012; McGlynn et al., 2015). By coupling FISH-TAMB to 16S rRNA FISH we have successfully and sensitively visualized intracellular mRNA amongst significantly more abundant rRNA, using advanced fluorescence microscopy techniques that are precise enough to capture FISH-TAMB hybridization in real time. Future applications in tandem with nanoscale secondary ion mass spectroscopy (nanoSIMS) and electron microscopy may further resolve the nature of direct electron transfer between ANMEs and their syntrophic partners.

Continued development of FISH-TAMB is necessary to understand the limits of its application in other systems (e.g. temperature, salinity, and pH extremes; sensitivity to spore forming, gram-positive *Bacteria*; double-membraned *Archaea* (Rachel et al., 2002; Näther and Rachel, 2004; Comolli et al., 2009; Perras et al., 2014; Probst et al., 2014); the detection limit for transcript copy numbers, etc.). We note that careful probe design is required upstream to ensure the ability of the MB structure to retain a quenched fluorophore in the absence of target mRNA. With these considerations in mind, FISH-TAMB sequences can be sufficiently sensitive to identify varying degrees of transcriptional activity in target cells, including active players belonging to the low abundance ranks of the rare biosphere. As it does not discriminate based upon 16S rRNA phylogeny, FISH-TAMB is capable of identifying mRNA from functional genes which

may have been gained through lateral gene transfer. FISH-TAMB is a promising tool for characterizing the ecophysiologies of MDM, as well as the metabolic links between physically associated taxa. We envision future applications of FISH-TAMB that can be coupled with FACS, allowing for cost-efficient deep sequencing surveys of target populations, with resulting metagenomes informing efforts to improve isolation of uncultivated lineages.

2.6 DATA AVAILABILITY

Raw sequencing data from the BE326 BH2-Conc AOM enrichment metagenome have been deposited at NCBI Genbank under accession number PRJNA562560 (Sequence Read Archive accession number SRR100029121). Raw flow cytometry data and microscopy images are available upon request.

2.7 ACKNOWLEDGEMENTS

This chapter is largely based on Harris et al. (2017). I am indebted to Sibanye Gold, Ltd. and the staff at the Beatrix Gold Mine for their hospitality and granting us continued access to the BE326 BH2 borehole. I would like to thank Mike Pullin, Gilbert Tetteh, Sarah Hendrickson and Olukayode Kuloyo for their field assistance. Thank you to Peter Jaffe, Melany Ruiz Uriguen, Reika Yokochi, and Roland Purtschert for access to equipment for field work performed at BE326 BH2. Special thanks are extended to Rick Colwell, Hillary Morrison, and the Marine Biological Laboratory for supporting sequencing efforts through the Deep Carbon Observatory's Census of Deep Life. I would like to thank Gary Laevsky of the Princeton Confocal Imaging Core Facility and Ewa

Zarnowska and Tiang Liao of Bruker Florescence Microscopy for aiding us in cell imaging. Tina DeCoste of the Princeton Flow Cytometry Core Facility was also an integral player in helping us optimize the protocol. I would also like to personally thank the Bartlett lab at the Scripps Institution of Oceanography for hosting my research that contributed to this project, which was supported through the Deep Carbon Observatory Deep Life Cultivation Internship (Alfred P. Sloan Foundation). Finally, thank you to Prabhpreet Gill and the Princeton University Office of Technology Licensing for aiding us in filling a provisional patent application on the FISH-TAMB methodology.

This project was supported by funding from National Science Foundation grants DGE-1148900, DEB-1441717, EAR-1528492, DEB-1442059, and DEB-1441646. I was also supported by the Geosciences Graduate Student Research Fund (Princeton University). Metagenomic sequencing was supported by Phase 14 of the Census of Deep Life (Deep Carbon Observatory, Alfred P. Sloan Foundation) through the Marine Biological Laboratory in Woods Hole, MA. Pioneer work was supported by junior project funding from the Department of Geosciences, Princeton University to Anjali Taneja (’15).

2.8 SUPPLEMENTARY INFORMATION

2.8.1 SI MATERIALS AND METHODS

2.8.1.1 *Detailed sampling and geochemical characterization of BE326 BH2*.

Fracture fluid was collected 1.34 km below land surface within the Beatrix Gold Mine in South Africa’s Witwatersrand Basin. Gas, water, and biomass samples were collected from the exploratory borehole BE326 BH2 that was drilled in 2007. An autoclaved

stainless-steel manifold fitted with high-pressure ball valves was attached to the sealed borehole casing and purged with fracture water for 10 minutes prior to sample collection to flush out any contaminant ambient mine air. Autoclaved teflon tubing was retrofitted to the manifold's and flushed for a subsequent 10 minutes at a flow rate of ~800 ml min^{-1} for biomass collection into combusted, evacuated, and N_2-sparged 180 ml borosilicate serum vials sealed and crimped with butyl rubber stoppers. Temperature, pH, electrical conductivity, and total dissolved solids (TDS) were made using handheld probes (Hanna Instruments, Woonsocket, RI USA). Measurements for dissolved H_2S, H_2O_2, Fe^{2+}, and total Fe were made in the field using CHEMets® Visual Kits (CHEMetrics, Inc., Midland, VA USA). Anion measurements were made using a Dionex IC25 ion chromatograph coupled to an MSQ-quadruple mass spectrometer (Thermo Scientific, Waltham, MA USA).

"Little Eddie", the portable, 8.2 kg, fourth generation model of the high-volume gas extraction system EDGAR (Extraction of Dissolved Gases for Analysis of Radiokrypton), was connected to the manifold for gas sampling (Probst et al., 2006; Yokochi, 2016). Dissolved gases were collected into air-tight canvas bags on site and transferred into pre-evacuated, 160-ml borosilicate vials (Ward et al., 2004) upon return to the surface using a 50-ml gas-tight syringe (Trajan Scientific, Ringwood, Victoria, Australia). Gas vials were stored at 5˚C prior to measurement using gas chromatographers installed with a flame-ionizing detector (FID) (for CH_4 and CO_2) and a thermal conductivity detector (TCD) (for O_2, H_2, He, and N_2) (Peak Performer 1 series, Peak Laboratories, Mountain View, CA USA). Dissolved gas concentrations were calculated using the ratio of the gas flow rate to the water flow rate. We confirm that

anaerobic conditions were maintained during the sample collection process based on the dissolved gas composition (Table 2S.1).

2.8.1.2 ***BE326 BH2-Conc fracture fluid enrichments and*** **M. barkeri**. DSMZ medium 120a was prepared in an anaerobic glove bag (Coy Laboratory Products, Grass Lake, MI USA) containing a 95:5 N_2:H_2 atmosphere. The following were added to one liter of degassed distilled H_2O: 2 mM K_2HPO_4, 1.7 mM KH_2PO_4, 9.3 mM NH_4Cl, 2 mM $MgSO_4 \cdot 7H_2O$, 1.7 mM $CaCl_2 \cdot 2H_2O$, 2.25 g 4.3 mM NaCl, 2.00 ml of $FeSO_4 \cdot 7H_2O$ (0.1% w/v in 0.1 N H_2SO_4), 2.00 g yeast extract, 2.00 g casitone, 2.5 mM $NaHCO_3$, 1.3 mM $Na_2S \cdot 9H_2O$, 1.7 mM L-cys $HCl \cdot H_2O$, 1.0 ml of trace element solution SL-10 (per liter of distilled H_2O: 10.0 ml HCl [25%, 7.7 M], 1.50 g $FeCl_2 \cdot 4H_2O$, 70 mg $ZnCl_2$, 100 mg $MnCL_2 \cdot 4H_2O$, 6 mg H_3BO_3, 190 mg $CoCl_2 \cdot 6H_2O$, 2 mg $CuCl_2 \cdot 2H_2O$, 24 mg $NiCl_2 \cdot 6H_2O$, 36 mg $Na_2MoO_4 \cdot 6H_2O$), and 0.3 ml Na-resazurin solution (0.1% w/v). The medium was dispersed as 9-ml aliquots into 25-ml Balch tubes and sealed with 0.1 N NaOH-boiled butyl rubber stoppers and aluminum crimps. Balch tubes were sparged for 20 minutes at 30 psi with 100% ultra-high purity Ar gas (Airgas, Inc., Radnor, PA USA) and subsequently autoclaved. MD-VS™ vitamin solution (ATCC®, Manassas, VA USA), 100 µl of 1% (v/v), was added to each vial after autoclaving, and the headspace was replaced and over-pressurized to 1.5 x atmospheric pressure (atm) with 80:20 H_2:CO_2 gas (Airgas, Inc., Radnor, PA USA) by flushing for 15 minutes at 30 psi.

Freeze-dried *M. barkeri* cells (ATCC® 43569™) were revitalized by inoculation into 9 ml of DSMZ medium 120a (pH 7.2). The cultivations were maintained

anaerobically in 160-ml borosilicate serum vials at 37˚C. H_2 was the sole added electron donor.

For enrichment of sulfate-dependent anaerobic methanotrophy (S-AOM), 10 ml BE326 BH2-Conc fracture fluid was added to 90 ml modified artificial seawater medium in 160-ml borosilicate serum vials(Widdel and Bak, 1992; Holler et al., 2011). Per 1 liter of distilled, degassed H_2O was 376 mM NaCl, 49 mM 26 mM $MgCl_2$, 10 mM Na_2SO_4, 8.5 mM KCl, 2.5 mM $NaHCO_3$, 1.3 mM $Na_2S•9H_2O$, 1.7 mM L-cys $HCl•H_2O$, 1 ml of SL-10 trace metal solution (described above), 10 ml of MD-VS™ vitamin solution, 0.3 ml (0.1% w/v) Na-resazurin solution, final pH 8.2. Media sterilization, addition of vitamins, and anaerobic sparging followed the protocol described above for DSMZ 120a medium, with the exception that serum vial headspaces comprised 2% $^{13}CH_4$ (Isotec® Stable Isotopes, MilliporeSigma, St. Louis, MO USA) in a balance of ultra-high purity N_2 gas (Airgas, Inc., Radnor, PA USA).

2.8.1.3 E. coli *mcrA*$^+$ *expression clone transformation*. An *mcr*A insert was isolated and purified from *M. barkeri*. Triplicate 1-ml aliquots of *M. barkeri* (OD_{550} ~10^9 cells ml^{-1}) were centrifuged at 11,000 x g for 2 minutes. The supernatant was removed down to 10 µl and the cell pellet was stored at -80˚C prior to PCR amplification. Triplicate PCR amplifications were performed in 50-µl reaction volumes containing the thawed pellet, 1X PCR buffer, 200 µM dNTPs, 1% Tween-20, 1.5 U Taq DNA Polymerase (Takara Bio USA, Mountain View, CA USA), 0.2 mM Mlas forward primer (5'-GGTGGTGTMGGDTTCACMCARTA-3') (Luton et al., 2002; Steinberg and Regan, 2008), and 0.2 mM mcrA-rev reverse primer (5'-

CGTTCATBGCGTAGTTVGGRTAGT-3') (Steinberg and Regan, 2008). The amplification thermal program was performed on a C1000 Touch™ Thermal Cycler (Bio-Rad Laboratories, Inc., Hercules, CA USA) and consisted of a 5 minute initial denaturation step at 94˚C and 35 cycles of the following: 1 minute denaturation at 94˚C, 1 minute annealing at 55˚C, and 1 minute extension at 72˚C. Final extension lasted for 10 minutes at 72˚C. Positive amplification was confirmed by gel electrophoresis and PCR products were purified by ethanol precipitation. Two volumes of pre-chilled absolute ethanol were added to each PCR reaction tube and mixed by inversion. Reaction tubes were incubated at -20˚C for 30 minutes and subsequently centrifuged at 11,000 x g for 30 minutes. The supernatant was discarded, and the pellet was washed with 500 µl 75% ethanol prior to centrifugation at 11,000 x g for 5 minutes. The ethanol wash step was repeated once, the supernatant was discarded, and the pellet was resuspended in 1X TE buffer. Purified PCR products with 3'-A overhangs generated by Takara Taq DNA polymerase were ligated to pGEM®-T Easy vectors by incubating overnight at 4˚C and subsequently transformed into JM109 High Efficiency Competent *E. coli* cells according to the manufacturer's instructions (Promega Corporation, Madison, WI USA). Following transformation, *E. coli* were incubated for 1.5 hours at 37˚C in an orbital shaker at 150 rpm in a suspension of Luria broth containing 0.05 mg ml^{-1} ampicillin (LB/A). *E. coli* (~3.4 x 10^8 cells ml^{-1} by OD_{600} measurement) were serially diluted to ~10^2 cells ml^{-1} and plated on an LB cloning plate with 0.05 mg ml^{-1} ampicillin, 0.05 mg ml^{-1} IPTG, and 0.08 mg ml^{-1} X-gal (LB/AIX) for blue/white screening and incubated overnight at 37˚C. White colonies, presumably containing *mcr*A PCR products, were picked from the plate and

inoculated into LB/A medium. Sanger sequencing of the plasmid confirmed orientation of the *mcr*A insert.

2.8.1.4 E. coli *pmoA*$^+$ *expression clone transformation*. Total DNA was extracted from BE326 BH2 fracture fluid collected in 2011 using 2x CTAB lysis buffer and phenol/chloroform according to the procedure previously described(Lau et al., 2014). *pmo*A genes were PCR-amplified from total DNA using 0.4 mM each of A189m (5'-GGNGAYTGGGACTTYTGG-3') and A682m_a (5'-GAAYSCNGARAAGAACGM(C/A)-3')-modified primers (Holmes et al., 1995; Luesken et al., 2011). PCR amplification was confirmed by gel electrophoresis and PCR products were purified by ethanol precipitation before ligation with pGEM®-T Vectors. *E. coli* pmoA$^+$ were isolated as white colonies from LB/AIX cloning plates and inoculated in LB/A medium according to the procedure described above.

2.8.1.5 *FISH-TAMB formation optimization*. Aliquots of FISH-TAMB complexes of varying molar ratios (0:1, 5:1, 10:1, 15:1, 20:1, 25:1, 30:1) were mixed with 1× DNA loading dye (Thermo Fisher Scientific, Waltham, MA USA) and ran on a 1% (w/v) agarose gel containing ethidium bromide in 1× TAE buffer solution (40 mM Tris, pH 7.6; 20 mM acetic acid, 1 mM EDTA) for 30 minutes at 100 V. A 100 bp ladder (New England BioLabs®, Ipswich, MA USA) was used as a size-marker.

2.8.1.6 In vitro *MB:target oligonucleotide hybridization assays*. Triplicate 100-µl reaction mixtures containing either 0.4 µM MB or 1 µM FISH-TAMBs in 1x DPBS

were incubated at 37˚C for 10 minutes with 0.4 µM of oligonucleotide sequences complementary to MBs. Background signal (due to unbound MB probes) and potential non-specific hybridization fluorescence were respectively assessed by incubating MB and FISH-TAMBs in the absence of any target (blank) and an oligonucleotide sequence specific to particulate methane monooxygenase beta subunit (*pmo*A) (5'-GAAYSCNGARAAGAACGM-3') (Luesken et al., 2011). Fluorescence images were taken every 5 minutes for 100 minutes using a Typhoon 9410 Variable Mode Imager® (Molecular Dynamics, GE Healthcare, Little Chalfront, UK) (excitation 633 nm, detection bandwidth 655 - 685 nm, exposure time 5 min.).

Fluorescence intensity was measured as a function of temperature and salt concentration to determine stability profiles of the MB probe sequence in the presence and absence of MB targets (bound MB vs. unbound MB states). Three 50-µl reaction volumes were prepared for the unbound MB controls, comprising 16 nM MBs and Takara PCR buffer containing 1.5 mM $MgCl_2$ (1×), 7.5 mM $MgCl_2$ (5×), or 15 mM $MgCl_2$ (10×). Three bound MB reactions were set up using the same recipes except with the addition of 32 nM target oligo sequences. Reaction mixtures were incubated at 37˚C for 1 hour on a real-time qPCR 7900HT system (Applied Biosystems, Inc., Carlsbad, CA USA). Melting curve analysis was done for temperatures ranging from 25˚C to 95˚C with fluorescence signals measured every 0.2˚C. Optimal detection temperature for positive MB-target hybridization was determined as the temperature with the highest signal-to-background noise ratio, as indicated by the relative fluorescence intensities of bound MB and unbound MB, respectively.

2.8.1.7 ***Population gating parameters in flow cytometry***. Cell population gates were constrained using control samples comprising non-FISH-TAMB-treated cells in 1× DPBS. To correct for sources of background fluorescence three additional controls were prepared: 1) FISH-TAMB + LB medium in 1× DPBS, 2) FISH-TAMB + DSMZ medium 120a in 1× DPBS, and 3) FISH-TAMB only in 1× DPBS. Three replicates were prepared for each treatment and incubated at 37˚C for 15 minutes. Cell-sized objects were gated with respect to the side-scattered light area (SSC-A) and fluorescence signals of 0.5 µm microspheres along the 575/26 nm (PE) filter (320 V). This gate was sufficient to identify *E. coli* based on known autofluorescence properties (Benson et al., 1979; Renggli et al., 2013). *M. barkeri* and BE326 BH2-Conc cells were identified as sub-populations from the cell-sized objects gate on a 450/50 nm (F420) filter (321 V) that measures autofluorescence of the F420 enzyme (420 nm emission) (Doddema and Vogels, 1978; Dolfing and Mulder, 1985; Hendrickson and Leigh, 2008). FISH-TAMB-labeled cells were identified as appropriately autofluorescent cell-sized objects that also demonstrated at least a 10% increase in fluorescence on a 700/25 nm (Cy5) filter relative to the non-FISH-TAMB-treated cell populations. Gating was performed using BD FACSDiva V8.0.1 software (BD Biosciences, San Jose, CA USA).

2.8.2 SI RESULTS AND DISCUSSION

2.8.2.1 ***Conformational stability and target specificity of mcrA-targeting MBs***. Melting curve analysis was performed between 25˚C – 95˚C under three buffer conditions containing 1.5 mM, 7.5 mM, and 15 mM $MgCl_2$ to assess the stability and fluorescence intensity of MB in the presence and absence of target *mcr*A oligonucleotide

sequences (i.e. bound vs. unbound MB states). Results revealed maximum fluorescence of *mcr*A-bound MB at 25˚C under all investigated saline buffer solutions. (Table 2S.2, Figure 2S.1). This temperature corresponded with the highest signal-to-background noise ratio (195:1 relative to unbound MB in 1× PCR buffer containing 1.5 mM $MgCl_2$). Bound MB fluorescence intensity remained > 17× greater than unbound MB up to 64˚C before dropping down to 2× greater emission for higher temperatures up to 95˚C (Figure 2S.1). MB conformation remained intact at all assessed salinities, but signal-to-background noise improved with increased salt concentration between 55˚ - 65˚C (Table 2S.2). Thus, for this *mcr*A target sequence, FISH-TAMB demonstrates a large operational temperature range of 25˚C - 65˚C but may be limited from *in situ* studies of thermophilic methanogens and ANMEs.

In vitro and *in vivo* hybridization assays were performed to assess (i) hybridization of MB and FISH-TAMBs to target *mcr*A oligonucleotide sequences, (ii) whether resulting fluorescence from probe-target hybridization was differentiable from background fluorescence of unbound and potentially non-specifically bound MB probes, and (iii) optimal incubation time for detection of positive hybridization fluorescence. Gel imaging revealed that background autofluorescence of unbound MB significantly diminished when MB was non-covalently bound to R9, showing a minimum 20:1 R9:MB molar ratio for complete complexation of all free-floating MB in solution (Figure 2S.1). Thus, this molar ratio was selected for the formation of FISH-TAMBs utilized in subsequent experiments. It is possible that R9 may be playing a role in stabilizing the MB hairpin conformation, thus improving the quencher's absorption of background fluorophore emission. However, this stabilization appeared to be inhibitory to MB-target

hybridization when FISH-TAMBs were incubated with *mcr*A oligonucleotide sequences *in vitro* (Figure 2S.3E). Because positive fluorescence signals were detected when FISH-TAMBs encountered intracellular *mcr*A mRNA *in vivo* in *M. barkeri*, BE326 BH2-Conc, and *E. coli* mcrA$^+$ (Figure 2S.3F-H), we hypothesize that intracellular scavenging may physically dissociate R9 from MB allowing subsequent MB-target hybridization. While the exact mechanism remains unknown, the MB probes released from R9 appear to retain hairpin conformation following cellular penetration, as evidenced by minimal fluorescence in negative control *E. coli* pmoA$^+$ cells incubated with FISH-TAMBs (Figure 2S.3I).

2.8.3 SUPPLEMENTARY TABLES

Table 2S.1: Geochemical data for BE326 BH2 fracture fluid collected 24 June 2016. "< d.l.", below detection limit.

Temperature (˚C)	31.8
pH	8.2
pe	-3.8
TDS (ppt)	4.3
Conductivity (mS cm^{-1})	8.7
H_2S (ppm)	<0.1
H_2O_2 (ppm)	<0.1
Fe^{2+} (ppm)	0.1
Total Fe (ppm)	0.2
PO_4^{3-} (ppm)	<0.1
$HCOO^-$ (ppm)	< d.l.
CH_3COOH (ppm)	< d.l.
NO_2^- (ppm)	0.52 ± 0.05
NO_3^- (ppm)	0.01
SO_4^{2-} (ppt)	7.43 ± 0.19
Br^- (ppm)	9.14 ± 0.22
O_2	0.2%
N_2	5.0%
H_2	0.1%
CH_4	90.3%
CO_2	4.4%
He	0.02%
water:gas flow rate ratio	320:1

Table 2S.2. FISH-TAMB and 16S rRNA FISH probe sequences used in this study.

Probe Name	5' reporter/3' quencher/reporter	Sequence (5' – 3')	Reference
Eury_mcrA-rev_FISH-TAMB	Cy5/BHQ3	CCT GGC GTT CAT BGC GTA GTT VGG RTA GTC CAG G	(Steinberg and Regan, 2008)
pGEM-T-Easy_lacZα-rev_FISH-TAMB	Cy5/BHQ3	CCT GGC ACT AGT GAT ATC GAA TTC CCG CGC CAG G	this study
ANME-2_EelMS_932-16S-rRNA-FISH	Atto 565/Atto 565	AGC TCC ACC CGT TGT AGT	(Boetius et al., 2000; Orphan, 2001; Hatzenpichler et al., 2016)

Table 2S.3. Fluorescence of bound and unbound *mcr*A-targeting MB as a function of salinity and temperature.

Temp	Buffer Solution	Bound MB Relative Fluorescence	Unbound MB Relative Fluorescence*	Signal to Background (S:B) ratio
25˚C	1x PCR buffer containing 1.5 mM $MgCl_2$	3.9 x 10^3	0.2 x 10^2	195:1
	5x PCR buffer containing 7.5 mM $MgCl_2$	3.1 x 10^3	0.2 x 10^2	155:1
	10x PCR buffer containing 15 mM $MgCl_2$	2.5 x 10^3	0.2 x 10^2	125:1
35˚C	1x PCR buffer containing 1.5 mM $MgCl_2$	3.2 x 10^3	0.2 x 10^2	160:1
	5x PCR buffer containing 7.5 mM $MgCl_2$	2.7 x 10^3	0.2 x 10^2	135:1
	10x PCR buffer containing 15 mM $MgCl_2$	2.2 x 10^3	0.2 x 10^2	110:1
45˚C	1x PCR buffer containing 1.5 mM $MgCl_2$	2.5 x 10^3	0.2 x 10^2	125:1
	5x PCR buffer containing 7.5 mM $MgCl_2$	2.2 x 10^3	0.2 x 10^2	110:1
	10x PCR buffer containing 15 mM $MgCl_2$	1.8 x 10^3	0.2 x 10^2	90:1
55˚C	1x PCR buffer containing 1.5 mM $MgCl_2$	1.7 x 10^3	1.0 x 10^2	17:1
	5x PCR buffer containing 7.5 mM $MgCl_2$	1.6 x 10^3	0.2 x 10^2	80:1
	10x PCR buffer containing 15 mM $MgCl_2$	1.4 x 10^3	0.3 x 10^2	47:1

65˚C	1x PCR buffer containing 1.5 mM $MgCl_2$	6.0×10^2	2.0×10^2	3:1
	5x PCR buffer containing 7.5 mM $MgCl_2$	8.0×10^2	0.6×10^2	16:1
	10x PCR buffer containing 15 mM $MgCl_2$	8.0×10^2	0.6×10^2	13:1
75˚C	1x PCR buffer containing 1.5 mM $MgCl_2$	5.0×10^2	2.0×10^2	3:1
	5x PCR buffer containing 7.5 mM $MgCl_2$	3.0×10^2	1.0×10^2	3:1
	10x PCR buffer containing 15 mM $MgCl_2$	2.0×10^2	1.0×10^2	2:1
85˚C	1x PCR buffer containing 1.5 mM $MgCl_2$	4.0×10^2	1.7×10^2	2:1
	5x PCR buffer containing 7.5 mM $MgCl_2$	3.0×10^2	1.0×10^2	3:1
	10x PCR buffer containing 15 mM $MgCl_2$	2.2×10^2	1.0×10^2	2:1
95˚C	1x PCR buffer containing 1.5 mM $MgCl_2$	3.9×10^2	1.3×10^2	3:1
	5x PCR buffer containing 7.5 mM $MgCl_2$	2.1×10^2	0.7×10^2	3:1
	10x PCR buffer containing 15 mM $MgCl_2$	1.7×10^2	0.8×10^2	2:1

* Unbound MB fluorescence, due to absence of *mcr*A targets, is treated as background noise.

2.8.4 SUPPLEMENTARY FIGURES

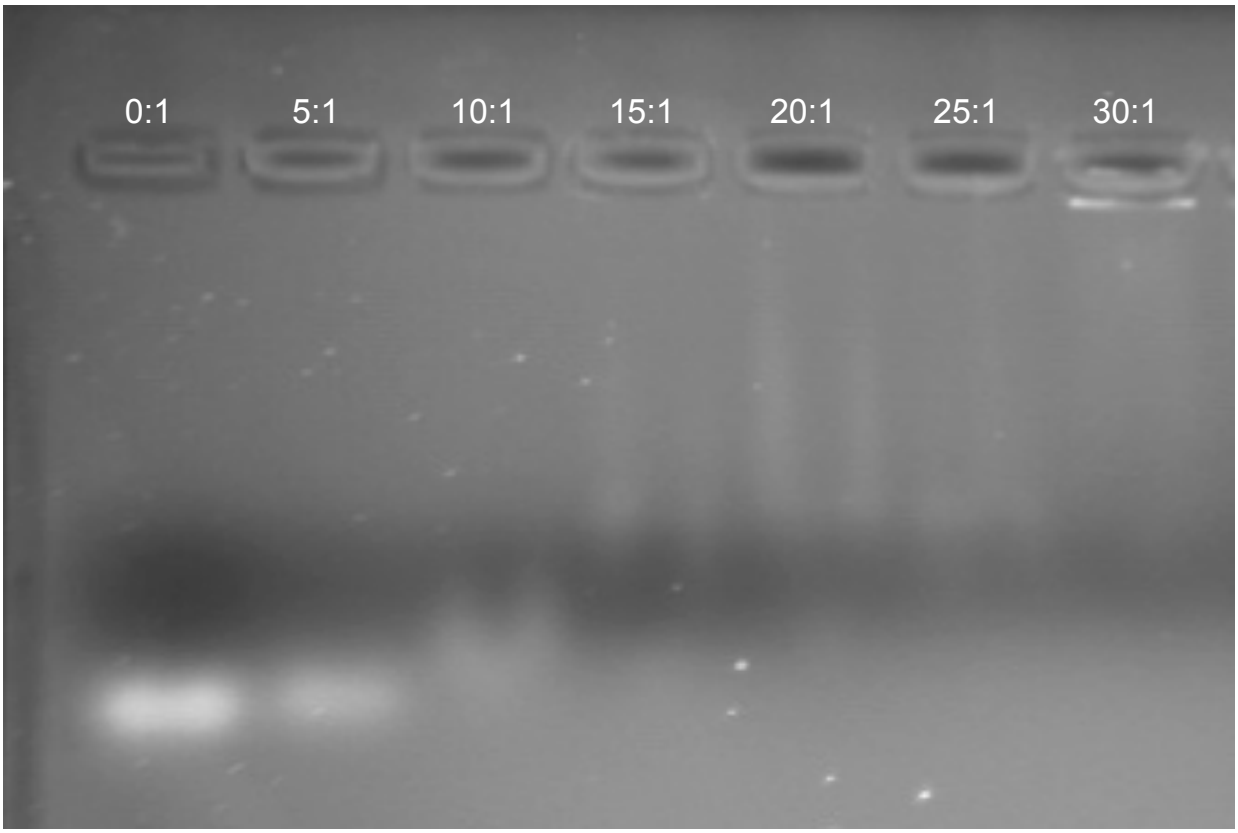

Figure 2S.1. Complexation between R9 cell-penetrating peptide and *mcr*A MB sequences in fixed R9:MB molar ratios. Unbound MB shows up as white bands in the gel and complete complexation of all MB to R9 is evidenced by the lack of a physical band. Optimal R9:MB ratio was determined to be 20:1.

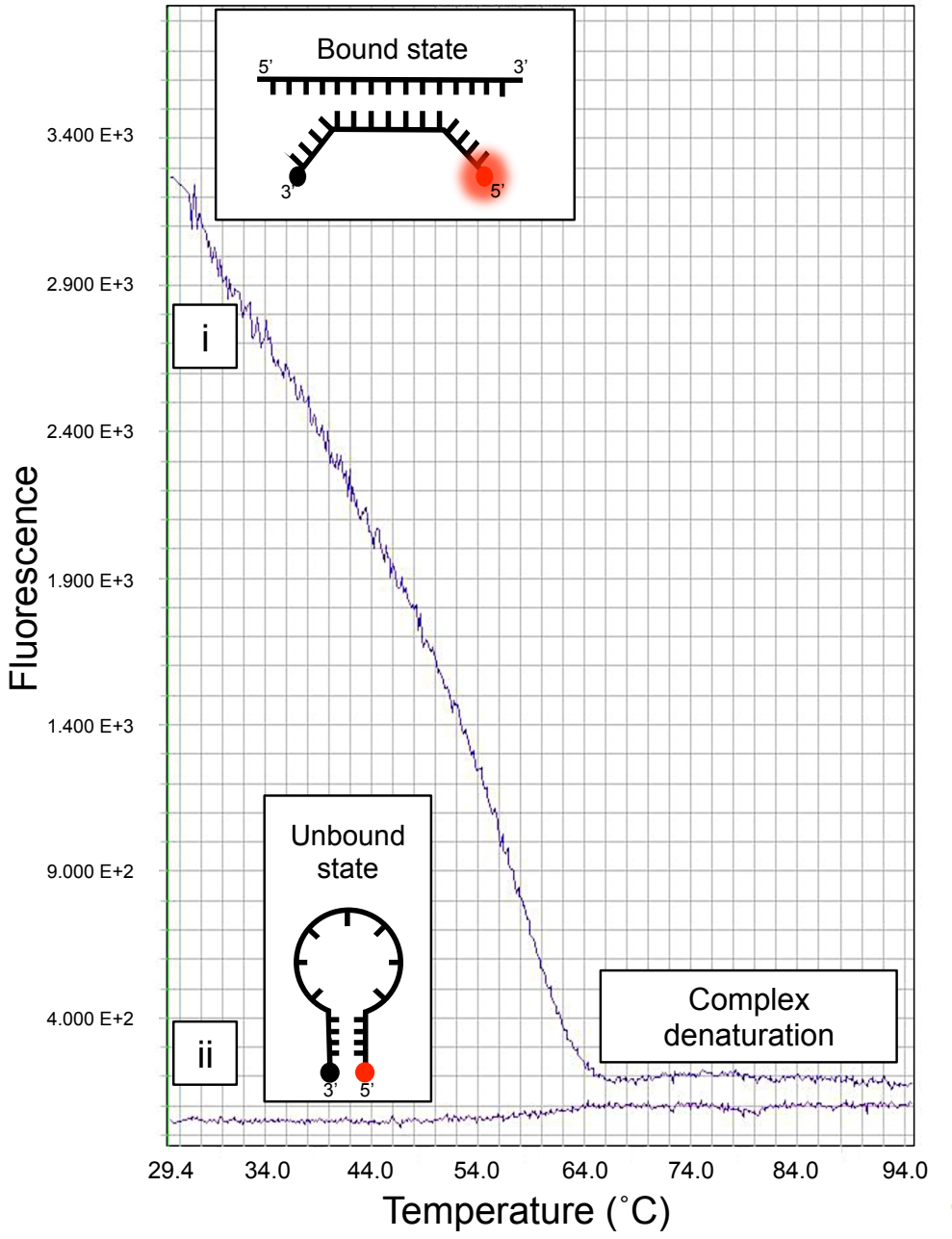

Figure 2S.2. Heat stability of *mcr*A MB sequence. *In vitro* melting curve analysis of *mcr*A-targeting MB in 5X PCR buffer containing 7.5 mM $MgCl_2$. (i) *mcr*A MB hybridized to target oligonucleotide sequence. (ii) Unbound *mcr*A MB.

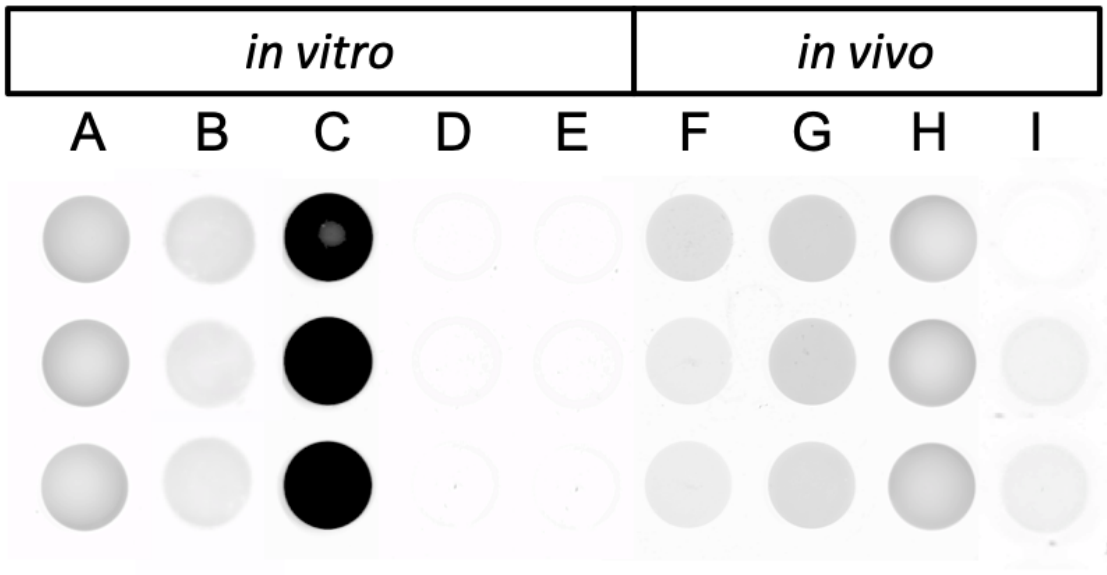

Figure 2S.3. MB and FISH-TAMB target specificity *in vitro* and *in vivo.* **(A)** 0.4 µM MB in 1x PBS. **(B)** 0.4 µM MB + *pmoA* target oligo. **(C)** 0.4 µM MB + *mcrA* target oligo. **(D)** 1 µM FISH-TAMB in 1x PBS. **(E)** 1 µM FISH-TAMB + *mcrA* target oligo. **(F)** 1 µM FISH-TAMB + *M. barkeri*. **(G)** 1 µM FISH-TAMB + BE326 BH2-Conc. **(H)** 1 µM FISH-TAMB + *E. coli* mcrA^{+}. **(I)** 1 µM FISH-TAMB + *E. coli* pmoA^{+}. Images taken after 20 minutes incubation with a Typhoon 9410 Variable Mode Imager®. Excitation 633 nm. Emission 675/10 nm. Exposure time 5 minutes per image.

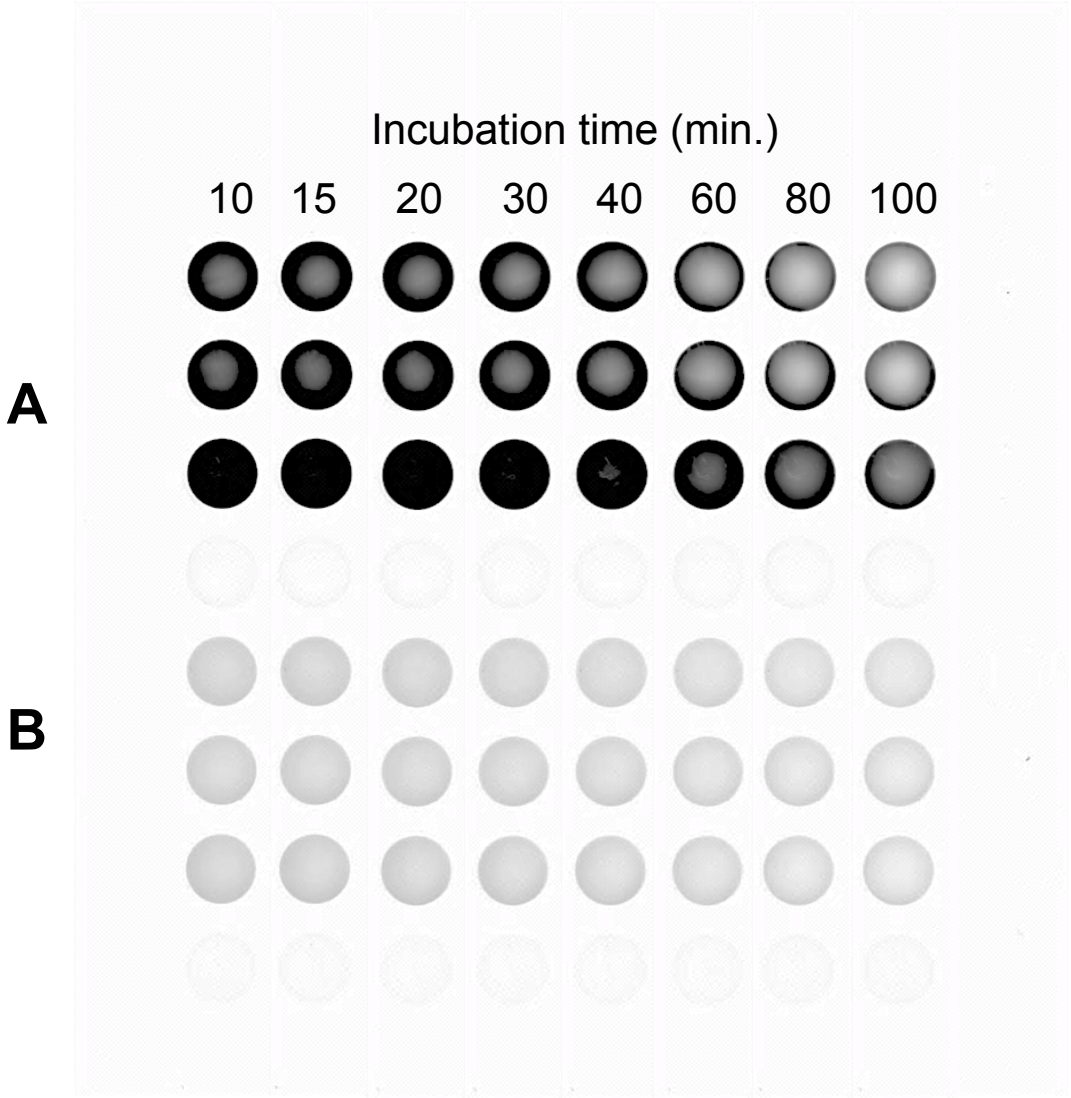

Figure 2S.4. Unbound MB fluorescence lifetime. An *in vitro* hybridization time series experiment monitored Cy5 fluorescence in **(A)** bound (0.4 µM MB + 0.4 µM *mcr*A target oligo) and **(B)** unbound MB (0.4 µM MB in 1x PBS). Images taken with a Typhoon 9410 Variable Mode Imager®. Excitation 633 nm. Emission 675/10 nm. Exposure time 5 minutes per image.

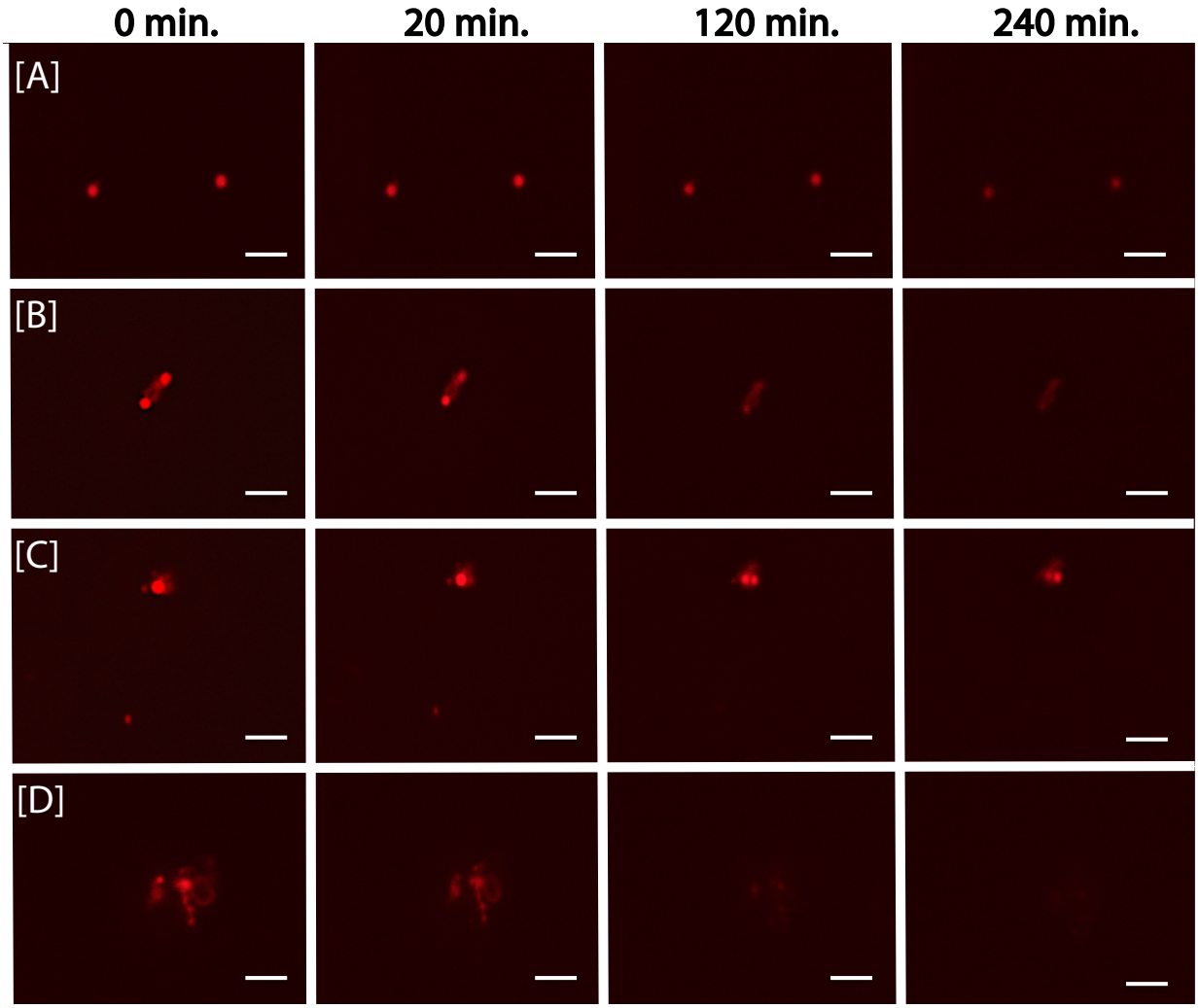

Figure 2S.5. Fluorescence lifetime of Cy5 in FISH-TAMB-hybridized cells. BE326 BH2-Conc methanogenic enrichments were incubated anaerobically with 1 µM FISH-TAMB and subsequently imaged via spinning disk photomicroscopy. Samples were excited with a 647 nm laser line and analyzed at 670 nm under a 100% CO_2 atmosphere. Micrographs were snapped every minute for 14 hours. Micrographs here represent the first four hours of observation. **(A)** Single cells. **(B)** Physically associated cells. **(C)** Cell pair in which an unlabeled cell becomes labeled between 20 and 120 minutes. **(D)** Cell aggregate. Scale bar 5 µm.

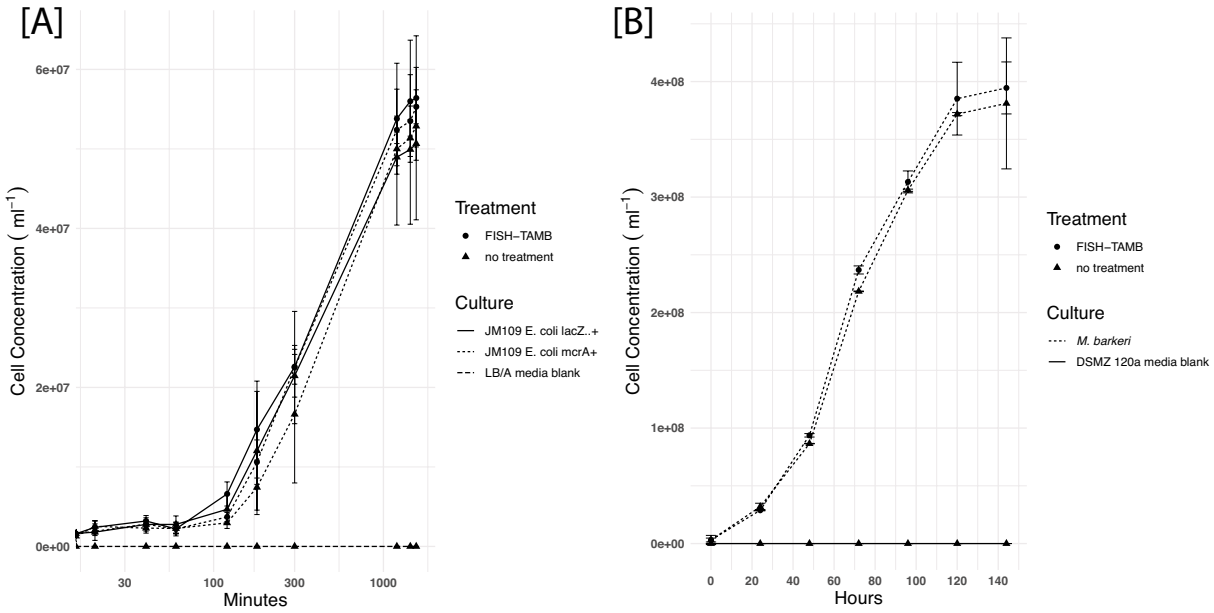

Figure 2S.6. FISH-TAMB viability assessment by growth curve analysis. Pure cultures of *E. coli* mcrA^{+} and *E. coli* lacZα^{+} **(A)** and *M. barkeri* **(B)** (~10^{6} cells ml^{-1}) were incubated with 1 μM FISH-TAMBs and inoculated into their respective growth media. Growth was measured spectrophotometrically (OD_{600} for *E. coli*, OD_{550} for *M. barkeri*) and growth rates compared to untreated control cultures.

2.9 REFERENCES

Amann R. I., Krumholz L. and Stahl D. A. (1990) Fluorescent-oligonucleotide probing of whole cells for determinative, phylogenetic, and environmental studies in microbiology. *J. Bacteriol.* **172**, 762–770. Available at: http://jb.asm.org/lookup/doi/10.1128/jb.172.2.762-770.1990.

Amann R. I., Ludwig W. and Schleifer K. H. (1995) Phylogenetic identification and in situ detection of individual microbial cells without cultivation. *Microbiol. Rev.* **59**, 143–69. Available at: http://mmbr.asm.org/content/59/1/143.short%5Cnhttp://www.ncbi.nlm.nih.gov/pubmed/7535888%5Cnhttp://www.pubmedcentral.nih.gov/articlerender.fcgi?artid=PMC239358.

Anderson K. L., Apolinario E. E. and Sowers K. R. (2012) Desiccation as a long-term survival mechanism for the archaeon Methanosarcina barkeri. *Appl. Environ. Microbiol.* **78**, 1473–1479.

Bankevich A., Nurk S., Antipov D., Gurevich A. A., Dvorkin M., Kulikov A. S., Lesin V. M., Nikolenko S. I., Pham S., Prjibelski A. D., Pyshkin A. V., Sirotkin A. V., Vyahhi N., Tesler G., Alekseyev M. A. and Pevzner P. A. (2012) SPAdes: A New Genome Assembly Algorithm and Its Applications to Single-Cell Sequencing. *J. Comput. Biol.* **19**, 455–477. Available at: http://www.liebertpub.com/doi/10.1089/cmb.2012.0021.

Bao G., Rhee W. J. and Tsourkas A. (2009) Fluorescent probes for live-cell RNA detection. *Annu. Rev. Biomed. Eng.* **11**, 25–47.

Benson R. C., Meyer R. a, Zaruba M. E. and McKhann G. M. (1979) Cellular

autofluorescence--is it due to flavins? *J. Histochem. Cytochem.* **27**, 44–48.

Berlanga M. and Guerrero R. (2016) Living together in biofilms: the microbial cell factory and its biotechnological implications. *Microb. Cell Fact.* **15**, 165. Available at: http://microbialcellfactories.biomedcentral.com/articles/10.1186/s12934-016-0569-5.

Boetius A., Ravenschlag K., Schubert C. J., Rickert D., Widdel F., Gieseke A., Amann R., Jørgensen B. B., Witte U. and Pfannkuche O. (2000) A marine microbial consortium apparently mediating anaerobic oxidation of methane. *Nature* **407**, 623–626. Available at: http://www.nature.com/doifinder/10.1038/35036572.

Borrel G., Adam P. S., McKay L. J., Chen L.-X., Sierra-García I. N., Sieber C. M. K., Letourneur Q., Ghozlane A., Andersen G. L., Li W.-J., Hallam S. J., Muyzer G., de Oliveira V. M., Inskeep W. P., Banfield J. F. and Gribaldo S. (2019) Wide diversity of methane and short-chain alkane metabolisms in uncultured archaea. *Nat. Microbiol.* **4**, 603–613. Available at: http://www.nature.com/articles/s41564-019-0363-3.

Boyd J. A., Jungbluth S. P., Leu A. O., Evans P. N., Woodcroft B. J., Chadwick G. L., Orphan V. J., Amend J. P., Rappé M. S. and Tyson G. W. (2019) Divergent methyl-coenzyme M reductase genes in a deep-subseafloor Archaeoglobi. *ISME J.* **13**, 1269–1279. Available at: http://www.nature.com/articles/s41396-018-0343-2.

Bryant M. P. and Boone D. R. (1987) Emended Description of Strain MST(DSM 800T), the Type Strain of Methanosarcina barkeri. *Int. J. Syst. Bacteriol.* **37**, 169–170.

Chen S.-C. C., Musat N., Lechtenfeld O. J., Paschke H., Schmidt M., Said N., Popp D., Calabrese F., Stryhanyuk H., Jaekel U., Zhu Y.-G. G., Joye S. B., Richnow H.-H.

H., Widdel F. and Musat F. (2019) Anaerobic oxidation of ethane by archaea from a marine hydrocarbon seep. *Nature* **568**, 108–111. Available at: http://www.nature.com/articles/s41586-019-1063-0.

Chen S., Zhou Y., Chen Y. and Gu J. (2018) fastp: an ultra-fast all-in-one FASTQ preprocessor. *Bioinformatics* **34**, i884–i890. Available at: https://academic.oup.com/bioinformatics/article/34/17/i884/5093234.

Choi H. M. T., Calvert C. R., Husain N., Huss D., Barsi J. C., Deverman B. E., Hunter R. C., Kato M., Lee S. M., Abelin A. C. T., Rosenthal A. Z., Akbari O. S., Li Y., Hay B. A., Sternberg P. W., Patterson P. H., Davidson E. H., Mazmanian S. K., Prober D. A., van de Rijn M., Leadbetter J. R., Newman D. K., Readhead C., Bronner M. E., Wold B., Lansford R., Sauka-Spengler T., Fraser S. E. and Pierce N. A. (2016) Mapping a multiplexed zoo of mRNA expression. *Development* **143**, 3632–3637. Available at: http://dev.biologists.org/lookup/doi/10.1242/dev.140137.

Comolli L. R., Baker B. J., Downing K. H., Siegerist C. E. and Banfield J. F. (2009) Three-dimensional analysis of the structure and ecology of a novel, ultra-small archaeon. *ISME J.* **3**, 159–167. Available at: http://www.nature.com/articles/ismej200899.

DeLong E., Wickham G. and Pace N. (1989) Phylogenetic stains: ribosomal RNA-based probes for the identification of single cells. *Science* **243**, 1360–1363. Available at: http://www.sciencemag.org/content/243/4896/1360.abstract.

DePas W. H., Starwalt-Lee R., Van Sambeek L., Ravindra Kumar S., Gradinaru V. and Newman D. K. (2016) Exposing the Three-Dimensional Biogeography and Metabolic States of Pathogens in Cystic Fibrosis Sputum via Hydrogel Embedding,

Clearing, and rRNA Labeling. *MBio* **7**. Available at: http://mbio.asm.org/lookup/doi/10.1128/mBio.00796-16.

Doddema H. J. and Vogels G. D. (1978) Improved identification of methanogenic bacteria by fluorescence microscopy. *Appl. Environ. Microbiol.* **36**, 752–4. Available at: http://www.pubmedcentral.nih.gov/articlerender.fcgi?artid=243133&tool=pmcentrez&rendertype=abstract.

Dolfing J. and Mulder J. W. (1985) Comparison of methane production rate and coenzyme f(420) content of methanogenic consortia in anaerobic granular sludge. *Appl. Environ. Microbiol.* **49**, 1142–1145. Available at: http://www.pubmedcentral.nih.gov/articlerender.fcgi?artid=238520&tool=pmcentrez&rendertype=abstract.

Evans P. N., Boyd J. A., Leu A. O., Woodcroft B. J., Parks D. H., Hugenholtz P. and Tyson G. W. (2019) An evolving view of methane metabolism in the Archaea. *Nat. Rev. Microbiol.* **17**, 219–232. Available at: http://www.nature.com/articles/s41579-018-0136-7.

Evans P. N., Parks D. H., Chadwick G. L., Robbins S. J., Orphan V. J., Golding S. D. and Tyson G. W. (2015) Methane metabolism in the archaeal phylum Bathyarchaeota revealed by genome-centric metagenomics. *Science* **350**, 434–8. Available at: http://www.sciencemag.org/content/350/6259/434.short.

Fetzer S., Bak F. and Conrad R. (1993) Sensitivity of methanogenic bacteria from paddy soil to oxygen and desiccation. *FEMS Microbiol. Ecol.* **12**, 107–115. Available at: https://academic.oup.com/femsec/article-lookup/doi/10.1111/j.1574-

6941.1993.tb00022.x.

Fuseler K. (1996) A common pathway of sulfide oxidation by sulfate-reducing bacteria. *FEMS Microbiol. Lett.* **144**, 129–134. Available at: http://doi.wiley.com/10.1016/0378-1097(96)00337-0.

Gifford S. M., Sharma S., Rinta-Kanto J. M. and Moran M. A. (2011) Quantitative analysis of a deeply sequenced marine microbial metatranscriptome. *ISME J.* **5**, 461–472. Available at: http://dx.doi.org/10.1038/ismej.2010.141.

Glöckner F. O., Amann R., Alfreider A., Pernthaler J., Psenner R., Trebesius K. and Schleifer K.-H. (1996) An In Situ Hybridization Protocol for Detection and Identification of Planktonic Bacteria. *Syst. Appl. Microbiol.* **19**, 403–406. Available at: https://linkinghub.elsevier.com/retrieve/pii/S0723202096800695.

Goel G., Kumar A., Puniya A. K., Chen W. and Singh K. (2005) Molecular beacon: a multitask probe. *J. Appl. Microbiol.* **99**, 435–442. Available at: http://doi.wiley.com/10.1111/j.1365-2672.2005.02663.x.

Guilhen C., Charbonnel N., Parisot N., Gueguen N., Iltis A., Forestier C. and Balestrino D. (2016) Transcriptional profiling of Klebsiella pneumoniae defines signatures for planktonic, sessile and biofilm-dispersed cells. *BMC Genomics* **17**, 237. Available at: http://www.biomedcentral.com/1471-2164/17/237.

Hallam S. J., Girguis P. R., Preston C. M., Richardson P. M. and DeLong E. F. (2003) Identification of methyl coenzyme M reductase A (mcrA) genes associated with methane-oxidizing archaea. *Appl. Environ. Microbiol.* **69**, 5483–5491.

Harris R. L., Lau M. C. Y., Cadar A., Bartlett D. H., Cason E., van Heerden E. and Onstott T. C. (2018) Draft Genome Sequence of " Candidatus Bathyarchaeota"

Archaeon BE326-BA-RLH, an Uncultured Denitrifier and Putative Anaerobic Methanotroph from South Africa's Deep Continental Biosphere ed. J. C. Dunning Hotopp. *Microbiol. Resour. Announc.* **7**, e01295-18. Available at: http://mra.asm.org/content/7/20/e01295-18.abstract.

Harris R., Lau M. C. Y., van Heerden E., Cason E., Vermeulen J.-G., Taneja A., Kieft T. L., DeCoste C., Laevsky G. and Onstott T. C. (2017) Labeling of prokaryotic mRNA in live cells using fluorescent in situ hybridization of transcript-annealing molecular beacons (FISH-TAMB). *bioRxiv*. Available at: http://biorxiv.org/content/early/2017/08/19/178368.abstract.

Hatzenpichler R., Connon S. A., Goudeau D., Malmstrom R. R., Woyke T. and Orphan V. J. (2016) Visualizing in situ translational activity for identifying and sorting slow-growing archaeal−bacterial consortia. *Proc. Natl. Acad. Sci.* **113**, E4069–E4078. Available at: http://www.pnas.org/lookup/doi/10.1073/pnas.1603757113.

He L., Zhang C. L., Dong H., Fang B. and Wang G. (2012) Distribution of glycerol dialkyl glycerol tetraethers in Tibetan hot springs. *Geosci. Front.* **3**, 289–300.

He S., Kunin V., Haynes M., Martin H. G., Ivanova N., Rohwer F., Hugenholtz P. and McMahon K. D. (2010) Metatranscriptomic array analysis of 'Candidatus Accumulibacter phosphatis'-enriched enhanced biological phosphorus removal sludge. *Environ. Microbiol.* **12**, 1205–1217. Available at: http://doi.wiley.com/10.1111/j.1462-2920.2010.02163.x.

Hendrickson E. L. and Leigh J. A. (2008) Roles of coenzyme F420-reducing hydrogenases and hydrogen- and F420-dependent methylenetetrahydromethanopterin dehydrogenases in reduction of F420 and

production of hydrogen during methanogenesis. *J. Bacteriol.* **190**, 4818–4821.

Hinrichs K. U., Hayes J. M., Sylva S. P., Brewer P. G., DeLong E. F., Brewert P. G. and DeLong E. F. (1999) Methane-consuming archaebacteria in marine sediments. *Nature* **398**, 802–805.

Hoehler T. M., Alperin M. J., Albert D. B. and Martens S. C. (1994) Field and laboratory studies of methane oxidation in an anoxic sediment: evidence for a methanogen-sulfate-reducer consortium. *Glob. Biogeochem Cycles* **8**, 451–464.

Holler T., Widdel F., Knittel K., Amann R., Kellermann M. Y., Hinrichs K.-U., Teske A., Boetius A. and Wegener G. (2011) Thermophilic anaerobic oxidation of methane by marine microbial consortia. *ISME J.* **5**, 1946–1956. Available at: http://www.nature.com/doifinder/10.1038/ismej.2011.77.

Hollibaugh J. T., Gifford S., Sharma S., Bano N. and Moran M. A. (2011) Metatranscriptomic analysis of ammonia-oxidizing organisms in an estuarine bacterioplankton assemblage. *ISME J.* **5**, 866–878. Available at: http://www.nature.com/articles/ismej2010172.

Holmes A. J., Costello A., Lidstrom M. E. and Murrell J. C. (1995) Evidence that participate methane monooxygenase and ammonia monooxygenase may be evolutionarily related. *FEMS Microbiol. Lett.* **132**, 203–208.

Hutten T. J., Bongaerts H. C. M., van der Drift C. and Vogels G. D. (1980) Acetate, methanol and carbon dioxide as substrates for growth of Methanosarcina barkeri. *Antonie Van Leeuwenhoek* **46**, 601–610. Available at: http://link.springer.com/10.1007/BF00394016.

Hyatt D., Chen G.-L., LoCascio P. F., Land M. L., Larimer F. W. and Hauser L. J. (2010)

Prodigal: prokaryotic gene recognition and translation initiation site identification. *BMC Bioinformatics* **11**, 119. Available at: https://bmcbioinformatics.biomedcentral.com/articles/10.1186/1471-2105-11-119.

Jen C. J., Chou C. H., Hsu P. C., Yu S. J., Chen W. E., Lay J. J., Huang C. C. and Wen F. S. (2007) Flow-FISH analysis and isolation of clostridial strains in an anaerobic semi-solid bio-hydrogen producing system by hydrogenase gene target. *Appl. Microbiol. Biotechnol.* **74**, 1126–1134.

Kalyuzhnaya M. G., Zabinsky R., Bowerman S., Baker D. R., Lidstrom M. E. and Chistoserdova L. (2006) Fluorescence in situ hybridization-flow cytometry-cell sorting-based method for separation and enrichment of type I and type II methanotroph populations. *Appl. Environ. Microbiol.* **72**, 4293–4301.

Kostakioti M., Hadjifrangiskou M. and Hultgren S. J. (2013) Bacterial Biofilms: Development, Dispersal, and Therapeutic Strategies in the Dawn of the Postantibiotic Era. *Cold Spring Harb. Perspect. Med.* **3**, a010306–a010306. Available at: http://perspectivesinmedicine.cshlp.org/lookup/doi/10.1101/cshperspect.a010306.

Larsson H. M., Lee S. T., Roccio M., Velluto D., Lutolf M. P., Frey P. and Hubbell J. A. (2012) Sorting Live Stem Cells Based on Sox2 mRNA Expression ed. J. Najbauer. *PLoS One* **7**, e49874. Available at: https://dx.plos.org/10.1371/journal.pone.0049874.

Laso-Pérez R., Wegener G., Knittel K., Widdel F., Harding K. J., Krukenberg V., Meier D. V., Richter M., Tegetmeyer H. E., Riedel D., Richnow H.-H., Adrian L., Reemtsma T., Lechtenfeld O. J. and Musat F. (2016) Thermophilic archaea activate

butane via alkyl-coenzyme M formation. *Nature* **539**, 396–401. Available at: http://www.nature.com/articles/nature20152.

Lau M. C. Y., Cameron C., Magnabosco C., Brown C. T., Schilkey F., Grim S., Hendrickson S., Pullin M., Sherwood Lollar B., van Heerden E., Kieft T. L. and Onstott T. C. (2014) Phylogeny and phylogeography of functional genes shared among seven terrestrial subsurface metagenomes reveal N-cycling and microbial evolutionary relationships. *Front. Microbiol.* **5**, 531. Available at: http://journal.frontiersin.org/article/10.3389/fmicb.2014.00531/abstract.

Lau M. C. Y., Harris R. L., Oh Y., Yi M. J., Behmard A. and Onstott T. C. (2018) Taxonomic and Functional Compositions Impacted by the Quality of Metatranscriptomic Assemblies. *Front. Microbiol.* **9**, 3389–1235. Available at: https://www.frontiersin.org/article/10.3389/fmicb.2018.01235/full.

Lau M. C. Y., Kieft T. L., Kuloyo O., Linage-Alvarez B., van Heerden E., Lindsay M. R., Magnabosco C., Wang W., Wiggins J. B., Guo L., Perlman D. H., Kyin S., Shwe H. H., Harris R. L., Oh Y., Yi M. J., Purtschert R., Slater G. F., Ono S., Wei S., Li L., Sherwood Lollar B. and Onstott T. C. (2016) An oligotrophic deep-subsurface community dependent on syntrophy is dominated by sulfur-driven autotrophic denitrifiers. *Proc. Natl. Acad. Sci.* **113**, E7927–E7936. Available at: http://www.pnas.org/lookup/doi/10.1073/pnas.1612244113.

Lazar C. S., Baker B. J., Seitz K. W. and Teske A. P. (2017) Genomic reconstruction of multiple lineages of uncultured benthic archaea suggests distinct biogeochemical roles and ecological niches. *ISME J.* **11**, 1118–1129. Available at: http://dx.doi.org/10.1038/ismej.2016.189.

Li L., Xue S. and Xi J. (2019) Anaerobic oxidation of methane coupled to sulfate reduction: Consortium characteristics and application in co-removal of H2S and methane. *J. Environ. Sci.* **76**, 238–248. Available at: https://linkinghub.elsevier.com/retrieve/pii/S1001074218308611.

Liu B. R., Huang Y.-W. and Lee H.-J. (2013a) Mechanistic studies of intracellular delivery of proteins by cell-penetrating peptides in cyanobacteria. *BMC Microbiol.* **13**, 57. Available at: http://www.pubmedcentral.nih.gov/articlerender.fcgi?artid=3637573&tool=pmcentrez&rendertype=abstract.

Liu B. R., Liou J.-S., Huang Y.-W., Aronstam R. S. and Lee H.-J. (2013b) Intracellular Delivery of Nanoparticles and DNAs by IR9 Cell-penetrating Peptides ed. J. Najbauer. *PLoS One* **8**, e64205. Available at: https://dx.plos.org/10.1371/journal.pone.0064205.

Lueders T., Chin K. J., Conrad R. and Friedrich M. (2001) Molecular analyses of methyl-coenzyme M reductase α-subunit (mcrA) genes in rice field soil and enrichment cultures reveal the methanogenic phenotype of a novel archaeal lineage. *Environ. Microbiol.* **3**, 194–204.

Luesken F. A., Zhu B., van Alen T. A., Butler M. K., Diaz M. R., Song B., Op den Camp H. J. M., Jetten M. S. M. and Ettwig K. F. (2011) pmoA primers for detection of anaerobic methanotrophs. *Appl. Environ. Microbiol.* **77**, 3877–3880.

Luton P. E., Wayne J. M., Sharp R. J. and Riley P. W. (2002) The mcrA gene as an alternative to 16S rRNA in the phylogenetic analysis of methanogen populations in landfill. *Microbiology* **148**, 3521–3530.

Maestrojuan G. M. and Boone D. R. (1991) Characterization of Methanosarcina barkeri MST and 227, Methanosarcina mazei S-6T, and Methanosarcina vacuolata Z-761T. *Int. J. Syst. Bacteriol.* **41**, 267–274.

Magnabosco C., Tekere M., Lau M. C. Y., Linage B., Kuloyo O., Erasmus M., Cason E., van Heerden E., Borgonie G., Kieft T. L., Olivier J. and Onstott T. C. (2014) Comparisons of the composition and biogeographic distribution of the bacterial communities occupying South African thermal springs with those inhabiting deep subsurface fracture water. *Front. Microbiol.* **5**, 679. Available at: http://journal.frontiersin.org/article/10.3389/fmicb.2014.00679/abstract.

Magnabosco C., Timmers P. H. A., Lau M. C. Y., Borgonie G., Linage-Alvarez B., Kuloyo O., Alleva R., Kieft T. L., Slater G. F., van Heerden E., Sherwood Lollar B. and Onstott T. C. (2018) Fluctuations in populations of subsurface methane oxidizers in coordination with changes in electron acceptor availability. *FEMS Microbiol. Ecol.* **94**, fiy089. Available at: https://academic.oup.com/femsec/article/doi/10.1093/femsec/fiy089/4995908.

McGlynn S. E., Chadwick G. L., Kempes C. P. and Orphan V. J. (2015) Single cell activity reveals direct electron transfer in methanotrophic consortia. *Nature* **526**, 531–535. Available at: http://dx.doi.org/10.1038/nature15512.

McKay L. J., Dlakić M., Fields M. W., Delmont T. O., Eren A. M., Jay Z. J., Klingelsmith K. B., Rusch D. B. and Inskeep W. P. (2019) Co-occurring genomic capacity for anaerobic methane and dissimilatory sulfur metabolisms discovered in the Korarchaeota. *Nat. Microbiol.* **4**, 614–622. Available at: http://www.nature.com/articles/s41564-019-0362-4.

Menzel P., Ng K. L. and Krogh A. (2016) Fast and sensitive taxonomic classification for metagenomics with Kaiju. *Nat. Commun.* **7**, 11257. Available at: http://www.nature.com/articles/ncomms11257.

Milucka J., Ferdelman T. G., Polerecky L., Franzke D., Wegener G., Schmid M., Lieberwirth I., Wagner M., Widdel F. and Kuypers M. M. M. (2012) Zero-valent sulphur is a key intermediate in marine methane oxidation. *Nature* **491**, 541–546.

Möller C. and van Heerden E. (2006) Isolation of a soluble and membrane-associated Fe(III) reductase from the thermophile, Thermus scotoductus (SA-01). *FEMS Microbiol. Lett.* **265**, 237–243. Available at: https://academic.oup.com/femsle/article-lookup/doi/10.1111/j.1574-6968.2006.00499.x.

Moran J. J., Beal E. J., Vrentas J. M., Orphan V. J., Freeman K. H. and House C. H. (2008) Methyl sulfides as intermediates in the anaerobic oxidation of methane. *Environ. Microbiol.* **10**, 162–173.

Mota C. R., So M. J. and de los Reyes F. L. (2012) Identification of Nitrite-Reducing Bacteria Using Sequential mRNA Fluorescence In Situ Hybridization and Fluorescence-Assisted Cell Sorting. *Microb. Ecol.* **64**, 256–267.

Nakamura Y., Yamamoto Nao, Kino Y., Yamamoto Nozomi, Kamei S., Mori H., Kurokawa K. and Nakashima N. (2016) Establishment of a multi-species biofilm model and metatranscriptomic analysis of biofilm and planktonic cell communities. *Appl. Microbiol. Biotechnol.* **100**, 7263–7279. Available at: http://link.springer.com/10.1007/s00253-016-7532-6.

Näther D. J. and Rachel R. (2004) The outer membrane of the hyperthermophilic

archaeon Ignicoccus: dynamics, ultrastructure and composition. *Biochem. Soc. Trans.* **32**, 199–203. Available at: http://www.biochemsoctrans.org/cgi/doi/10.1042/bst0320199.

Nikolakakis K., Lehnert E., McFall-Ngai M. J. and Ruby E. G. (2015) Use of Hybridization Chain Reaction-Fluorescent In Situ Hybridization To Track Gene Expression by Both Partners during Initiation of Symbiosis ed. P. D. Schloss. *Appl. Environ. Microbiol.* **81**, 4728–4735. Available at: http://aem.asm.org/lookup/doi/10.1128/AEM.00890-15.

Nitin N., Santangelo P. J., Kim G., Nie S. and Bao G. (2004) Peptide-linked molecular beacons for efficient delivery and rapid mRNA detection in living cells. *Nucleic Acids Res.* **32**, e58. Available at: http://nar.oxfordjournals.org/content/32/6/e58.abstract.

Orphan V. J. (2001) Methane-Consuming Archaea Revealed by Directly Coupled Isotopic and Phylogenetic Analysis. *Science (80-.).* **293**, 484–487. Available at: http://www.sciencemag.org/cgi/doi/10.1126/science.1061338.

Orphan V. J., House C. H., Hinrichs K.-U., Mckeegan K. D. and Delong E. F. (2001) Methane-Consuming Archaea Revealed by Directly Coupled Isotopic and Phylogenetic Analysis. *Source Sci. New Ser. Cell Mol. Cell Proc. Natl. Acad. Sci. U.S.A. Nat. Cell X. Z. Su al. Cell D. I. Baruch al. Cell* **293**, 484–487. Available at: http://www.jstor.org/stable/3084093%5Cnhttp://www.jstor.org/stable/3084093?seq=1&cid=pdf-reference#references_tab_contents%5Cnhttp://about.jstor.org/terms.

Orphan V. J., House C. H., Hinrichs K.-U., McKeegan K. D. and DeLong E. F. (2002) Multiple archaeal groups mediate methane oxidation in anoxic cold seep sediments.

Proc. Natl. Acad. Sci. **99**, 7663–7668. Available at: http://www.pnas.org/content/99/11/7663.abstract.

Pernthaler A. and Amann R. (2004) Simultaneous fluorescence in situ hybridization of mRNA and rRNA in environmental bacteria. *Appl. Environ. Microbiol.* **70**, 5426–33. Available at: http://www.ncbi.nlm.nih.gov/pubmed/15345429.

Perras A. K., Wanner G., Klingl A., Mora M., Auerbach A. K., Heinz V., Probst A. J., Huber H., Rachel R., Meck S. and Moissl-Eichinger C. (2014) Grappling archaea: ultrastructural analyses of an uncultivated, cold-loving archaeon, and its biofilm. *Front. Microbiol.* **5**, 397. Available at: http://journal.frontiersin.org/article/10.3389/fmicb.2014.00397/abstract.

Peterson J. R., Thor S., Kohler L., Kohler P. R. A., Metcalf W. W. and Luthey-Schulten Z. (2016) Genome-wide gene expression and RNA half-life measurements allow predictions of regulation and metabolic behavior in Methanosarcina acetivorans. *BMC Genomics* **17**, 924. Available at: http://bmcgenomics.biomedcentral.com/articles/10.1186/s12864-016-3219-8.

Poretsky R. S., Bano N., Buchan A., LeCleir G., Kleikemper J., Pickering M., Pate W. M., Moran M. A. and Hollibaugh J. T. (2005) Analysis of Microbial Gene Transcripts in Environmental Samples. *Appl. Environ. Microbiol.* **71**, 4121–4126. Available at: http://aem.asm.org/cgi/doi/10.1128/AEM.71.7.4121-4126.2005.

Poretsky R. S., Hewson I., Sun S., Allen A. E., Zehr J. P. and Moran M. A. (2009) Comparative day/night metatranscriptomic analysis of microbial communities in the North Pacific subtropical gyre. *Environ. Microbiol.* **11**, 1358–1375. Available at: http://doi.wiley.com/10.1111/j.1462-2920.2008.01863.x.

Pratscher J., Vollmers J., Wiegand S., Dumont M. G. and Kaster A.-K. (2018) Unravelling the Identity, Metabolic Potential and Global Biogeography of the Atmospheric Methane-Oxidizing Upland Soil Cluster α. *Environ. Microbiol.* **20**, 1016–1029. Available at: http://doi.wiley.com/10.1111/1462-2920.14036.

Probst A. J., Weinmaier T., Raymann K., Perras A., Emerson J. B., Rattei T., Wanner G., Klingl A., Berg I. A., Yoshinaga M., Viehweger B., Hinrichs K.-U., Thomas B. C., Meck S., Auerbach A. K., Heise M., Schintlmeister A., Schmid M., Wagner M., Gribaldo S., Banfield J. F. and Moissl-Eichinger C. (2014) Biology of a widespread uncultivated archaeon that contributes to carbon fixation in the subsurface. *Nat. Commun.* **5**, 5497. Available at: http://www.nature.com/articles/ncomms6497.

Probst P., Yokochi R. and Sturchio N. C. (2006) Method for extraction of dissolved gases from groundwater for radiokrypton analysis. *Eos Trans. AGU* **87**, Fall Meet. Suppl., Abstract H41B-0414.

Rachel R., Wyschkony I., Riehl S. and Huber H. (2002) The ultrastructure of Ignicoccus : Evidence for a novel outer membrane and for intracellular vesicle budding in an archaeon. *Archaea* **1**, 9–18. Available at: http://www.hindawi.com/journals/archaea/2002/307480/abs/.

Renggli S., Keck W., Jenal U. and Ritz D. (2013) Role of Autofluorescence in Flow Cytometric Analysis of Escherichia coli Treated with Bactericidal Antibiotics. *J. Bacteriol.* **195**, 4067–4073. Available at: http://jb.asm.org/cgi/doi/10.1128/JB.00393-13.

Rinke C., Schwientek P., Sczyrba A., Ivanova N. N., Anderson I. J., Cheng J.-F., Darling A. E., Malfatti S., Swan B. K., Gies E. a, Dodsworth J. A., Hedlund B. P., Tsiamis

G., Sievert S. M., Liu W.-T., Eisen J. A., Hallam S. J., Kyrpides N. C., Stepanauskas R., Rubin E. M., Hugenholtz P. and Woyke T. (2013) Insights into the phylogeny and coding potential of microbial dark matter. *Nature* **499**, 431–437. Available at: http://www.ncbi.nlm.nih.gov/pubmed/23851394.

Rosenthal A. Z., Zhang X., Lucey K. S., Ottesen E. A., Trivedi V., Choi H. M. T., Pierce N. A. and Leadbetter J. R. (2013) Localizing transcripts to single cells suggests an important role of uncultured deltaproteobacteria in the termite gut hydrogen economy. *Proc. Natl. Acad. Sci.* **110**, 16163–16168. Available at: http://www.pnas.org/cgi/doi/10.1073/pnas.1307876110.

Rumbo-Feal S., Gómez M. J., Gayoso C., Álvarez-Fraga L., Cabral M. P., Aransay A. M., Rodríguez-Ezpeleta N., Fullaondo A., Valle J., Tomás M., Bou G. and Poza M. (2013) Whole Transcriptome Analysis of Acinetobacter baumannii Assessed by RNA-Sequencing Reveals Different mRNA Expression Profiles in Biofilm Compared to Planktonic Cells ed. G. F. Kaufmann. *PLoS One* **8**, e72968. Available at: https://dx.plos.org/10.1371/journal.pone.0072968.

Santangelo P., Nitin N. and Bao G. (2006) Nanostructured probes for RNA detection in living cells. *Ann. Biomed. Eng.* **34**, 39–50.

Seitz K. W., Lazar C. S., Hinrichs K.-U., Teske A. P. and Baker B. J. (2016) Genomic reconstruction of a novel, deeply branched sediment archaeal phylum with pathways for acetogenesis and sulfur reduction. *ISME J* **10**, 1696–1705. Available at: http://dx.doi.org/10.1038/ismej.2015.233.

Simkus D. N., Slater G. F., Lollar B. S., Wilkie K., Kieft T. L., Magnabosco C., Lau M. C. Y., Pullin M. J., Hendrickson S. B., Wommack K. E., Sakowski E. G., Heerden

E. van, Kuloyo O., Linage B., Borgonie G. and Onstott T. C. (2016) Variations in microbial carbon sources and cycling in the deep continental subsurface. *Geochim. Cosmochim. Acta* **173**, 264–283. Available at: https://linkinghub.elsevier.com/retrieve/pii/S0016703715005852.

Sogin M. L., Sogin M. L., Morrison H. G., Morrison H. G., Huber J. a, Huber J. a, Mark Welch D., Mark Welch D., Huse S. M., Huse S. M., Neal P. R., Neal P. R., Arrieta J. M., Arrieta J. M., Herndl G. J. and Herndl G. J. (2006) Microbial diversity in the deep sea and the underexplored "rare biosphere". *Proc. Natl. Acad. Sci. U. S. A.* **103**, 12115–20. Available at: http://www.ncbi.nlm.nih.gov/pubmed/16880384.

Sokol D. L., Zhang X., Lu P. and Gewirtz a M. (1998) Real time detection of DNA.RNA hybridization in living cells. *Proc. Natl. Acad. Sci. U. S. A.* **95**, 11538–43. Available at: http://www.pubmedcentral.nih.gov/articlerender.fcgi?artid=21676&tool=pmcentrez&rendertype=abstract.

Sørensen K. B., Finster K. and Ramsing N. B. (2001) Thermodynamic and Kinetic Requirements in Anaerobic Methane Oxidizing Consortia Exclude Hydrogen, Acetate, and Methanol as Possible Electron Shuttles. *Microb. Ecol.* **42**, 1–10. Available at: http://www.ncbi.nlm.nih.gov/pubmed/12035076.

Spang A., Saw J. H., Jørgensen S. L., Zaremba-Niedzwiedzka K., Martijn J., Lind A. E., van Eijk R., Schleper C., Guy L. and Ettema T. J. G. (2015) Complex archaea that bridge the gap between prokaryotes and eukaryotes. *Nature* **521**, 173–179. Available at: http://www.nature.com/doifinder/10.1038/nature14447.

Stehbens S., Pemble H., Murrow L. and Wittmann T. (2012) Imaging Intracellular

Protein Dynamics by Spinning Disk Confocal Microscopy. In *Methods in Enzymology* pp. 293–313. Available at: https://linkinghub.elsevier.com/retrieve/pii/B978012391857400015X.

Steinberg L. M. and Regan J. M. (2009) mcrA-targeted real-time quantitative PCR method to examine methanogen communities. *Appl. Environ. Microbiol.* **75**, 4435–4442.

Steinberg L. M. and Regan J. M. (2008) Phylogenetic comparison of the methanogenic communities from an acidic, oligotrophic fen and an anaerobic digester treating municipal wastewater sludge. *Appl. Environ. Microbiol.* **74**, 6663–71. Available at: http://aem.asm.org/cgi/content/long/74/21/6663 [Accessed February 4, 2017].

Thorup C., Schramm A., Findlay A. J., Finster K. W. and Schreiber L. (2017) Disguised as a Sulfate Reducer: Growth of the Deltaproteobacterium Desulfurivibrio alkaliphilus by Sulfide Oxidation with Nitrate ed. D. K. Newman. *MBio* **8**. Available at: http://mbio.asm.org/lookup/doi/10.1128/mBio.00671-17.

Tyagi S. and Kramer F. R. (1996) Molecular Beacons: Probes that Fluoresce upon Hybridization. *Nat. Biotechnol.* **14**, 303–308. Available at: http://www.nature.com/articles/nbt0396-303.

Valentine D. L. and Reeburgh W. S. (2000) New perspectives on anaerobic methane oxidation. *Env. Microbiol* **2**, 477–484.

Vanwonterghem I., Evans P. N., Parks D. H., Jensen P. D., Woodcroft B. J., Hugenholtz P. and Tyson G. W. (2016) Methylotrophic methanogenesis discovered in the archaeal phylum Verstraetearchaeota. *Nat. Microbiol.* **1**, 16170. Available at: http://dx.doi.org/10.1038/nmicrobiol.2016.170%5Cnhttp://www.ncbi.nlm.nih.gov/p

ubmed/27694807.

Wang Y., Wegener G., Hou J., Wang F. and Xiao X. (2019) Expanding anaerobic alkane metabolism in the domain of Archaea. *Nat. Microbiol.* **4**, 595–602. Available at: http://www.nature.com/articles/s41564-019-0364-2.

Ward J. A., Slater G. F., Moser D. P., Lin L. H., Lacrampe-Couloume G., Bonin A. S., Davidson M., Hall J. A., Mislowack B., Bellamy R. E. S., Onstott T. C. and Sherwood Lollar B. (2004) Microbial hydrocarbon gases in the Witwatersrand Basin, South Africa: Implications for the deep biosphere. *Geochim. Cosmochim. Acta* **68**, 3239–3250.

Widdel F. and Bak F. (1992) *The Prokaryotes*. eds. A. Balows, H. G. Trüper, M. Dworkin, W. Harder, and K.-H. Schleifer, Springer New York, New York, NY. Available at: http://link.springer.com/10.1007/978-1-4757-2191-1.

Yilmaz S., Haroon M. F., Rabkin B. A., Tyson G. W. and Hugenholtz P. (2010) Fixation-free fluorescence in situ hybridization for targeted enrichment of microbial populations. *ISME J.* **4**, 1352–1356. Available at: http://www.nature.com/doifinder/10.1038/ismej.2010.73%5Cnhttp://dx.doi.org/10.1038/ismej.2010.73.

Yokochi R. (2016) Recent developments on field gas extraction and sample preparation methods for radiokrypton dating of groundwater. *J. Hydrol.* **540**, 368–378.

Zaremba-Niedzwiedzka K., Caceres E. F., Saw J. H., Bäckström D., Juzokaite L., Vancaester E., Seitz K. W., Anantharaman K., Starnawski P., Kjeldsen K. U., Stott M. B., Nunoura T., Banfield J. F., Schramm A., Baker B. J., Spang A. and Ettema T. J. G. (2017) Asgard archaea illuminate the origin of eukaryotic cellular complexity.

Nature **541**, 353–358. Available at: http://dx.doi.org/10.1038/nature21031.

CHAPTER 3

Draft genome sequence of *Candidatus* "Bathyarchaeota" archaeon BE326-BA-RLH, an uncultured putative anaerobic methanotroph from South Africa's deep continental biosphere

Keywords: metagenomics, Bathyarchaeota, anaerobic methane oxidation

3.1 ABSTRACT

Metagenomic sequencing of fracture fluid from South Africa recovered a nearly complete genome belonging to the archaeal phylum *Candidatus* "Bathyarchaeota". Metagenomic-assembled genome *Ca.* BE326-BA-RLH possesses a complete Wood-Ljundal pathway, but also genes involved in methane metabolism and dissimilatory nitrate reduction to ammonium. This study presents the first genomic evidence for potential anaerobic methane oxidation in the *Ca.* "Bathyarchaeota".

3.2 INTRODUCTION

The uncultured *Ca.* "Bathyarchaeota" is a deeply branching and diverse phylum of deep biosphere inhabitants, whose recently inferred role in methanogenesis supports an early evolution of biogenic methane cycling (Evans et al., 2015; Lloyd, 2015). We report a near-complete metagenome-assembled genome (MAG) of *Ca.* "Bathyarchaeota" archaeon BE326-BA-RLH assembled from metagenomic data obtained from a Subsurface chemoLithoautotrophic Microbial Ecosystem (SLiME) (Stevens and McKinley, 1995) in oligotrophic fracture fluid (33.2˚C, pH 7.5, pe = -0.48) from 1.34 kmbls at Beatrix Gold Mine, South Africa.

3.3 MATERIALS AND METHODS

3.3.1 *Site description and sample collection, BE326 BH2 borehole, Beatrix Mine*

. Fracture fluid was collected in 2015 from the BE326 BH2 borehole following established procedures (Lau et al., 2014; Magnabosco et al., 2014). A sterile stainless-steel manifold fitted with high-pressure ball valves was attached to sealed borehole casing and purged with water for 10 minutes (flow rate ~ 8 L min^{-1}) to minimize contamination by mine air. Ethanol-sterilized Teflon™ tubing was connected to the manifold and flushed for another 10 minutes (flow rate of ~800 mL min^{-1}). Biomass was collected onto a pre-autoclaved 0.2 μm 25-cm long Memtrex NY filter (Cat. No. MNY-92-1-AAS, General Electric Co., Minnetonka, MN) for 49 days (flow rate ~100 mL min^{-1}). Upon retrieval, water was decanted from the filter and replaced with sterile RNA preservation solution (20 mM ethylenediaminetetraacetic acid [EDTA], 0.3 M sodium citrate, 4.3 M ammonium sulfate; pH adjusted to 5.2 using concentrated H_2SO_4) (Brown

and Smith, 2009). The filter was aseptically transferred into double Ziploc® bags and stored overnight at 4˚C to allow RNA preservation solution to completely saturate all membrane layers. The filter was shipped back to Princeton University in a liquitd N_2-charged dry shipper and stored at -80˚C until processing.

3.3.2 ***Genomic DNA isolation and metagenomic sequencing***. Total nucleic acids and proteins were isolated from the MNY filter following the procedure by Lau et al. (2014). The MNY filter was cut into 2-cm thick discs using a bleached band saw and subsequently sliced into 2 cm^2 slices using a flame-sterilized razor. Cells were lysed by treating filter slices in 2X cationic detergent cetyltrimethylammonium bromide (CTAB) lysis buffer (pH 8.0) containing lysozyme (5 mg mL^{-1} final concentration) (MilliporeSigma, Burlington, MA USA) and Proteinase K (0.2 mg mL^{-1} final concentration) (MilliporeSigma) and incubated for 30 minutes at 60˚C. Phenol/chloroform/isoamyl alcohol (25:24:1) was added to the lysate (4:5 v/v) and then incubated in a 60˚C water bath for 1 min and an ice bath for 5 min before centrifugation at 4300 × g for 10 min at 23˚C. DNA and RNA were precipitated by adding isopropanol (1:1 v/v), incubated on ice for 30 min, and centrifuged at 4300 × g for 15 min at 23˚C. The supernatant was decanted, and the pellet was rinsed using 20˚C-chilled 75% (v/v) ethanol. Pellets were left to air dry under a laminar flow hood for 1 hour then resuspended in 1X TE buffer (Tris-EDTA, pH 8) and stored in 1.5 mL Eppendorf tubes (Eppendorf, Hamburg, Germany).

DNA was collected from an aliquot of total nucleic acids following treatment with RNase A (10 μg mL^{-1} final concentration) (ThermoFisher Scientific, Waltham, MA

USA) and two added volumes of 100% (v/v) molecular grade ethanol. The mixture was incubated at -20˚C for 30 min and subsequently centrifuged at 11,500 × g at 23˚C. The metagenomic library was prepared using the PrepX DNA library kit and automated Apollo 324™ system (WaferGen Biosystems, Inc., Fremont, CA USA). The library DNA concentration was quantified on a Qubit® 2.0 fluorometer using a Qubit™ 1X dsDNA HS assay (Invitrogen, Carlsbad, CA USA). Library DNA was pooled at equal molar amounts and paired end (2 x 100 nt) metagenomic sequencing was performed for 300 cycles at the Marine Biological Laboratory using the Illumina HiSeq 2000 platform (Illumina Inc., San Diego, CA USA).

3.3.3 ***Metagenome assembly, MAG binning, and annotation***. Tools on the Galaxy web platform at https://galaxy.princeton.edu (Afgan et al., 2018) were used to quality filter raw reads. Filter FASTQ v.1.1.1 removed reads having 90% of bases with Phred quality scores <30. Remove Sequencing Artifacts v.1.0.1 removed homopolymers. Trim Galore! v.0.4.3.1 removed reads that matched the Illumina Universal adapter sequence anywhere with a max error rate of 0.1, match times of 1, minimum overlap length of 20, including "Ns" as matches. Trim v.0.0.1 removed 5 bases from the 3' end, and then reads shorter than 50 bases and those containing "Ns". The resulting quality reads were assembled using SPAdes v.3.11.0 (--meta option) (Bankevich et al., 2012). Scaffolds were binned into MAGs using MetaBAT v.2.11.2 (Kang et al., 2015). Quality-filtered metagenome reads were mapped back to assembled MAGs using Bowtie2 v.2.3.2 (default --very-sensitive mode options) to recruit more reads belonging to the bin (Langmead and Salzberg, 2012). Protein-encoding genes were identified using Prodigal

v.2.6.3 (Hyatt et al., 2010) and annotated using NCBI BLAST v.2.2.29+ (Camacho et al., 2009), Prokka v.1.13 (Lupetti et al., 2014), GraftM v.0.11.1 (Boyd et al., 2018), and HHpred v.3.0.0beta (Soding et al., 2005). Tetranucleotide frequency (TNF) and variance of TNF (σ^2_{TNF}) were calculated in R using tools in the seqinr and Biostrings packages (Charif and Lobry, 2007; Pagès et al., 2017). A summary of the methodological pipeline is visualized in Figure 3.1.

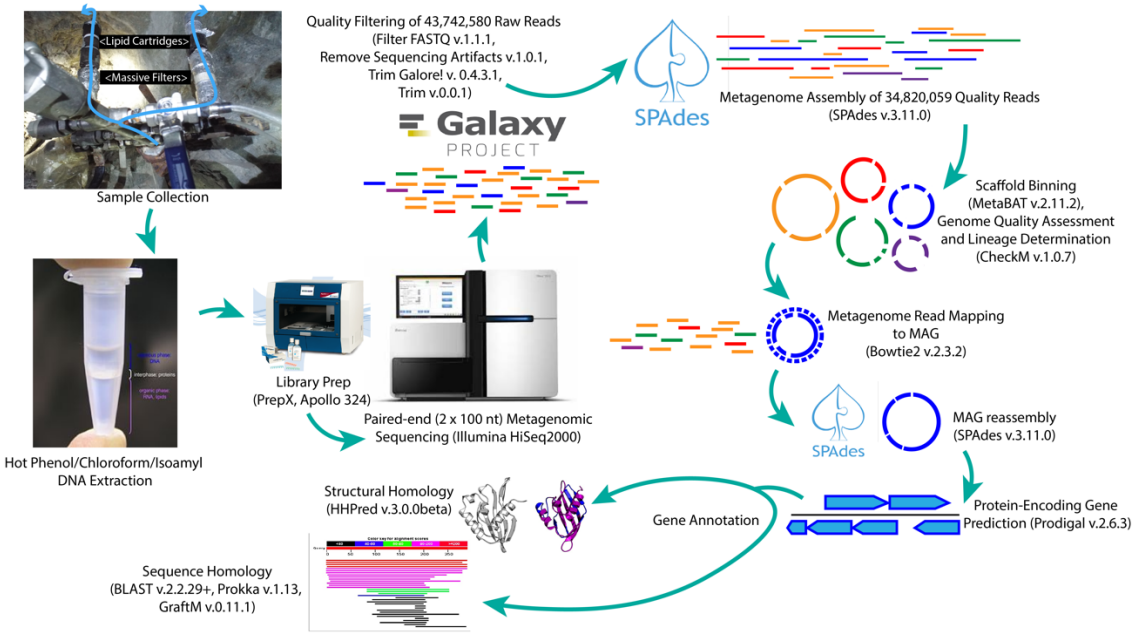

Figure 3.1. Overview of bioinformatic workflow from sample collection to MAG annotation.

3.3.4. ***16S rRNA gene phylogeny***. The 16S rRNA gene of *Ca.* "Bathyarchaeota" archaeon BE326-BA-RLH was referenced against 455 sequences belonging to 25 *Ca.* "Bathyarchaeota" subgroups and three outgroups (*Crenarchaeota*, *Ca.* "Korcharchaeota", and *Ca.* "YNPFFA"), concatenated in a previous review by Zhou et al. (2018) and made publicly available at https://github.com/ChaoLab/Bathy16Stree. A multiple sequence

alignment of 16S rRNA gene sequences was compiled using Clustal Omega v.1.2.4 (Sievers and Higgins, 2014). Gaps were removed from aligned sequences using an automated trimming heuristic function in trimAl v.1.2b (--automated1) (Capella-Gutierrez et al., 2009) and a maximum likelihood tree was inferred from 100 non-parametric bootstrapping iterations of the GTRGAMMA model in RAxML v.8.2.11 (Stamatakis, 2014).

3.3.5 *Sequence phylogeny of methyl-coenzyme M reductase subunit A (mcrA)*.

BE326-BH2 metagenome assembly scaffolds identified by GraftM as *mcr*A sequences were aligned with 174 unique *mcr*A amino acid sequences (> 200 aa residues) assembled from previous publications (Evans et al., 2015; Jungbluth et al., 2017; Wang et al., 2019) representing known and putative CH_4/short alkane metabolizers in the *Euryarchaeota*, *Ca.* "Bathyarchaeota", *Ca.* "Nezhaarchaeota", *Ca.* "Archaeoglobi", and *Ca.* "Korarchaeota". Multiple sequence alignment and alignment trimming was performed using Clustal Omega and trimAl as described above. In the absence of a rooted outgroup, the best-fit model of nucleotide substitution to assess phylogenetic relatedness was informed using jModelTest v.2.10.0 (Guindon and Gascuel, 2003; Darriba et al., 2012). The resulting maximum likelihood tree was constructed using 100 non-parametric bootstrapping iterations of the PROTGAMMAILGF model in RAxML.

Phylogenetic trees were visualized using FigTree v.1.4.4 (https://github.com/rambaut/figtree/releases) and enhanced to group related taxa using Adobe Illustrator 2020 v.24.1.0.

3.4 RESULTS AND DISCUSSION

3.4.1 ***MAG assembly statistics***. From an initial pool of 43,742,580 raw sequenced reads, a total of 34,820,059 quality-filtered paired end reads were recovered from genomic DNA extracted from the BE326-BH2 borehole. From the metagenome assembly, MetaBAT binned a near-complete (estimated at 89.79%), low-contamination (3.74%) MAG with 0% strain heterogeneity. Quality-filtered BE326-BH2 metagenome reads that mapped to the scaffolds in this initial bin were reassembled using SPAdes (default option). The resulting draft genome (2.09 Mb, 44.9% GC) comprises 227 contigs with an N_{50} length of 14,564 bp and has an 86% coding density (Table 3.1) and contains 23 30S and 29 50S ribosomal proteins, a single copy of 16S, 23S, and 5S rRNA genes, and 91 tRNA genes.

Table 3.1. Statistics summary of CH_4-metabolizing *Ca.* "Bathyarchaeota" genomes

	BE326-BA-RLH (this study)	BA1[a]	BA2[a]
Completeness (%)	89.8[b]	91.6	93.8
Contamination (%)	3.7	2.8	3.7
Total length (bp)	2,097,091	1,931,714	1,455,689
GC content (%)	44.9	47.1	44.2
Num. contigs	227	96	58
N_{50} contigs	14,564[c]	32,677	43,519
Num. coding sequences	2,229	2,403	1,761
Coding density (%)	86.0	80.8	83.6
Average coverage (×)	21.1	35.8	49.8
Relative abundance (%)	0.36[d]	0.92	1.03

[a] Source: Evans et al. (2015)
[b] Based on lineage-specific marker genes determined via CheckM (Parks et al., 2015)
[c] Calculated from Prodigal (Hyatt et al., 2010)
[d] Estimated from the percentage of reads mapped back to the metagenome assembly.

3.4.2 *Phylogeny of* Ca. *"Bathyarchaeota" archaeon BE326-BA-RLH*. The phylogeny of the MAG was identified as an unknown archaeon according to CheckM v.1.0.7 (Parks et al., 2015), but a BLASTn search determined that the 16S rRNA gene (1139 bp) shares 97% similarity to uncultured *Ca.* "Bathyarchaeota" (EU559699, EU155992, EU155991), and 87% and 86% similarity to putative *Ca.* "Bathyarchaeota" methanogens BA2 (LIHK01000010) and BA1 (LIHJ01000085), respectively (SRX1122679) (Evans et al., 2015). A maximum likelihood tree of aligned 16S rRNA gene sequences placed this MAG as belonging to a deeply divergent clade interpreted as *Ca.* "Bathyarchaeota" Subgroup-18 (Figure 3.2). This subgroup is apparently monophyletic with Subgroup-3, represented by previously identified putatively methanogenic *Ca.* "Bathyarchaeota" BA1 and BA2 (Evans et al., 2015), providing increasingly supportive evidence for a deep root of methane metabolisms amongst the *Archaea* (Lloyd, 2015).

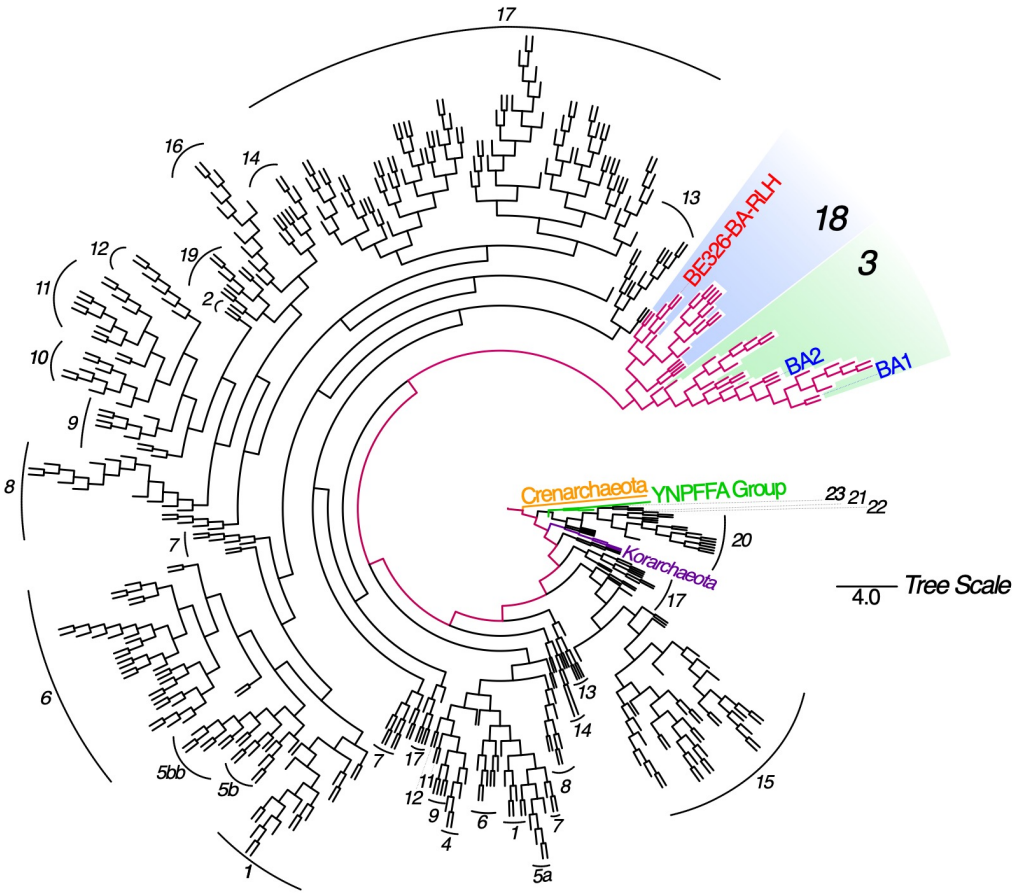

Figure 3.2. 16S rRNA gene phylogenetic tree showing the placement of *Ca.* "Bathyarchaeota" archaeon BE326-BA-RLH among other *Ca.* "Bathyarchaeota" OTUs. *Crenarchaeota*, *Ca.* "Korarchaeota", and *Ca.* "YNPFFA" are referenced as outgroups. Monophyly of subgroups 18 and 3 indicated by pink branches. Reference NCBI accession numbers of 16S rRNA genes used in the building of this tree are available at https://github.com/ChaoLab/Bathy16Stree and Appendix C, File 3C.1.fasta. Scale bar refers to average number of substitutions per site.

3.4.3 *Metabolic potential for methane metabolism*. *Ca.* "Bathyarchaeota"

BE326-BA-RLH encodes proteins involved in methanogenesis via the Wood-Ljundal pathway, including a complete CODH/ACS operon, tungsten-containing formylmethanofuran dehydrogenase (*Fwd*DACB), two copies of formylmethanofuran tetrahydromethanopterin formyltransferase (*Ftr*), methenyl tetrahydromethanopterin

cyclohydrolase (*Mch*), methylene tetrahydromethanopterin dehydrogenase (*Mtd*B), 5,10-methylenetetrahydromethanopterin reductase (*Mer*), tetrahydromethanopterin S-methyltransferase (*Mtr*H), and the nickel-iron (NiFe)-containing CoB-CoM heterodisulfide reductase (*Hdr*ABC), along with associated NiFe hydrogenase maturation proteins (e.g., *Hyp*CEF). Similar to *Ca.* "Bathyarchaeota" BA1 and BA2, as well as the *Methanomassiliicoccales*, we did not detect the membrane-bound *Hdr*E (Evans et al., 2015; Zhou et al., 2018). Electron shuttling in the methanogenesis pathway is apparently mediated by energy-conserving ferredoxin and coenzyme F420, the latter of which is encoded by two operons encoding F420-reducing hydrogenase (*Frh*ABDG). The metabolic potential to utilize H_2 is not apparent, given an absence of membrane-bound hydrogenases such as energy conserving hydrogenase (*Ech*) and methanophenazine-recycling hydrogenase (*Vht*/*Vho*).

The metabolic potential for growth on methylated compounds is also indicated by the detection of a trimethylamine corrinoid protein (*Mtt*C) adjacent to *Mtr*. Additionally, we detected 7 copies of methyl sulfide methyltransferase-associated sensors (*Msm*S), one of which was found immediately adjacent to alpha and beta units of sulfide dehydrogenase (*Sud*AB), as well as coenzyme PQQ synthesis protein E (*Pqq*E), which may speak to quinoproteins participating in the oxidation of thiol groups. Evidence for motility is indicated by archaeal flagellin (*Fla*I) and methyl-accepting chemotaxis proteins, including the *Che*A histidine kinase, *Che*W signal transducer, and *Che*B and *Che*Y phosphoryl regulators. Several genes in an incomplete reductive TCA cycle were also detected, suggesting *Ca.* "Bathyarchaeota" BE326-BA-RLH possesses metabolic plasticity to fix carbon (Figure 3.3).

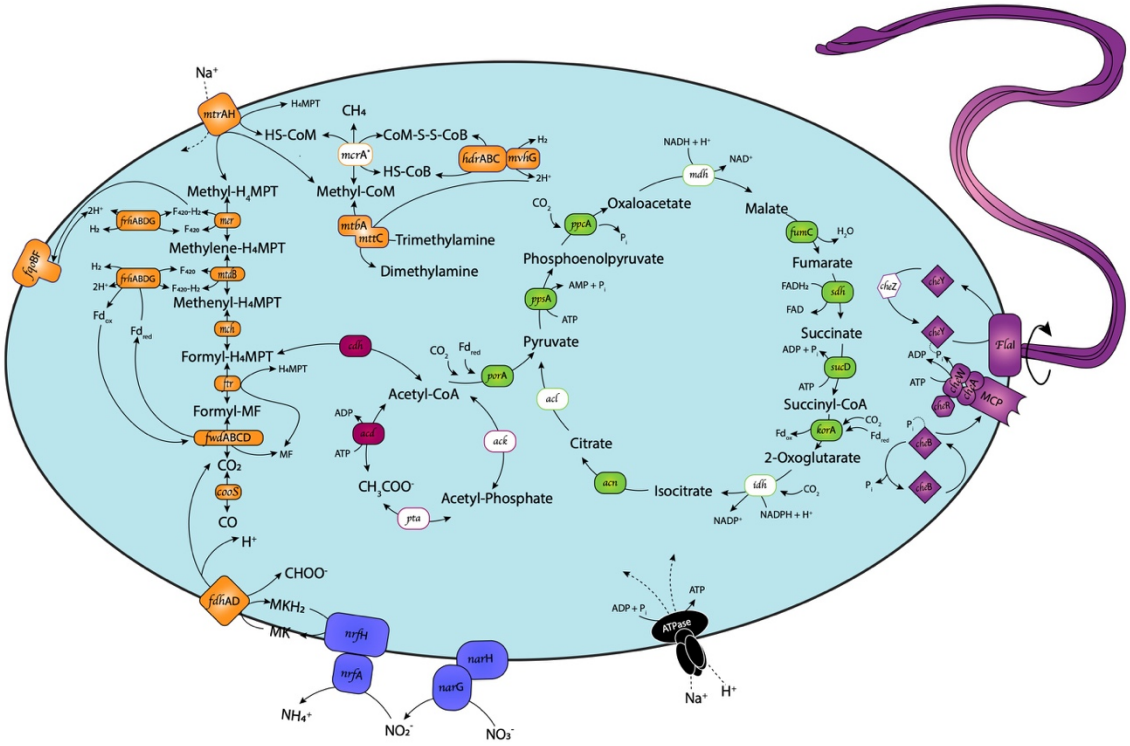

Figure 3.3. Key metabolic pathways in *Ca.* "Bathyarchaeota" archaeon BE326-BA-RLH. Genes are color-coded by pathway, with missing genes indicated with a white fill. Gene abbreviations are provided in Appendix A, Table A.1.

A partial methyl-coenzyme M reductase subunit A (*Mcr*A) sequence was identified in a 265-bp-long contig in the metagenome assembly, which shared 70% identity to an amino acid sequence of an uncultured archaeon (AGA20295) based on BLASTp search. A maximum likelihood tree of 175 *mcr*A amino acid sequences for this and 175 reference sequences placed this *Mcr*A as a deep branch rooting the *Ca.* "Bathyarchaeota" clade (Figure 3.4). A comparison of GC content versus tetranucleotide frequency variance of the putative *Mcr*A sequence with *Ca.* Bathyarchaeota BE326-BA-RLH genome scaffolds did not rule out this *Mcr*A from belonging to the MAG (Figure 3.5). Given the short length of the contig, we anticipate it was too short to be added to

the bin by MetaBAT without also increasing the potential of recruiting contaminant reads.

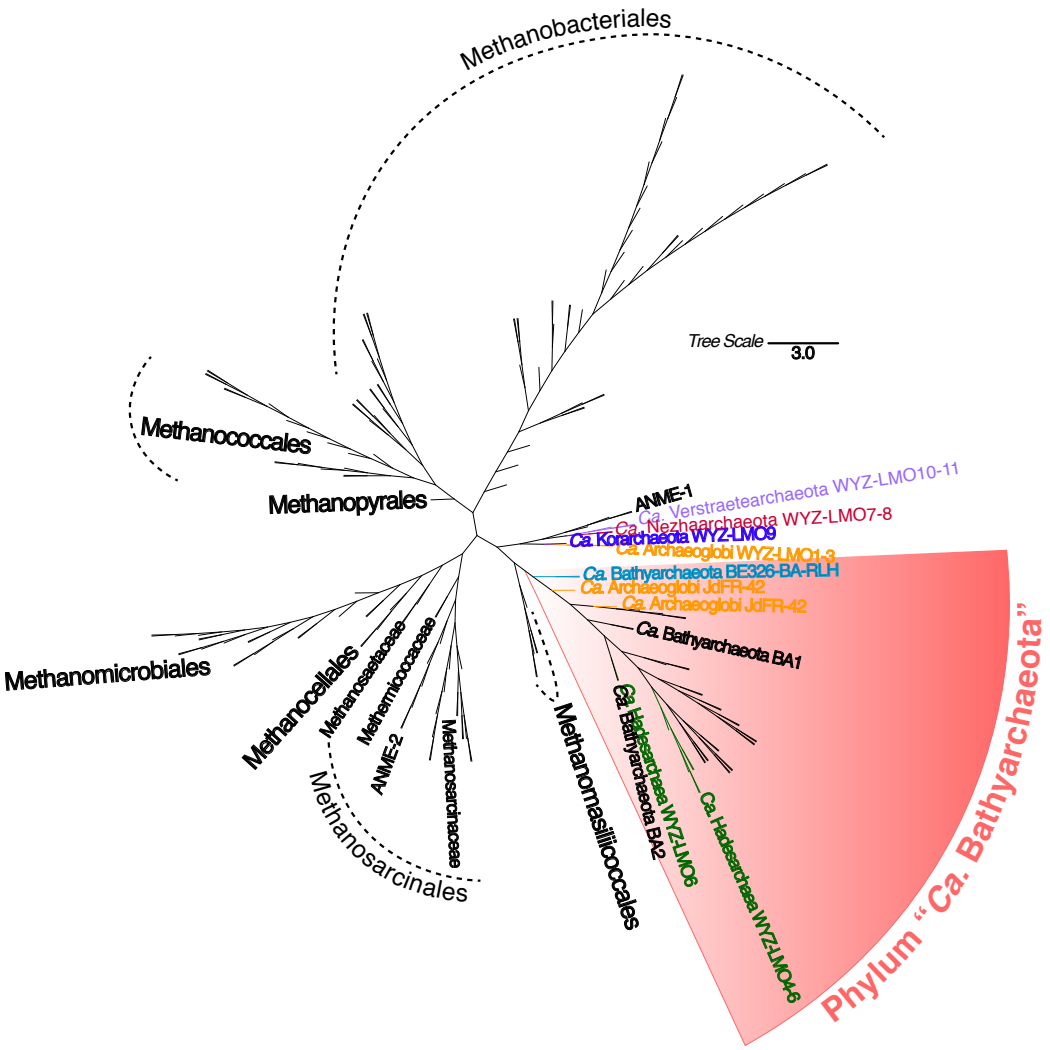

Figure 3.4. Maximum likelihood tree placing the putative *Ca.* "Bathyarchaeota" BE326-BA-RLH *mcr*A sequence at the root of the *Ca.* "Bathyarchaeota" phylum. Scale bar refers to number of average substitutions per position. A fasta file of amino acid sequences used in the building of this tree are available in Appendix C, File 3C.2.fasta

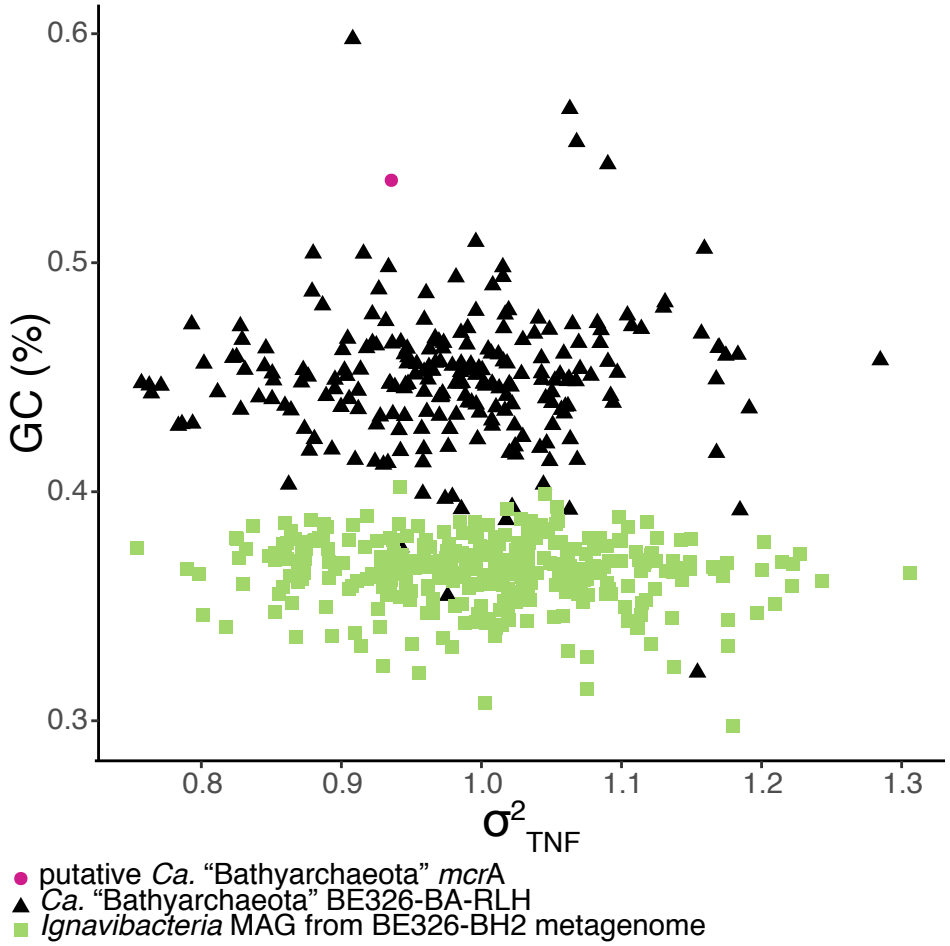

Figure 3.5. GC content versus tetranucleotide frequency variance (σ^2_{TNF}) of the putative *Ca.* "Bathyarchaeota" *Mcr*A sequence (pink circle) relative to scaffold sequences recruited to *Ca.* BE326-BA-RLH (black triangles) and a reference *Ignavibacteria* MAG binned from the BE326-BH2 metagenome assembly (green squares).

BE326-BA-RLH contains genes encoding for periplasmic nitrate reductase (*Nar*H) and nitrite reductase (*Nrf*HA), which suggests the metabolic capacity to perform dissimilatory nitrate reduction to ammonium (DNRA) (Figure 3.3). Formate dehydrogenase (*Fdh*AD) was found adjacent to tungsten-containing formylmethanofuran dehydrogenase (*Fwd*DACB), supporting metabolic potential of formate-dependent CO_2 reduction to CH_4. However, we also note that the *Nrf* operon is adjacent to *Fdh*.

Therefore, formate may also serve as a possible electron shuttle between reverse methanogenesis and DNRA. To our knowledge *Ca.* BE326-BA-RLH is the first described *Ca.* "Bathyarchaeota" genome encoding genes that may couple anaerobic methane oxidation (AOM) to known oxidants. This study provides further support that members of Bathyarchaeota may perform AOM (Biddle et al., 2006; Evans et al., 2015; Lever, 2016).

3.5 DATA AVAILABILITY.

The BE326-BH2 borehole whole shotgun 2015 metagenome and draft genome sequences of *Ca.* "Bathyarchaeota" archaeon BE326-BA-RLH have been deposited at NCBI GenBank under accession numbers QZGF00000000 (SRR7867194) and QYYE00000000 (SRR7866305), respectively. The version described in this chapter is QYYE01000000. Fasta files of 16S rRNA genes and *Mcr*A amino acid sequences used to generate Figures 3.2 and 3.4 are respectively available in Appendix C as File 3C.1.fasta and File 3C.2.fasta.

3.6 ACKNOWLEDGEMENTS

This chapter is largely based on Harris et al. (2018). This research was supported by funding from National Science Foundation grants DEB-1441646 and DGE-1148900, NASA grant NNX17AK87G, and the Deep Carbon Observatory Deep Life Cultivation Internship (Alfred P. Sloan Foundation). I am grateful to Sibanye Gold Ltd. and the management of Beatrix Mine for granting sampling access to the BE326-BH2 borehole. I thank Esta van Heerden, Errol Cason, and Jan-G Vermeulen from the University of the

Free State for their field assistance during sample collection. Metagenomic sequencing services were provided by the Marine Biological Laboratory (Woods Hole, MA USA) via Phase 11 of the Deep Carbon Observatory's Census of Deep Life Program (Alfred P. Sloan Foundation) and I am grateful for the assistance of Susan Huse, Joseph Vineis, Andrew Voorhis, and Hilary Morrison in this endeavor.

Any opinions, findings, and conclusions or recommendations expressed in this material are mine and do not necessarily reflect the views of the National Science Foundation.

3.7 REFERENCES

Afgan E., Baker D., Batut B., van den Beek M., Bouvier D., Čech M., Chilton J., Clements D., Coraor N., Grüning B. A., Guerler A., Hillman-Jackson J., Hiltemann S., Jalili V., Rasche H., Soranzo N., Goecks J., Taylor J., Nekrutenko A. and Blankenberg D. (2018) The Galaxy platform for accessible, reproducible and collaborative biomedical analyses: 2018 update. *Nucleic Acids Res.* **46**, W537–W544. Available at: https://academic.oup.com/nar/article/46/W1/W537/5001157.

Bankevich A., Nurk S., Antipov D., Gurevich A. A., Dvorkin M., Kulikov A. S., Lesin V. M., Nikolenko S. I., Pham S., Prjibelski A. D., Pyshkin A. V., Sirotkin A. V., Vyahhi N., Tesler G., Alekseyev M. A. and Pevzner P. A. (2012) SPAdes: A New Genome Assembly Algorithm and Its Applications to Single-Cell Sequencing. *J. Comput. Biol.* **19**, 455–477. Available at: http://www.liebertpub.com/doi/10.1089/cmb.2012.0021.

Biddle J. F., Lipp J. S., Lever M. A., Lloyd K. G., Sørensen K. B., Anderson R.,

Fredricks H. F., Elvert M., Kelly T. J., Schrag D. P., Sogin M. L., Brenchley J. E., Teske A., House C. H. and Hinrichs K.-U. (2006) Heterotrophic Archaea dominate sedimentary subsurface ecosystems off Peru. *Proc. Natl. Acad. Sci. U. S. A.* **103**, 3846–3851.

Boyd J. A., Woodcroft B. J. and Tyson G. W. (2018) GraftM: a tool for scalable, phylogenetically informed classification of genes within metagenomes. *Nucleic Acids Res.* **46**, e59–e59. Available at: https://academic.oup.com/nar/article/46/10/e59/4942468.

Brown A. L. and Smith D. W. (2009) Improved RNA preservation for immunolabeling and laser microdissection. *RNA* **15**, 2364–2374. Available at: http://rnajournal.cshlp.org/cgi/doi/10.1261/rna.1733509.

Camacho C., Coulouris G., Avagyan V., Ma N., Papadopoulos J., Bealer K. and Madden T. L. (2009) BLAST+: architecture and applications. *BMC Bioinformatics* **10**, 421. Available at: http://www.biomedcentral.com/1471-2105/10/421.

Capella-Gutierrez S., Silla-Martinez J. M. and Gabaldon T. (2009) trimAl: a tool for automated alignment trimming in large-scale phylogenetic analyses. *Bioinformatics* **25**, 1972–1973. Available at: https://academic.oup.com/bioinformatics/article-lookup/doi/10.1093/bioinformatics/btp348.

Charif D. and Lobry J. R. (2007) SeqinR 1.0-2: A Contributed Package to the R Project for Statistical Computing Devoted to Biological Sequences Retrieval and Analysis.

Darriba D., Taboada G. L., Doallo R. and Posada D. (2012) jModelTest 2: more models, new heuristics and parallel computing. *Nat. Methods* **9**, 772–772. Available at: http://www.nature.com/articles/nmeth.2109.

Evans P. N., Parks D. H., Chadwick G. L., Robbins S. J., Orphan V. J., Golding S. D. and Tyson G. W. (2015) Methane metabolism in the archaeal phylum Bathyarchaeota revealed by genome-centric metagenomics. *Science* **350**, 434–8. Available at: http://www.sciencemag.org/content/350/6259/434.short.

Guindon S. and Gascuel O. (2003) A Simple, Fast, and Accurate Algorithm to Estimate Large Phylogenies by Maximum Likelihood ed. B. Rannala. *Syst. Biol.* **52**, 696–704. Available at: http://academic.oup.com/sysbio/article/52/5/696/1681984.

Harris R. L., Lau M. C. Y., Cadar A., Bartlett D. H., Cason E., van Heerden E. and Onstott T. C. (2018) Draft Genome Sequence of " Candidatus Bathyarchaeota" Archaeon BE326-BA-RLH, an Uncultured Denitrifier and Putative Anaerobic Methanotroph from South Africa's Deep Continental Biosphere ed. J. C. Dunning Hotopp. *Microbiol. Resour. Announc.* **7**, e01295-18. Available at: http://mra.asm.org/content/7/20/e01295-18.abstract.

Hyatt D., Chen G.-L., LoCascio P. F., Land M. L., Larimer F. W. and Hauser L. J. (2010) Prodigal: prokaryotic gene recognition and translation initiation site identification. *BMC Bioinformatics* **11**, 119. Available at: https://bmcbioinformatics.biomedcentral.com/articles/10.1186/1471-2105-11-119.

Jungbluth S. P., Amend J. P. and Rappé M. S. (2017) Metagenome sequencing and 98 microbial genomes from Juan de Fuca Ridge flank subsurface fluids. *Sci. Data* **4**, 170037. Available at: http://www.nature.com/articles/sdata201737.

Kang D. D., Froula J., Egan R. and Wang Z. (2015) MetaBAT, an efficient tool for accurately reconstructing single genomes from complex microbial communities. *PeerJ* **3**, e1165. Available at: https://peerj.com/articles/1165.

Langmead B. and Salzberg S. L. (2012) Fast gapped-read alignment with Bowtie 2. *Nat. Methods* **9**, 357–9. Available at: http://www.ncbi.nlm.nih.gov/pubmed/22388286.

Lau M. C. Y., Cameron C., Magnabosco C., Brown C. T., Schilkey F., Grim S., Hendrickson S., Pullin M., Sherwood Lollar B., van Heerden E., Kieft T. L. and Onstott T. C. (2014) Phylogeny and phylogeography of functional genes shared among seven terrestrial subsurface metagenomes reveal N-cycling and microbial evolutionary relationships. *Front. Microbiol.* **5**, 531. Available at: http://journal.frontiersin.org/article/10.3389/fmicb.2014.00531/abstract.

Lever M. A. (2016) A New Era of Methanogenesis Research. *Trends Microbiol.* **24**, 84–86. Available at: https://linkinghub.elsevier.com/retrieve/pii/S0966842X15002966.

Lloyd K. (2015) Beyond known methanogens. *Science* **350**, 384–384. Available at: https://www.sciencemag.org/lookup/doi/10.1126/science.aad4066.

Lupetti M., Hengster J., Uphues T. and Scrinzi A. (2014) Attosecond Photoscopy of Plasmonic Excitations. *Phys. Rev. Lett.* **113**, 113903. Available at: http://arxiv.org/abs/1401.4290.

Magnabosco C., Tekere M., Lau M. C. Y., Linage B., Kuloyo O., Erasmus M., Cason E., van Heerden E., Borgonie G., Kieft T. L., Olivier J. and Onstott T. C. (2014) Comparisons of the composition and biogeographic distribution of the bacterial communities occupying South African thermal springs with those inhabiting deep subsurface fracture water. *Front. Microbiol.* **5**, 679. Available at: http://journal.frontiersin.org/article/10.3389/fmicb.2014.00679/abstract.

Pagès H., Aboyoun P., Gentleman R. and DebRoy S. (2017) Biostrings: Efficient manipulation of biological strings. *R Packag. version 2.46.0*.

Parks D. H., Imelfort M., Skennerton C. T., Hugenholtz P. and Tyson G. W. (2015) CheckM: assessing the quality of microbial genomes recovered from isolates, single cells, and metagenomes. *Genome Res.* **25**, 1043–1055. Available at: http://genome.cshlp.org/lookup/doi/10.1101/gr.186072.114.

Sievers F. and Higgins D. G. (2014) Clustal Omega, Accurate Alignment of Very Large Numbers of Sequences. In *Methods in Molecular Biology* pp. 105–116. Available at: http://link.springer.com/10.1007/978-1-62703-646-7_6.

Soding J., Biegert A. and Lupas A. N. (2005) The HHpred interactive server for protein homology detection and structure prediction. *Nucleic Acids Res.* **33**, W244–W248. Available at: https://academic.oup.com/nar/article-lookup/doi/10.1093/nar/gki408.

Stamatakis A. (2014) RAxML version 8: a tool for phylogenetic analysis and post-analysis of large phylogenies. *Bioinformatics* **30**, 1312–1313. Available at: https://academic.oup.com/bioinformatics/article-lookup/doi/10.1093/bioinformatics/btu033.

Stevens T. O. and McKinley J. P. (1995) Lithoautotrophic Microbial Ecosystems in Deep Basalt Aquifers. *Science* **270**, 450–455. Available at: https://www.sciencemag.org/lookup/doi/10.1126/science.270.5235.450.

Wang Y., Wegener G., Hou J., Wang F. and Xiao X. (2019) Expanding anaerobic alkane metabolism in the domain of Archaea. *Nat. Microbiol.* **4**, 595–602. Available at: http://www.nature.com/articles/s41564-019-0364-2.

Zhou Z., Pan J., Wang F., Gu J.-D. and Li M. (2018) Bathyarchaeota: globally distributed metabolic generalists in anoxic environments. *FEMS Microbiol. Rev.* **42**, 639–655. Available at: https://academic.oup.com/femsre/article/42/5/639/5000165.

CHAPTER 4

Tracing piezotolerant anaerobic methane oxidation in deep sub-seafloor microbial communities from IODP 370 Site C0023A in the Nankai Trough accretionary complex

Keywords: anaerobic methane oxidation, ANME, piezotolerant microorganisms

4.1 ABSTRACT

Deep marine sediments are one of the largest reservoirs of microbial biomass on Earth, but very little is known about the extent of the ecophysiological activities they play host to, particularly in high-temperature regimes. To address these unknowns, sub-seafloor sediment cores were collected during International Ocean Discovery Program (IODP) Expedition 370 from Site C0023A in the Nankai Trough accretionary complex. In this study we incubated sub-core sediment slurries from depths ranging from 257 – 865 m below seafloor for 350 days at high hydrostatic pressure (40 MPa) under approximate *in situ* temperatures with isotopically heavy methane ($^{13}CH_4$) and a variety of electron acceptors – sulfate, ferrihydrite, manganese oxide, nitrate, and nitrite – to assess for piezophilic and thermophilic anaerobic oxidation of methane (AOM). Isotopic enrichments of dissolved inorganic carbon ($\delta^{13}C_{DIC}$) from sediment slurries provided evidence for AOM *in vitro* at 40 MPa up to 80˚C, documenting the first evidence for thermophilic AOM above 70˚C and piezophilic AOM above 10 MPa. Metagenomic evidence for nitrite- and nitrate-dependent AOM was supported at 616 mbsf via the identification of *Candidatus* "Methylomirabilis oxyfera" and ANME-2d phylotype *Candidatus* "Methanoperedens nitroreducens". ANME-2d and methanogens *Ca.* "Bathyarchaeota" BA1 and BA2 were also identified from the metagenome at 257 mbsf. Fluorescent *in situ* hybridization performed on 40 MPa-recovered cells identified anaerobic methanotrophs belonging to the ANME-1 phylotype, while a 16S rRNA gene amplicon survey and maximum likelihood phylogenetic analysis revealed the presence of sister lineages to *Candidatus* "Bathyarchaeota" BE326-BA-RLH, which is thought to couple AOM to dissimilatory nitrate reduction to ammonia. This study demonstrates how we may be overlooking high-pressure regimes as habitable environments for ANMEs, providing evidence for new upper temperature and pressure records in the deep, hot biosphere.

4.2 INTRODUCTION

Anaerobic oxidation of methane (AOM) is a significant but poorly constrained biological sink in the global carbon cycle. Several studies estimate AOM is responsible for consuming ~80-90% of CH_4 produced in marine sediments (Reeburgh, 2007; Conrad, 2009; Kirschke et al., 2013). However, this may be an underestimation of the true size of the sub-seafloor AOM sink, as these fluxes have been primarily derived from modeling sulfate-methane transition zones in continental shelf sediments and are unable to account for cryptic CH_4 cycling where methanogenesis and AOM proceed simultaneously at small temporospatial scales (Egger et al., 2018; Beulig et al., 2019). Recent breakthroughs have vastly improved our understanding of the mechanisms by which AOM proceeds (Milucka et al., 2012; Sivan et al., 2014; McGlynn et al., 2015; Wegener et al., 2015), and we now know that anaerobic methane-oxidizing *Archaea* (ANMEs) are capable of utilizing electron acceptors other than sulfate, including nitrate and oxidized species of iron and manganese (Beal et al., 2009; Haroon et al., 2013; Ettwig et al., 2016; Cai et al., 2018; Leu et al., 2020). *Candidatus* "Methylomirabilis oxyfera" is the first bacterium identified to carry out AOM, oxidizing CH_4 with nitrite via an "intra-aerobic" pathway utilizing particulate methane-monooxygenase (pMMO) characteristic of aerobic methanotrophs (Ettwig et al., 2010).

Despite a growing diversity of ANME metabolisms, the extent and distribution of AOM in the high pressure, high temperature deep biosphere is seriously underexplored. Euryarchaeal ANMEs share close phylogenetic and metabolic heritage with methanogens belonging to the same phylum, including the piezophilic methanogen *Methanopyrus kandleri* strain 116, which has been shown to grow up to temperatures of 122˚C and

pressures of 40 MPa (Takai et al., 2008). An temperature limit for AOM of 72˚C was reported for Guaymas Basin hydrothermal sediments based on isotopically-labeled enrichments, and only 50˚C based on detection of ANME-1 16S rRNA gene amplicons from the same study (Holler et al., 2011). However, these incubations were performed in serum vials at 290 kPa, depressurized by nearly two orders of magnitude relative to the *in situ* pressure from where the samples were collected. ANME-2c have been enriched up to 10.1 MPa at 20˚C from Eckernförde Bay sediments, 50 times higher than the *in situ* pressure at the site of collection (Timmers et al., 2015). It is clear that much remains unknown about the temperature and pressure limits of anaerobic methanotrophy.

In this study we follow thermodynamically favorable outputs from geochemical modeling to investigate the potential of biological AOM to occur at high temperatures and hydrostatic pressures representative of the deep sub-seafloor biosphere of the Nankai Trough. To accomplish this, we performed $^{13}CH_4$ tracer incubations on sub-seafloor sediments ranging from 257 – 865 m below seafloor (4900 m water depth), collected from International Ocean Discovery Program (IODP) Site C0023A, drilled during IODP Expedition 370: The Temperature Limit of the Deep Biosphere off Muroto (Hinrichs et al., 2016). Sediments were incubated in sulfate-free artificial seawater medium for 350 days at 40 MPa under approximate *in situ* temperatures with 10 mM of SO_4^{2-}, Fe^{3+}, Mn^{4+}, NO_3^-, or NO_2^-, in addition to control incubations with no added oxidant and autoclaved kill controls. Measurements of the stable isotopic composition of dissolved inorganic carbon (DIC) were coupled with 16S rRNA gene sequencing and fluorescent *in situ* hybridization (FISH) and referenced to *in situ* geochemistry at Site C0023A to identify evidence of active, microbially-mediated under pressure and temperature conditions

faithful to the deep sub-seafloor biosphere of the Nankai Trough. Parallel to these high pressure incubation experiments, we performed AOM enrichments on sediment samples from 257 and 616 mbsf, investigating the same electron acceptor conditions and temperatures as the high pressure enrichments, but at 0.15 MPa and with natural abundance CH_4. From these enrichments we measured isotopic shifts in two clumped isotopes of methane – $^{12}CH_2D_2$ and $^{13}CH_3D$ – and also performed metagenomics.

4.3 MATERIALS AND METHODS

4.3.1 ***Site C0023A description, Nankai Trough accretionary complex***. IODP Expedition 370: T-Limit of the Deep Biosphere off Muroto was designed around the question of elucidating the upper temperature limit of microbial life in the deep oligotrophic sub-seafloor (Hinrichs et al., 2016). Site C0023A is located in the Nankai Trough on the subduction boundary between the Philippine Sea and Eurasian plates (N 32.367˚, E 134.978˚), encompassing a gradual temperature gradient ranging from ~ 2˚C at the sediment/seafloor interface to ~130˚C at the basement (Figure 4.1). Beginning at 4776 m water depth, drilling was performed between 10 September and 10 November 2016, recovering 112 cores between 189 and 1180 m below sea floor (mbsf). Downhole temperature logging was performed down to 410.5 mbsf using an advanced piston corer temperature tool (APCT-3) (Heesemann et al., 2006) and used to infer a temperature model at depth, *d*:

$$T_d = d^2\left(-1.69 \times 10^{-5}\right) + 0.113663d + 10 \qquad (4.1)$$

where *T* is in ˚C and *d* is in mbsf. A thorough account of drilling operations is described in the expedition methodology report (Morono et al., 2017). Geochemical profiles of

major gases and aqueous species from Site C0023A are presented in Figure 4.2 and are publicly available at http://sio7.jamstec.go.jp/j-cores.data/370/C0023A/. Detailed information regarding lithostratigraphy, structural geology, and geochemistry can be found in the post-cruise preliminary report (Heuer et al., 2017).

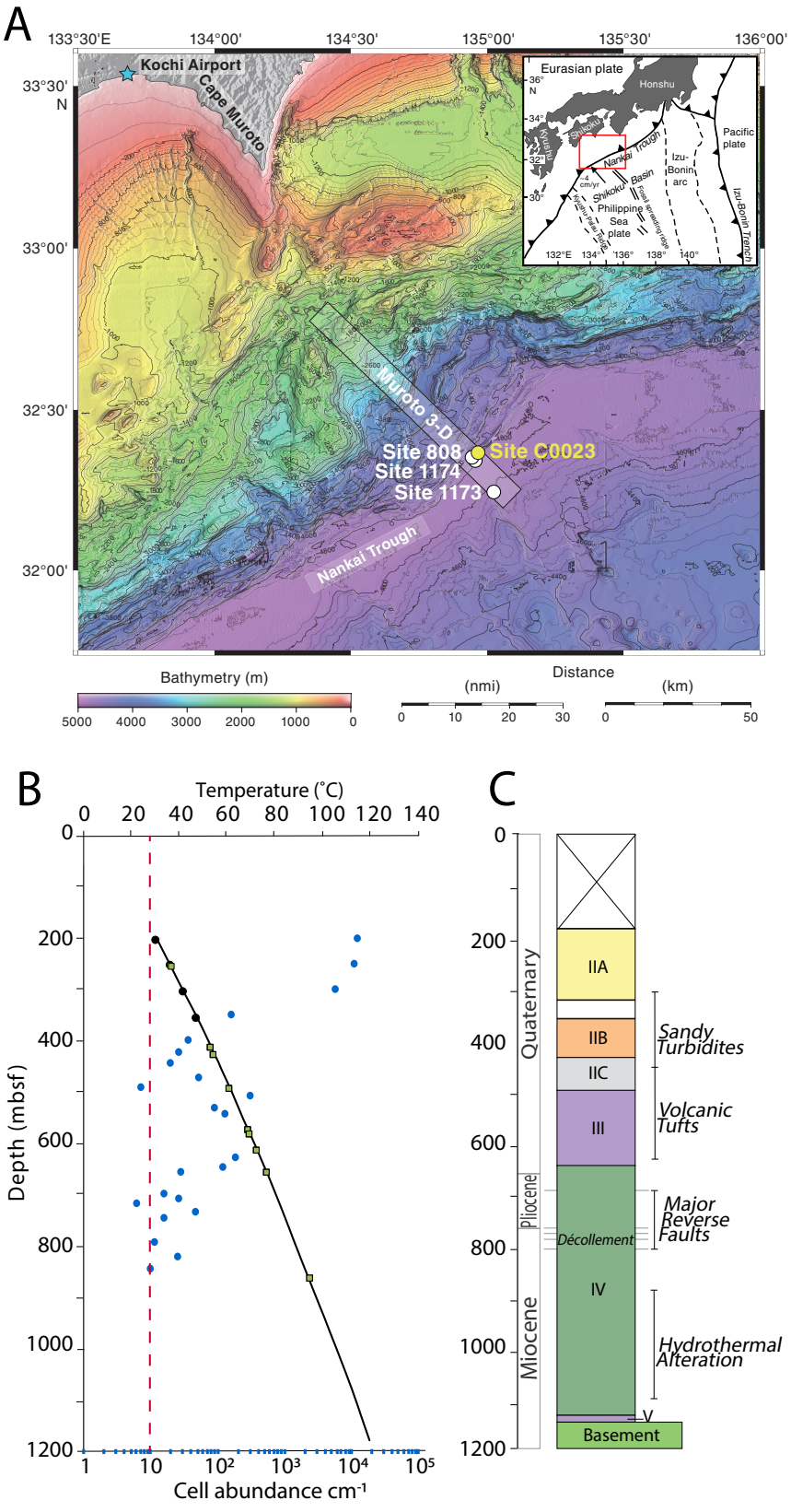

Figure 4.1. **(A)** Regional bathymetry map around IODP 370 Site C0023A and neighboring ODP drilling sites (white text). Inset: Plate configuration of the region with the bathymetry map area outlined in red. **(B)** Downhole temperature, and cell abundance profile of Site C0023A. Black dots indicate *in situ* temperature measurements taken at the time of drilling. Core sediments of depths investigated in this study are indicated by green squares. Projected temperature profile (black line) inferred using Eq. (1). Shipboard cell counts represented by blue circles. Red dashed line indicates the minimum quantification limit (MQL) for statistically meaningful values. **(C)** Litho-stratigraphy of Site C0023A. Major formations are indicated by Roman numerals. IIA, Axial trench wedge facies; IIB, Outer trench wedge facies; IIC, Trench-to-basin facies; III, Upper Shikoku Basin facies; IV, Lower Shikoku Basin facies; V, Acidic volcaniclastics. Figure modified from Heuer, V.B. et al. (2017) with permission.

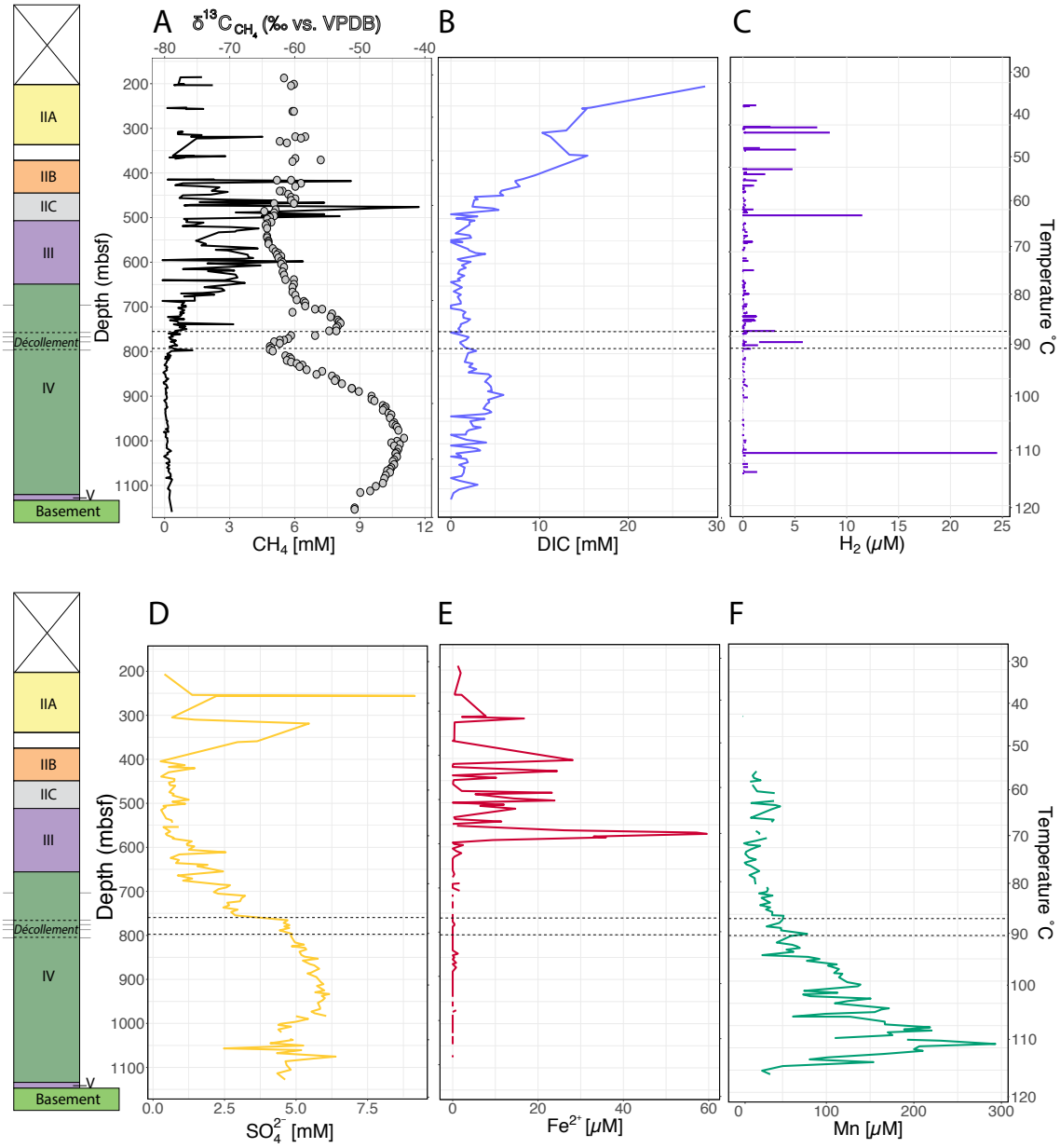

Figure 4.2. Geochemical profiles at Site C0023A for **A)** CH_4 (black) and $\delta^{13}C_{CH_4}$ (grey circles), **B)** dissolved inorganic carbon (DIC), **C)** H_2, **D)** sulfate, **E)** dissolved ferrous iron, and **F)** dissolved manganese. Stratigraphy for reference. Isotopic composition of methane is referenced relative to the Vienna Pee Dee Belemnite standard (VPDB). Data are available at http://sio7.jamstec.go.jp/j-cores.data/370/C0023A/.

4.3.2 ***Shipboard processing of microbiological core samples***. Samples dedicated to microbiological investigations were selected from parent core material by passing a rigorous multistep protocol to ensure minimal risk of contamination (Morono et al., 2017). Briefly, freshly retrieved core sections were visually inspected and subjected to X-ray computed tomography (CT scans) to quickly filter out any intervals containing obvious fractures or drilling disturbances (Tonai et al., 2019). Passing core material was aseptically processed to cut WRC segments (~30 cm length) within four hours of arrival on deck. Using autoclaved spatulas, outer layers were mechanically shaved off WRC surfaces to remove contaminating drilling fluid, which was indicated by a perfluorocarbon tracer. WRCs were packed in ethanol-cleaned, UV-sterilized packaging inside a UV-sterilized anaerobic chamber (95:5 (v/v) N_2:H_2 atmosphere; Coy Laboratory Products Inc., Grass Lake, MI USA) containing a tabletop air filtration unit (KOACH T 500-F; MGN International Inc., Temecula, CA USA) and ionizer (Winstat BF-X2MB; Shishido Electrostatic Ltd., Tokyo, Japan) to reduce static attraction of potentially contaminating airborne particles. Interior surfaces of the glove bag were routinely decontaminated with RNase *AWAY*™ (ThermoFisher Scientific, Waltham, MA USA) and irradiated with UV light. Working surfaces were replaced with a fresh sheet of aluminum foil between samples. Shipboard counts of contaminant airborne particles and microbial cells were performed at regular intervals in core-processing locations throughout the duration of the cruise. Drilling fluid was also collected from the delivery pump, preparation tank, and core surfaces for biological and chemical contamination analyses. Packaged WRCs were shipped to shore on ice by helicopter for immediate cell enumeration at the Kochi Core Center (KCC) in Kochi, Japan. WRC samples intended

for the high-pressure AOM tracer experiment described in this study were shipped overnight on blue ice to Princeton University for storage in the dark at 4˚C for two weeks and then shipped overnight on blue ice to the Scripps Institution of Oceanography at UCSD. Samples were stored in the dark at 4˚C for future processing. The WRCs utilized in this study originated from 257, 414, 429, 496, 574, 583, 616, 659, and 865 mbsf (Figure 4.1B).

4.3.3 ***Vegetative cell and endospore counts***. WRC samples dedicated to *in situ* cell counts were transferred to an International Organization for Standards (ISO) Class I ultra-clean room at KCC for processing as described in Morono et al. (2017). To minimize potential contamination, ~ 5mm of the outer surface of pre-scraped WRCs were aseptically shaved off with a sterilized ceramic knife on 500˚C-combusted aluminum foil inside a Coy anaerobic chamber as described above. Approximately 10 cm^3 of sediment was collected from each WRC interior and powderized with a 500˚C-combusted mortar and pestle before transfer into a sterile 50 mL centrifuge tube. Sediments were fixed at 4˚C for 6 hours in a 20 mL suspension of 3% (w/v) NaCl and 10% (v/v) formalin. Samples were homogenized by vortexing and slurries were subjected to a Nycodenz density gradient separation to detach cells from the matrix (Morono et al., 2017). The entire aqueous layer was collected and filtered onto 0.22 μm polycarbonate filters and stained in SYBR™ Green I DNA stain according to the manufacturer's protocol (ThermoFischer Scientific). Total vegetative cell counts were obtained photomicroscopically via direct counts (Inagaki et al., 2015) on a BX-51 Olympus epifluorescent microscope (Olympus Corporation, Tokyo Japan) equipped with a cooled

ORCA-AG CCD camera (Hamamatsu photonics K.K., Osaka, Japan), an in-house automatic slide loader (Morono et al., 2009; Morono and Inagaki, 2010) and MetaMorph v.7.5 software (Molecular Devices, Downington, PA, USA). SYBR-I was excited with a 490/20 nm band-pass filter and emission was detected on a 528/38 nm filter. Automated cell counting was performed as previously described (Morono et al., 2009).

Bacterial endospores were enumerated from 79 WRCs spanning 256 – 1122 mbsf at Site C0023A. At each depth, the diagnostic endospore biomarker dipicolinic acid (DPA) was extracted from WRC sediment in biological duplicates and stored in 4 mL Tris buffer (0.2 M, pH 7.6). One replicate was spiked with a 200 nM DPA standard to quantify low concentrations of DPA below this detection limit (Heuer et al., *in prep*). DPA signatures were detected using high performance liquid chromatography (HPLC) following an established protocol (Fichtel et al., 2007b), normalized to source sediment mass, and converted to spore counts (2.2×10^{-16} mol DPA spore^{-1}) (Fichtel et al., 2007).

4.3.4 ***16S rRNA gene amplicon sequencing and analysis of inoculum***. WRC samples intended for DNA extraction were immediately stored upon arrival at KCC at -80˚C until further processing. DNA was extracted from 5 g of frozen inner WRC material using gamma irradiated components of a PowerLyzer PowerSoil DNA Isolation Kit following the manufacturer's instructions (MO BIO Laboratories, Carlsbad, CA USA). Isolated DNA was concentrated via ethanol precipitation as previously described (Inagaki et al., 2015), eluted into 50 µL 1X TE buffer, and stored at -20˚C until further processing.

To determine microbial community composition, V4 regions of bacterial and archaeal 16S rRNA genes were PCR-amplified using the 515F/806R universal primer set

(Caporaso et al., 2012; Hoshino and Inagaki, 2012; Hoshino and Inagaki, 2017). PCR reaction mixtures (25 μL) were prepared using 2× MightyAmp DNA polymerase Ver.3 and associated dNTP buffer according to the manufacturer's protocol (TaKaRa Bio, Shiga, Japan). Each mixture contained 2 μL template DNA and 0.3 μM forward and reverse primers. PCR was initiated on either a Veriti Thermal Cycler or StepOnePlus Thermal Cycler (ThermoFisher Scientific) at 98˚C for 2 minutes, followed by 35 denaturation cycles at 95˚C for 5 seconds, 55˚C annealing cycles for 15 seconds, and 68˚C extension for 30 seconds. Amplification products were purified using AMPure XP beads (Beckman Coulter Inc., Brea, CA USA) and then transferred into a new PCR reaction mix containing 515F/806R-MiSeq barcoded primers (Walters et al., 2011) and KAPA HiFi Hot-Start DNA polymerase according to the manufacturer's instructions (F. Hoffmann-La Roche, Ltd., Basel, Switzerland). A second PCR amplification was performed using an initial denaturation at 95˚C for 3 minutes, followed by 10 cycles of 30-second denaturation at 95˚C, 30-second annealing at 55˚C, 30-second elongation at 72˚C, and final elongation at 72˚C for 5 minutes. PCR products were purified twice using AMPure XP beads and DNA concentration was measured using a NanoDrop 3300 fluorospectrometer and PicoGreen (ThermoFisher Scientific). Purified amplification products were pooled at equal molar ratios and were sequenced for 600 cycles (2 x 300 bp) on a MiSeq platform (Illumina Inc., San Diego, CA USA) located at KCC. Microbial community profiling was assessed using QIIME v.1.9.1 (Caporaso et al., 2012), where operational taxonomic units (OTUs) were clustered with a 97% sequence similarity cutoff using UPARSE (Edgar, 2013), and taxonomy was assigned referencing the SILVA release 132 database (Quast et al., 2012). The vegan v.2.5-2 package in R (Oksanen et al.,

2019) was used to assess OTU richness and evenness at each depth, where Shannon diversity indices (H) were calculated following Lemos et al. (2011),

$$H = -\sum_{i=1}^{n} (p_i \ln p_i) \tag{4.2}$$

where n is the number of OTUs and p_i is the proportion of the microbial community represented by OTU i.

A maximum likelihood phylogenetic tree was constructed using RAxML v.8.2.11 (GTRCAT mode, 100 nonparametric bootstrapping iterations) (Stamatakis, 2014) for identified *Archaea* sequences and 74 reference 16S rRNA gene sequences obtained from NCBI GenBank. The deep biosphere bacterium *Ca*. "Desulforudis audaxviator" MP104C (Chivian et al., 2008) was selected as the taxonomic outgroup to root the tree.

4.3.5 ***Free energy model of AOM reactions at site C0023A***. To assess the thermodynamic favorability of CH_4 metabolisms within the geochemical constraints of each investigated depth at Site C0023A, we calculated the *in situ* Gibbs free energy yield (ΔG_{rxn}) of hydrogenotrophic methanogenesis, reverse methanogenesis, and five AOM redox reactions (Table 4.1; Figure 4.5) using The Geochemists Workbench® v.8.0.5 (Aqueous Solutions LLC, Champaign, IL USA). For each depth investigated in the high-pressure AOM tracer study, we calculated ΔG_{rxn} for each metabolism within the constraints of the *in situ* temperature, geochemistry, and dissolved gas concentrations reported in the expedition's data repository, publicly accessible at http://sio7.jamstec.go.jp/j-cores.data/370/C0023A/. Aqueous species reported with concentrations below the detection limit were assigned with a 0.1 μM value in the model. If a measurement was not made for a particular species, the value from the next closest

depth was adopted into the model. Pyrolusite (MnO_2) and $Fe(OH)_3$ were swapped as solid mineral phases of Mn^{4+} and Fe^{3+}, respectively. Detailed geochemical constraints for each depth can be found in Table 4S.3.

Table 4.1. Net redox reactions modeled for Site C0023A.

$$H^+ + HCO_3^- + 4H_2 \leftrightarrow CH_4 + 3H_2O$$

$$CH_4 + 3H_2O \leftrightarrow H^+ + HCO_3^- + 4H_2$$

$$SO_4^{2-} + CH_4 + H^+ \leftrightarrow H_2S + HCO_3^- + H_2O$$

$$8NO_2^- + 3CH_4 + 5H^+ \leftrightarrow 3HCO_3^- + 4N_2 + 7H_2O$$

$$8NO_3^- + 5CH_4 + 3H^+ \leftrightarrow 5HCO_3^- + 4N_2 + 9H_2O$$

$$4MnO_2 + CH_4 + 7H^+ \leftrightarrow HCO_3^- + 4Mn^{2+} + 5H_2O$$

$$8Fe(OH)_3 + CH_4 + 15H^+ \leftrightarrow HCO_3^- + 8Fe^{2+} + 21H_2O$$

4.3.6 *$^{13}CH_4$ tracer microcosm experiment at high hydrostatic pressure*.

Microcosms were set up inside an anaerobic glove bag (Coy Laboratory Products, Grass Lake, MI USA) under a 5:95 H_2:N_2 atmosphere. Fresh aluminum foil was placed on the working surface of the glove bag and ethanol-sterilized nitrile gloves were used over the glove bag's butyl rubber gloves to minimize potential contamination of low-biomass samples. The surface of each C0023A WRC was scraped using an ethanol-sterilized scalpel to remove sediment exposed to KCC's anaerobic packaging. For each WCR, ~ 1 g (wet weight) of freshly exhumed interior sediment was transferred into high-pressure modified Hungate tubes (Figure 4.3; Bowles et al., 2011) containing 5 mL anoxic sulfate-free artificial seawater medium at pH 8.0 (Widdel and Bak, 1992; Holler et al., 2011) and

supplemented with 10 mM (final concentration) of one of the following electron acceptors: SO_4^{2-}, NO_2^-, NO_3^- , Mn^{4+} (in the form of MnO_2), or Fe^{3+} (in the form of $Fe_2O_3 \bullet H_2O$), in addition to a no-added oxidant control. $Fe_2O_3 \bullet H_2O$ and MnO_2 were synthesized as previously described (Cornell and Schwertmann, 2003; Händel et al., 2013). The headspace of each microcosm was replaced with 2:98 $^{13}CH_4$:N_2 (1 atm), prepared by mixing via gas-tight syringes (Trajan Scientific and Medical, Melbourne, Australia) in sealed Tedlar® bags (DuPont, Wilmington, DE USA). An autoclaved kill control was included at each assessed depth for both sites as a reference for determining significant biological AOM. All treatments were assessed in biological triplicate.

Microcosms were inverted and placed inside stainless-steel hydrostatic vessels with a pin-retained piston closure pre-heated in gravity ovens to approximate *in situ* temperatures (Table 4S.1; see Figure 4.1B for reference temperature profile). Vessels were sealed and pressurized to 40 ± 0.5 MPa using a hydrostatic pump as previously described (Yayanos, 1995) and subsequently returned to gravity ovens for incubation. Subsamples of the enrichments were collected at 0, 14, 60, 200, and 350 days to monitor CH_4 concentrations and the evolution of $\delta^{13}C_{DIC}$. Briefly, hydrostatic vessels were removed from ovens and depressurized for retrieval of Hungate tube microcosms. From each sample, a 500 µl aliquot of the slurry was anaerobically transferred using Ar-sparged syringes and needles into combusted borosilicate serum vials pre-treated with saturated $HgCl_2$ to kill any microbes contained in the sample (Sherwood Lollar et al., 1993a; Sherwood Lollar et al., 1993b). Vials were sealed under a 100% N_2 atmosphere with crimped 0.1 NaOH-treated butyl rubber stoppers (Bellco Glass, Inc., Vineland, NJ USA). Following sample transfer, serum vials were over-pressurized with N_2 gas to

minimize the risk of mixing with atmospheric CO_2. To exsolve all DIC out of solution, vials were supplemented with 100 µL of 0.5 N H_3PO_4, and heated overnight in a water bath at 70˚C. CH_4 concentrations and $\delta^{13}C_{DIC}$ were analyzed from the headspace using a Picarro cavity ringdown spectrometer equipped with a G2101-I Isotopic CO_2 analyzer (Picarro, Inc., Sunnyvale, CA USA). Resulting isotopic values were calculated according to

$$\delta^{13}C_{DIC} = \left(\frac{\left(\frac{^{13}C_{DIC}}{^{12}C_{DIC}} \right)_{sample}}{\left(\frac{^{13}C_{DIC}}{^{12}C_{DIC}} \right)_{standard}} - 1 \right) \times 1000 \text{ ‰} \quad (4.3)$$

with respect to the [$^{13}C/^{12}C$] ratio of the Vienna Pee Dee Belemnite standard. AOM was determined to have a significant influence on $\delta^{13}C_{DIC}$ in a given treatment if its average $\delta^{13}C_{DIC} \pm$ standard deviation (SD) was greater than the average $\delta^{13}C_{DIC}$ + 3 × SD of the kill control ($\delta^{13}C_{DIC_{d.kill}}$) for the same depth.

DIC production rates (r_{DIC}) for each sample were calculated according to

$$r_{DIC}\ (\text{pmol cm}^{-3}\text{day}^{-1}) = \frac{\left(\frac{\delta^{13}C_{DIC_d} - \delta^{13}C_{DIC_{d.kill}}}{\delta^{13}C_{^{13}CH_4} - \delta^{13}C_{DIC_{d.kill}}} \right) DIC_d \left(\frac{\rho_d}{g_d} \right)}{t} \quad (4.4)$$

where DIC_d is the sum of $^{13}C_{DIC}$ and $^{12}C_{DIC}$ in pmol at depth d, ρ_d is the bulk density of the sediment at depth d in grams cm^{-3} (http://sio7.jamstec.go.jp/j-cores.data/370/C0023A/), and g_d is the grams of sediment incubated from depth d, and t is the number of days of incubation.

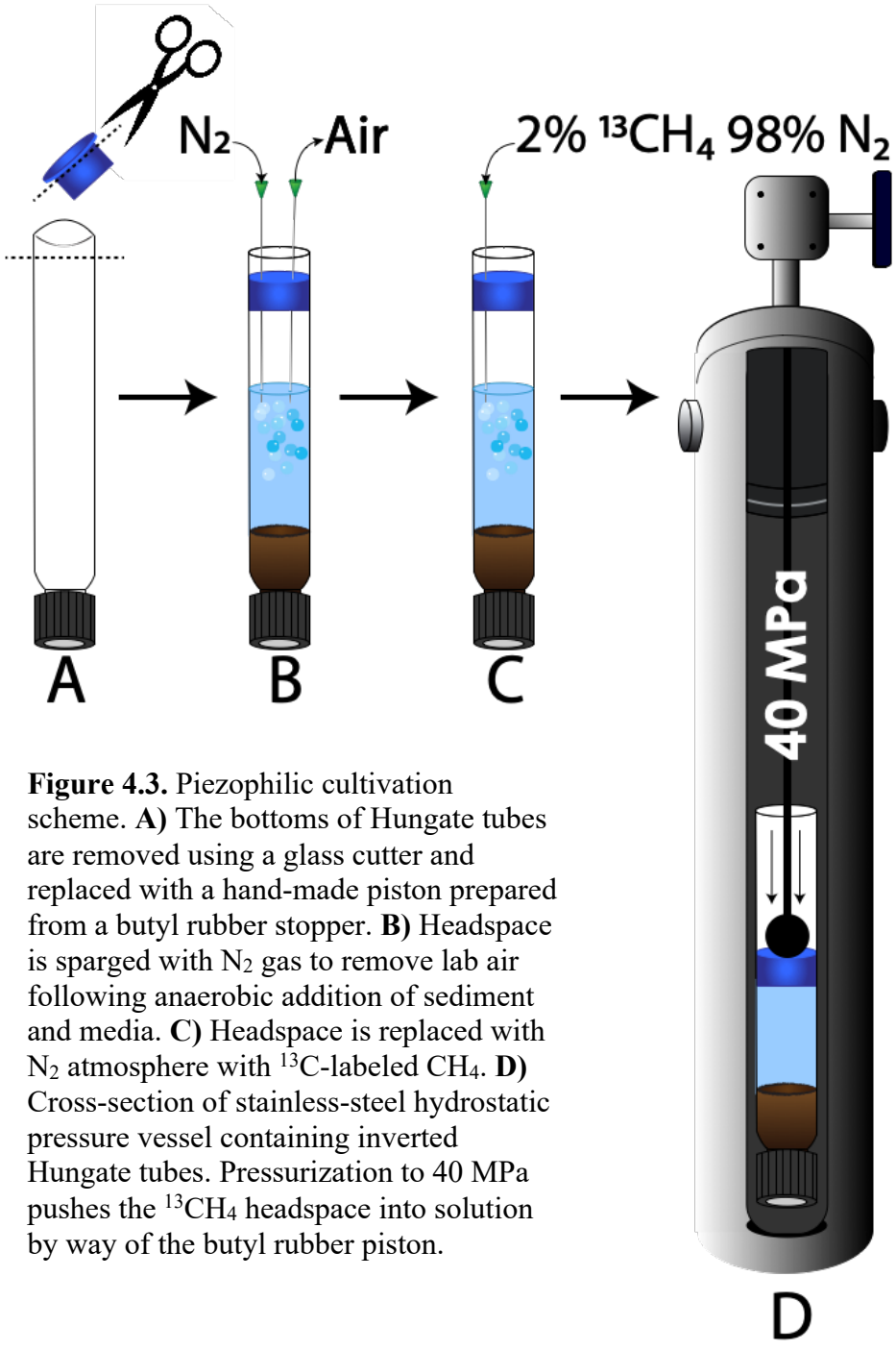

Figure 4.3. Piezophilic cultivation scheme. **A)** The bottoms of Hungate tubes are removed using a glass cutter and replaced with a hand-made piston prepared from a butyl rubber stopper. **B)** Headspace is sparged with N_2 gas to remove lab air following anaerobic addition of sediment and media. **C)** Headspace is replaced with N_2 atmosphere with ^{13}C-labeled CH_4. **D)** Cross-section of stainless-steel hydrostatic pressure vessel containing inverted Hungate tubes. Pressurization to 40 MPa pushes the $^{13}CH_4$ headspace into solution by way of the butyl rubber piston.

4.3.7 ***Microcosm sample preservation for fluorescent in situ hybridization (FISH).*** Subsamples from $^{13}CH_4$ tracer microcosms were collected and fixed for downstream fluorescent *in situ* hybridization (FISH). The fluid fraction of C0023A

sediment slurries were centrifuged at 2,000 × g for 5 minutes to pellet planktonic cells. The supernatant was pipetted off and cells were fixed according in a 1:1 mixture of chilled absolute ethanol and 1× phosphate buffered saline (PBS) and stored overnight at -20˚C. Fixed samples were then filtered and washed through 0.2 µm polycarbonate membrane filters (Whatman International Ltd., Maidstone, UK) using nuclease-free water. As a final step, absolute chilled ethanol was filtered through samples, which were left to air dry in a laminar flow hood. Filters were stored at -20˚C until further processing.

Sediments subsamples from the microcosm experiments were fixed following an established protocol (Llobet-Brossa et al., 1998). Freshly prepared, 0.2 µm filtered formalin was diluted in filter-sterilized 1× PBS to a final concentration of 4% (v/v). Sediment slurries were submerged in the 4% formalin solution for 2 hours at room temperature. Following fixation, samples were centrifuged at 16,000 × g for 5 minutes. The supernatant was poured off and sediments were washed 3 times with 1× PBS (pH 7.6), centrifuging at 16,0000 × g for 5 minutes between washed. After the final washing step, fixed sediments were stored in a 1:1 PBS:ethanol mix at -20˚C until further processing.

ANMEs from AOM enrichments were visualized by coupling FISH-TAMB (Harris et al., 2017) to 16S rRNA FISH (e.g., Karner and Fuhrman, 1997; Williams et al., 1998; Christensen et al., 1999; Pernthaler et al., 2002). Briefly, enrichment aliquots were anaerobically incubated with 1 µM Cy5-labeled FISH-TAMB probes modified from a reverse primer targeting the alpha subunit of methyl coenzyme-M reductase (*mcr*A) in methanogens and ANMEs belonging to the *Euryarchaeota* (Steinberg and Regan, 2008). Following FISH-TAMB treatment, cells were fixed according to the planktonic fixation

protocol described above. Samples were hybridized following an established protocol (Glöckner et al., 1996) with 50 ng μl^{-1} dual- labeled oligonucleotide probes (Biomers.net, Ulmer, Germany; ATTO-TEC GmbH, Siegen, Germany) specific to *Archaea* belonging to the ANME-1 (Boetius et al., 2000) and ANME-2 (Boetius et al., 2000; Orphan, 2001; Hatzenpichler et al., 2016), as well as *Candidatus* "Methylomirabilis oxyfera" belonging to NC-10 *Bacteria* (Ettwig et al., 2008). Approximate cell counts were obtained by counterstaining each filter with 1 μM of the DNA stain 4,6-diaminidino-2-phynylindole (DAPI). Probe sequences and associated fluorophores are described in Table 4S.2.

Cells were imaged using an Olympus BX60 epifluorescence microscope outfitted with a mercury burner and a tungsten-halogen lamp for excitation. Cells were imaged in brightfield and filtered transmitted light as appropriate for the emission spectra of fluorescent dyes (Table 4S.2). Individual filter cube sets were specific to DAPI (352 – 477 nm), FITC (590 – 650 nm), TRITC (532 – 613 nm), and Texas Red (633-738 nm).

4.3.8 ***Natural abundance CH_4 incubations for metagenomics.*** Parallel to the 40 MPa experiments, 0.15 MPa AOM enrichment microcosms were prepared from 257 and 616 mbsf WRC sediments. For each assessed depth, 10 g (wet weight) triplicates of WRC interior sediment were weighed out and transferred into combusted 160-mL borosilicate serum vials containing 100 mL anoxic artificial sulfate-free seawater media (Widdel and Bak, 1992; Holler et al., 2011). Serum vials were sealed with 0.1 N NaOH-boiled butyl rubber stoppers (Bellco Glass, Inc., Vineland, NJ USA) and silver aluminum crimps (Supelco Inc., Bellefonte, PA USA), and the headspace was subsequently replaced with 100% natural abundance CH_4 to a final pressure of 1.5 atm (0.15 MPa). Each incubation

was supplemented with 10 mM of either SO_4^{2-}, NO_3^-, NO_2^-, Mn^{4+}, or Fe^{3+} as described above. A no-added oxidant control was included to assess endogenous AOM activity from remnant oxidants available in the inoculum, and an autoclaved sample was included as a kill control. Serum vials containing were incubated upside-down in gravity ovens at approximate *in situ* temperatures (257 mbsf at 40˚C; 616 mbsf at 70˚C). Oxidant depletion was monitored using a Dionex IC25 ion chromatograph coupled to an MSQ-quadruple mass spectrometer (Thermo Scientific, Waltham, MA USA).

After 500 days' continuous incubation, total DNA was extracted from single biological replicates from each electron acceptor condition using the Qiagen DNeasy PowerSoil Kit (Qiagen Sciences, Inc., Hilden, Germany) and accompanying protocol. DNA was concentrated via ethanol precipitation, wherein 0.2 mL of 5M NaCl was added to each 5 mL elution and the volume was inverted 5 times to mix. Next, 10.4 mL of chilled absolute molecular grade ethanol was added and mixed by gentle inversion 5 times. Mixtures were centrifuged in 50 mL Falcon tubes (Corning, Inc., Corning, NY USA) at 15,000 × g for 30 minutes. Liquid was subsequently decanted, the pellet was washed with chilled 70% molecular grade ethanol, and Falcon tubes were left to dry inside a UV-irradiated laminar flow hood. DNA was resuspended in 100 µL 1× TE buffer and quantified using a Qubit 1× high sensitivity dsDNA assay kit on a Qubit 2.0 analyzer following the manufacturer's instructions (ThermoFisher Scientific, Waltham, MA USA). Low DNA yields for several samples (Table 4S.4) resulted in needing to pool and re-concentrate DNA via ethanol precipitation again to have enough material for metagenomic sequencing.

Two metagenome libraries, one for 257 mbsf and one for 616 mbsf, comprised

AOM enrichments for SO_4^{2-}, NO_3^-, NO_2^-, Mn^{4+}, Fe^{3+}, and no-added oxidant controls, were prepared using a PrepX DNA library kit and an automated Apollo 324 system (WaferGen Biosystems, Inc., Fremont CA USA). Paired-end (2 x 100 nt) DNA sequencing was performed on a HiSeq 2000 platform (Illumina, Inc., San Diego, CA USA) located at the Marine Biological Laboratory in Woods Hole, MA USA. Quality filtering of sequenced reads and subsequent metagenome assembly and annotation was performed as described in Chapter 1.

4.4 RESULTS & DISCUSSION

4.4.1 ***AOM reactions are exergonic at site C0023A***. Despite significant differences in *in situ* geochemistry (Figure 4.2, Table 4S.3), each investigated depth yielded exergonic ΔG_{rxn} values for AOM net reactions coupled to available electron acceptors. This included depths greater than 574 mbsf, where the *in situ* temperature exceeds 70˚C, presently the highest temperature where AOM activity has been recorded (Holler et al., 2011). Assuming a microbial cell requires a minimum of -20 kJ/mol $2e^-$ free energy change from a reaction to generate ATP (Schink, 1997), any inhabitant ANMEs at Site C0023A performing AOM would fall either right on the so-called "thermodynamic limit" (e.g. sulfate-dependent AOM) or well above it (Figure 4.4). Mn(IV)-, nitrite-, and nitrate-dependent AOM reactions were highly exergonic (≤ -100 kJ/mol $2e^-$) throughout the depth profile, even when the coupled electron acceptor was limiting (e.g. 0.1 μM inputs for NO_2^- or NO_3^-). Fe(III)-dependent AOM also proceeded favorably at each investigated depth.

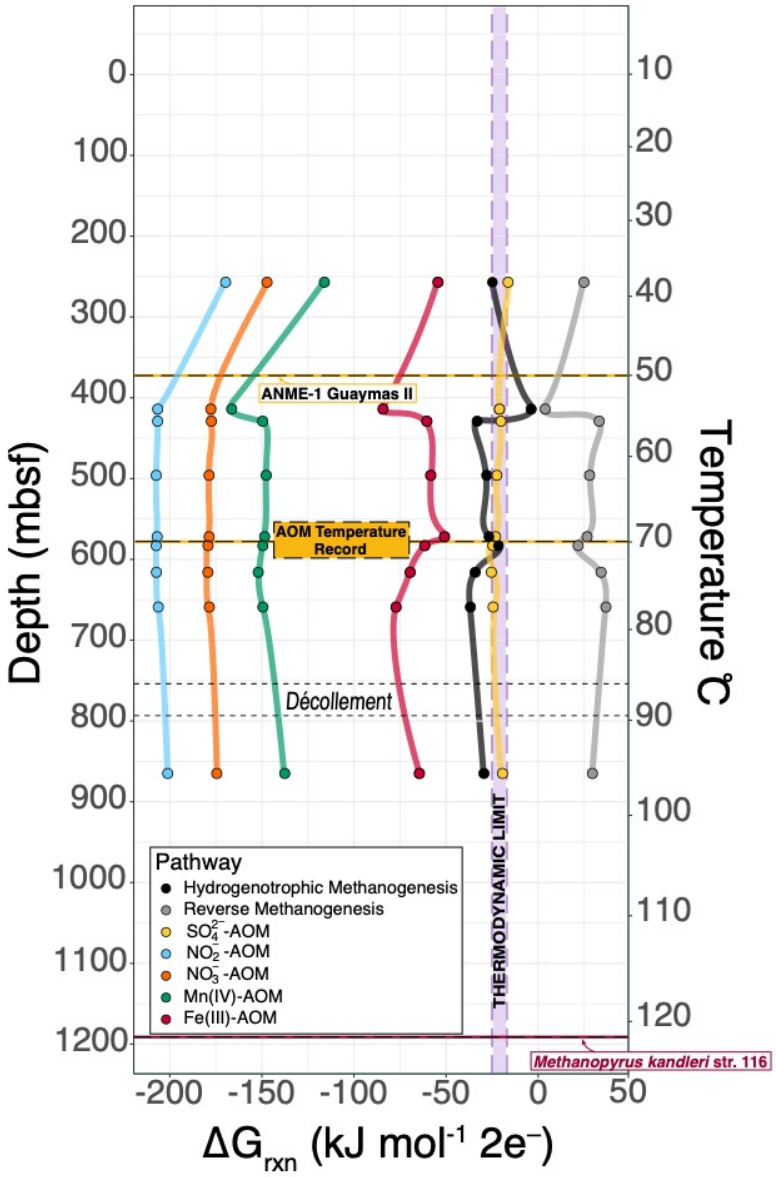

Figure 4.4. ΔG_{rxn} for hydrogenotrophic methanogenesis, reverse methanogenesis, and five proposed AOM pathways coupled to known mediating electron acceptors at Site C0023A. Geochemical constraints for each investigated depth were derived from the IODP Expedition 370 post-cruise report. Optimal growth temperatures of the most heat-tolerant methanogen, *Methanopyrus kandleri* strain 116 (Takai et al., 2008), and ANME phylotype (ANME-1-Guayamas II) (Holler et al., 2011) are referenced by colored dashed lines at their respective highest recorded temperatures. Line at 70˚C represents known upper temperature limit of AOM activity (Holler et al., 2011).

High concentrations of CH_4 with depleted carbon isotopic signatures ($\delta^{13}C_{CH_4}$) were available throughout much of the depth profile (Figure 4.2A). At depths shallower than ~700 mbsf, the $\delta^{13}C_{CH_4}$ averaged -61.3 ± 3.0 ‰, indicating formation via biogenic methanogenesis (Figure 4.2A). This interpretation is consistent with our thermodynamic model's predictions that hydrogenotrophic methanogenesis had free energy yields above

the thermodynamic limit (with the exception of two depths, 414 and 583 mbsf) (Figure 4.4). A positive excursion of the $\delta^{13}C_{CH_4}$ peaking around ~730 mbsf coincides with a deep sulfate-methane transition zone (SMTZ) (Figure 4.2A,D), and has been interpreted as isotopic evidence for *in situ* thermophilic sulfate-dependent AOM (Heuer et al., *in prep*). For the depths investigated in our high pressure incubations, the ΔG_{rxn} of sulfate-dependent AOM stays relatively constant on the thermodynamic limit (Figure 4.4). Previous studies have shown this phenomenon is closely tied to competition between hydrogenotrophic microorganisms for H_2 in anoxic marine sediments, forcing terminal metabolic reactions utilizing the most predominant electron acceptors to operate right at the thermodynamic limit (Lovley et al., 1982; Lovley and Goodwin, 1988; Hoehler et al., 1994; Hoehler et al., 1998). This is certainly reflected in the geochemistry of C0023A. For each depth assessed in our thermodynamic model, sulfate was the most abundant electron acceptor and H_2 concentrations were low (nM range) relative to other intervals of the depth profile (Figure 4.2C,D; Table 4S.3).

The large free energy yields of many of these reactions confirmed our expectations that AOM should be possible under high temperature and pressure conditions, even when the oxidant coupled to AOM is in low concentration (e.g. 100 nM). Based on the results of this model, we anticipated observing isotopic evidence of AOM activity (i.e. ^{13}C enrichment of the DIC pool) at all depths in our high-pressure incubation experiment.

4.4.2 ***Distributions of vegetative cells and endospores at site C0023A***. Initial cell counts from WRC sediments yielded *in situ* cell concentrations several order of

magnitude lower than previous reports from nearby Site 1174, drilled during ODP Leg 190 (Moore et al., 2001). At site C0023A, intact vegetative cells were detectable throughout the depth profile in very low abundance (< 10^4 cells cm^{-3}) down to ~ 600 mbsf, beyond which counts were lower than the minimum quantitative limit (MQL) (10 cells) to be statistically meaningful. Cell concentrations rose above the MQL just above the décollement ~ 800 mbsf (Figure 4.1B) (Heuer et al., 2017). Initial cell counts for WRC sediment analyzed in this study were highest in sediments from 257 mbsf (~ 2.31 × 10^4 cells cm^{-3}) but dropped within the range of 10^2 or fewer cells cm^{-3} (Table 4.2) for all other investigated depths. The meaningful quantitative limit (MQL) was defined as 10 cells, and the sediment sample from 616 mbsf recorded the minimum detection limit (MDL) of 1 cell, falling within a putative "lifeless zone" at depths between ~70 – 75˚C. This drop in microbial abundance co-occurs with the lithological boundary of the Upper and Lower Shikoku Basins (Units III and IV, respectively), where an abundance of tuff layers, mechanical strengthening of the formation, and increased porewater Li^+ concentrations point to *in situ* mineral alteration, possibly driven by hydrothermal fluid flow from a deeper source (Heuer et al., *in prep*; Horsfield et al., 2006).

Whereas vegetative cell counts drop by more than two orders of magnitude below 257 mbsf, bacterial endospores remain in high abundance (~10^5 endospores cm^{-3}) down to 574 mbsf. At depths of 574, 616, and 865 mbsf, endospore estimates drop below the methodological detection limit of 2.2 × 10^4 spores cm^{-3}, but in between rise above 10^5 spores cm^{-3} just above the décollement at 659 mbsf (Table 4.2). Rates of microbial bio- and necromass turnover in the deep sub-seafloor have been shown to be significantly influenced by temperature. Recent model calculations of D:L aspartic acid racemization

have estimated surprisingly fast vegetative cell turnover times in deeply buried, 1.4 million year-old marine sediments from the Peru Margin – on the order of years to decades (Braun et al., 2017). However, at 2.4˚C, these sediments are significantly colder than the comparatively hotter and older sediments of site C0023A in the Nankai Trough, which span back ~13-16 million years to the middle Miocene (Morono et al., 2017; Hagino, 2018). Turnover times for vegetative cells in hydrothermal sediments, such as those from the Guaymas Basin, have been estimated to be on the order of only days to months (Møller et al., 2018). Liang et al.'s (2019) investigation of aspartic acid racemization rates in the thermophilic spore-former *Geobacillus stearothermophilus* demonstrated a complete loss of viability of spores within 125 days at their optimal growth temperature (65˚C) and within only 3 days at 95˚C. Thus, the identification of bacterial endospores from high temperature, multi-million year-old regimes at site C0023A likely indicates recent sporulation. While the potential for recent geological processing as described above offers one explanation for the high ratio of endospores to vegetative cells, an alternative interpretation is that sporulation was triggered by the stresses of the drilling process, such as significant temperature changes and depressurization upon arrival on deck.

Table 4.2. *In situ* cell concentrations of WRC samples incubated in the high hydrostatic pressure tracer experiment. Values reported as direct microscopic counts of SYBR-I stained cells. Abbreviations: *BMQL*, below meaningful quantitative limit (10 cells cm^{-3}); *BEDL*, below endospore detection limit (2.2×10^4 spores cm^{-3}).

Depth (mbsf)	*In situ* Temp (˚C)	Approx. vegetative cells (± 10) cm^{-3}	Approx. endospores cm^{-3}
257	37.6	2.31×10^4	$3.73 \pm 1.5 \times 10^4$
414	53.7	36	$1.3 \pm 0.5 \times 10^5$
429	55.2	26	$1.8 \pm 0.4 \times 10^5$
496	61.7	6^{BMQL}	$10 \pm 4 \times 10^4$
574	69.2	155	*BEDL*
583	70	155	*BEDL*
616	73.1	1^{BMQL}	*BEDL*
659	77.1	28	$6.2 \pm 0.1 \times 10^5$
865	95.2	8^{BMQL}	*BEDL*

4.4.3 ***Observations of trace AOM at high hydrostatic pressure***. The starting isotopic composition of sediment slurries, recording $\delta^{13}C_{DIC_d}$ values between approximately -14‰ to -26‰. These values were more negative than the $\delta^{13}C_{DIC}$ of the artificial seawater media (-11.61± 1.3 ‰; [DIC] = 10 μM) (Figure 5), indicating *in situ* sediment porewater DIC (which was not measured in this study) must be comparatively depleted in ^{13}C.

Positive $\delta^{13}C_{DIC_d}$ excursions were observed for 29 out of 54 investigated electron acceptor conditions (excluding the kill controls) for the duration of the incubation, demonstrating the highest average $\delta^{13}C_{DIC_d}$ for a majority of conditions at 350 days (Figure 4.5). Across all investigated electron acceptors, samples from 659 mbsf showed the largest excursion average relative to its starting isotopic composition. Nitrate-incubated samples from 659 m also yielded the largest overall enrichment, with its $\delta^{13}C_{DIC}$ increasing 24.63 ± 5.01‰ from the start of the experiment. This depth is also proximal a +10‰ excursion of the *in situ* $\delta^{13}C_{CH_4}$ (Figure 4.2A), which has been

interpreted to also be strongly suggestive of thermophilic biological AOM (Heuer et al., *in prep*).

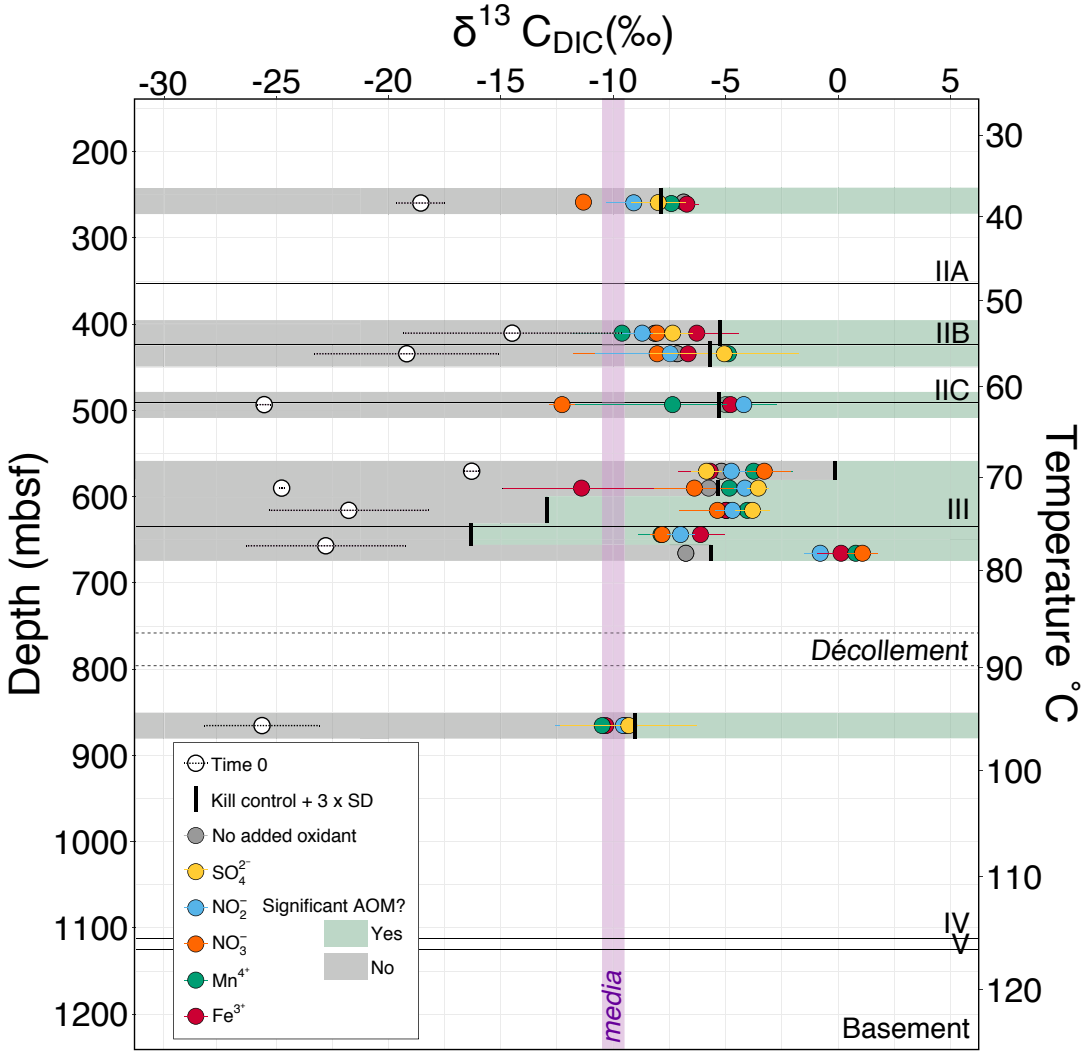

Figure 4.5. Average $\delta^{13}C_{DIC}$ ±SD of C0023A sediments after 350 days' incubation at 40 MPa under *in situ* temperature conditions. Time 0 $\delta^{13}C_{DIC_d}$ ± SD of unamended sediment slurries are indicated by white circles. Significant biological AOM was determined when $\delta^{13}C_{DIC_d}$ ± SD > $\delta^{13}C_{DIC_{d.kill}}$ ± 3 × SD. Significant values are each investigated depth are highlighted within green bars. $\delta^{13}C_{DIC}$ ± SD of sulfate-free artificial seawater medium is indicated in violet.

While the most positive $\delta^{13}C_{DIC_d}$ were generally observed at the end of the experiment, the r_{DIC} values were greatest within the first 14 days of incubation, with the

highest rate of production occurring in Fe(III)-amended slurries from 429 mbsf (r_{DICmax} = 3.3 ± 1.3 × 10^{-3} pmol cm^{-3} day^{-1}) (Figure 4.6; Table 4S.5). With the exception of samples from 616 mbsf, net AOM DIC production was observed throughout the depth profile, most prolifically in microcosms supplemented with Fe(III), Mn(IV), or NO_2^- (n = 6 depths each). We observed high replicability of r_{DIC} across biological replicates, with standard deviations of mean r_{DIC} < 0.3 pmol cm^{-3} day^{-1}.

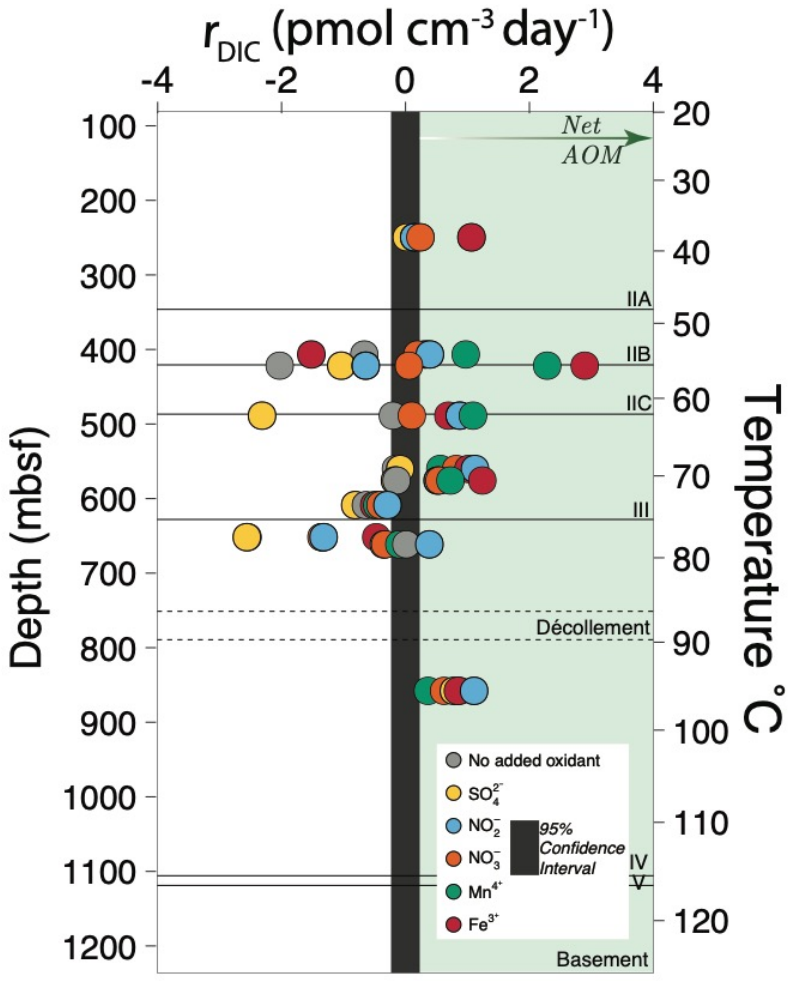

Figure 4.6. Rates of AOM DIC production (r_{DIC}) after 14 days' incubation in C0023A sediments. Rates calculated relative to the kill control at each depth according to equation (5). Gray bar represents 95% confidence interval of production relative to kill controls. SD values are smaller than point size (< 0.3 pmol cm^{-3} day^{-1}).

Net AOM DIC production was also observed at 14 days in NO_3^- supplemented samples (n = 3), while SO_4^{2-} and the no added electron acceptor control only demonstrated significant production in microcosms from 865 mbsf (Figure 4.6). AOM DIC production rates began to slow by the second sampling point at 60 days, with rates of production at 257 mbsf at least one order of magnitude greater than samples from other depths (r_{DICmax} = 1.26 ± 0.02 pmol cm^{-3} day^{-1}, Mn(IV)-enrichment, 257 mbsf) (Table 4S.5). Measurements made at 200 and 350 days showed rates of production < 0.2 pmol cm^{-3} day, again, with the highest rates being reported in 257 mbsf sediment slurries (Table 4S.5).

While it is difficult to disambiguate the relative contributions of AOM and other heterotrophic metabolisms to the DIC pool, the distribution and magnitude of metabolic rates reported in this study are generally consistent with radiotracer-inferred rates of hydrogenotrophic methanogenesis in C0023A sediments, which averaged < 1 pmol cm^{-3} day below depths where the temperature exceeded ~50˚C (Heuer et al., *in prep*; Figure 4S.7E). We note that the maximum AOM DIC rates reported from 429 mbsf Mn(IV)- and Fe(III)-amended slurries are respectively 2-3× greater than the maximum rate of methanogenesis reported for the same range of depths (Figure 4S.7E). The AOM rates observed at high hydrostatic pressure in this study are consistent with findings of other high pressure AOM tracer studies (Bowles et al., 2011; Timmers et al., 2015), and thus supportive of the existence of thermo-piezotolerant ANMEs. Future experiments employing other methodologies such as radiotracers or metatranscriptomics, ideally on more biomass-rich samples, are necessary to more definitively assess this question.

4.4.4 ***16S rRNA gene diversity and metagenomics of site C0023A***. A survey of 16S rRNA gene amplicon sequencing was performed on WRC samples spanning the depth profile at Site C0023A. A total of 535,679 quality-filtered amplicon sequences were recovered from WRC sediment samples relevant to our high pressure AOM tracer study. By comparison, a total of 31,255,507 and 6,209,754 quality-filtered reads were generated from 257 mbsf and 616 mbsf metagenome libraries.

A comparison of Shannon indices of 16S rDNA showed a range of low microbial diversity at the phylum level, ranging from 0.91 at 429 mbsf to 1.95 at 257 mbsf (Figure 4.7). *Proteobacteria* disproportionately dominated community composition at every depth, ranging from 63% relative abundance at 257 mbsf to 82.7% at 659 mbsf. (Figure 4.7). With the exception of 257 mbsf, where *Chloroflexi* were abundant (17%), *Actinobacteria* and endospore-forming *Firmicutes* were the second- and third-most abundant phyla present throughout the depth profile. The detection of *Firmicutes* in high relative abundance in multi-million year-old sediment is also consistent with the interpretation of recent sporulation, as DNA from long-dormant cells would degrade after prolonged exposure to high *in situ* temperatures (Liang et al., 2019). Nine candidate bacterial phyla were also present at ≥ 0.1% relative abundance, several of which (e.g. *Ca*. "Aerophobetes", *Ca.* "Sumerlaeota", *Ca.* "Atribacteria", *Ca.* "Armatimonadetes") are endemic to the deep sub-seafloor.

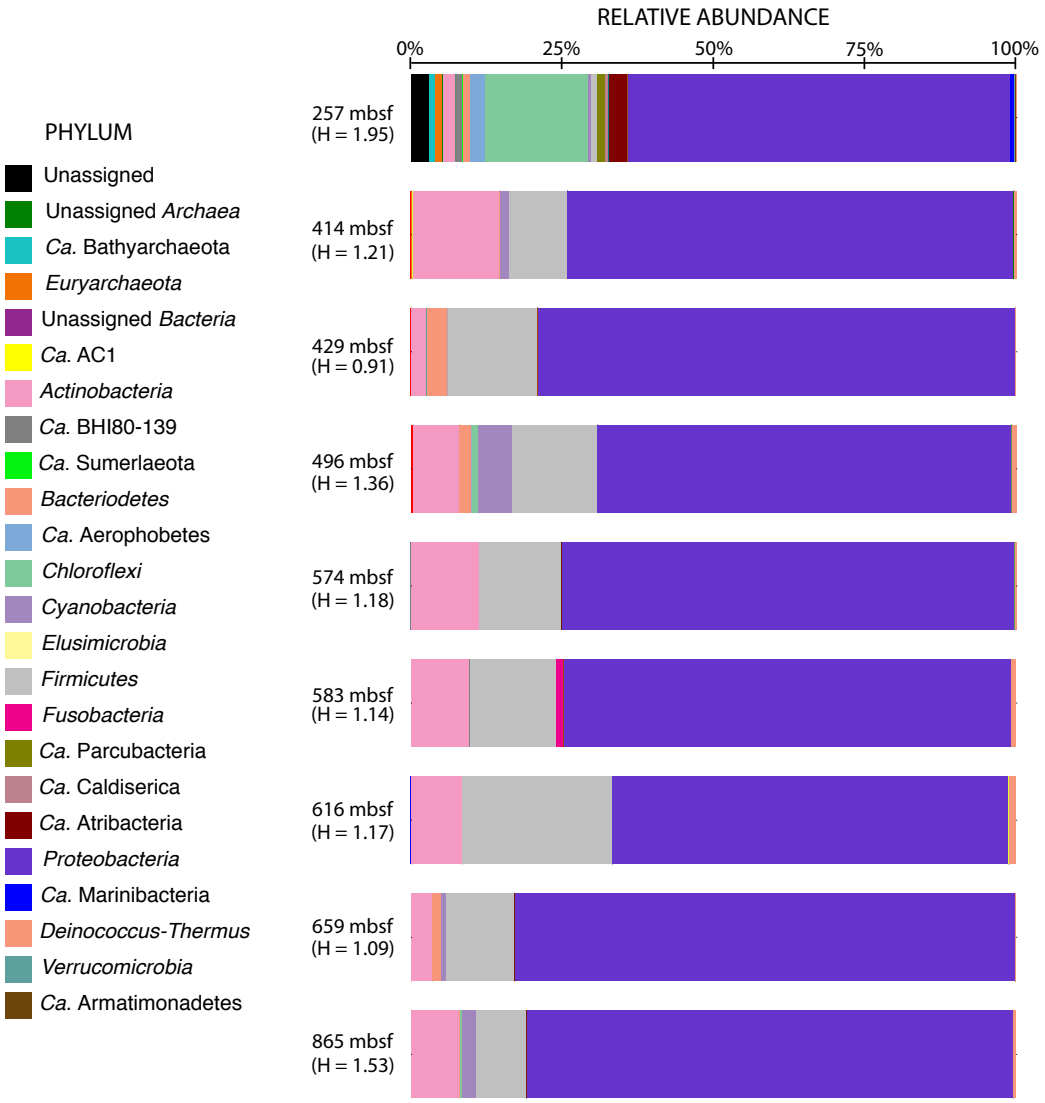

Figure 4.7. *In situ* microbial community composition at the phylum level for site C0023A OTUs with ≥ 0.1% relative abundance. Phylum-level richness and evenness at each depth is represented by its Shannon diversity index (H).

A total of 49 16S rDNA sequences were identified as *Archaea* and were recovered from only three depths: 257 (47 sequences), 414 (1 sequence), and 583 mbsf (1 sequence). The two most abundant phyla represented amongst archaeal sequences were the *Euryarchaeota* (1.3% total relative abundance; 64% of *Archaea*) and *Candidatus* "Bathyarchaeota" (0.9% total relative abundance; 36% of *Archaea*). The

candidate class *Ca.* "Hadesarchaea" accounted for 92.5% of *Euryarchaeota* assignments. Conspicuously, we did not identify any sequences belonging to known methanogenic or ANME phylotypes from the 16S rRNA gene survey. While this may imply that ANMEs are not present at the depth intervals investigated in this study, several factors may explain their apparent absence from amplicon libraries. Known biases of the 515F/806R universal primer set against several archaeal clades, including whole phyla such as the *Crenarchaeota* and *Thaumarchaeota* (Hugerth et al., 2014) occur, but also for the ANME-encompassing orders *Methanosarcinales* and *Methanomicrobiales* (Trembath-Reichert et al., 2016). Significant underestimations of the relative abundance of *Euryarchaeota* in amplicon libraries have previously been associated with low 16S rRNA gene copy numbers in methanogenic orders relative to other clades (Campanaro et al., 2018) and to *Bacteria* (Kembel et al., 2012).

A maximum likelihood tree of Site C0023A *Archaea* aligned to 16S rRNA gene sequences of reference genomes and deep biosphere lineages confirmed this apparent absence of canonical euryarchaeal ANMEs (Figure 4.8). However, metagenomics of 257 and 616 mbsf 0.15 MPa enrichments did reveal much greater microbial diversity, though *Archaea* still comprised < 1% of community composition at both depths (Appendix C, file 4C.1.html for 257 mbsf and 4C.2.html for 616 mbsf). We identified 17 sequences at 257 mbsf and 13 sequences at 616 mbsf belonging to the methanogenic euryarchaeal class *Methanomicrobia* at 257 mbsf (Figure 4.9A), including, at both depths, members of the ANME-2d family *Ca.* "Methanoperedenaceae", which have been described to independently couple AOM to nitrate, ferric iron, and manganese reduction (Haroon et al., 2013; Cai et al., 2018; Leu et al., 2020). We were also able to recover two sequences

belonging to the nitrite-reducing anaerobic methanotrophic bacterium, *Ca.* "Methylomirabilis oxyfera" (Figure 4.9B; Ettwig et al., 2010).

From the 16S rDNA survey we also identified two *Ca.* "Bathyarchaeota" OTUs, 257m.5F.3_2461 and 257m.5F.3_11668, belonging to the same clade as *Ca*. "Bathyarchaeota" archaeon BE326-BA-RLH, a putatively denitrifying anaerobic methanotroph characterized from a South African ultra-deep mine (Figure 4.8; Chapter 3; Harris et al., 2018). BLASTn pairwise alignments of 257m.5F.3_2461 and 257m.5F.3_11668 to *Ca.* BE326-BA-RLH respectively yielded 89.33% and 90.5% sequence similarity (E-values 4e-96 and 2e-100). With respect to each other, 257m.5F.3_2461 and 257m.5F.3 were 96.44% similar (E-value 3e-121), suggesting these amplicons belong to the same genus, if not also the same species, according to the arbitrary 97% 16S rRNA gene sequence similarity cutoff for species delineation (Stackebrandt and Goebel, 1994). While similar 16S rRNA gene phylogeny does not necessarily beget CH_4 metabolisms in these two OTUs, their identification does warrant continued investigation into the potential role *Ca.* "Bathyarchaeota" play in deep sub-seafloor hydrocarbon cycling, including the oxidation of higher alkanes (e.g., Wang et al., 2019). Notably, the majority of *Ca*. "Bathyarchaeota" sequences recovered from both metagenomes belong to Subgroup-3 (Figure 4.9C). This clade includes the methanogens *Ca.* "Bathyarchaeota" BA1 and BA2, of which 13 and 14 sequences were respectively identified from the 257 mbsf metagenome (Figure 4.9C).

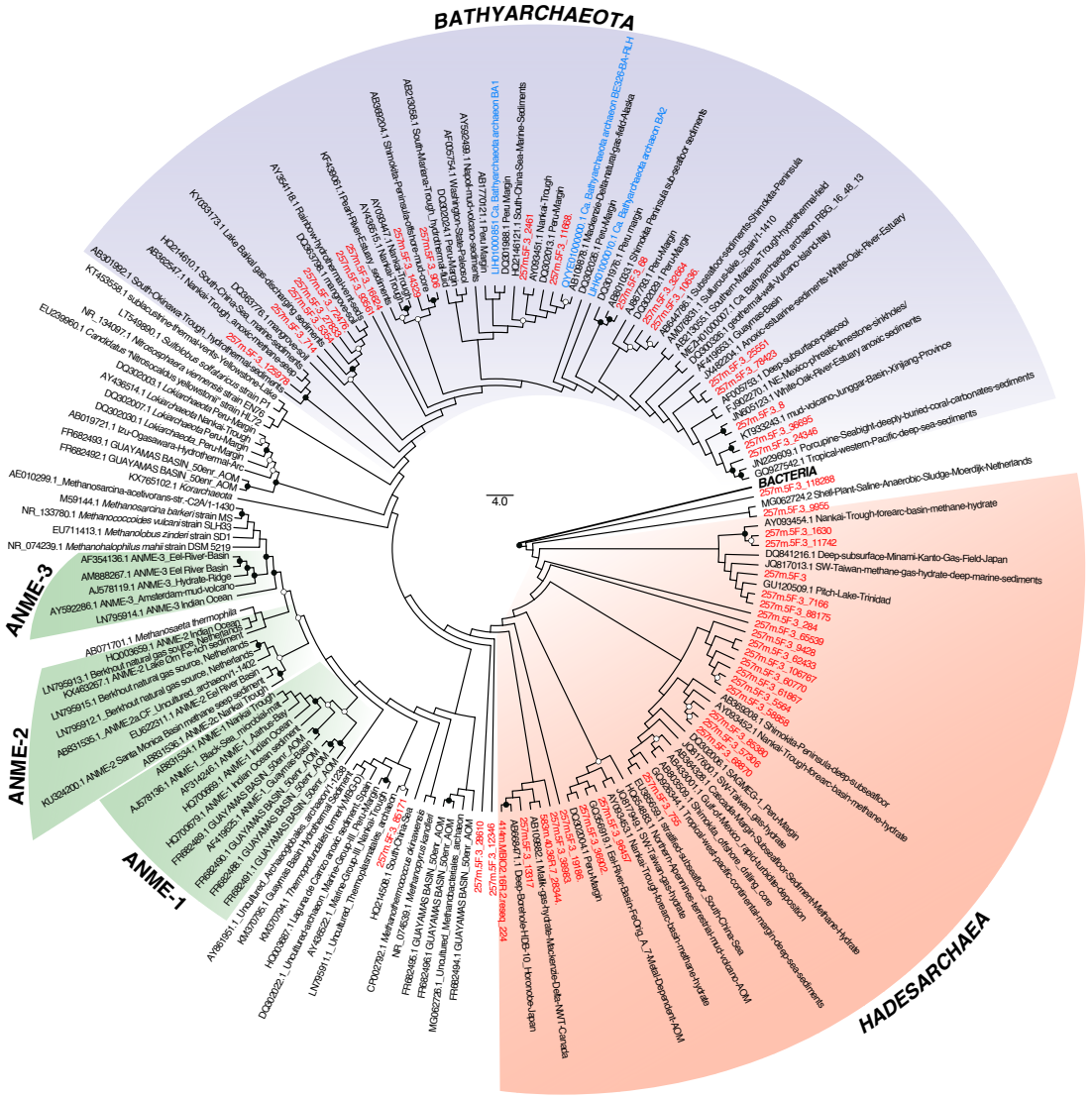

Figure 4.8. Phylogenetic diversity of 123 aligned 16S rRNA gene sequences belonging to *Archaea* amplified from Site C0023A WRC sediment (red text), reference genomes, and deep biosphere lineages. Nonparametric bootstrap values are shown as white (≥ 70%) and black (≥ 90%) circles at designated nodes. *Ca.* "Bathyarchaeota" lineages with metagenomic evidence for CH_4 metabolism are denoted by blue text. *Ca.* "Desulforudis audaxviator" MP104C (CPP00860.1) used as taxonomic outgroup (denoted as *Bacteria*). NCBI accession numbers and either environmental context or genome name provided for reference sequences.

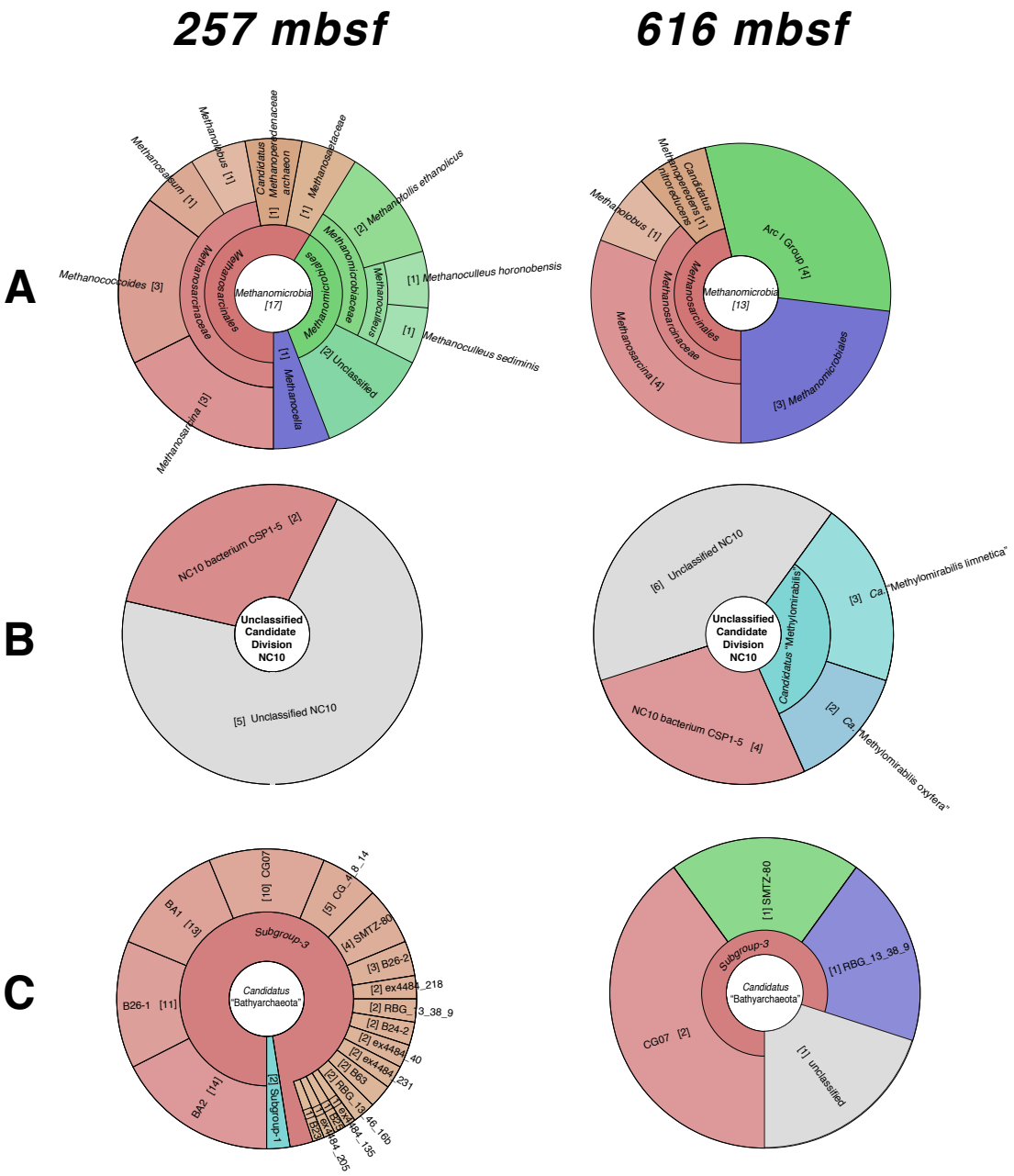

Figure 4.9. Putative CH_4-metabolizing taxa belonging to **(A)** *Methanomicrobia*, **(B)** Candidate Division NC10, and **(C)** *Candidatus* "Bathyarchaeota" recovered from 257 mbsf and 616 mbsf metagenomes (0.15 MPa enrichments). Numbers in brackets refer to number of sequences recovered belonging to that taxonomic classification.

4.4.5 ***Detection of ANME-1 via FISH at high hydrostatic pressure***. We performed FISH-TAMB and 16S rRNA FISH to search for evidence of ANMEs 40 MPa,

$^{13}CH_4$-incubated sediments. We were able to photomicrograph from a sulfate-supplemented 257 mbsf microcosm at 350 days an isolated example of what appeared to be a single cell (identified by DAPI staining, Figure 4.10B) that fluoresced with our ANME-1-specific 16S rRNA FISH (Figure 4.10C) and *mcr*A FISH-TAMB dyes (Figure 4.10D). Contrasting with the 16S rRNA gene survey, which presented the microbial community from the lens of amplified DNA, our FISH probes hybridize to RNA, offering a more faithful representation of the active metabolic landscape.

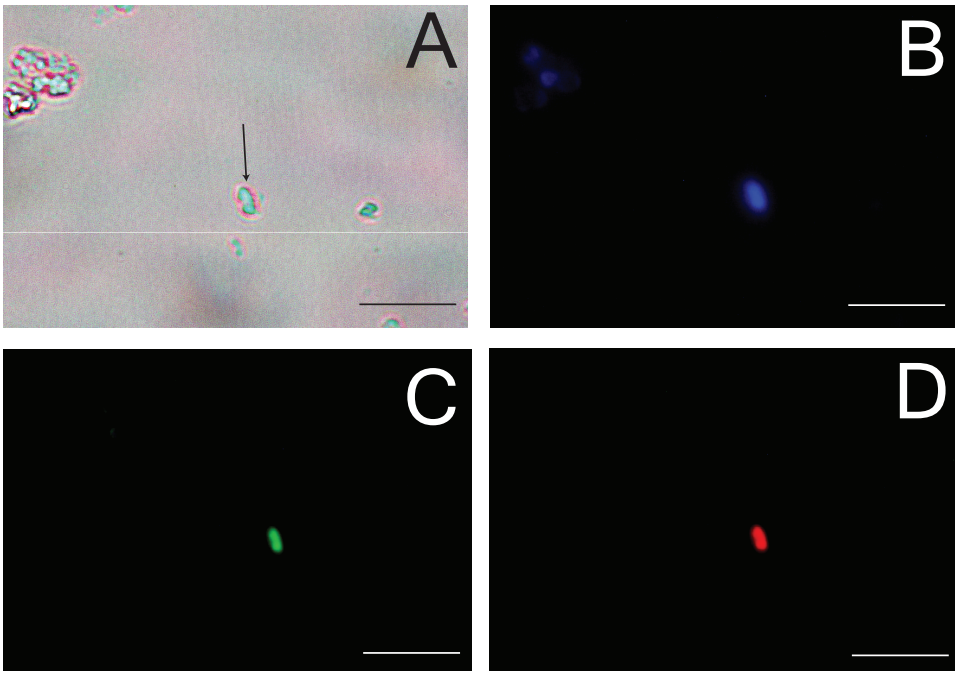

Figure 4.10. Photomicrographic evidence of ANME-1 from 257 mbsf, Site C0023A in 40 MPa microcosms supplemented with 10 mM sulfate and $^{13}CH_4$. **(A)** transmitted light, **(B)** DAPI stain, **(C)** 16S rRNA FISH **(D)** and FISH-TAMB targeting euryarchaeal *mcr*A mRNA **(E)**. Magnification 100×. Scale bar 5 µm.

The bright fluorescence intensity of the imaged cell with both 16S rRNA- and *mcr*A mRNA-specific probes is potentially indicative of very high transcriptional activity. Large transcript to gene copy number ratios appear to be characteristic of CH_4-metabolizing *Euryarchaeota*, particularly with genes involved in the methanogenesis

pathway (Zakrzewski et al., 2012; Bremges et al., 2015; Lau et al., 2016; Campanaro et al., 2018; Chapter 5 of this dissertation). ANME-1 have also been found without syntrophic partners (see Timmers et al., 2017 and references therein). Given the established specificity of the 16S rRNA probe sequence to ANME-1 (Boetius et al., 2000), as well as the consistent planktonic, rod-shaped morphology (Cui et al., 2015), we consider these images to be representative of a true positive detection of active ANME-1 enriched at 40 MPa.

4.5 CONCLUSIONS

4.5.1 ***The high-temperature, high-pressure deep biosphere as a new frontier for AOM research***. The gradual thermal gradient and diverse geochemical landscape of the Nankai Trough subduction zone provide excellent opportunities to assess the limits of microbial life in the deep hot biosphere. Photomicrographic evidence of ANME-1 in sulfate-supplemented sediment slurries recovered from 257 mbsf, the identification of ANME, *Ca.* "M. oxyfera", and Subgroup-3 *Ca.* "Bathyarchaeota" from metagenomics, and the identification of 16S rDNA OTUs closely related to *Ca.* "Bathyarchaeota" BE326-BA-RLH support the presence of piezotolerant AOM. This study presents stable isotopic evidence of microbially-mediated AOM proceeding in deep sub-seafloor sediments enriched at 40 MPa and temperatures of up to 80˚C, the highest combinatorial pressure and temperature at which AOM has been inferred *in vitro* to date.

4.6 DATA AVAILABILITY

Expedition 370 drilling records and associated core analyses, including 16S rRNA gene amplicon data, from Site C0023A are publicly available for download through the JCORES data base at http://sio7.jamstec.go.jp/j-cores.data/370/C0023A/. Raw isotopic data, photomicrographs, and code generated by this study are available upon request. Metagenomic sequencing data are available on request until the publication of this chapter at which time it will be available on NCBI GenBank.

4.7 ACKNOLWEDGEMENTS

This research was supported with samples and data provided by the International Ocean Discovery Program (IODP). I am thankful for the crew of the *Chikyu*, the staff of the Kochi Core Center, and the Expedition 370 chief scientists, Verena Heuer, Kai-Uwe Hinrichs, Fumio Inagaki, Yuki Morono, and Lena Maeda. I am especially thankful to the following Expedition 370 scientists whose data helped construct and contextualize the findings of this chapter: Verena Heuer (DIC, acetate, the $\delta^{13}C_{acetate}$, C1/C2 ratios), Yuki Morono (cell counts), Tatsuhiko Hoshino (16S rRNA gene sequencing), Florence Shubotz (CH_4 and $\delta^{13}C_{CH_4}$ measurements; radiotracer methanogenesis experiments), and Bernhard Viehweger (DPA-based endospore enumerations). This chapter was supported in part by the Deep Carbon Observatory (DCO) Deep Life Cultivation Internship, sponsored by the Alfred P. Sloan Foundation, as well as the National Science Foundation Graduate Student Research Fellowship (DGE-1148900). Metagenomic sequencing support was provided through Phase 14 of the DCO's Census of Deep Life and performed at the Marine Biological Laboratory. I am indebted to Doug Bartlett and his

lab at SIO for providing me a home away from home as I performed the high-pressure $^{13}CH_4$ tracer experiments.

4.8 EXPEDITION 370 SCIENTISTS

Lena Maeda, Margaret Cramm, Susann Henkel, Kira Homola, Tatsuhiko Hoshino, Akira Ijiri, Hiroyuki Imachi, Masanori Kaneko, Lorenzo Lagostina, Hayley Manners, Harry-Luke McClelland, Kyle Metcalfe, Natsumi Okutsu, Donald Pan, Maija Jocelyn Raudsepp, Justine Sauvage, Florence Schubotz, Arthur Spivack, Tina Treude, Bernhard Viehweger, David T. Wang, Emily Whitaker, Masataka Kinoshita.

4.9 SUPPLEMENTARY INFORMATION

Table 4S.1. Source core material for sediment samples incubated in high pressure $^{13}CH_4$ tracer experiment. Incubation temperatures juxtaposed to *in situ* temperature conditions calculated from equation (4.1).

Sample Source Core	Top Depth (mbsf)	In situ Temp (˚C)	Incubation Temp (˚C)
C0023A-5F-2	257.285	37.6	40
C0023A-16R-4	414.85	53.7	50
C0023A-18R-2	429.21	55.2	50
C0023A-25R-3	496.365	61.7	60
C0023A-35R-1	574.45	69.2	60
C0023A-36R-1	583	70	60
C0023A-39R-5	616.865	73.1	70
C0023A-44R-2	659.63	77.1	70 & 80
C0023A-83R-4	865.81	95.2	80

Table 4S.2. FISH-TAMB and 16S rRNA FISH probe sequences used in this study.

Probe Name ***(Methodology)***	**5' Reporter; 3' Quencher/Reporter**	**Sequence (5' – 3')**	**Reference(s)**
Eury_mcrA_rev *(FISH-TAMB)*	Cy5; BHQ3	CCTGGCGTTCAT-BGCGTAGTTVGG-RTAGTCCAGG	(Steinberg and Regan, 2008; Harris et al., 2017)
ANME-2_EelMS_932 *(16S rRNA FISH)*	Atto 565; Atto 565	AGCTCCACCCGT-TGTAGT	(Boetius et al., 2000; Orphan, 2001; Hatzenpichler et al., 2016)
ANME-1_350 *(16S rRNA FISH)*	Atto 425; Atto 425	AGTTTTCGCGCC-TGATGC	(Boetius et al., 2000)

Table 4S.3. Site C0023A *in situ* geochemistry for AOM free energy model. Inputs derived from expedition bulk porewater chemistry and dissolved gas reports (http://sio7.jamstec.go.jp/j-cores.data/370/C0023A/). Abbreviations: n.e., no entry; †assigned last recorded pH in depth profile; 0.1 µM, default entry if measurement was reported as below detection limit; 1 free g, default entry for hard mineral phases.

Depth (mbsf)	**257**	**414**	**429**	**496**	**574**	**583**	**616**	**659**	**865**
Temp (˚C)	37.6	53.7	55.2	61.7	69.2	70	73.1	77.1	95.2
H^+ (pH)	7.99	8.02	7.67	7.73	7.54†	7.54†	7.54†	7.54†	7.54†
Cl- (mM)	560.67	580.87	579.29	554.22	551.60	544.71	520.70	486.38	467.11
H_2S (µM)	0.40	*0.1*	*0.1*	*0.1*	*0. 1*	*0.1*	*0.1*	*0.1*	0.40
$Fe(OH)_3$ (free g)	*1*	*1*	*1*	*1*	*1*	*1*	*1*	*1*	*1*
Pyrolusite (free g)	*1*	*1*	*1*	*1*	*1*	*1*	*1*	*1*	*1*
CH_4 (mM)	1.87	5.83	0.30	1.47	1.83	4.49	3.08	1.48	0.18
Fe^{2+}(µM)	2.08	0.12	24.48	23.87	59.58	9.38	2.03	0.40	0.81
Mn^{2+} (µM)	*0.1*	7.20	20.16	40.19	22.95	19.45	7.37	12.10	101.74
HCO_3^- (mM)	15.32	7.25	7.76	2.99	2.05	2.05	0.99	0.99	7.77
NO_2^- (µM)	*0.1*	*0.1*	*0.1*	*0.1*	*0.1*	*0.1*	*0.1*	*0.1*	*0.1*
NO_3^- (µM)	11.71	*0.1*	*0.1*	*0.1*	*0.1*	*0.1*	*0.1*	*0.1*	*0.1*
SO_4^{2-} (mM)	2.22	0.55	0.55	0.68	0.487	1.36	0.92	0.86	5.64
H_2 (µM)	0.002	1.13	0.49	0.02	0.02	0.004	0.36	0.81	0.39
NH_4^+ (mM)	6.85	3.65	3.17	1.48	1.12	1.01	0.91	0.89	0.30
Na^+ (mM)	511.63	529.90	524.64	493.82	489.80	487.04	462.30	445.58	415.35
Br^- (mM)	1.06	1.08	1.11	1.02	1.02	1.00	0.93	0.86	0.82
K^+ (mM)	7.53	4.74	4.90	2.27	2.00	1.96	1.48	0.87	0.72
Mg^{2+} (mM)	13.39	6.04	5.53	4.37	2.94	2.66	1.43	2.33	2.73
Ca^{2+} (mM)	9.23	15.35	17.55	20.97	23.14	23.92	24.21	22.76	33.87
Li^+ (µM)	*n.e.*	148.66	186.53	330.05	600.18	614.24	492.82	349.78	665.42

Table 4S.4. DNA yields from 0.15 MPa microcosm experiments. Abbreviations: bdl, below detection limit; NAO, no added oxidant

Depth (mbsf)	*Condition*	*ng/μL*
257	[Extraction blank]	bdl
	NAO	0.064
	Sulfate	0.046
	Fe(III)	0.052
	Mn(IV)	0.051
	Nitrite	7.16
	Nitrate	2.83
	Kill	bdl
	Pooled Library	3.46
616	[Extraction blank]	bdl
	NAO	0.03
	Sulfate	bdl
	Fe(III)	bdl
	Mn(IV)	0.04
	Nitrite	0.04
	Nitrate	bdl
	Kill	bdl
	Pooled Library	0.04

Table 4S.5. Rates of new AOM DIC production, r_{DIC}, since previous sampling point in pmol cm^{-3} day^{-1}. Values calculated according to equation (4.4). Abbreviations: NAO, no added oxidant control; K, kill control; -, replicate lost during depressurization.

	14 days		60 days		200 days		350 days	
Sample ID	r_{DIC}	SD	r_{DIC}	SD	r_{DIC}	SD	r_{DIC}	SD
257m_NAO_40C	1.62E-01	1.65E-01	9.08E-02	5.62E-02	6.44E-03	3.43E-03	1.59E-01	1.77E-02
257m_K_40C	0.00E+00	2.66E-02	0.00E+00	3.09E-03	0.00E+00	2.62E-04	0.00E+00	2.09E-03
257m_SO42-_40C	1.73E-02	2.92E-02	6.74E-01	5.19E-02	1.93E-03	1.94E-02	4.62E-02	3.23E-02
257m_NO2-_40C	-9.89E-03	1.61E-03	6.08E-01	2.98E-02	7.80E-03	1.39E-01	-1.99E-02	3.36E-02
257m_NO3-_40C	2.41E-01	3.84E-02	1.13E+00	1.03E-01	4.82E-02	1.62E-02	-2.60E-02	9.65E-03
257m_MnO2_40C	2.47E-01	2.99E-03	1.26E+00	2.02E-02	-9.92E-03	8.38E-02	1.32E-01	5.38E-02
257m_Fe2O3_40C	1.19E+00	1.95E-03	1.03E+00	2.43E-02	-7.18E-02	1.40E-02	1.72E-01	1.35E-02
414m_NAO_50C	-7.68E-01	2.88E-05	-1.52E-06	4.06E-07	4.48E-08	6.91E-08	6.76E-08	6.39E-08
414m_K_50C	0.00E+00	1.44E-08	0.00E+00	1.28E-08	0.00E+00	1.04E-08	0.00E+00	8.84E-09
414m_SO42-_50C	3.56E-01	8.71E-07	-3.13E-06	7.84E-07	-5.62E-08	4.80E-08	-3.49E-08	2.31E-08
414m_NO2-_50C	2.75E-01	3.53E-05	-6.64E-06	8.84E-07	-4.14E-07	4.63E-07	-4.23E-07	3.96E-07
414m_NO3-_50C	1.94E-01	4.29E-06	-2.78E-06	4.96E-07	9.36E-07	3.60E-07	4.88E-07	3.52E-07
414m_MnO2_50C	1.09E+00	1.73E-06	-3.62E-06	1.21E-06	1.49E-07	2.77E-08	1.07E-06	6.36E-08
414m_Fe2O3_50C	-1.69E+00	5.42E-05	-2.34E-06	2.76E-06	-3.00E-07	1.54E-06	-4.38E-09	4.88E-07
429m_NAO_50C	-2.30E+00	4.47E-06	3.52E-06	2.21E-07	-9.98E-07	2.03E-06	1.53E-07	1.98E-06
429m_K_50C	0.00E+00	5.33E-08	0.00E+00	5.25E-08	0.00E+00	4.97E-08	0.00E+00	2.54E-09
429m_SO42-_50C	-1.18E+00	2.14E-06	6.27E-06	2.83E-06	-4.81E-07	4.41E-07	-1.31E-06	4.10E-07
429m_NO2-_50C	-8.98E-01	1.34E-05	1.56E-06	2.59E-06	-7.35E-08	5.13E-07	8.98E-08	8.14E-07
429m_NO3-_50C	3.83E-02	1.44E-06	4.80E-06	5.37E-07	-9.26E-07	8.27E-07	-3.85E-07	1.09E-06
429m_MnO2_50C	2.65E+00	1.15E-04	-9.28E-07	3.61E-06	-4.50E-07	6.68E-08	6.53E-07	1.59E-07
429m_Fe2O3_50C	3.29E+00	1.28E-05	2.09E-06	2.57E-07	-7.02E-07	6.25E-07	5.07E-08	9.04E-07
496m_NAO_60C	-2.35E-01	2.34E-03	-1.18E-03	1.51E-03	-2.46E-04	5.61E-04	3.23E-04	8.45E-04

496m_K_60C	0.00E+00	1.22E-07	0.00E+00	3.26E-04	0.00E+00	1.92E-04	0.00E+00	1.77E-04
574m_NAO_60C	-1.80E-01	4.28E-04	1.80E-03	6.97E-05	4.31E-05	3.22E-03	1.40E-03	3.52E-03
574m_K_60C	0.00E+00	1.08E-05	0.00E+00	2.91E-05	0.00E+00	8.06E-05	0.00E+00	1.61E-04
583m_NAO_60C	-1.68E-01	3.72E-03	4.00E-03	5.18E-05	3.23E-05	1.02E-04	8.11E-04	9.06E-05
583m_K_60C	0.00E+00	2.11E-05	0.00E+00	8.45E-05	0.00E+00	1.16E-04	0.00E+00	3.21E-03
496m_SO42-_60C	-2.54E+00	8.25E-04	-	-	-	-	-	-
496m_NO2-_60C	7.99E-01	2.33E-03	-5.42E-03	2.19E-04	1.28E-03	2.82E-04	4.54E-03	3.29E-03
496m_NO3-_60C	8.83E-02	4.27E-03	1.96E-04	3.23E-04	-8.05E-04	3.47E-04	1.12E-03	5.73E-04
496m_MnO2_60C	1.18E+00	2.92E-04	1.28E-03	3.48E-03	-1.04E-03	1.05E-03	-7.73E-06	9.13E-04
496m_Fe2O3_60C	7.79E-01	4.13E-03	-1.42E-03	1.34E-03	-3.12E-04	7.90E-04	2.36E-03	4.29E-04
574m_SO42-_60C	-9.65E-02	1.97E-04	5.02E-03	8.75E-03	0.00E+00	6.36E-04	0.00E+00	5.27E-05
574m_NO2-_60C	1.07E+00	3.46E-03	2.60E-03	1.68E-03	2.21E-03	2.24E-03	2.22E-02	1.86E-03
574m_NO3-_60C	8.76E-01	1.82E-04	1.25E-03	1.55E-03	-1.81E-05	3.50E-03	6.61E-02	6.03E-03
574m_MnO2_60C	5.99E-01	5.16E-03	1.30E-03	1.95E-03	-3.92E-04	4.42E-04	3.88E-02	1.09E-02
574m_Fe2O3_60C	1.13E+00	1.24E-04	-2.68E-03	3.69E-03	1.37E-03	3.13E-03	7.17E-03	3.83E-02
583m_SO42-_60C	-1.89E-01	2.33E-03	3.20E-03	9.01E-05	-1.42E-03	1.18E-04	7.13E-03	1.73E-04
583m_NO2-_60C	4.05E-01	7.28E-03	2.53E-03	4.14E-03	1.84E-03	2.44E-03	9.81E-03	2.27E-03
583m_NO3-_60C	5.79E-01	2.41E-03	-4.51E-03	1.20E-04	-1.13E-03	4.20E-04	1.54E-03	1.66E-03
583m_MnO2_60C	7.80E-01	6.82E-03	6.92E-05	7.24E-05	-1.32E-04	9.05E-04	1.05E-02	8.31E-04
583m_Fe2O3_60C	1.38E+00	3.31E-03	-6.84E-04	3.76E-04	-4.96E-04	2.40E-04	-4.51E-03	1.38E-03
616m_NAO_70C	-7.13E-01	1.94E-03	2.84E-02	3.21E-03	-1.50E-02	4.89E-04	3.87E-02	1.36E-04
616m_K_70C	0.00E+00	2.89E-04	0.00E+00	1.21E-04	0.00E+00	3.13E-05	0.00E+00	3.00E-05
616m_SO42-_70C	-8.93E-01	1.46E-03	-6.63E-04	3.53E-04	4.65E-03	1.73E-04	6.52E-03	1.77E-04
616m_NO2-_70C	-4.84E-01	1.87E-03	6.62E-02	2.48E-03	-2.30E-02	2.09E-03	-3.51E-03	1.53E-03
616m_NO3-_70C	-4.69E-01	2.04E-04	-2.57E-04	5.29E-04	7.24E-04	3.02E-05	-6.89E-04	1.44E-04
616m_MnO2_70C	-5.17E-01	3.20E-03	-1.60E-03	6.42E-03	-3.23E-03	1.77E-04	8.38E-03	2.48E-04
616m_Fe2O3_70C	-5.36E-01	1.11E-02	-3.67E-04	3.71E-03	-3.19E-03	1.43E-04	6.63E-03	7.41E-04

659m_NAO_70C	-2.81E+00	-	-	-	-	-	-	-
659m_K_70C	0.00E+00	1.13E-04	0.00E+00	9.33E-05	0.00E+00	1.64E-04	0.00E+00	3.23E-04
659m_SO42-_70C	-2.81E+00	4.22E-03	1.01E-03	2.09E-04	1.51E-03	1.11E-04	-1.63E-02	1.04E-04
659m_NO2-_70C	-1.62E+00	2.41E-04	2.01E-03	6.62E-04	-3.33E-03	1.46E-05	-1.06E-03	1.73E-05
659m_NO3-_70C	-1.52E+00	1.77E-04	1.97E-03	6.90E-04	-3.68E-03	7.73E-05	-6.21E-04	6.80E-05
659m_MnO2_70C	-1.48E+00	5.60E-04	-7.14E-03	2.61E-03	-1.32E-03	6.58E-05	-4.21E-03	2.91E-05
659m_Fe2O3_70C	-1.46E+00	4.29E-03	9.49E-05	2.16E-05	-7.50E-04	8.69E-05	3.91E-02	1.69E-04
659m_NAO_80C	3.94E-03	1.22E-03	1.94E-03	-6.77E-07	-1.08E-03	-7.30E-06	8.04E-05	-1.38E-05
659m_K_80C	0.00E+00	-4.85E-04	0.00E+00	-1.37E-07	0.00E+00	-2.78E-07	0.00E+00	1.89E-05
659m_SO42-_80C	-3.87E-01	5.20E-05	-5.83E-02	1.47E-07	0.00E+00	0.00E+00	7.36E-03	4.21E-05
659m_NO2-_80C	2.59E-01	8.15E-03	-2.65E-02	4.89E-07	7.67E-06	-1.09E-04	1.44E-04	1.76E-05
659m_NO3-_80C	-3.86E-01	1.70E-03	-3.02E-01	1.48E-08	-4.17E-04	-2.27E-05	4.26E-04	7.58E-05
659m_MnO2_80C	-1.25E-01	1.20E-03	-2.45E-01	7.51E-08	-4.56E-04	-3.68E-05	-5.74E-04	-8.19E-06
659m_Fe2O3_80C	-5.00E-01	4.09E-04	-1.64E-01	-3.37E-07	-4.64E-04	2.04E-06	-5.35E-04	1.53E-04
865m_NAO_80C	9.43E-01	5.63E-04	1.20E-01	-2.65E-07	-2.89E-04	7.53E-04	-8.12E-04	-7.22E-04
865m_K_80C	0.00E+00	-7.57E-05	0.00E+00	-8.62E-08	0.00E+00	2.96E-05	1.87E-04	-2.84E-05
865m_SO42-_80C	8.54E-01	5.75E-04	-6.76E-02	6.33E-07	2.81E-03	-6.01E-05	1.60E-05	-6.46E-05
865m_NO2-_80C	1.05E+00	3.14E-03	2.52E-01	7.22E-06	1.78E-04	-2.01E-03	-1.69E-05	-1.23E-04
865m_NO3-_80C	6.60E-01	-9.18E-04	-1.99E-02	-1.23E-07	-5.68E-05	1.82E-05	9.61E-05	9.26E-06
865m_MnO2_80C	3.81E-01	3.44E-04	-1.00E-01	-1.34E-07	-6.45E-04	1.36E-04	1.73E-04	-1.49E-04
865m_Fe2O3_80C	9.48E-01	7.79E-04	2.74E-01	2.22E-06	1.84E-03	-2.80E-03	8.59E-05	-1.52E-04

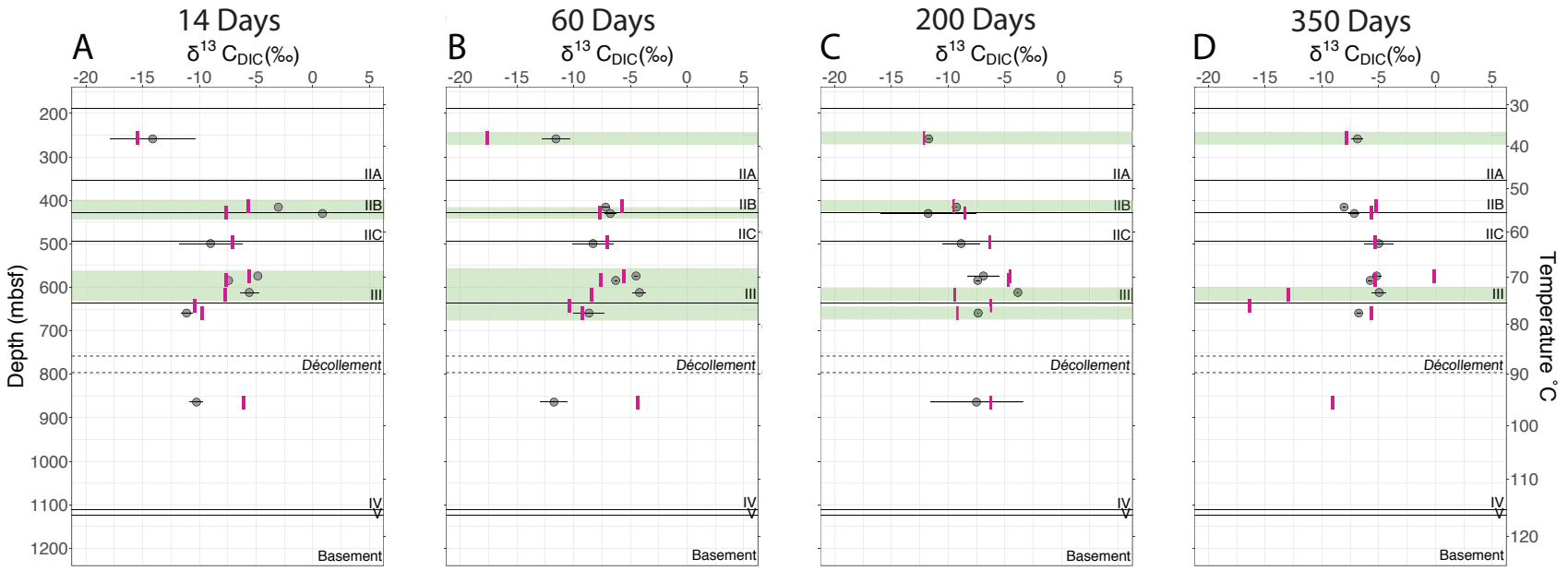

Figure 4S.1. Average $\delta^{13}C_{DIC} \pm$ SD (vs. VPDB) of unamended C0023A sediments (i.e., no added oxidant) incubated at 40 MPa under *in situ* temperatures after **(A)** 14 days, **(B)** 60 days, **(C)** 200 days, and **(D)** 350 days. Pink bars: $\delta^{13}C_{DIC_{d.kill}} \pm 3 \times$ SD. Green highlights: Depths with statistically significant biological AOM.

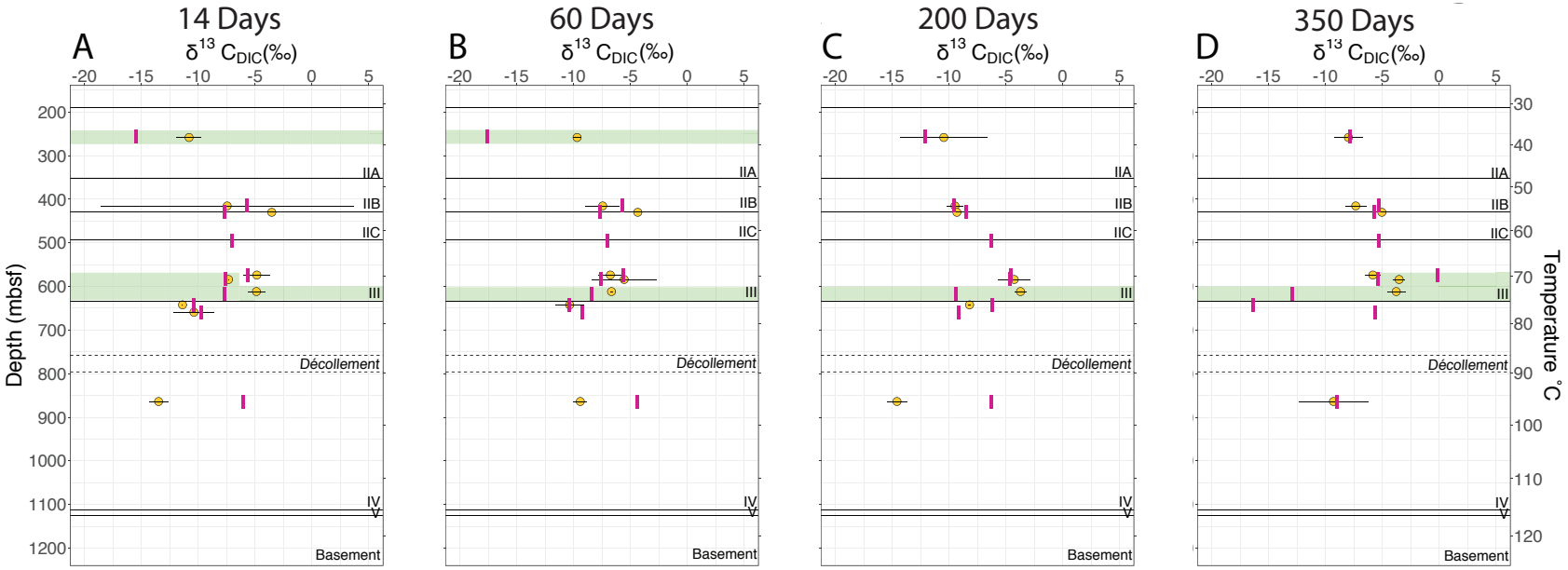

Figure 4S.2. Average $\delta^{13}C_{DIC} \pm$ SD (vs. VPDB) of sulfate amended C0023A sediments incubated at 40 MPa under *in situ* temperatures after **(A)** 14 days, **(B)** 60 days, **(C)** 200 days, and **(D)** 350 days. Pink bars: $\delta^{13}C_{DIC_{d.kill}} \pm 3 \times$ SD. Green highlights: Depths with statistically significant biological AOM.

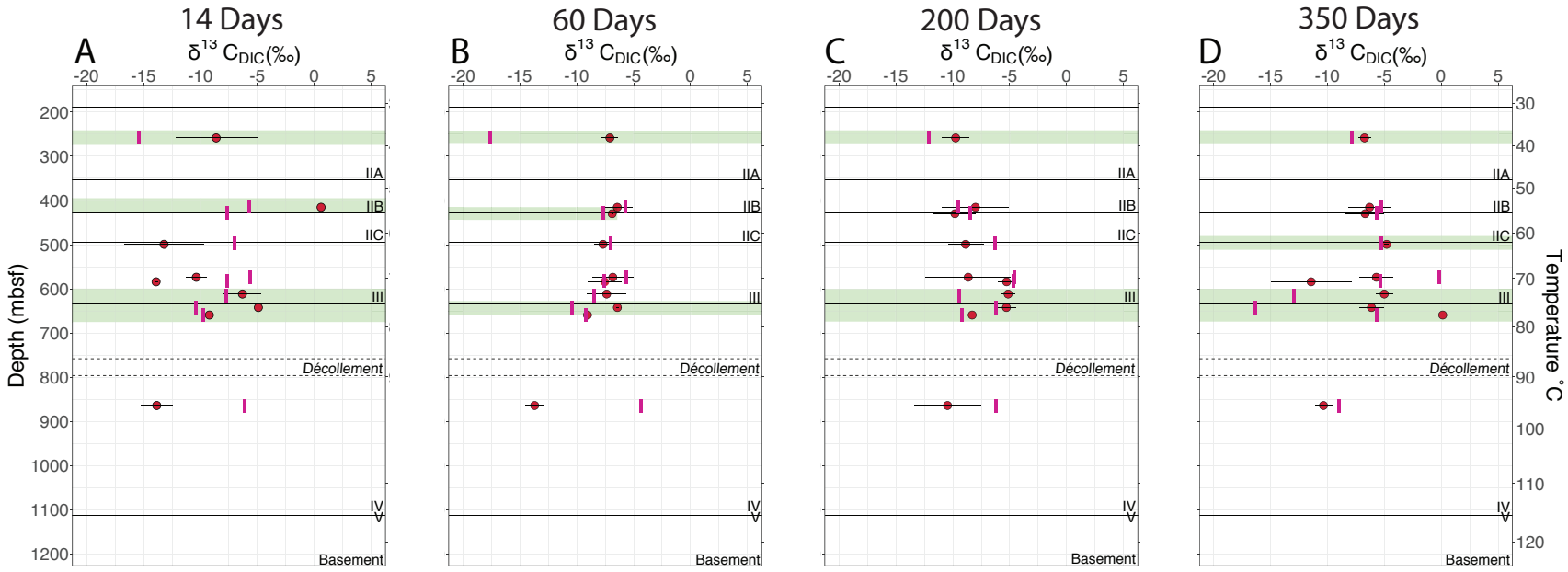

Figure 4S.3. Average $\delta^{13}C_{DIC} \pm$ SD (vs. VPDB) of Fe(III) amended C0023A sediments incubated at 40 MPa under *in situ* temperatures after **(A)** 14 days, **(B)** 60 days, **(C)** 200 days, and **(D)** 350 days. Pink bars: $\delta^{13}C_{DIC_{d.kill}} \pm 3 \times$ SD. Green highlights: Depths with statistically significant biological AOM.

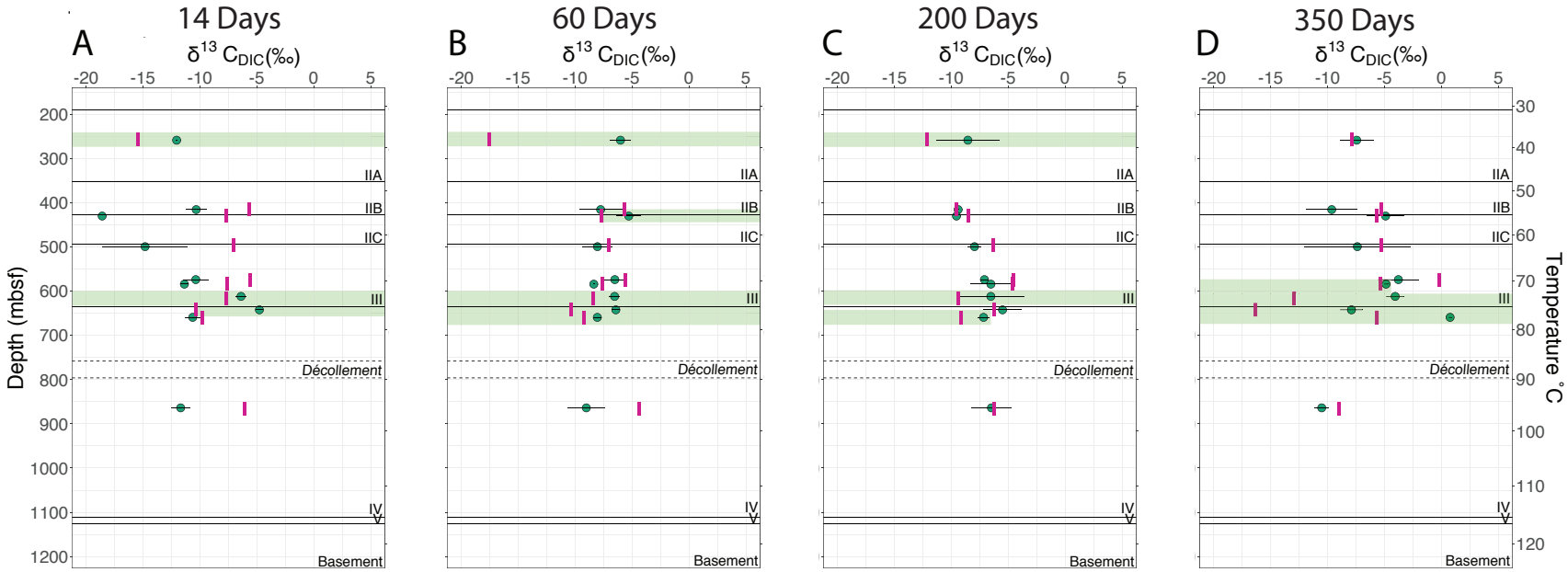

Figure 4S.4. Average $\delta^{13}C_{DIC} \pm$ SD (vs. VPDB) of Mn(IV) amended C0023A sediments incubated at 40 MPa under *in situ* temperatures after **(A)** 14 days, **(B)** 60 days, **(C)** 200 days, and **(D)** 350 days. Pink bars: $\delta^{13}C_{DIC_{d.kill}} \pm 3 \times$ SD. Green highlights: Depths with statistically significant biological AOM.

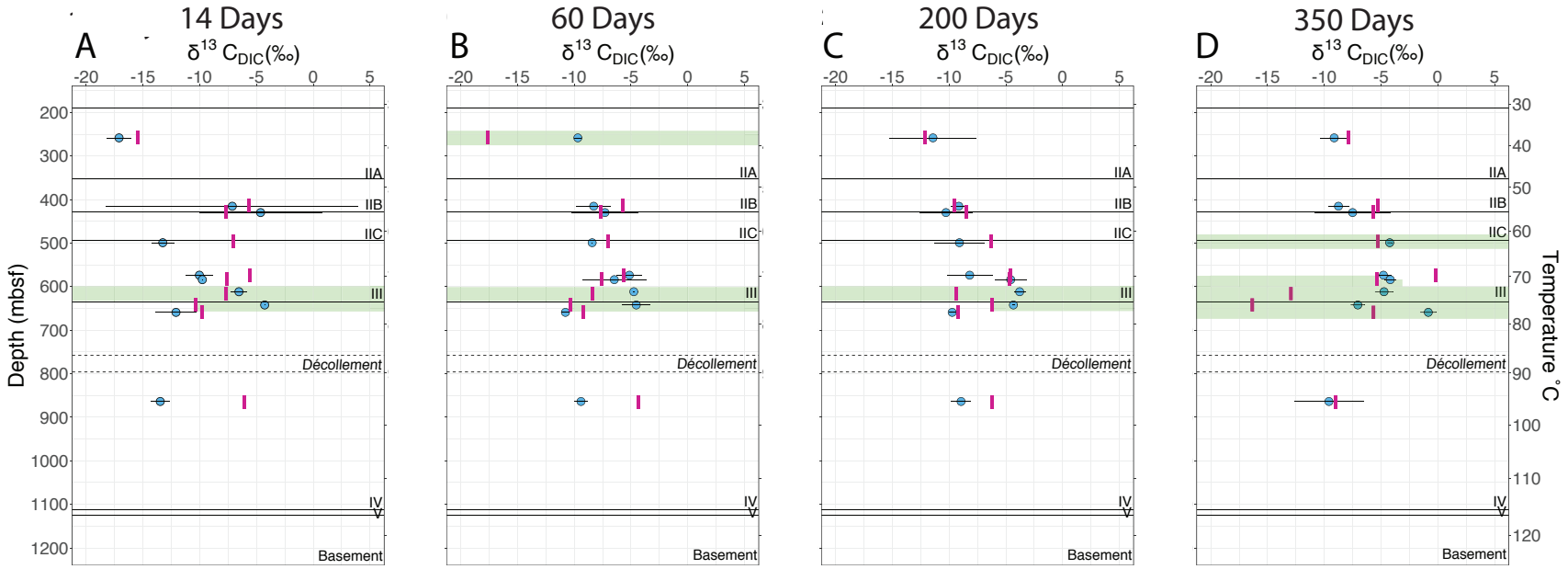

Figure 4S.5. Average $\delta^{13}C_{DIC} \pm$ SD (vs. VPDB) of nitrite amended C0023A sediments incubated at 40 MPa under *in situ* temperatures after **(A)** 14 days, **(B)** 60 days, **(C)** 200 days, and **(D)** 350 days. Pink bars: $\delta^{13}C_{DIC_{d.kill}} \pm 3 \times$ SD. Green highlights: Depths with statistically significant biological AOM.

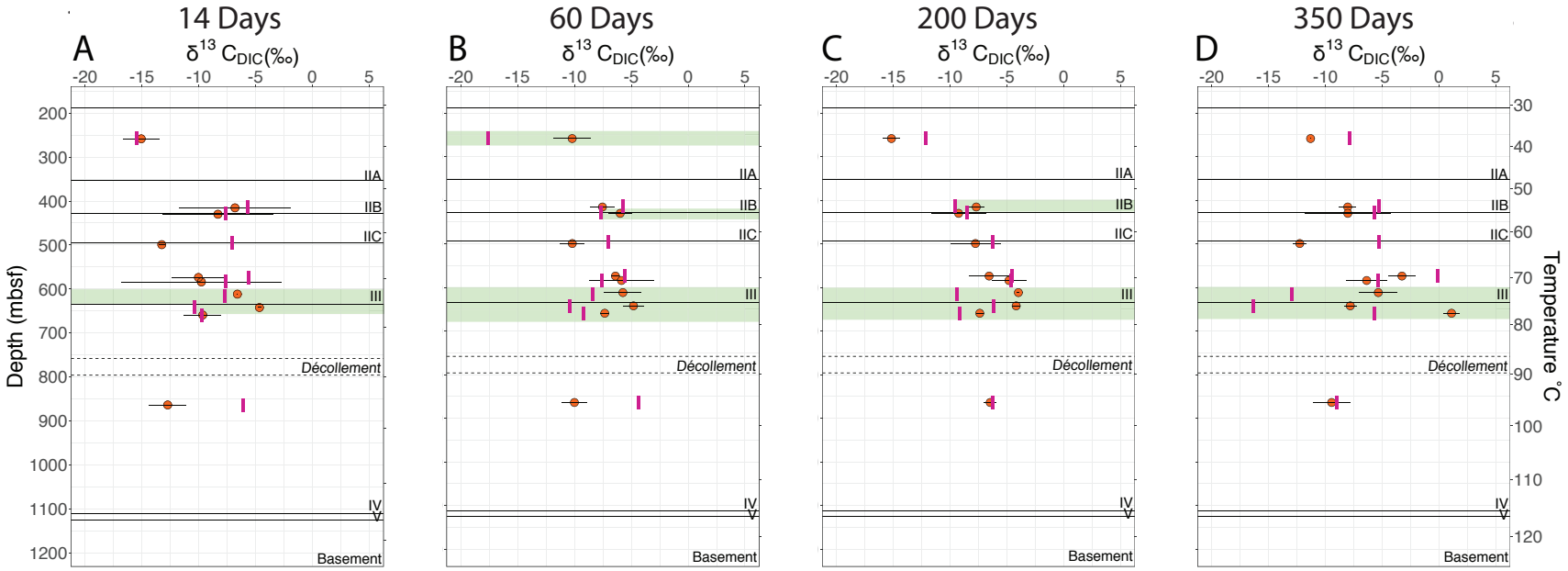

Figure 4S.6. Average $\delta^{13}C_{DIC} \pm$ SD (vs. VPDB) of nitrate amended C0023A sediments incubated at 40 MPa under *in situ* temperatures after **(A)** 14 days, **(B)** 60 days, **(C)** 200 days, and **(D)** 350 days. Pink bars: $\delta^{13}C_{DIC_{d.kill}} \pm 3 \times$ SD. Green highlights: Depths with statistically significant biological AOM.

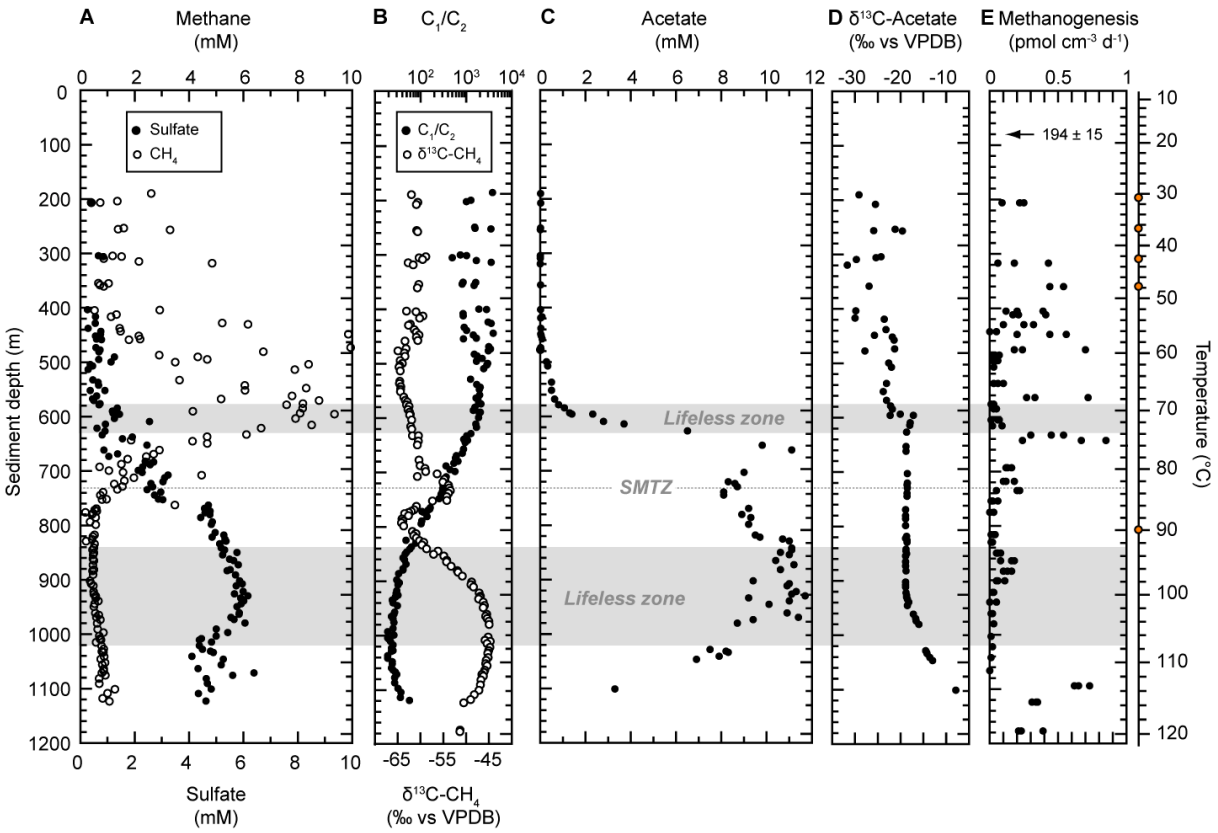

Figure 4S.7. Geochemical signals of microbial metabolism at Site C0023. **(A)** Dissolved methane and sulfate, **(B)** C_1/C_2 ratios (Heuer et al., 2016) and $\delta^{13}C$-CH_4, (C) dissolved acetate, (D) $\delta^{13}C$-acetate, and (E) potential rates of methanogenesis (MG) based on conversion of ^{14}C-CO_2 to ^{14}C-CH_4; note the high average value at 80 mbsf, scale has been adjusted to display rates in more deeply buried sediments. Red symbols on temperature axis designate the points where discrete temperature measurements were made (Morono et al., 2017). Abbreviations: VPDB, Vienna Pee Dee Belemnite standard; SMTZ, sulfate-methane transition zone. Figure used with permission from Heuer et al., *in prep*.

4.10 REFERENCES

Beal E. J., House C. H. and Orphan V. J. (2009) Manganese- and Iron-Dependent Marine Methane Oxidation. *Science (80-.).* **325**, 184–187. Available at: https://www.sciencemag.org/lookup/doi/10.1126/science.1169984.

Beulig F., Røy H., McGlynn S. E. and Jørgensen B. B. (2019) Cryptic CH4 cycling in the sulfate–methane transition of marine sediments apparently mediated by ANME-1

archaea. *ISME J.* **13**, 250–262. Available at: http://www.nature.com/articles/s41396-018-0273-z.

Boetius A., Ravenschlag K., Schubert C. J., Rickert D., Widdel F., Gieseke A., Amann R., Jørgensen B. B., Witte U. and Pfannkuche O. (2000) A marine microbial consortium apparently mediating anaerobic oxidation of methane. *Nature* **407**, 623–626. Available at: http://www.nature.com/doifinder/10.1038/35036572.

Bowles M. W., Samarkin V. A. and Joye S. B. (2011) Improved measurement of microbial activity in deep-sea sediments at in situ pressure and methane concentration. *Limnol. Oceanogr. Methods* **9**, 499–506. Available at: http://doi.wiley.com/10.4319/lom.2011.9.499.

Braun S., Mhatre S. S., Jaussi M., Røy H., Kjeldsen K. U., Pearce C., Seidenkrantz M.-S., Jørgensen B. B. and Lomstein B. A. (2017) Microbial turnover times in the deep seabed studied by amino acid racemization modelling. *Sci. Rep.* **7**, 5680. Available at: http://www.nature.com/articles/s41598-017-05972-z.

Bremges A., Maus I., Belmann P., Eikmeyer F., Winkler A., Albersmeier A., Pühler A., Schlüter A. and Sczyrba A. (2015) Deeply sequenced metagenome and metatranscriptome of a biogas-producing microbial community from an agricultural production-scale biogas plant. *Gigascience* **4**, 33. Available at: https://academic.oup.com/gigascience/article-lookup/doi/10.1186/s13742-015-0073-6.

Cai C., Leu A. O., Xie G.-J., Guo J., Feng Y., Zhao J.-X., Tyson G. W., Yuan Z. and Hu S. (2018) A methanotrophic archaeon couples anaerobic oxidation of methane to Fe(III) reduction. *ISME J.* **12**, 1929–1939. Available at:

http://www.nature.com/articles/s41396-018-0109-x.

Campanaro S., Treu L., Kougias P. G., Zhu X. and Angelidaki I. (2018) Taxonomy of anaerobic digestion microbiome reveals biases associated with the applied high throughput sequencing strategies. *Sci. Rep.* **8**, 1926. Available at: http://www.nature.com/articles/s41598-018-20414-0.

Caporaso J. G., Lauber C. L., Walters W. A., Berg-Lyons D., Huntley J., Fierer N., Owens S. M., Betley J., Fraser L., Bauer M., Gormley N., Gilbert J. A., Smith G. and Knight R. (2012) Ultra-high-throughput microbial community analysis on the Illumina HiSeq and MiSeq platforms. *ISME J.* **6**, 1621–1624. Available at: http://www.nature.com/articles/ismej20128.

Chivian D., Brodie E. L., Alm E. J., Culley D. E., Dehal P. S., DeSantis T. Z., Gihring T. M., Lapidus A., Lin L.-H., Lowry S. R., Moser D. P., Richardson P. M., Southam G., Wanger G., Pratt L. M., Andersen G. L., Hazen T. C., Brockman F. J., Arkin A. P. and Onstott T. C. (2008) Environmental Genomics Reveals a Single-Species Ecosystem Deep Within Earth. *Science* **322**, 275–278. Available at: https://www.sciencemag.org/lookup/doi/10.1126/science.1155495.

Christensen H., Hansen M. and Sorensen J. (1999) Counting and size classification of active soil bacteria by fluorescence in situ hybridization with an rRNA oligonucleotide probe. *Appl. Environ. Microbiol.* **65**, 1753–61. Available at: http://www.ncbi.nlm.nih.gov/pubmed/10103277.

Conrad R. (2009) The global methane cycle: recent advances in understanding the microbial processes involved. *Environ. Microbiol. Rep.* **1**, 285–292. Available at: http://doi.wiley.com/10.1111/j.1758-2229.2009.00038.x.

Cornell R. M. and Schwertmann U. (2003) Introduction to the Iron Oxides. In *The Iron Oxides* Wiley. pp. 1–7. Available at: https://onlinelibrary.wiley.com/doi/abs/10.1002/3527602097.ch1.

Cui M., Ma A., Qi H., Zhuang X. and Zhuang G. (2015) Anaerobic oxidation of methane: an "active" microbial process. *Microbiologyopen* **4**, 1–11. Available at: http://doi.wiley.com/10.1002/mbo3.232.

Edgar R. C. (2013) UPARSE: highly accurate OTU sequences from microbial amplicon reads. *Nat. Methods* **10**, 996–998. Available at: http://www.nature.com/articles/nmeth.2604.

Egger M., Riedinger N., Mogollón J. M. and Jørgensen B. B. (2018) Global diffusive fluxes of methane in marine sediments. *Nat. Geosci.* **11**, 421–425. Available at: http://www.nature.com/articles/s41561-018-0122-8.

Ettwig K. F., Butler M. K., Le Paslier D., Pelletier E., Mangenot S., Kuypers M. M. M., Schreiber F., Dutilh B. E., Zedelius J., de Beer D., Gloerich J., Wessels H. J. C. T., van Alen T., Luesken F., Wu M. L., van de Pas-Schoonen K. T., Op den Camp H. J. M., Janssen-Megens E. M., Francoijs K.-J., Stunnenberg H., Weissenbach J., Jetten M. S. M. and Strous M. (2010) Nitrite-driven anaerobic methane oxidation by oxygenic bacteria. *Nature* **464**, 543–548. Available at: http://dx.doi.org/10.1038/nature08883.

Ettwig K. F., Shima S., van de Pas-Schoonen K. T., Kahnt J., Medema M. H., op den Camp H. J. M., Jetten M. S. M. and Strous M. (2008) Denitrifying bacteria anaerobically oxidize methane in the absence of Archaea. *Environ. Microbiol.* **10**, 3164–3173. Available at: http://doi.wiley.com/10.1111/j.1462-2920.2008.01724.x.

Ettwig K. F., Zhu B., Speth D., Keltjens J. T., Jetten M. S. M. and Kartal B. (2016) Archaea catalyze iron-dependent anaerobic oxidation of methane. *Proc. Natl. Acad. Sci.* **113**, 12792–12796. Available at: http://www.pnas.org/lookup/doi/10.1073/pnas.1609534113.

Fichtel J., Köster J., Rullkötter J. and Sass H. (2007a) Spore dipicolinic acid contents used for estimating the number of endospores in sediments. *FEMS Microbiol. Ecol.* **61**, 522–532. Available at: https://academic.oup.com/femsec/article-lookup/doi/10.1111/j.1574-6941.2007.00354.x.

Fichtel J., Köster J., Scholz-Böttcher B., Sass H. and Rullkötter J. (2007b) A highly sensitive HPLC method for determination of nanomolar concentrations of dipicolinic acid, a characteristic constituent of bacterial endospores. *J. Microbiol. Methods* **70**, 319–327. Available at: https://linkinghub.elsevier.com/retrieve/pii/S0167701207001741.

Glöckner F. O., Amann R., Alfreider A., Pernthaler J., Psenner R., Trebesius K. and Schleifer K.-H. (1996) An In Situ Hybridization Protocol for Detection and Identification of Planktonic Bacteria. *Syst. Appl. Microbiol.* **19**, 403–406. Available at: https://linkinghub.elsevier.com/retrieve/pii/S0723202096800695.

Hagino K. (2018) Data report: calcareous nannofossils from the middle Miocene to Pleistocene, IODP Expedition 370 Site C0023. In *Proceedings of the International Ocean Discovery Program Volume 370* Available at: http://publications.iodp.org/proceedings/370/201/370_201.html.

Händel M., Rennert T. and Totsche K. U. (2013) A simple method to synthesize birnessite at ambient pressure and temperature. *Geoderma* **193**–**194**, 117–121.

Available at: https://linkinghub.elsevier.com/retrieve/pii/S0016706112003333.

Haroon M. F., Hu S., Shi Y., Imelfort M., Keller J., Hugenholtz P., Yuan Z. and Tyson G. W. (2013) Anaerobic oxidation of methane coupled to nitrate reduction in a novel archaeal lineage. *Nature* **500**, 567–570. Available at: http://dx.doi.org/10.1038/nature12375.

Harris R. L., Lau M. C. Y., Cadar A., Bartlett D. H., Cason E., van Heerden E. and Onstott T. C. (2018) Draft Genome Sequence of " Candidatus Bathyarchaeota" Archaeon BE326-BA-RLH, an Uncultured Denitrifier and Putative Anaerobic Methanotroph from South Africa's Deep Continental Biosphere ed. J. C. Dunning Hotopp. *Microbiol. Resour. Announc.* **7**, e01295-18. Available at: http://mra.asm.org/content/7/20/e01295-18.abstract.

Harris R., Lau M. C. Y., van Heerden E., Cason E., Vermeulen J.-G., Taneja A., Kieft T. L., DeCoste C., Laevsky G. and Onstott T. C. (2017) Labeling of prokaryotic mRNA in live cells using fluorescent in situ hybridization of transcript-annealing molecular beacons (FISH-TAMB). *bioRxiv*. Available at: http://biorxiv.org/content/early/2017/08/19/178368.abstract.

Hatzenpichler R., Connon S. A., Goudeau D., Malmstrom R. R., Woyke T. and Orphan V. J. (2016) Visualizing in situ translational activity for identifying and sorting slow-growing archaeal−bacterial consortia. *Proc. Natl. Acad. Sci.* **113**, E4069–E4078. Available at: http://www.pnas.org/lookup/doi/10.1073/pnas.1603757113.

Heesemann M., Villinger H., Fisher A. T., Tréhu A. M. and and White S. (2006) Data report: testing and deployment of the new APC3 tool to determine in situ temperatures while piston coring. In *Proceedings of the IODP, 311* Integrated Ocean

Drilling Program. Available at: http://iodp.tamu.edu/publications/exp311/108/108_.htm.

Heuer V. B., Inagaki F., Morono Y., Kubo Y., Maeda L. and the Scientists of Expedition 370 (2016) Temperature Limit of the Deep Biosphere off Muroto. *Proc. Int. Ocean Discov. Progr. Vol. 370* **370**.

Heuer V. B., Inagaki F., Morono Y., Kubo Y., Maeda L. and Expedition 370 Scientists (2017) Expedition 370 Preliminary Report: Temperature Limit of the Deep Biosphere off Muroto. *Int. Ocean Discov. Progr.* Available at: http://dx.doi.org/10.14379/iodp.pr.370.2017.

Heuer V. B., Inagaki F., Morono Y., Kubo Y., Maeda L., Spivack A., Viehweger B., Treude T., Beulig F., Schubotz F., Tonai S., Bowden S., Cramm M., Henkel S., Hirose T., Homola K., Hoshino T., Ijiri A., Imachi H., Kamiya N., Kaneko M., Lagostina L., Manners H., McClelland H.-L., Metcalfe K., Okutsu N., Pan D., Raudsepp M. J., Glombitza C., Sauvage J., Tsang M.-Y., Wang D. T., Whitaker E., Yamamoto Y., Yang K., Adhikari R. R., Kallmeyer J., Wendt J., Wörmer L., Yamada Y., Kinoshita M. and Hinrichs K.-U. *in prep.* Temperature limits to deep subseafloor life in the Nankai Trough subduction zone.

Hinrichs K.-U., Inagaki F., Heuer V. B., Kinoshita M., Morono Y. and Kubo Y. (2016) Expedition 370 Scientific Prospectus T-Limit of the Deep Biosphere off Muroto (T-Limit) Deciphering factors that constrain the extent of the deep. *Int. Ocean Discov. Progr.*

Hoehler T. M., Alperin M. J., Albert D. B. and Martens C. S. (1994) Field and laboratory studies of methane oxidation in an anoxic marine sediment: Evidence for a

methanogen-sulfate reducer consortium. *Global Biogeochem. Cycles*.

Hoehler T. M., Alperin M. J., Albert D. B. and Martens C. S. (1998) Thermodynamic control on hydrogen concentrations in anoxic sediments. *Geochim. Cosmochim. Acta*.

Holler T., Widdel F., Knittel K., Amann R., Kellermann M. Y., Hinrichs K.-U., Teske A., Boetius A. and Wegener G. (2011) Thermophilic anaerobic oxidation of methane by marine microbial consortia. *ISME J.* **5**, 1946–1956. Available at: http://www.nature.com/doifinder/10.1038/ismej.2011.77.

Horsfield B., Schenk H., Zink K., Ondrak R., Dieckmann V., Kallmeyer J., Mangelsdorf K., Diprimio R., Wilkes H. and Parkes R. (2006) Living microbial ecosystems within the active zone of catagenesis: Implications for feeding the deep biosphere. *Earth Planet. Sci. Lett.* **246**, 55–69. Available at: https://linkinghub.elsevier.com/retrieve/pii/S0012821X06002731.

Hoshino T. and Inagaki F. (2017) Application of Stochastic Labeling with Random-Sequence Barcodes for Simultaneous Quantification and Sequencing of Environmental 16S rRNA Genes ed. G. E. Fox. *PLoS One* **12**, e0169431. Available at: https://dx.plos.org/10.1371/journal.pone.0169431.

Hoshino T. and Inagaki F. (2012) Molecular quantification of environmental DNA using microfluidics and digital PCR. *Syst. Appl. Microbiol.* **35**, 390–395. Available at: https://linkinghub.elsevier.com/retrieve/pii/S0723202012000781.

Hugerth L. W., Wefer H. A., Lundin S., Jakobsson H. E., Lindberg M., Rodin S., Engstrand L. and Andersson A. F. (2014) DegePrime, a Program for Degenerate Primer Design for Broad-Taxonomic-Range PCR in Microbial Ecology Studies ed.

F. E. Löffler. *Appl. Environ. Microbiol.* **80**, 5116–5123. Available at: http://aem.asm.org/lookup/doi/10.1128/AEM.01403-14.

Inagaki F., Hinrichs K. U., Kubo Y., Bowles M. W., Heuer V. B., Hong W. L., Hoshino T., Ijiri A., Imachi H., Ito M., Kaneko M., Lever M. A., Lin Y. S., Methe B. A., Morita S., Morono Y., Tanikawa W., Bihan M., Bowden S. A., Elvert M., Glombitza C., Gross D., Harrington G. J., Hori T., Li K., Limmer D., Liu C. H., Murayama M., Ohkouchi N., Ono S., Park Y. S., Phillips S. C., Prieto-Mollar X., Purkey M., Riedinger N., Sanada Y., Sauvage J., Snyder G., Susilawati R., Takano Y., Tasumi E., Terada T., Tomaru H., Trembath-Reichert E., Wang D. T. and Yamada Y. (2015) Exploring deep microbial life in coal-bearing sediment down to 2.5 km below the ocean floor. *Science* **349**, 420–424. Available at: https://www.sciencemag.org/lookup/doi/10.1126/science.aaa6882.

Karner M. and Fuhrman J. A. (1997) Determination of Active Marine Bacterioplankton: a Comparison of Universal 16S rRNA Probes, Autoradiography, and Nucleoid Staining. *Appl. Environ. Microbiol.* **63**, 1208–13. Available at: http://www.ncbi.nlm.nih.gov/pubmed/16535563.

Kembel S. W., Wu M., Eisen J. A. and Green J. L. (2012) Incorporating 16S Gene Copy Number Information Improves Estimates of Microbial Diversity and Abundance ed. C. von Mering. *PLoS Comput. Biol.* **8**, e1002743. Available at: https://dx.plos.org/10.1371/journal.pcbi.1002743.

Kirschke S., Bousquet P., Ciais P., Saunois M., Canadell J. G., Dlugokencky E. J., Bergamaschi P., Bergmann D., Blake D. R., Bruhwiler L., Cameron-Smith P., Castaldi S., Chevallier F., Feng L., Fraser A., Heimann M., Hodson E. L.,

Houweling S., Josse B., Fraser P. J., Krummel P. B., Lamarque J.-F., Langenfelds R. L., Le Quéré C., Naik V., O'Doherty S., Palmer P. I., Pison I., Plummer D., Poulter B., Prinn R. G., Rigby M., Ringeval B., Santini M., Schmidt M., Shindell D. T., Simpson I. J., Spahni R., Steele L. P., Strode S. A., Sudo K., Szopa S., van der Werf G. R., Voulgarakis A., van Weele M., Weiss R. F., Williams J. E. and Zeng G. (2013) Three decades of global methane sources and sinks. *Nat. Geosci.* **6**, 813–823. Available at: http://www.nature.com/articles/ngeo1955.

Lau M. C. Y., Kieft T. L., Kuloyo O., Linage-Alvarez B., van Heerden E., Lindsay M. R., Magnabosco C., Wang W., Wiggins J. B., Guo L., Perlman D. H., Kyin S., Shwe H. H., Harris R. L., Oh Y., Yi M. J., Purtschert R., Slater G. F., Ono S., Wei S., Li L., Sherwood Lollar B. and Onstott T. C. (2016) An oligotrophic deep-subsurface community dependent on syntrophy is dominated by sulfur-driven autotrophic denitrifiers. *Proc. Natl. Acad. Sci.* **113**, E7927–E7936. Available at: http://www.pnas.org/lookup/doi/10.1073/pnas.1612244113.

Lemos L. N., Fulthorpe R. R., Triplett E. W. and Roesch L. F. W. (2011) Rethinking microbial diversity analysis in the high throughput sequencing era. *J. Microbiol. Methods* **86**, 42–51. Available at: https://linkinghub.elsevier.com/retrieve/pii/S0167701211001138.

Leu A. O., Cai C., McIlroy S. J., Southam G., Orphan V. J., Yuan Z., Hu S. and Tyson G. W. (2020) Anaerobic methane oxidation coupled to manganese reduction by members of the Methanoperedenaceae. *ISME J.* **14**, 1030–1041. Available at: http://www.nature.com/articles/s41396-020-0590-x.

Liang R., Lau M. C. Y., Baars O., Robb F. T. and Onstott T. C. (2019) Aspartic acid

racemization constrains long-term viability and longevity of endospores. *FEMS Microbiol. Ecol.* **95**. Available at: https://academic.oup.com/femsec/article/doi/10.1093/femsec/fiz132/5553460.

Llobet-Brossa E., Rosselló-Mora R. and Amann R. (1998) Microbial Community Composition of Wadden Sea Sediments as Revealed by Fluorescence In Situ Hybridization. *Appl. Environ. Microbiol.* **64**, 2691–2696. Available at: https://aem.asm.org/content/64/7/2691.

Lovley D. R., Dwyer D. F. and Klug M. J. (1982) Kinetic Analysis of Competition Between Sulfate Reducers and Methanogens for Hydrogen in Sediments †. *Appl. Environ. Microbiol.* **43**, 1373–1379. Available at: https://aem.asm.org/content/43/6/1373.

Lovley D. R. and Goodwin S. (1988) Hydrogen concentrations as an indicator of the predominant terminal electron-accepting reactions in aquatic sediments. *Geochim. Cosmochim. Acta* **52**, 2993–3003. Available at: https://linkinghub.elsevier.com/retrieve/pii/0016703788901639.

McGlynn S. E., Chadwick G. L., Kempes C. P. and Orphan V. J. (2015) Single cell activity reveals direct electron transfer in methanotrophic consortia. *Nature* **526**, 531–535. Available at: http://dx.doi.org/10.1038/nature15512.

Milucka J., Ferdelman T. G., Polerecky L., Franzke D., Wegener G., Schmid M., Lieberwirth I., Wagner M., Widdel F. and Kuypers M. M. M. (2012) Zero-valent sulphur is a key intermediate in marine methane oxidation. *Nature* **491**, 541–546. Available at: http://www.nature.com/articles/nature11656.

Møller M. H., Glombitza C., Lever M. A., Deng L., Morono Y., Inagaki F., Doll M., Su

C. and Lomstein B. A. (2018) D:L-Amino Acid Modeling Reveals Fast Microbial Turnover of Days to Months in the Subsurface Hydrothermal Sediment of Guaymas Basin. *Front. Microbiol.* **9**. Available at: http://journal.frontiersin.org/article/10.3389/fmicb.2018.00967/full.

Moore G. F., Taira A., Bangs N. L., Kuramoto S., Shipley T. H., Alex C. M., Gulick S. S., Hills D. J., Ike T., Ito S., Leslie S. C., McCutcheon A. J., Mochizuki K., Morita S., Nakamura Y., Park J.-O., Taylor B. L., Toyama G., Yagi H. and Zhao Z. (2001) Leg 190 Summary. In *Proceedings of the Ocean Drilling Program, 190 Initial Reports*

Morono Y. and Inagaki F. (2010) Automatic Slide-Loader Fluorescence Microscope for Discriminative Enumeration of Subseafloor Life. *Sci. Drill.* **9**, 32–36. Available at: http://www.sci-dril.net/9/32/2010/.

Morono Y., Inagaki F., Heuer V. B., Kubo Y., Maeda L., Bowden S., Cramm M., Henkel S., Hirose T., Homola K., Hoshino T., Ijiri A., Imachi H., Kamiya N., Kaneko M., Lagostina L., Manners H., McClelland H.-L., Metcalfe K., Okutsu N., Pan D., Raudsepp M. J., Sauvage J., Schubotz F., Spivack A., Tonai S., Treude T., Tsang M.-Y., Viehweger B., Wang D. T., Whitaker E., Yamamoto Y. and Yang K. (2017) Expedition 370 methods. In *Proceedings of the International Ocean Discovery Program Volume 370*

Morono Y., Terada T., Masui N. and Inagaki F. (2009) Discriminative detection and enumeration of microbial life in marine subsurface sediments. *ISME J.* **3**, 503–511. Available at: http://www.nature.com/articles/ismej20091.

Oksanen J., Blanchet F. G., Friendly M., Kindt R., Legendre P., McGlinn D., Minchin P.

R., O'Hara R. B., Simpson G. L., Solymos P., Stevens M. H. H., Szoecs E. and Wagner H. (2019) vegan: Community Ecology Package. R package version 2.5-2. *Cran R*.

Orphan V. J. (2001) Methane-Consuming Archaea Revealed by Directly Coupled Isotopic and Phylogenetic Analysis. *Science* **293**, 484–487. Available at: http://www.sciencemag.org/cgi/doi/10.1126/science.1061338.

Pernthaler A., Preston C. M., Pernthaler J., DeLong E. F. and Amann R. (2002) Comparison of Fluorescently Labeled Oligonucleotide and Polynucleotide Probes for the Detection of Pelagic Marine Bacteria and Archaea. *Appl. Environ. Microbiol.* **68**, 661–667. Available at: http://aem.asm.org/cgi/doi/10.1128/AEM.68.2.661-667.2002.

Quast C., Pruesse E., Yilmaz P., Gerken J., Schweer T., Yarza P., Peplies J. and Glöckner F. O. (2012) The SILVA ribosomal RNA gene database project: improved data processing and web-based tools. *Nucleic Acids Res.* **41**, D590–D596. Available at: http://academic.oup.com/nar/article/41/D1/D590/1069277/The-SILVA-ribosomal-RNA-gene-database-project.

Reeburgh W. S. (2007) Oceanic Methane Biogeochemistry. *Chem. Rev.* **107**, 486–513. Available at: https://pubs.acs.org/doi/10.1021/cr050362v.

Schink B. (1997) Energetics of syntrophic cooperation in methanogenic degradation. *Microbiol. Mol. Biol. Rev.* **61**, 262–280.

Sherwood Lollar B., Frape S. K., Fritz P., Macko S. A., Welhan J. A., Blomqvist R. and Lahermo P. W. (1993a) Evidence for bacterially generated hydrocarbon gas in Canadian shield and fennoscandian shield rocks. *Geochim. Cosmochim. Acta* **57**,

5073–5085. Available at: https://linkinghub.elsevier.com/retrieve/pii/001670379390609Z.

Sherwood Lollar B., Frape S. K., Weise S. M., Fritz P., Macko S. A. and Welhan J. A. (1993b) Abiogenic methanogenesis in crystalline rocks. *Geochim. Cosmochim. Acta* **57**, 5087–5097. Available at: https://linkinghub.elsevier.com/retrieve/pii/0016703793906109.

Sivan O., Antler G., Turchyn A. V, Marlow J. J. and Orphan V. J. (2014) Iron oxides stimulate sulfate-driven anaerobic methane oxidation in seeps. *Proc. Natl. Acad. Sci.* **111**, E4139–E4147. Available at: http://www.pnas.org/content/111/40/E4139.abstract.

Stackebrandt E. and Goebel B. M. (1994) Taxonomic Note: A Place for DNA-DNA Reassociation and 16S rRNA Sequence Analysis in the Present Species Definition in Bacteriology. *Int. J. Syst. Evol. Microbiol.* **44**, 846–849. Available at: https://www.microbiologyresearch.org/content/journal/ijsem/10.1099/00207713-44-4-846.

Stamatakis A. (2014) RAxML version 8: a tool for phylogenetic analysis and post-analysis of large phylogenies. *Bioinformatics* **30**, 1312–1313. Available at: https://academic.oup.com/bioinformatics/article-lookup/doi/10.1093/bioinformatics/btu033.

Steinberg L. M. and Regan J. M. (2008) Phylogenetic comparison of the methanogenic communities from an acidic, oligotrophic fen and an anaerobic digester treating municipal wastewater sludge. *Appl. Environ. Microbiol.* **74**, 6663–71. Available at: http://aem.asm.org/cgi/content/long/74/21/6663.

Takai K., Nakamura K., Toki T., Tsunogai U., Miyazaki M., Miyazaki J., Hirayama H., Nakagawa S., Nunoura T. and Horikoshi K. (2008) Cell proliferation at 122 degrees C and isotopically heavy CH4 production by a hyperthermophilic methanogen under high-pressure cultivation. *Proc. Natl. Acad. Sci. U. S. A.* **105**, 10949–10954. Available at: papers://0be24a46-325a-4116-a3c6-fd8a3b614472/Paper/p11728.

Timmers P. H. A., Widjaja-Greefkes H. C. A., Ramiro-Garcia J., Plugge C. M. and Stams A. J. M. (2015) Growth and activity of ANME clades with different sulfate and sulfide concentrations in the presence of methane. *Front. Microbiol.* **6**. Available at: http://journal.frontiersin.org/Article/10.3389/fmicb.2015.00988/abstract.

Timmers P. H. A., Welte C. U., Koehorst J. J., Plugge C. M., Jetten M. S. M. and Stams A. J. M. (2017) Reverse Methanogenesis and Respiration in Methanotrophic Archaea. *Archaea* **2017**, 1–22. Available at: https://www.hindawi.com/journals/archaea/2017/1654237/.

Tonai S., Kubo Y., Tsang M.-Y., Bowden S., Ide K., Hirose T., Kamiya N., Yamamoto Y., Yang K., Yamada Y., Morono Y., Heuer V. B. and Inagaki F. (2019) A New Method for Quality Control of Geological Cores by X-Ray Computed Tomography: Application in IODP Expedition 370. *Front. Earth Sci.* **7**. Available at: https://www.frontiersin.org/article/10.3389/feart.2019.00117/full.

Trembath-Reichert E., Case D. H. and Orphan V. J. (2016) Characterization of microbial associations with methanotrophic archaea and sulfate-reducing bacteria through statistical comparison of nested Magneto-FISH enrichments. *PeerJ* **4**, e1913. Available at: https://peerj.com/articles/1913.

Walters W. A., Caporaso J. G., Lauber C. L., Berg-Lyons D., Fierer N. and Knight R.

(2011) PrimerProspector: de novo design and taxonomic analysis of barcoded polymerase chain reaction primers. *Bioinformatics* **27**, 1159–1161. Available at: https://academic.oup.com/bioinformatics/article-lookup/doi/10.1093/bioinformatics/btr087.

Wang Y., Wegener G., Hou J., Wang F. and Xiao X. (2019) Expanding anaerobic alkane metabolism in the domain of Archaea. *Nat. Microbiol.* **4**, 595–602. Available at: http://www.nature.com/articles/s41564-019-0364-2.

Wegener G., Krukenberg V., Riedel D., Tegetmeyer H. E. and Boetius A. (2015) Intercellular wiring enables electron transfer between methanotrophic archaea and bacteria. *Nature* **526**, 587–590. Available at: http://www.nature.com/articles/nature15733.

Widdel F. and Bak F. (1992) *The Prokaryotes*. eds. A. Balows, H. G. Trüper, M. Dworkin, W. Harder, and K.-H. Schleifer, Springer New York, New York, NY. Available at: http://link.springer.com/10.1007/978-1-4757-2191-1.

Williams S. C., Hong Y., Danavall D. C. A., Howard-Jones M. H., Gibson D., Frischer M. E. and Verity P. G. (1998) Distinguishing between living and nonliving bacteria: Evaluation of the vital stain propidium iodide and its combined use with molecular probes in aquatic samples. *J. Microbiol. Methods* **32**, 225–236. Available at: http://linkinghub.elsevier.com/retrieve/pii/S0167701298000141.

Yayanos A. A. (1995) Microbiology to 10,500 Meters in the Deep Sea. *Annu. Rev. Microbiol.* **49**, 777–805. Available at: http://micro.annualreviews.org/cgi/doi/10.1146/annurev.micro.49.1.777.

Zakrzewski M., Goesmann A., Jaenicke S., Jünemann S., Eikmeyer F., Szczepanowski

R., Al-Soud W. A., Sørensen S., Pühler A. and Schlüter A. (2012) Profiling of the metabolically active community from a production-scale biogas plant by means of high-throughput metatranscriptome sequencing. *J. Biotechnol.* **158**, 248–258. Available at: https://linkinghub.elsevier.com/retrieve/pii/S0168165612000685.

CHAPTER 5

Regulatory responses of *Methanosarcina barkeri* to freezing temperatures and perchlorates: Transcriptomic insights into the potential for biological methanogenesis on Mars

Keywords: Methanogens, transcriptomics, perchlorates, Mars

5.1 ABSTRACT

Observations of trace methane (CH_4) in the Martian atmosphere are of significant relevance to the astrobiology community given the overwhelming contribution of biological methanogenesis to atmospheric CH_4 on Earth. However, it remains poorly understood how microorganisms might be able to survive under oxidative stresses characteristic of modern Mars. In this study we performed comparative transcriptomics on RNA from the methanogenic archaeon, *Methanosarcina barkeri*, which was grown in liquid culture at both 30˚C and 0˚C under high concentrations of perchlorates, highly oxidizing chaotropic salts which have been found across the Martian surface. Consistent with prior studies, we report quantifiable but inhibited methanogenesis in cultures supplemented with perchlorates. However, this suppression was not exacerbated in combination with growth at 0˚C. We present transcriptomic evidence of direct regulatory responses to increased osmotic stress, nitrogen limitation, and changing substrate availability. Regulatory switches to methylamine-based methanogenesis over hydrogenotrophy suggest competition for H_2 with perchlorate reduction, which we propose is catalyzed abiotically by trace nickel and maintained by siphoning diffused H_2. These results provide new insights into previously documented interactions between perchlorates, methanogens, and their environment and expands our understanding of the potential for methanogens' survival beyond Earth and their possible contribution to Martian CH_4.

5.2 INTRODUCTION

The story of Martian atmospheric methane (CH_4) remains enigmatic and under intense debate. In the past 15 years, a growing body of evidence has unfolded to suggest episodic appearances (and disappearances) of ppbv-level CH_4 (Krasnopolsky et al., 2004; Formisano et al., 2004; Geminale et al., 2008; Mumma et al., 2009; Webster et al., 2015; Webster et al., 2018; Korablev et al., 2019). Myriad abiotic mechanisms have been suggested as potential CH_4 sources, including cometary impacts (Fries et al., 2016), UV degradation of meteoritic and interplanetary dust particle (IDP) organics (Keppler et al., 2012; Moores and Schuerger, 2012; Schuerger et al., 2012), and Fischer-Tropsch-type synthesis coupled to serpentinization of ultramafic silicates in the subsurface, which is subsequently released to the surface through seeps (Etiope et al., 2013; Oehler and Etiope, 2017) (Figure 5.1). On Earth, however, nearly 70% of CH_4 is of biological origin, generated by methanogenic *Archaea* (Conrad, 2009). This has led to an extensive debate considering the biological origin of Martian CH_4. Understandably, the quest to comprehend the nature of CH_4 cycling on Mars is a fervent one, as it may be the most conspicuous biosignature detected on Mars to date.

Methanogens are not only among the most deeply rooted microorganisms in the tree of life, but they are also among the most successful: they have proliferated into nearly every habitable anaerobic environment and possess conserved adaptions for growth and survival under stressful conditions including exposure to prolonged desiccation (Kendrick and Kral, 2006; Anderson et al., 2012; Kral and Altheide, 2013), high salinity (Sowers and Gunsalus, 1988; Maestrojuan et al., 1992; Sowers et al., 1993; Sowers and Gunsalus, 1995; Roessler et al., 2002), strong oxidants (Shcherbakova et al.,

2015; Kral et al., 2016), and extremes in temperature, pH, and pressure (Rivkina et al., 2002; Rivkina et al., 2004; Rivkina et al., 2007; Takai et al., 2008; Sinha et al., 2017). Thus, they are ideal candidates in the consideration of biology's potential contribution to Martian CH_4 and have thus been the subject of extensive study to infer how hostile conditions simulating modern Mars may allow – or inhibit – biological methanogenesis (Kendrick and Kral, 2006; Chastain and Kral, 2010; Kral et al., 2011; Kral and Altheide, 2013; Shcherbakova et al., 2015; Kral et al., 2016; Sinha et al., 2017; Mickol and Kral, 2017).

Perchlorate salts are highly soluble, chaotropic compounds that appear to be pervasive on Mars (Hecht et al., 2009; Navarro-González et al., 2010; Glavin et al., 2013; Kounaves et al., 2014a; Kounaves et al., 2014b; Clark and Kounaves, 2016). Perchlorates are of great interest to Martian habitability studies for their hygroscopicity and low eutectic temperatures, allowing for the formation of stable liquid water brines at temperatures as low as -74.6˚C and 55% relative humidity (Pestova et al., 2005; Chevrier et al., 2009; Marion et al., 2010; Stillman and Grimm, 2011; Toner et al., 2014; Nikolakakos and Whiteway, 2015). Previous work has reported decreased CH_4 production in methanogenic cultures supplemented with increasing concentrations of perchlorate salts (Shcherbakova et al., 2015; Kral et al., 2016). To date, the mechanisms resulting in this apparent inhibition of methanogenesis have not been fully explored. In this chapter I utilize transcriptomics to evaluate regulatory responses of the methanogenic archaeon *Methanosarcina barkeri* during a 28-day exposure to high concentrations of sodium-, magnesium-, and calcium-perchlorate salts at 30˚C and 0˚C to understand how

perchlorate salts inhibit methanogenesis and how they would influence their survival on Mars.

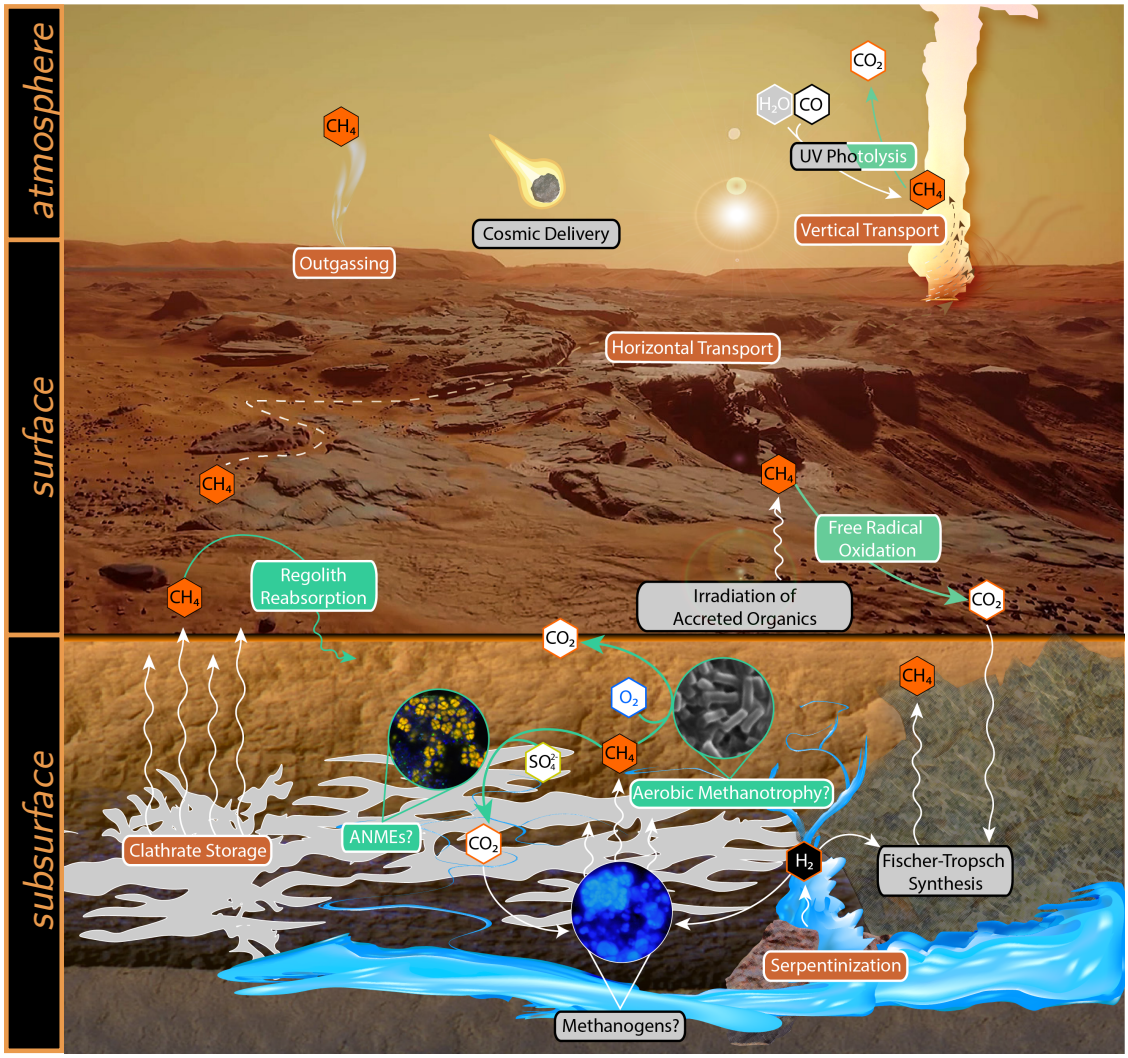

Figure 5.1. Proposed model for Martian CH_4 cycle. Sources indicated by grey boxes. Sinks are highlighted by green boxes and accompanying arrows (Atreya et al., 2007; Moores and Schuerger, 2012; Harris et al., 2019; Seto et al., 2019). Reservoirs, transport systems, and substrate-generating intermediates are denoted by orange boxes. This figure was generated using images from Mars Reconnaissance Orbiter and *Mars 2030* virtual reality game (produced by NASA in collaboration with the MIT AeroAstro Lab and Fusion Media Group, Doral FL) in accordance with the fair use doctrine of United States copyright law. Abbreviations: ANMEs, anaerobic methanotrophs.

5.3 MATERIALS AND METHODS

5.3.1 ***Materials and culture conditions***. *Methanosarcina barkeri* wild-type strain MS (ATCC® 51582™) was grown hydrogenotrophically (15 mL of 80:20 H_2:CO_2 headspace pressurized to 1.5 bar) in anaerobic balch tubes (Chemglass Life Sciences LLC, Vineland, NJ USA) containing 9 mL DSMZ medium 120a, 10 mg/L EDTA (pH 7.0 to 7.2) (Bryant and Boone, 1987), supplemented with trace element solution SL-10 (Widdel et al., 1983) and vitamin supplement MD-VS (ATCC®, Manassas, VA USA). Media assaying for perchlorate tolerance were augmented to 10 mM (final concentration) $NaClO_4$, $Mg(ClO_4)_2$, or $Ca(ClO_4)_2$. Balch tubes were inoculated with 1 mL cell suspensions containing ~4 x 10^7 cells and grown in batches of 9 biological replicates plus one autoclave-sterilized media blank for 28 days. For each experimental treatment (perchlorate-free control, $NaClO_4$, $Mg(ClO_4)_2$, or $Ca(ClO_4)_2$), optical density measurements (OD) and CH_4 production were monitored weekly in parallel experiments incubated at 30˚C or 0˚C (Figure 5.2).

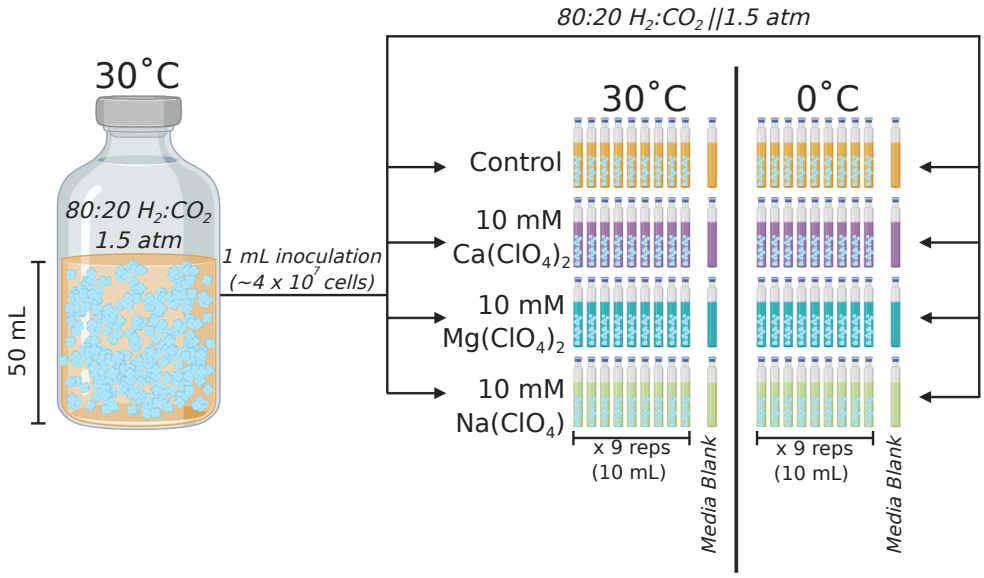

Figure 5.2. Experimental growth conditions investigating temperature and perchlorate effects on *M. barkeri*.

OD measurements were performed spectrophotometrically at 600 nm using a Genesys 30 Visible Spectrometer (Thermo-Scientific Corp., Madison, WI USA). At the end of the incubation experiment, direct cell counts were performed on enrichment aliquots fluorescently stained with Acridine Orange (AO) dye (catalog #318337, Sigma-Aldrich Chemical, Co., Milwaukee, WI USA) (50 μM final concentration) following an established procedure (Francisco et al., 1973). Stained cells were enumerated in a Spotlite hemocytometer counting chamber (McGaw Park, IL USA) with a Zeiss Axioskope 40 epifluorescence microscope (ZEISS Microscopy, Jena, Germany) at 600× magnification using an AO filter cube set (excitation 470/20 nm; emission >510 nm).

Headspace gas samples were collected via gas-tight syringes (catalog #24886, Restek U.S., Bellefonte, PA USA) to measure CH_4 evolution using a Trace 1310 gas chromatograph equipped with a flame-ionizing detector (GC-FID) (ThermoFisher Scientific, Waltham, MA USA). To avoid injecting atmospheric O_2 and residual carrier-over of trace gases within the syringes between samples, all syringes were flushed three times with ultra-high purity nitrogen gas (UHP N_2) between samples.

5.3.2 ***RNA isolation and purification.*** After 28 days' incubation, culture and blank volume contents were briefly vortexed and aseptically transferred into sterile 15 mL Falcon® tubes (Corning Inc., Corning, NY USA) at incubation temperature inside a Coy anaerobic chamber (Coy Laboratory Products Inc., Grass Lake, MI USA). Tubes were centrifuged at 3,000 × g for 1 minute using an IEC Centra CL2 centrifuge (Thermo Electron Company, Milford, MA USA) to pellet cells. Media was poured off for pH and electrical conductivity measurements, leaving behind 1 mL. To ensure quantifiable RNA yields downstream, the nine biological replicates from each condition were consolidated

into three sets of three samples each for extraction (3 mL pelleted cell suspension/tube). RNAlater solution (ThermoFisher Scientific, Waltham, MA USA) was added to a final volume of ~12 mL. Samples were left to equilibrate at incubation temperature for 3 hours, transferred to 4℃ for 24 hours, and then stored at -80˚C until overnight shipment on dry ice to Princeton University for RNA extraction.

Samples preserved at -80℃ in RNAlater were thawed on ice in a sealed container before contents were transferred to 50 mL Falcon® tubes. An equal volume (12 mL) of nuclease-free water (Qiagen, Hilden, Germany) was added to RNAlater-preserved samples, briefly vortexed, and centrifuged at 5,000 × g for 10 minutes using a Sorvall Legend XI centrifuge (ThermoFisher Scientific, Waltham, MA USA). The supernatant was subsequently discarded, and RNA was extracted following a modified protocol from a Zymo Quick-RNA Miniprep Plus Kit (Zymo Research, Irvine, CA USA). RNA lysis buffer and nuclease-free water were added to each sample in a 5:1 ratio, and sterile 0.7 mm garnet bashing beads (Qiagen, Hilden, Germany) were added to facilitate mechanical lysis during subsequent vortexing. Samples were then vortexed for 1 minute and centrifuged at 10,000 × g at 4℃ for 1 minute using an Eppendorf 5810R (Eppendorf, Hamburg, Germany) to pellet cell debris. The supernatant containing total nucleic acids was transferred to a yellow Spin-Away™ column (Zymo Research, Irvine, CA USA) fitted in a 2 ml collection tube. Samples were centrifuged at 10,000 x g for 1 minute using an AccuSpin Micro 17 (ThermoFisher Scientific, Waltham, MA USA) to separate out genomic DNA. Following centrifugation, the Spin-Away™ filter was discarded and the filtrate was collected from the column for RNA purification.

Total nucleic acids were then precipitated by adding 1 mL of chilled absolute ethanol. Pellets were mixed by pipetting and then transferred to green Zymo-Spin™ IIICG column filters fitted in clean collection tubes. Samples were centrifuged at 10,000 × g for 30 seconds to collect precipitated nucleic acids on the column, subsequently treated with 400 µL RNA wash buffer, and centrifuged for 30 seconds at 10,000 × g. The wash buffer was discarded and columns were treated with 80 µL DNAse I reaction mixture (per 80 µL: 5 µL DNAse 1 [1 U/µL], 8 µL 10X DNAse I reaction buffer [Zymo Research, Irvine, CA USA], 3 µL nuclease-free water, 64 µL RNA wash buffer [Zymo Research, Irvine, CA USA]) to degrade trace genomic DNA and left to incubate on ice in the dark for 15 minutes. DNAse-treated samples were then centrifuged at 10,000 × g for 30 seconds. The reaction buffers were discarded, column filters were washed three times with 400, 700, and 400 µl of RNA Prep Buffer (Zymo Research, Irvine, CA USA), centrifuging twice for 30 seconds at 10,000 × g and at 16,000 × g for 2 minutes for the final wash. Total RNA was then eluted into sterile, nuclease-free PCR tubes on ice using nuclease-free water pre-heated to 95℃. Total RNA was quantified using a Qubit hs RNA assay kit coupled to a Qubit 2.0 analyzer (ThermoFisher Scientific, Waltham, MA USA) following the manufacturer's protocol. RNA quality was subsequently assessed using a 2100 Bioanalyzer (Agilent Technologies Inc., Santa Clara, CA USA). RNA samples were kept at -20˚C until library preparation and sequencing.

All RNA extraction steps were performed using nuclease-free pipette tips (Corning Inc., Corning, NY USA) in a UV-sterilized laminar flow hood. All surfaces, pipettes, and gloves were wiped down at each step with RNaseZap® solution (ThermoFisher Scientific, Waltham, MA USA) to minimize potential RNase

contamination. Parallel extraction blanks of extraction kit reagents and blank growth media co-incubated with *M. barkeri* enrichment cultures were performed to ensure cleanliness of the extraction procedure and sterility of uninoculated growth media.

5.3.3 ***RNA library prep and RNA-Seq.*** Ribosomal RNA was depleted from total RNA using a Ribo-Zero Bacterial rRNA Removal Kit (Illumina, Inc., San Diego, CA USA) following the manufacturer's instructions and using the provided universal probe sequence. Bi-directional library prep was performed for each treatment and its constituent 3 sequencing replicates using the Nextera DNA Flex Library Prep Kit (Illumina, Inc., San Diego, CA USA) on the automated Apollo™ 324 system (Takara Bio USA, Inc., Mountain View, CA, USA). RNA-Seq was carried out for 318 cycles on two lanes of a NovaSeq SP Flowcell (Illumina, Inc., San Diego, CA USA) (2 x 150 bp) at the Princeton University genomics core facility.

5.3.4 ***Annotation and comparative transcriptomics*****.** Quality filtering of paired-end reads was performed using fastp v.0.12.6 (Chen et al., 2018), removing reads <50 nt, containing >1 Ns, Phred quality scores < 30, and sample barcode sequences. Using Bowtie2 v.2.3.2 (Langmead and Salzberg, 2012), retained, quality-filtered reads from each experiment were mapped to coding sequence (CDS) regions subset from the complete *M. barkeri* MS reference genome obtained from NCBI GenBank (accession no. NZ_CP009528.1). CDS-mapped reads were then sorted, indexed, and processed for extraction from the sequenced transcriptome using Samtools v.1.5 (Li et al., 2009) and BEDTools v.2.17.0 (Quinlan and Hall, 2010). Gene annotation was performed using

NCBI BLASTn v.2.2.29+ (Camacho et al., 2009) against a reference *M. barkeri* MS CDS assembly database generated using option -makeblastdb. Protein assignment was determined as the entry with the greatest sequence identity alignment with the query sequence, the lowest E-value, and largest bit score. Differential expression analysis of investigated treatments relative to the 30˚C and 0˚C perchlorate-free controls, within-group (i.e. biological replicate) variance estimation, and transcript fragment counts per million mapped reads (FPM) were performed using DESeq2 (Love et al., 2014). Metabolic pathway involvement of identified genes was determined by referencing the Kyoto Encyclopedia of Genes and Genomes (KEGG) (Ogata et al., 1999).

5.4 RESULTS

5.4.1 ***Transcriptome assembly statistics***. *M. barkeri* possesses the second largest described genome amongst the *Archaea* (Maeder et al., 2006). This genome comprises a 4.53 megabase (Mb) circular chromosome and a 40 kilobase (kb) plasmid, which collectively encode 3,760 genes, 3,470 of which are protein-encoding CDS regions (3.17 Mb). RNA sequencing yielded a total of 1,500,716,043 quality paired end reads across 24 libraries (8 conditions × 3 replicates/condition) with a mean Phred (sequence quality) score of 36. On average 1.60 ± 0.66 % of 30˚C and 1.50 ± 0.51% of 0˚C quality-filtered reads mapped back to CDS regions (n = 12 libraries/temperature condition; Table 5S.2), consistent with expectations that mRNA typically comprises 1-5% of total RNA in prokaryotic cells (Sorek and Cossart, 2010). Per individual open reading frame, the average FPM was consistent across all conditions (Figures 5S.2-5S.3, Table 5S.3).

5.4.2 ***Methanogenesis and associated regulatory responses***. Methane production was observed in all investigated conditions (Figure 5.3). At 30˚C, the addition of $Ca(ClO_4)_2$, $Mg(ClO_4)_2$, and $Na(ClO_4)$ reduced net CH_4 production by 48%, 32%, and 24%, respectively, relative to the perchlorate-free control. Significant reduction in CH_4 was observed across all treatments at 0˚C with respect to 30˚C, with no significant differences in production yields between perchlorate-incubated samples and the perchlorate-free control (Figure 5.3). No CH_4 production was observed in the media blank controls (data not shown). We note that it was difficult to assess culture growth via OD_{600} measurements (Figure 5S.1) due to precipitates formation in the media over time.

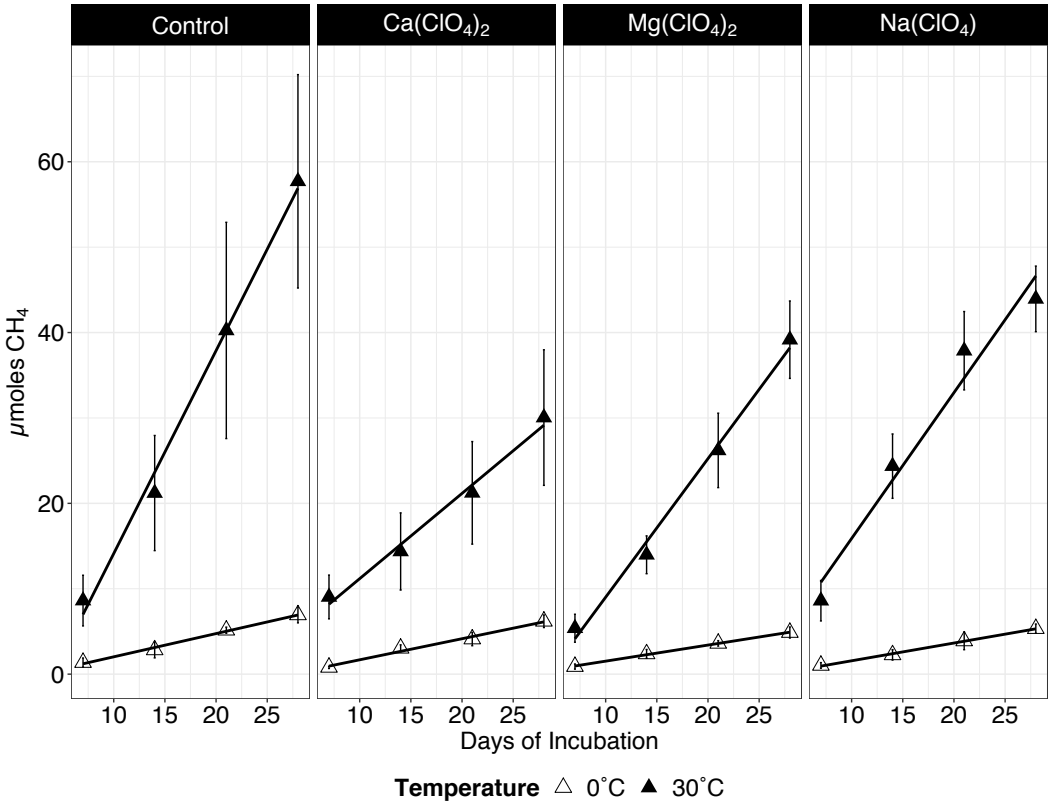

Figure 5.3. Cumulative CH_4 formation by *M. barkeri* strain MS grown (from left to right) without perchlorates (Control), $Ca(ClO_4)$, $Mg(ClO_4)_2$, or $Na(ClO_4)$ at 30˚C (filled triangles) and 0˚C (open triangles).

Both temperature and perchlorate exposure demonstrated distinct metabolic responses in *M. barkeri*'s CH_4 production pathways (Figures 5.4 – 5.7). When grown at 0˚C, the perchlorate-free control demonstrated significant up-regulation of several genes in the hydrogenotrophic pathway relative to the 30˚C perchlorate-free control (Figure 5.4), including $\log_2$-fold changes (LFC) in formylmethanofuran dehydrogenase subunit B (*Fmd*B) (LFC = 0.34 ± 0.12, $P = 0.02$), methenyl-tetrahydrosarcinapterin (H_4SPT) cyclohydrolase (*Mch*) (LFC = 0.21 ± 0.08, $P = 0.04$), and periplasmic heterodisulfide reductase (*Hdr*DE) ($LFC_{HdrD} = 0.23 \pm 0.07$, $P = 0.01$; $LFC_{HdrE} = 0.22 \pm 0.09$, $P = 0.03$). Likewise, significant down-regulation was observed in the sodium ion (Na^+) transporter methyl-H_4SPT:coenzyme M methyltransferase complex (*Mtr*A) (LFC = -0.51 ± 0.22, $P = 0.02$), as well as the F_{420}-reducing subunit of the periplasmic energy conserving hydrogenase (*Ech*F) (LFC = -0.33 ± 0.15, $P = 0.03$).

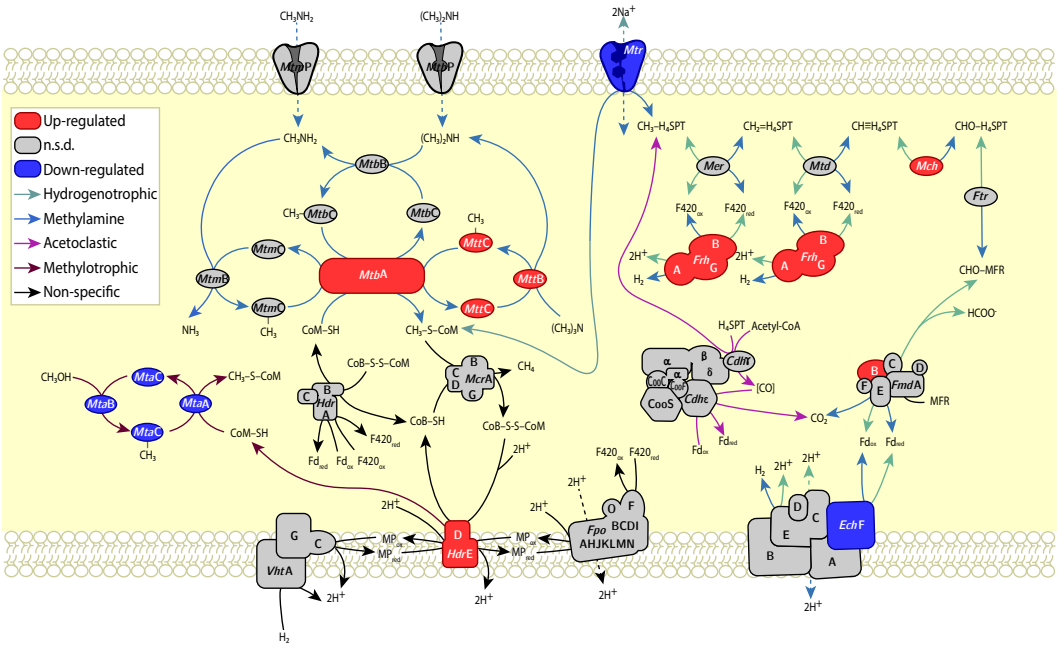

Figure 5.4. Regulatory responses in methanogenesis pathways in *M. barkeri* strain MS grown perchlorate-free at 0˚C. Significant differential expression (Wald test, $P < 0.05$) relative to the 30˚C perchlorate-free control. Abbreviations: n.s.d., no significant difference; Non-specific, common to multiple methanogenesis pathways.

At 30˚C, methanogenesis-associated regulatory responses shared across all perchlorate conditions included up-regulation of several subunits of molybdenum-containing formylmethanofuran dehydrogenase, *Fmd*, which catalyzes the CO_2 reduction step of the hydrogenotrophic pathway (Figures 5.5A, 5.6A, 5.7A). These subunits include *Fmd*B ($LFC_{Ca} = 0.44 \pm 0.14$, $P = 0.006$; $LFC_{Mg} = 0.44 \pm 0.14$, $p < 0.001$; $LFC_{Na} = 0.44 \pm 0.14$, $p < 0.001$), *Fmd*C ($LFC_{Ca} = 0.32 \pm 0.14$, $P = 0.05$; $LFC_{Mg} = 0.39 \pm 0.13$, $P = 0.01$; $LFC_{Na} = 0.45 \pm 0.13$, $P < 0.001$), and *Fmd*D (LFC $LFC_{Mg} = 0.52 \pm 0.15$, $P = 0.002$; $LFC_{Na} = 0.59 \pm 0.15$, $P = 0.001$). *Fmd*E also exhibited significant up-regulation under $Mg(ClO_4)_2$ and $Na(ClO_4)$ exposure ($LFC_{Mg} = 0.51 \pm 0.12$, $p < 0.001$; $LFC_{Na} = 0.43 \pm$

0.13, $P = 0.002$) (Figures 5.5A, 5.6A). Unique to the $Mg(ClO_4)_2$ incubations was the up-regulation of *Fmd*A (LFC = 0.40 ± 0.10, $P = 0.001$).

Supplying reduced ferredoxin to *Fmd*, *Ech*F was down-regulated in the presence of $Mg(ClO_4)_2$ and $Na(ClO_4)$ at 30˚C ($LFC_{Mg} = -0.77 \pm 0.20$, $p < 0.001$; $LFC_{Na} = -0.70 \pm 0.20$, $p < 0.001$) (Figures 5.5A, 5.6A). Contrasting to this, most subunits of *Ech* were significantly up-regulated in $Ca(ClO_4)_2$ conditions ($LFC_{EchA} = 0.62 \pm 0.14$, $p < 0.001$; $LFC_{EchB} = 0.60 \pm 0.19$, $P = 0.004$; $LFC_{EchE} = 0.35 \pm 0.12$, $P = 0.01$) (Figure 5.7A). Among other hydrogenases demonstrating significant up-regulation was methanophenazine-dependent hydrogenase, *Vht*, specifically, the large subunit *Vht*A ($LFC_{Ca} = 0.31 \pm 0.12$, $P = 0.04$; $LFC_{Mg} = -0.32 \pm 0.12$; $P = 0.03$) and cytochrome b subunit *Vht*C ($LFC_{Ca} = 0.31 \pm 0.12$, $P = 0.04$). Regardless of type of perchlorate exposure, all subunits of both coenzyme F_{420} hydrogenases (*Frh*αβγ) were significantly up-regulated at 0˚C ($LFC_{Frh\alpha} = 0.38 \pm 0.12$, $P = 0.01$; $LFC_{Frh\beta} = 0.17 \pm 0.07$, $P = 0.05$; $LFC_{Frh\gamma} = 0.29 \pm 0.13$, $P = 0.04$) (Figure 5.4).

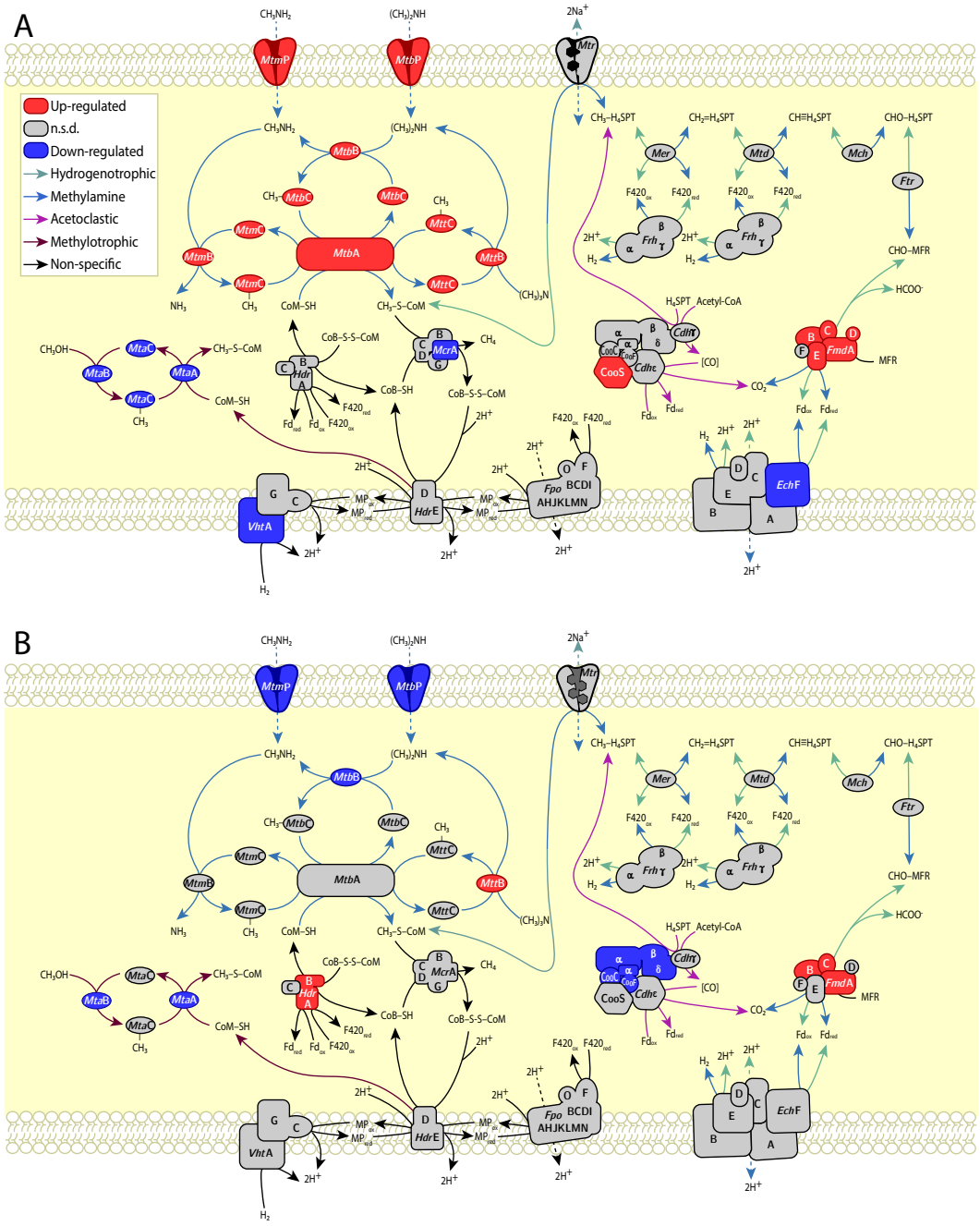

Figure 5.5. Regulatory responses in methanogenesis pathways in $Mg(ClO_4)_2$-incubated *M. barkeri* strain MS grown at 30˚C **(A)** relative to the 30˚C perchlorate-free control and 0˚C **(B)** relative to the 0˚C perchlorate-free control. Significant differential expression (Wald test, $P < 0.05$). Abbreviations: n.s.d., no significant difference; Non-specific, common to multiple methanogenesis pathways.

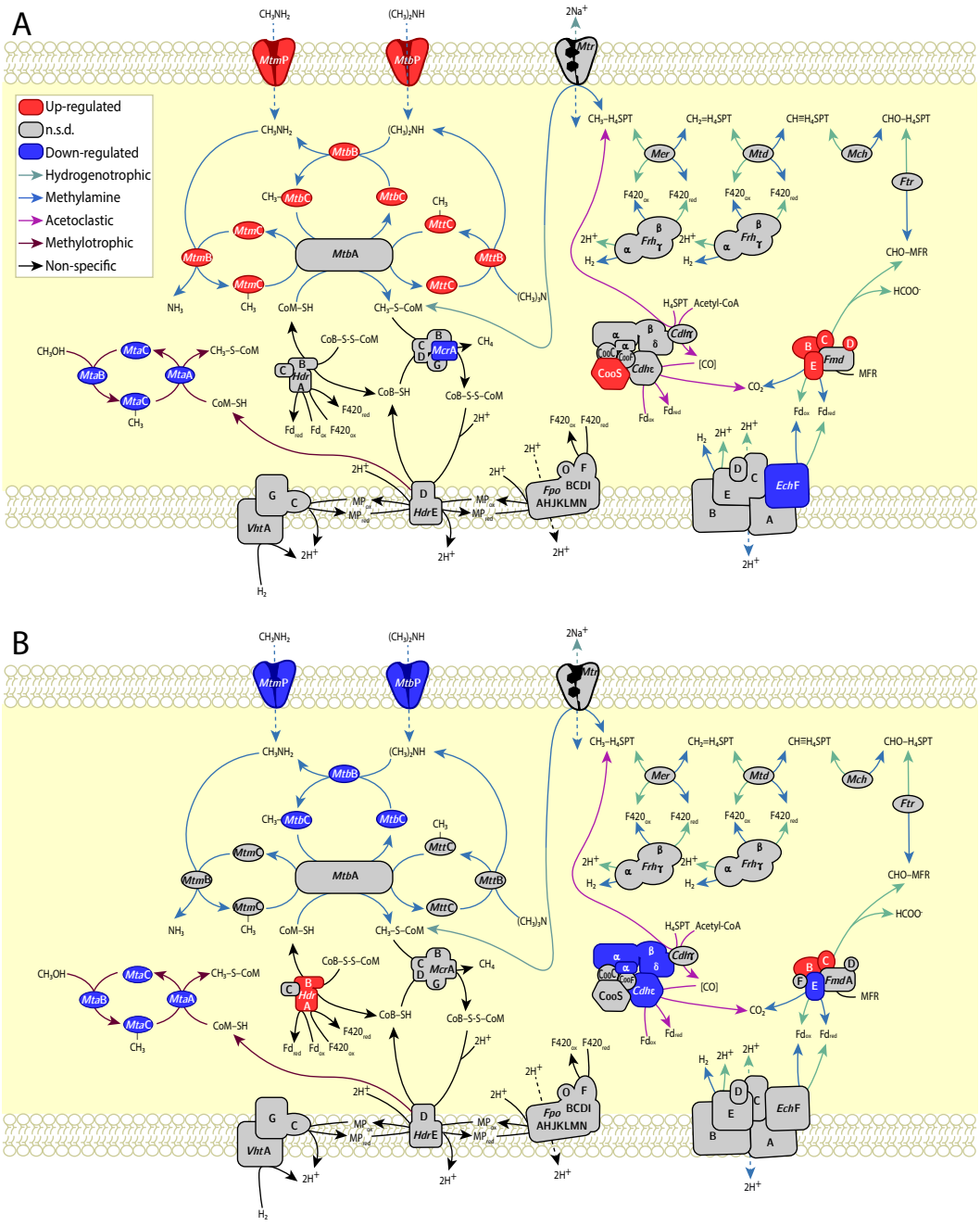

Figure 5.6. Regulatory responses in methanogenesis pathways in $Na(ClO_4)$-incubated *M. barkeri* strain MS grown at 30˚C **(A)** relative to the 30˚C perchlorate-free control and 0˚C **(B)** relative to the 0˚C perchlorate-free control. Significant differential expression (Wald test, $P < 0.05$). Abbreviations: n.s.d., no significant difference; Non-specific, common to multiple methanogenesis pathways. Full names of proteins and metabolites are respectively listed in Appendix A, Table A.2 and Table A.3.

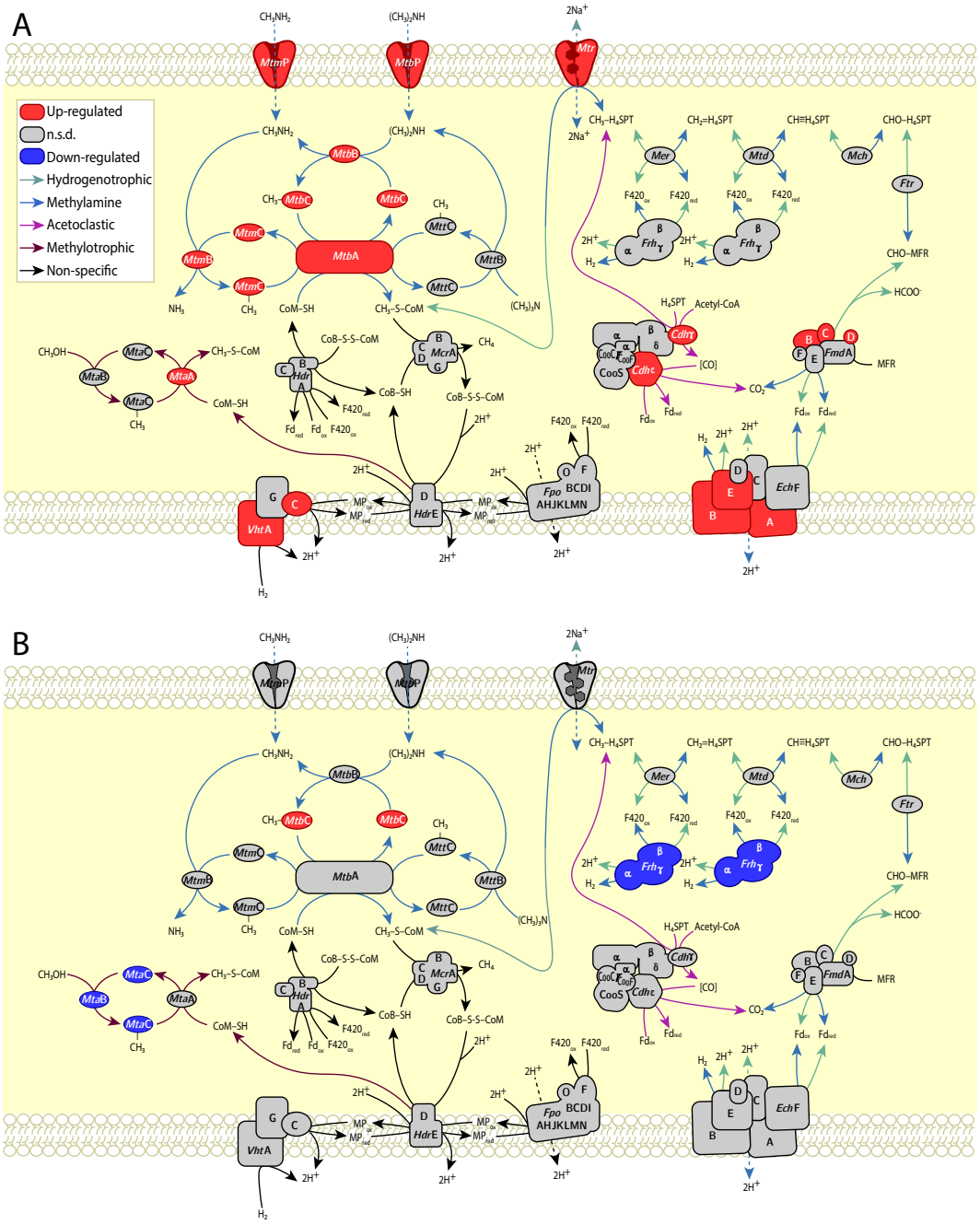

Figure 5.7. Regulatory responses in methanogenesis pathways in $Ca(ClO_4)_2$-incubated *M. barkeri* strain MS grown at 30˚C **(A)** relative to the 30˚C perchlorate-free control and at 0˚C **(B)** relative to the 0˚C perchlorate-free control. Abbreviations: n.s.d., no significant difference; Non-specific, common to multiple methanogenesis pathways. Complete names of proteins and metabolites are respectively listed in Appendix A, Table A.2 and Table A.3.

Despite H_2 being the only reducing equivalent provided for the production of CH_4 in our incubations, the up-regulation of complete methylamine-dependent methanogenesis pathways was conspicuous in the 30˚C perchlorate treatments. The addition of $Ca(ClO_4)_2$, $Mg(ClO_4)_2$, and $Na(ClO_4)$ resulted in significant and complete up-regulation of all three (mono-, di-, and trimethylamine) pathways, including associated membrane permeases (Figures 5.4 – 5.7).

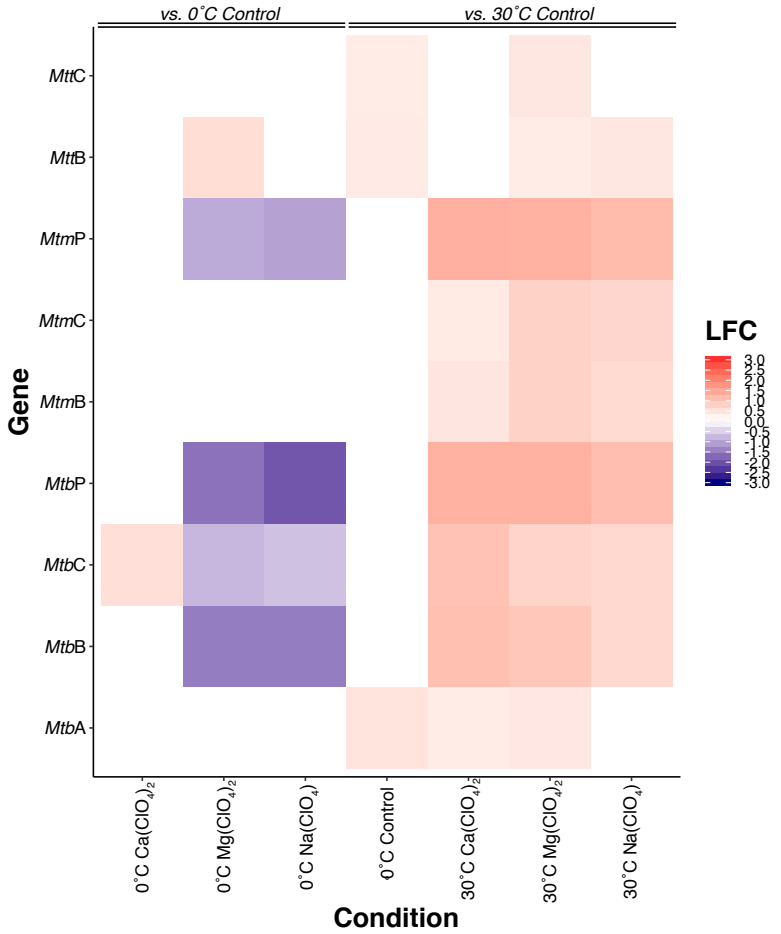

Figure 5.8. Differential expression (Log_2-fold change, LFC) of methylamine-specific methanogenesis genes in *M. barkeri* MS. Perchlorate-grown 30˚C and 0˚C perchlorate-free control cultures are relative to 30˚C perchlorate-free control. 0˚C perchlorate-grown cultures are relative to 0˚C perchlorate-free control. An absence of a bar means no significant differential expression from control. (Wald test, $P < 0.05$). Full names of proteins encoded by listed genes are provided in Appendix A, Table A.4.

Despite the up-regulation of several genes in the methanogenesis pathway, the terminal step encoding methyl-coenzyme M (CH_3-CoM) reductase subunit alpha (*Mcr*A) was down-regulated at 30˚C in $Mg(ClO_4)_2$ (Figure 5.5A) (LFC = -0.40 ± 0.16, $P = 0.03$) and $Na(ClO_4)$ (Figure 7A) enrichments (LFC = -0.36 ± 0.16, $P = 0.04$). Although this reduction in expression is consistent with decreased CH_4 production observed in these treatments (Figure 3), both $Mg(ClO_4)_2$ and $Na(ClO_4)$-grown enrichments generated greater net CH_4 than $Ca(ClO_4)_2$-grown *M. barkeri*, which showed no significant differences in expression of the *Mcr* complex from the 30˚C perchlorate-free control. Furthermore, no elements of *Mcr* were significantly differentially expressed at 0˚C in perchlorate-free media (Figure 5.4). Therefore, the decreased expression of *Mcr*A is not sufficient to explain the associated decrease in CH_4 evolution in perchlorate enrichments at 30˚C.

Elements of the carbon monoxide dehydrogenase/acetyl-CoA synthase complex (CODH/ACS) demonstrated significant regulatory changes as a function of temperature and perchlorate exposure. *Coo*S, was up-regulated in 30˚C $Mg(ClO_4)_2$ and $Na(ClO_4)$ treatments ($LFC_{Mg} = 0.40 \pm 0.13$, $P = 0.008$; $LFC_{Na} = 0.49 \pm 0.13$, $P = 0.001$) (Figures 6-7). Carbon monoxide dehydrogenase subunit epsilon (*Cdh*ε), which recycles ferredoxin in the reversible conversion between CO and CO_2, was up-regulated with $Ca(ClO_4)_2$ at 30˚C (LFC = 0.53 ± 0.14, $P = 0.002$) (Figure 5.7A), but was down-regulated in the 0˚C $Na(ClO_4)$ treatment (LFC = -1.00 ± 0.21, $P < 0.001$) (Figure 5.6B). *M. barkeri* grown at 30˚C with $Ca(ClO_4)_2$ also demonstrated significant up-regulation of 5-H_4SPT:corrinoid Fe-S protein methyltransferase (*Cdh*γ) (LFC = 0.39 ± 0.16, $P = 0.04$), which plays a key

role in the generation H_4SPT and acetyl-CoA for biomass synthesis in the Wood-Ljundal pathway (Figure 5.7A).

With respect to the 0˚C perchlorate-free control, both alpha and beta chains of ACS, respectively encoded by *Cdh*α and *Cdh*β, were down-regulated in 0˚C Na(ClO_4)-supplemented cultures ($LFC_{Cdh\alpha}$ = -1.03 ± 0.13, $P < 0.001$; $LFC_{Cdh\beta}$ = -0.76 ± 0.22, P = 0.003). *Cdh*α was also down-regulated in 0˚C Mg(ClO_4)$_2$ cultures (LFC = -0.73 ± 0.32, P = 0.009). *Cdh*δ, which encodes an iron-sulfur corrinoid protein, was also down-regulated at 0˚C in Mg(ClO_4)$_2$ (LFC = -0.67 ± 0.28, P = 0.007). We observed no significant differential expression of CODH/ACS complex genes in 0˚C Ca(ClO_4)$_2$-grown *M. barkeri* (Appendix A, Table A.14).

5.4.3 ***Regulation of nitrogen metabolism.*** We observed substantial up-regulation of ammonium transporters (*Amt*) in the 30˚C perchlorate treatments with respect to the 30˚C control. Only one ammonium transporter was up-regulated in the presence of Ca(ClO_4)$_2$ (LFC = 0.52 ± 0.24, $P = 0.0$4), but three *Amt* genes were amongst the most significantly up-regulated genes in both Mg(ClO_4)$_2$ and Na(ClO_4) treatments ($LFC_{Mg.1}$ = 1.34 ± 0.12, $P < 0.001$; $LFC_{Mg.2}$ = 1.27 ± 0.18, $P < 0.001$; $LFC_{Mg.3}$ = 1.21 ± 0.22, $P <$ 0.001; $LFC_{Na.1}$ = 1.33 ± 0.22, $P < 0.001$; $LFC_{Na.2}$ = 1.29 ± 0.18, $P < 0.001$; $LFC_{Na.3}$ = 1.16 ± 0.13, $P < 0.001$). Notably, we observed no significant differences in *Amt* expression at 0˚C in any treatment. Perchlorates must somehow be impacting nitrogen metabolism in *M. barkeri* at 30˚C to an extent that warrants substantial log-fold changes in transcription of *Amt*.

Despite an initial abundance of fixed nitrogen (9.3 mM NH_4Cl plus undefined components of complex nutrients such as yeast extract and casitone) and a lack of supplied N_2 in the headspace of *M. barkeri* incubations, we observed significant differential expression of nitrogenase proteins when cells were grown with perchlorates (Figure 5.9). Transcriptomes from $Mg(ClO_4)_2$ and $Na(ClO_4)$ amended media showed significant differential expression of 7 and 8 genes directly involved in nitrogenase activity, respectively. Conversely, only one nitrogenase component was differentially expressed at 0˚C and in $Ca(ClO_4)_2$ amended cultures: the Fe-protein dinitrogen reductase, *Nif*H, which is responsible for electron transfer to the $\alpha_2\beta_2$ N_2 binding site (encoded by *Nif*D and *Nif*K, respectively) via ATP hydrolysis.

To save cells from the energetic costs associated with N_2 fixation, regulatory P-II proteins (*Nif*I) will trigger N_2 fixation to switch off when fixed nitrogen becomes freely available (Lobo and Zinder, 1988; Lobo and Zinder, 1990; Kessler and Leigh, 1999; Kessler et al., 2001). Several copies of *Nif*I demonstrated a significant increase in expression in $Mg(ClO_4)_2$ and $Na(ClO_4)$-supplemented cultures (Figure 5.9), suggesting a concerted effort to dedicate cellular energy towards signaling the shut off of FeMo nitrogenase activity. However, the occurrence of this process is unverifiable based on transcriptomics alone. The observation of co-upregulation of both nitrogenases and P-II repressors is consistent with previous findings that the P-II orchestrated shutoff is a posttranslational regulatory process and does not affect transcription or mRNA stability of other *Nif* genes under conditions of intermittent NH_3 availability (Kessler et al., 2001).

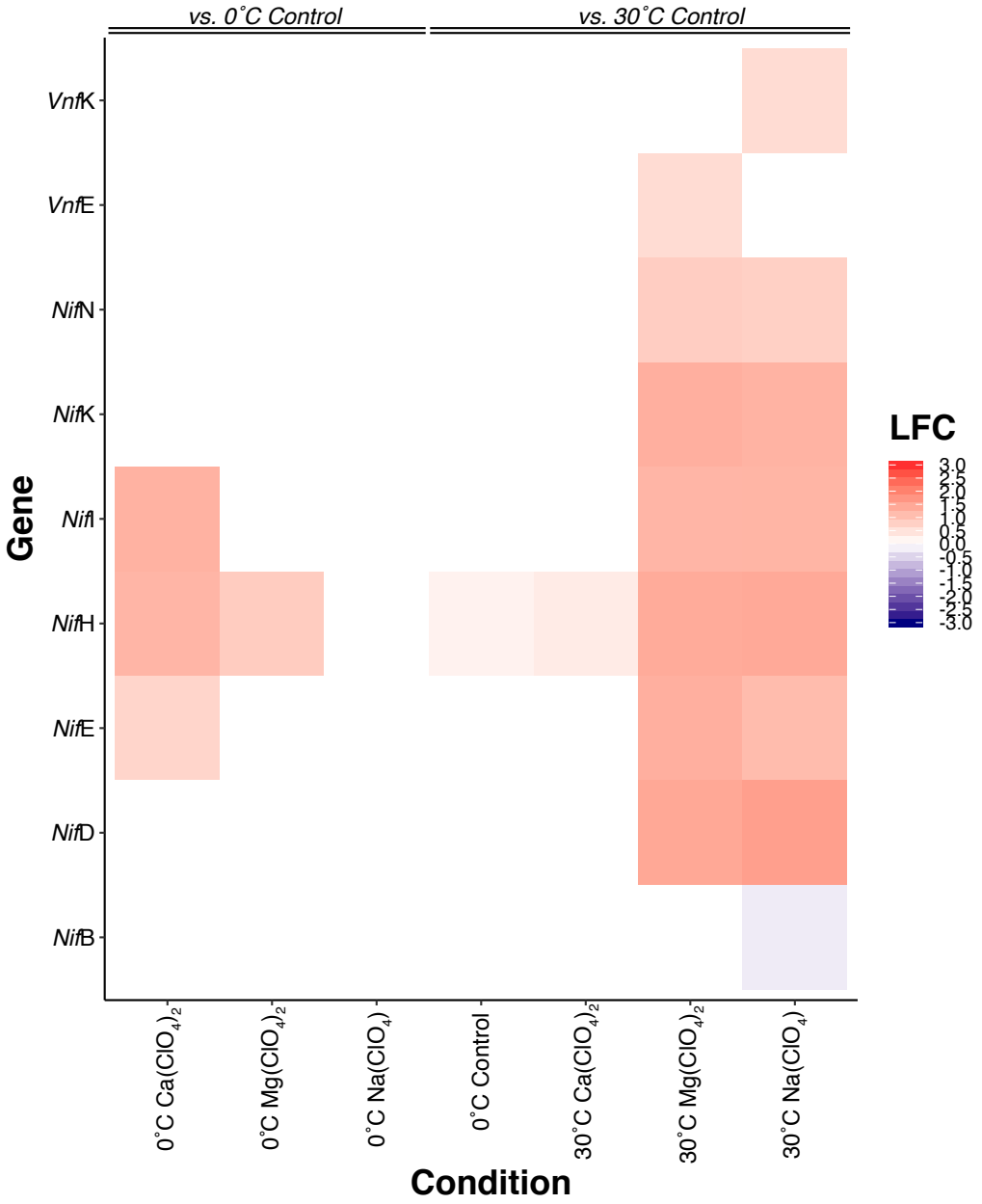

Figure 5.9. Differential expression (Log_2-fold change, LFC) of genes encoding nitrogenase proteins in *M. barkeri* MS. Perchlorate-amended 30˚C and 0˚C perchlorate-free control cultures are relative to 30˚C perchlorate-free control. 0˚C perchlorate-amended cultures are relative to 0˚C perchlorate-free control. Significance identified via Wald test ($P < 0.05$). Full names of proteins encoded by listed genes are found in Appendix A, Table A.5.

5.4.4 ***Osmoregulation***. Several regulatory responses suggested increased osmotic stress in perchlorate-supplemented cultures at 30˚C. In $Mg(ClO_4)_2$-grown *M. barkeri*, we

observed up-regulation of the complete operon for osmostress protectants uptake A ($LFC_{OpuA}A = 0.64 \pm 0.17$, $P < 0.001$; $LFC_{OpuA}B = 0.73 \pm 0.20$, $P < 0.001$; $LFC_{OpuA}C = 0.66 \pm 0.30$, $P = 0.02$). In $Na(ClO_4)$ enrichments, significant log_2-fold changes were also observed for *OpuA*A (LFC = 0.54 ± 0.17, $P = 4 \times 10^{-3}$) and *OpuA*B (LFC = 0.59 ± 0.20, $P = 7 \times 10^{-3}$). *OpuA* is responsible for the uptake of extracellular glycine betaine, belonging to a family of ABC transporters that hydrolyze ATP to import glycine betaine and other osmoprotectants such as proline (Kempf and Bremer, 1995; Kempf and Bremer, 1998; Hoffmann and Bremer, 2017). The *Opu* family also includes uptake systems for choline, a glycine betaine precursor (Hoffmann and Bremer, 2017), but *M. barkeri* lacks the cellular machinery for *de novo* glycine betaine synthesis (Hippe et al., 1979).

In addition to being an osmoprotectant, glycine betaine is also cryoprotective (Casanueva et al., 2010). Relative to the 0˚C perchlorate-free control, we observed significant down-regulation of *OpuA*A in 0˚C $Mg(ClO_4)_2$ (LFC = -0.94 ± 0.30, $P = 8.02 \times 10^{-3}$) and $Na(ClO_4)$ (LFC = -0.69 ± 0.31, $P = 3.14 \times 10^{-2}$) treatments. *OpuA*B was also down-regulated in 0˚C $Mg(ClO_4)_2$-grown cultures (LFC = -1.03 ± 0.38, $P = 1.56 \times 10^{-2}$). This likely signals a decreased cold shock response in *M. barkeri* due to the solubility and freezing point depression of perchlorate salts.

Evidence for osmotic stress is also reflected in the regulation of cell surface protein synthesis. Methanochondroitin is the primary constituent of the extracellular matrix that clumps *M. barkeri* cells into multicellular aggregates under optimal growth conditions (Kreisl and Kandler, 1986). Increased salinity ([NaCl] > 0.4 M) confers a decrease in methanochondroitin synthesis, thinning the methanochondroitin outer layer

and ultimately leading to the disaggregation of *M. barkeri* clumps into planktonic cells (Sowers et al., 1993). Glucuronic acid, generated from glucose degradation via UDP-glucose dehydrogenase (*UGDH*), is a major component of methanochondroitin (Kreisl and Kandler, 1986; Jarrell et al., 2010). We observed significant down-regulation of *UGDH* under $Mg(ClO_4)_2$ and $Na(ClO_4)$ conditions at 30˚C (LFC_{Mg} = -0.55 ± 0.17, $P = 3 \times 10^{-3}$; LFC_{Na} = -0.51 ± 0.17, $P = 7 \times 10^{-3}$), which may indicate conditions conducive to methanochondroitin thinning, though any increase in salinity associated with 10 mM perchlorate amendments in our incubations is minimal and likely insufficient to promote disaggregation. Electron microscopy is necessary to compare methanochondroitin thickness between conditions in order to assess this hypothesis.

5.4.5 ***Amino acid metabolic pathways***. We assessed the regulation of amino acid synthesis, degradation, and recycling to infer how freezing conditions and/or perchlorate exposure may have impacted the structural and functional activity of proteins. In addition to the 20 common amino acids, *M. barkeri* also encodes a 21st residue, pyrrolysine, via the 'amber' stop codon UAG (Srinivasan et al., 2002). A comparison of the genes encoding amino acid synthesis proteins showed large negative log_2-fold changes at 30˚C in $Mg(ClO_4)_2$ and $Na(ClO_4)$ amended cultures with respect to cysteine-producing proteins cysteine synthase (*Cys*K) and serine acetyltransferase (*Cys*E) (Figure 5.10A). Further examination of complete amino acid metabolic pathways (Appendix B, Figures B.1 – B.13) revealed that this pattern of substantial down-regulation of genes was characteristic of not only cysteine, but also other the sulfur-containing amino acid methionine (Figure 5.10B).

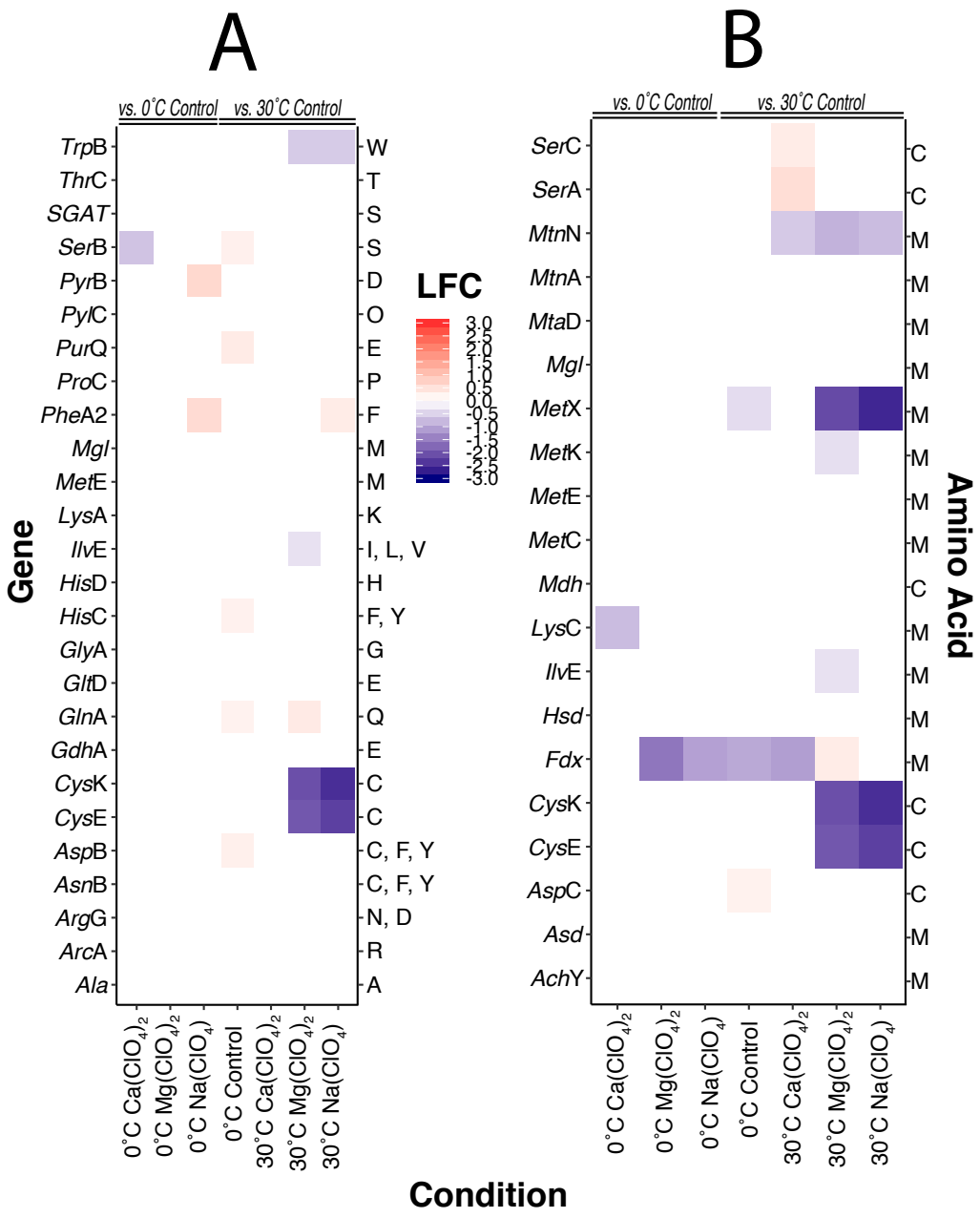

Figure 5.10. Differential expression (Log_2-fold change, LFC) of genes involved in **(A)** amino acid synthesis and **(B)** recycling of the sulfur-containing amino acids methionine and cysteine in *M. barkeri* MS. Perchlorate-amended 30˚C and 0˚C perchlorate-free control cultures are relative to 30˚C perchlorate-free control. 0˚C perchlorate-amended cultures are relative to 0˚C perchlorate-free control. Significant differential expression was identified via Wald test ($P < 0.05$). Full names of gene and amino acid abbreviations are respectively found in Appendix A, Table A.6 and Table A.7.

5.5 DISCUSSION

5.5.1 *Nitrogenase expression patterns provide insight into global metabolic state.*

Nitrogen fixation is an energetically expensive process, consuming at least 16 (and, by one calculation for methanogens (Lobo and Zinder, 1992), perhaps more than 50) moles of ATP per mole of N_2 fixed (Sohm et al., 2011). Previous work has demonstrated that expression of *Nif* operon components *NifD*, *Nif*K, and *Nif*H in *Methanococcus maripaludis* is characteristic of growth under diazotrophic conditions, but undetectable after prolonged exposure to NH_3 (Kessler et al., 1998). It is generally accepted that N_2 availability does not regulate nitrogenase activity (Halbleib and Ludden, 2000). In *M. barkeri*, NH_3 concentrations as low as 10 μM have been shown to be inhibitory to nitrogen fixation (Lobo and Zinder, 1988; Lobo and Zinder, 1990; Kessler and Leigh, 1999; Kessler et al., 2001). Our results appear inconsistent with these findings. Given the initial concentrations of fixed nitrogen in the growth media and the significant up-regulation of both ammonia transporters and genes involved in methylamine methanogenesis at 30˚C with the addition of perchlorate salts, it is surprising to observe a simultaneous up-regulation in nitrogenase gene expression (Figure 5.9).

It is possible, however, that the concurrent up-regulation of these genes is indicative of a physiological state of nitrogen starvation. In our experiments, *M. barkeri* growth is presumably limited by bioavailable fixed-N in the growth media. Nitrogen depletion at 30˚C is likely tied to our observation of stalled growth rates (Figure 5S.1). The up-regulation of ammonia transporters and methylamine permeases is consistent with a strategy of scavenging transiently available fixed-N. Methylamines were not present in the media and so the observation of significant up-regulation of methylamine-specific

methanogenesis pathways was unexpected, particularly because the decreased free energy yields of these reactions relative to the hydrogenotrophic pathway (Table 5.1). While we are presently unable to explain an exact mechanism of the formation of methylamines, we imagine possible interactions between perchlorates and amino acids in complex media components (e.g., from yeast extract and casitone in these experiments) could yield methylamine generation for uptake and utilization by *M. barkeri* for methanogenesis.

Table 5.1. Gibbs free energy change (ΔG°_{Rxn}) of methanogenesis net reactions at 30˚C and 0˚C. Values are presented in kJ/mol CH_4.

Reaction	30˚C	0˚C
$H^+ + HCO_3^- + 4H_2 \leftrightarrow CH_4 + 3H_2O$	-158	-167
$4CH_3OH \leftrightarrow 3CH_4 + H^+ + HCO_3^- + 3H_2O$	-121	-118
$4CH_3OH + H_2 \leftrightarrow CH_4 + H_2O$	-130	-130
$4CH_3NH_2 + 3H_2O + 3H^+ \leftrightarrow 3CH_4 + HCO_3^- + 4NH_4^+$	-136	-134
$CH_3NH_2 + H_2 + H^+ \leftrightarrow CH_4 + NH_4^+$	-143	-143
$2(CH_3)_2NH + 3H_2O + H^+ \leftrightarrow 3CH_4 + HCO_3^- + 2NH_4^+$	-103	-98
$(CH_3)_2NH + 2H_2 + H^+ \leftrightarrow 2CH_4 + 2NH_4^+$	-117	-116
$4(CH_3)_3N + 9H_2O + H^+ \leftrightarrow 9CH_4 + 3HCO_3^- + 4NH_4^+$	-91	-86
$(CH_3)_3N + 3H_2 + H^+ \leftrightarrow 3CH_4 + 3\ NH_4^+$	-108	-106
$CH_3COO^- + H^+ \leftrightarrow CH_4 + CO_2$	-25	-21

It has been suggested that glycine betaine may be a potential precursor of trimethylamine (TMA) (Oren, 1990; Seibel and Walsh, 2002). Given that *M. barkeri* does not possess a trimethylamine permease protein, TMA would need to be generated

intracellularly. The significant up-regulation of the glycine betaine-importing *OpuA*A operon provides one such mechanism to bring a TMA precursor into the cell.

The intermittent availability of fixed-N can also be tied to the observed expression of *Nif* genes, reflecting a strategy of *M. barkeri* "priming itself" for nitrogen fixation once NH_3 becomes limiting, presumably resulting from a decrease in bioavailable fixed-N due to unknown interactions between perchlorates and the media. Likewise, similar patterns in expression of regulatory P-II proteins point to an abundance of mRNA primed for translation to quickly prevent the unnecessary dumping of energy and electrons into N_2 reduction when NH_3 becomes available again (e.g., the generation of NH_3 from methylamine methanogenesis). The potential for translation of *Nif* transcripts under N limitation is also not unprecedented.

The overproduction of MoFe nitrogenase has been observed at the proteomic level in nitrogen-starved *Rhodopseudomonas palustris* (Arp and Zumft, 1983). Another study investigating *R. palustris* showed a four- to eight-fold increase in MoFe nitrogenase activity in cultures grown under prolonged N limitation, compared to *R. palustris* grown diazatrophically (Alef et al., 1981). It is possible that increased nitrogenase activity also occurred in our incubations, but an established link between reduced nitrogenase activity and increased osmotic stress (Burns et al., 1985; Deits and Howard, 1990; Brabban et al., 1999) suggests decreased nitrogenase activity is more likely. Relative to *Nif* homologues found in diazotrophic *Bacteria*, *M. barkeri*'s MoFe nitrogenase is three times more sensitive to increases in salinity with complete inhibition of nitrogenase activity occurring at 190 mM NaCl (Brabban et al., 1999). In the absence of proteomic data, it is

difficult to assess a correlation between the up-regulation of *Nif* genes and glycine betaine.

5.5.2 ***The potential of catalytic nickel and "leaky" H_2 as agnostic mediators of perchlorate reduction.*** Microbial perchlorate reduction has been observed in the *Proteobacteria* and halophilic *Archaea* (Logan et al., 2001; Coates and Achenbach, 2004; Yu et al., 2006; Bardiya and Bae, 2011; Liebensteiner et al., 2013; Oren et al., 2014), but to date no direct evidence has been shown demonstrating perchlorate reduction in methanogenic taxa. Perchlorate reduction has been observed in methanogenic enrichments, but the mechanism(s) driving this phenomenon remain poorly understood (Shcherbakova et al., 2015; Kral et al., 2016). Abiotic reduction of perchlorate has been shown in a sterile minimal salts methanogenic medium under a 2 bar atmosphere of 80:20 H_2:CO_2 supplemented with 5mM (final concentration) of either $Na(ClO_4)$ or $Mg(ClO_4)_2$ (Shcherbakova et al., 2015). In culture media containing *Methanobacterium arcticum* M2 (Shcherbakova et al., 2011), perchlorate reduction was increased by a factor of 1.7 and 2.6 for $Na(ClO_4)$ and $Mg(ClO_4)_2$, respectively, leading to the authors' suggestion that *M. arcticum* might be able to utilize perchlorate as an electron acceptor in the anaerobic oxidation of methane (AOM). These interpretations remain unverified.

Perchlorate reduction in *M. barkeri* enrichments has been observed to significantly increase when the basal growth medium is supplemented with complex nutrients such as yeast extract and trypticase peptone (Kral et al., 2016). Notably, reduction has been observed to run more to completion in enrichments supplemented with $Ca(ClO_4)_2$ relative to $Mg(ClO_4)_2$ and $Na(ClO_4)$ (Kral et al., 2016). While we did not

measure perchlorate concentrations in this study, we may still be able to infer, given the same growth media composition in this study as that used by Kral et al.(2016), that the strikingly similar regulatory patterns observed at 30˚C in $Mg(ClO_4)_2$ and $Na(ClO_4)$ transcriptomes but not in $Ca(ClO_4)_2$ transcriptomes (e.g. Figures 5.5A and 5.6A vs. Figure 5.7A and Figures 5.9-10) are reflective of comparatively advanced progression of $Ca(ClO_4)_2$ reduction. Ultimately, perchlorate measurements need to be made to confirm this, but at present we consider this the most likely explanation to explain the significant differences in expression which distinguish $Ca(ClO_4)_2$-supplemented *M. barkeri* from the other two perchlorate conditions. Measurements to monitor perchlorate concentration over the course of incubation are planned for future experiments to verify this interpretation.

If we are to accept the evidence and precedents supporting the occurrence of perchlorate reduction in our cultures, we must identify an electron donor that can facilitate this reaction to proceed. Kral et al. (2016) ruled out Na_2S and stainless steel as significant contributors to perchlorate reduction in methanogenic media, as they observed no significant differences in CH_4 production in cultures grown with these compounds versus those grown without. Although they do not explicitly address whether *M. barkeri* and other investigated methanogens could have mediated perchlorate reduction, they also argue their results were not supportive of perchlorate reduction being linked to CH_4 oxidation (abiotic or otherwise) (Kral et al., 2016).

The work of Shcherbakova et al. (2015) and Kral et al. (2016) suggests that the composition of methanogenic growth media is sufficient to kickstart abiotic perchlorate reduction, which is stimulated by the addition of complex organic nutrients, and is

enhanced further by changing gradients of electrochemical potential sustained by microbial metabolism. Therefore, we must conclude that the electron donor is available in the media and reacts more spontaneously with perchlorate with the addition of complex organic nutrients and metabolizing biomass. H_2 is a potential reducing agent of perchlorate ($\Delta G^{\circ'}$ = -289 kJ/mol H_2). However, the reaction is kinetically sluggish at ambient conditions due to its large activation energy (Abu-Omar, 2003).

The addition of metallic catalysts and adsorptive carbon substrates have been shown to overcome this energy barrier (Wang et al., 2008). Nickel has long been known as an excellent hydrogenation catalyst (Adkins and Cramer, 1930) and is an essential cofactor for hydrogenase activity in methanogens (Thauer et al., 2010). We postulate that free nickel sourced from the trace element solution could catalyze abiotic perchlorate reduction observed in sterile methanogenic media (Shcherbakova et al., 2015; Kral et al., 2016). Conspicuous regulatory shifts observed in Ni-containing hydrogenases at 30˚C but not at 0˚C is intriguing (notably the active sites *Ech*E, *Vht*A, *Frh*α; see Figures 5.5 – 5.7). These results suggest the need to investigate whether H_2-dependent perchlorate reduction could be enzymatically stimulated when adsorbed to a Ni-containing active site.

In methylamine methanogenesis, H_2 is recycled by the partial reversal of the methanogenesis pathway, generated via the oxidation of $F_{420}H_2$ by *Frh* and the oxidation of ferredoxin by *Ech* (blue arrows in Figures 5.5 - 5.7). H_2 generated by the oxidation of $F_{420}H_2$ and ferredoxin diffuses across the membrane to be oxidized by *Vht* in an energy conserving scheme to recycle methanophenazine (MP) (Ide et al., 1999; Meuer et al., 2002; Deppenmeier, 2004; Kulkarni et al., 2018). Ferredoxin oxidation by *Ech* also results in the translocation of $2H^+$ through *Ech*, contributing to the production of a proton

gradient (high outside the cell) (Kulkarni et al., 2018). Evidence for the generation of this proton gradient is indicated in our incubations based on drops in pH (up to 0.77 pH units) (Table 5S.1). Based on up-regulation of the genes for methylamine methanogenesis, we attribute the differential expression of *Ech*, *Vht*, and *Frh* hydrogenases (Figures 5.5 – 5.7) and ferredoxin (Appendix A, Tables A.9, A.11, A.13) as the sources of this proton motive force in the 30˚C perchlorate-supplemented incubations.

Methanogenesis, however, results in a net consumption of the proton motive force (Table 5.1), so one would expect to observe an increase in pH if all moles of substrate are made into the maximum number of moles of CH_4 afforded by the reaction. The joint observations of significant pH drops with decreased CH_4 production in perchlorate-supplemented enrichments suggest that hydrogenotrophic methanogenesis must somehow be inhibited, and intermediate H_2 generated during methylamine methanogenesis is not being recycled back to *Vht*. We theorize that the thermodynamic spontaneity of H_2-dependent perchlorate reduction (in the presence of an Ni catalyst) results in it outcompeting the endergonic first step of hydrogenotrophic methanogenesis (CO_2 + MFR + H_2 → CHO-MFR + H_2O + H^+; $\Delta G^{\circ'}$ = +16 kJ/mol H_2) (Bobik et al., 1990) (Figure 5.11). Likewise, we imagine H_2 intermediates generated during energy conserving steps of methylamine methanogenesis are siphoned off to reduce perchlorate in lieu of reducing MP via *Vht* ($\Delta G^{\circ'}$ = -289 kJ/mol H_2 for perchlorate reduction (Wang et al., 2008) vs. $\Delta G^{\circ'}$ = -50 kJ/mol H_2 for MP reduction (Thauer et al., 2008; Mand and Metcalf, 2019)) (Figure 5.11). Such interpretations warrant further investigation, but do fit within previously reported narratives of observed decreases in CH_4 production in perchlorate-supplemented methanogenic cultures (Shcherbakova et al., 2015; Kral et al., 2016).

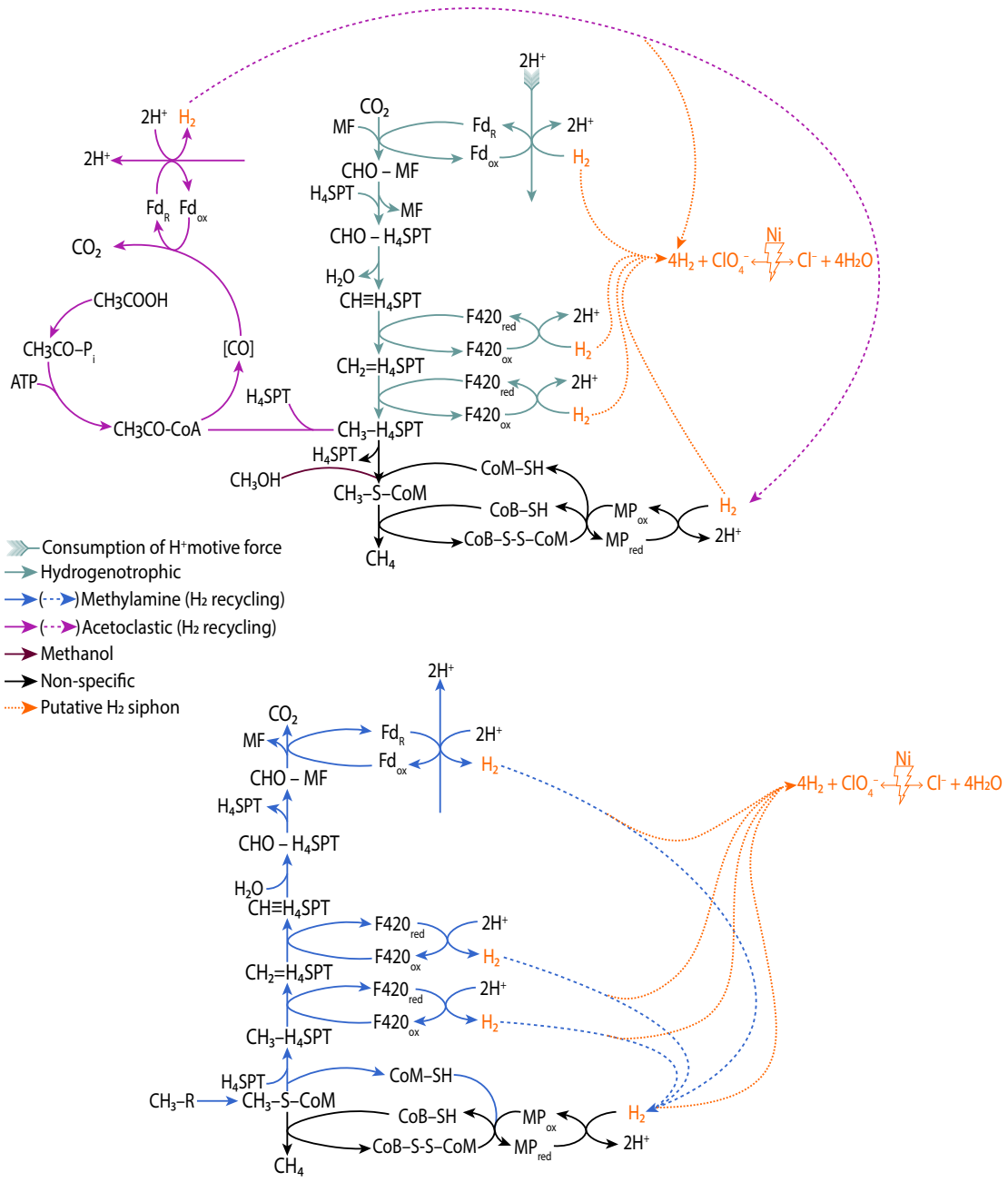

Figure 5.11. Proposed perchlorate reduction H_2 siphoning scheme from methanogenesis pathways in *M. barkeri*. Abbreviations: Non-specific, common to multiple pathways; MF, methanofuran; CHO-MF, formyl-methanofuran; H_4SPT, tetrahydrosarcinapterin; CHO-H_4SPT, formyl-tetrahydrosarcinapterin; CH≡H_4SPT, methenyl-tetrahydrosarcinapterin; CH_2=H_4SPT, methylene-tetrahydrosarcinapterin; CH_3-H_4SPT, methyl-tetrahydrosarcinapterin; CoM-SH, coenzyme M; CoB-SH, coenzyme B; CoB-S-S-CoM, CoB-CoM heterodisulfide; CH_3-S-CoM, methyl-coenzyme M; CH_3-R, methylamine; MP, methanophenazine; Fd, ferredoxin; F420, coenzyme F420.

5.5.3 ***Evidence for selection against sulfur-containing amino acids***. Cysteine and methionine are exceptionally sensitive to oxidation by reactive radical species (Bin et al., 2017). Both residues have shown strong binding affinities to both perchlorate and perchloric acid, resulting in the oxidation of methionine to methionine sulfoxide and cysteine to sulfonic acid (Armesto et al., 2000). The susceptibility of cysteine and methionine to react with perchlorate risks degradation of protein structure and function.

The extensive and substantial down-regulation of cysteine and methionine metabolic pathways we observed in the presence of Na- and Mg-perchlorates (Figure 5.10) suggests a concerted effort by *M. barkeri* to reduce the synthesis of these residues in the presence of a chaotropic agent. Likewise, in line with our inference that $Ca(ClO_4)_2$ reduction may have already proceeded to completion in 30˚C cultures, the absence of this response in $Ca(ClO_4)_2$ transcriptomes would imply a return to transcriptional activity indistinguishable from *M. barkeri* grown in perchlorate-free media. The veracity of this interpretation can be assessed by future perchlorate measurements and, ideally, proteomics.

5.6 CONCLUSIONS

5.6.1 ***Implications for Martian methane***. Our work corroborates previous findings demonstrating the progression of biological methanogenesis amidst exposure to oxidative perchlorate salts (Shcherbakova et al., 2015; Kral et al., 2016). Investigation into this phenomenon at the transcriptomic level provides novel insights into complicated interactions between perchlorates, methanogens, and their environment. For the first time we are able to identify perchlorate-associated decreases in CH_4 production are linked to

radical and unexpected shifts in methanogenesis metabolisms, wherein *M. barkeri* forgoes hydrogenotrophic methanogenesis for comparatively low energy yielding methylamine pathways, utilizing substrates of uncertain provenance yet must somehow be ultimately sourced back to perchlorate reactions. Based on transcriptomic data supported by prior observations in the published literature, we hypothesize that hydrogenotrophic methanogenesis is outcompeted by abiotic perchlorate reduction siphoning H_2 from energy-conserving reactions. Either through exceptional enzymatic ingenuity or an exceptional coincidence of chemistry, *M. barkeri* might be capable of utilizing glycine betaine not only to maintain osmotic balance, but also as a potential source of carbon for methanogenesis.

These findings better constrain our growing understanding of how microbial life responds to strong oxidants, freezing temperatures, osmotic stress, and nutrient limitation – i.e., conditions characteristic of any habitable Martian environment where we may hope to find extant life (Weiss et al., 2000; Beaty et al., 2006; Rummel, 2009; Davila et al., 2010; COSPAR, 2011; Kral et al., 2011; Kral and Altheide, 2013; Oren et al., 2014; Rummel et al., 2014; Shcherbakova et al., 2015; Kral et al., 2016; Sinha et al., 2017; Michalski et al., 2018; Jones et al., 2018; Sholes et al., 2019). Notably, our study shows that metabolic disruption by perchlorates at 30˚C is not reflected at 0˚C, which is more appropriately representative of the conditions at Mars Special Regions (Rummel et al., 2014). This finding offers new perspectives to contextualize observations of Martian CH_4, particularly *in situ* measurements made by the Curiosity rover (Webster et al., 2015; Webster et al., 2018), as diffuse emissions of trace CH_4 are not inconsistent with our observations of decreased methanogenesis under freezing temperatures. This work offers

a glimpse into the remarkable adaptability of methanogens to survive under oxidative stresses that mimic the Martian subsurface. The inferences made from this study provide many exciting opportunities for further research to better understand methanogen ecophysiology in the context of a potential role in the Martian methane story.

5.7 DATA AVAILABILITY

RNA-Seq data will be made public at NCBI GenBank upon acceptance of this manuscript for publication. The source code of all transcriptomic analyses presented in this chapter are available upon request and will be made publicly available upon acceptance for publication. Appendix Tables A.8 – A.14 are available for viewing at https://tinyurl.com/rjlu2gb.

5.8 ACKNOWLEDGEMENTS

I am thankful for our collaboration with Andrew Schuerger (University of Florida), who is the lead investigator of the grant that funded this research and who also grew *M. barkeri* analyzed in this chapter. A special thank you to Yuri Tamama (Princeton '22) for her assistance in isolating RNA from these enrichments, and Wei Wang (Princeton Genomics Core Facility) for library prep and sequencing. I would like to thank Xinning Zhang and Katja Luxem for sharing thoughtful insights into nitrogenases which helped inform interpretations made in this chapter. This research was supported by NASA Exobiology Grant NNX17AK87G. Thanks to the Princeton Environmental Institute for supporting Yuri's stipend in the 2019 PEI summer internship program.

5.9 SUPPLEMENTARY INFORMATION

5.9.1 SUPPLEMENTARY FIGURES

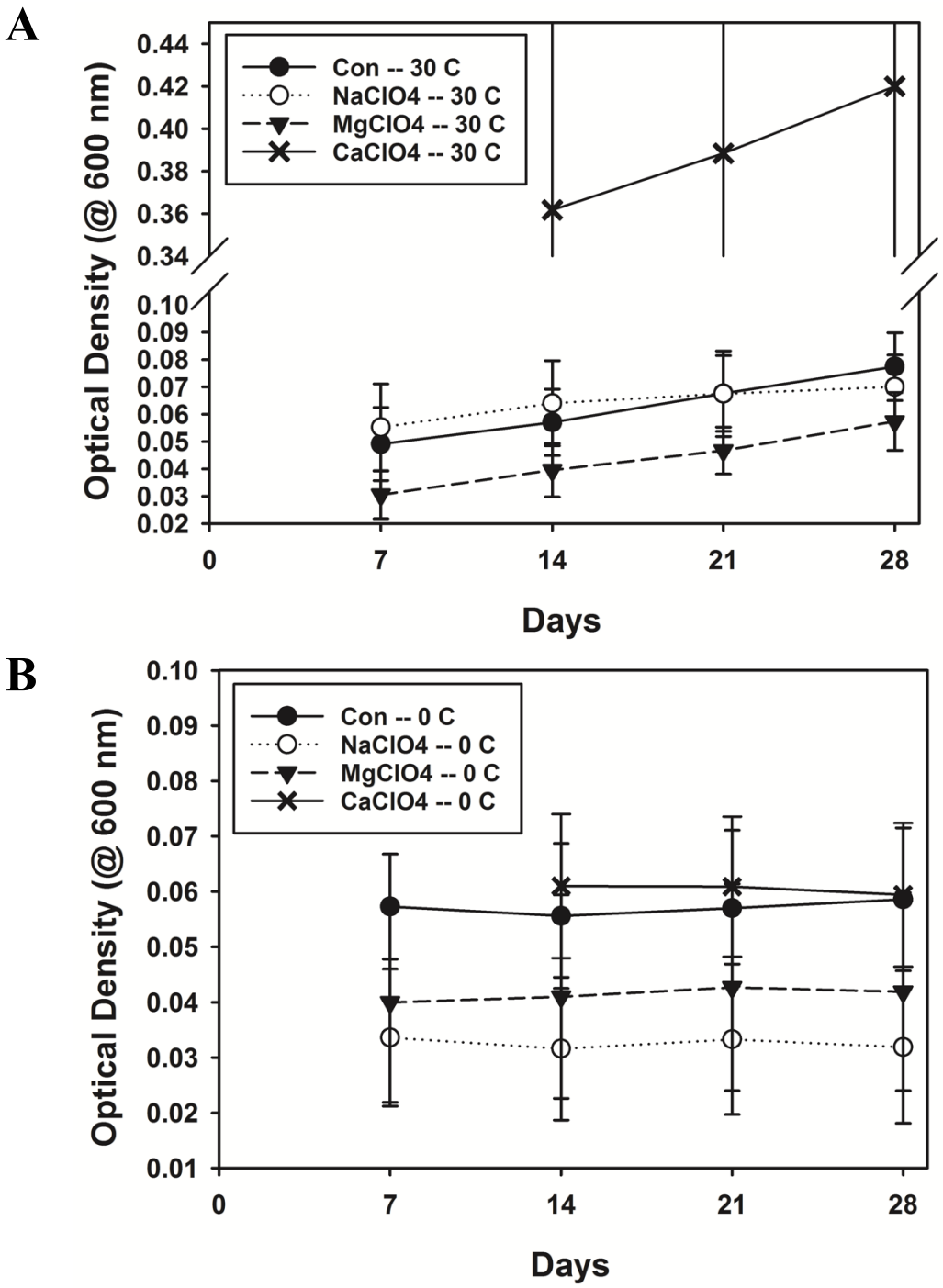

Figure 5S.1. Weekly OD_{600} ± SD of *Methanosarcina barkeri* grown at 30˚C **(A)** and 0˚C **(B)**.

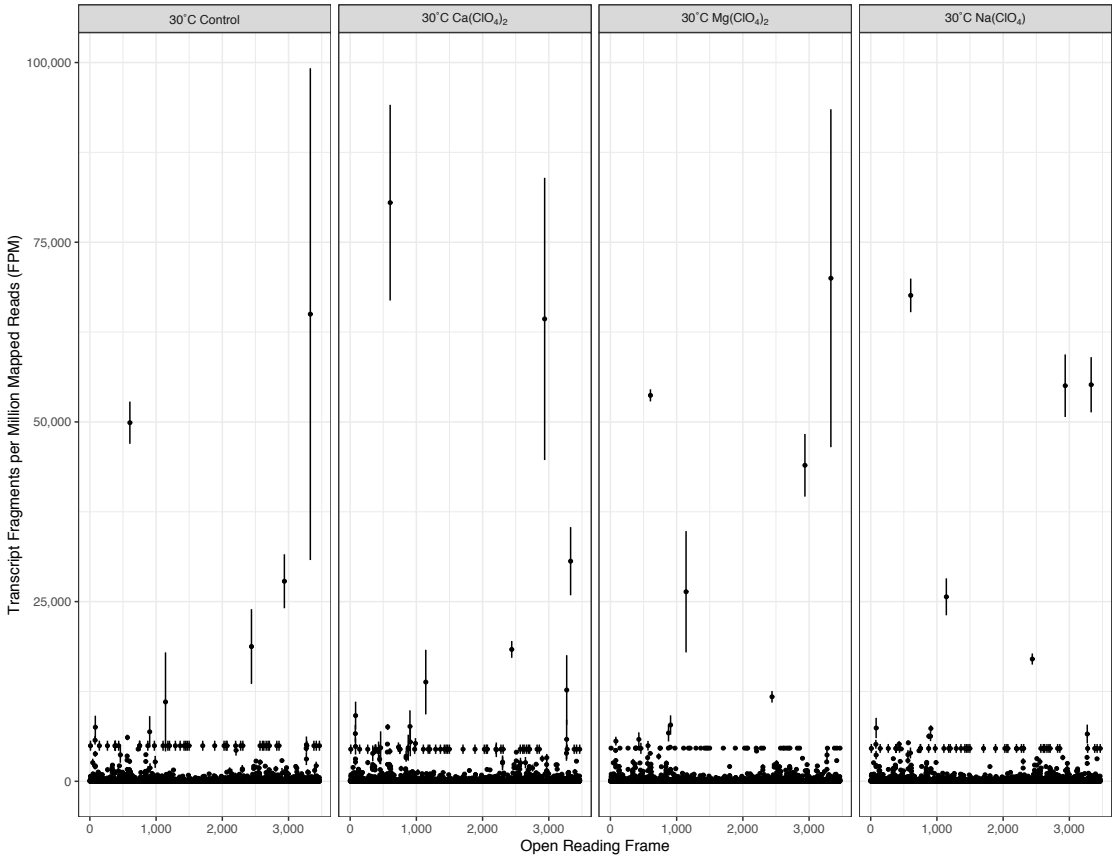

Figure 5S.2. Average ± SD transcript fragment counts per million mapped reads (FPM) at 30˚C. (n = 3 libraries per condition). Open reading frame number indicates position in genome (where ORF = 1 is the origin of replication). ORFs reference gene products found in Table 5S.3.

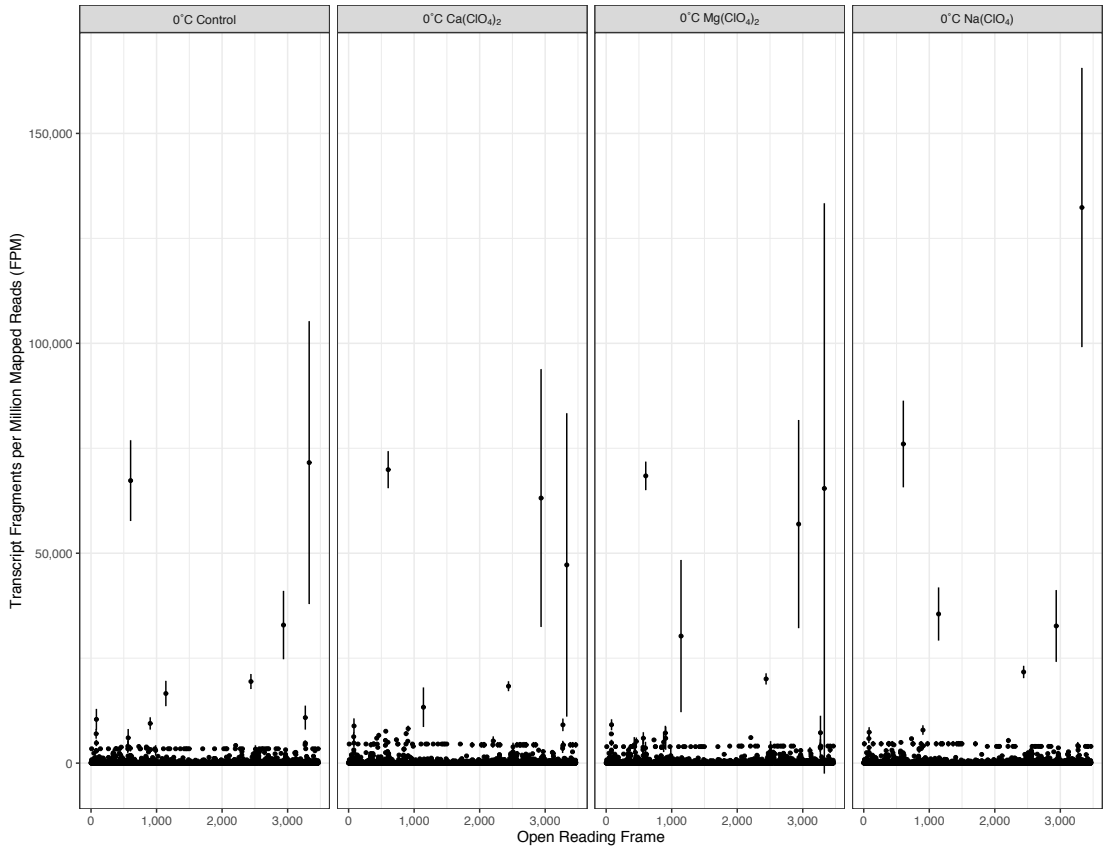

Figure 5S.3. Average ± SD transcript fragment counts per million mapped reads (FPM) at 0˚C. (n = 3 libraries per condition). Open reading frame number indicates position in genome (where ORF = 1 is the origin of replication). ORFs reference gene products found in Table 5S.3.

5.9.2 SUPPLEMENTARY TABLES

Table 5S.1 Average pH of *M. barkeri* cultures.

	30˚C		0˚C	
Condition	Day 0	Day 28	Day 0	Day 28
Control	7.0	6.51	7.0	6.81
$Mg(ClO_4)_2$	7.2	6.49	7.2	6.76
$Na(ClO_4)$	7.25	6.48	7.25	6.86
$Ca(ClO_4)_2$	7.0	6.78	7.0	6.53

Table 5S.2 RNA-Seq mapping results of quality-filtered reads, reported as average % mapping (± SD) (n = 3 libraries per condition). Abbreviations: CDS, coding sequence.

Temperature (˚C)	Condition	% mapped to reference genome	% mapped rRNA genes	% mapped CDS regions
30	Control	95.47 (2.28)	90.74 (3.44)	1.14 (0.22)
30	$Na(ClO_4)$	97.29 (0.79)	93.68 (1.80)	1.39 (0.58)
30	$Mg(ClO_4)_2$	97.55 (0.74)	89.81 (1.13)	2.94 (0.11)
30	$Ca(ClO_4)_2$	97.05 (1.50)	94.27 (1.50)	0.91 (0.23)
0	Control	97.15 (0.93)	91.81 (1.29)	1.71 (0.42)
0	$Na(ClO_4)$	97.18 (0.59)	92.42 (1.18)	1.67 (0.04)
0	$Mg(ClO_4)_2$	97.58 (0.76)	93.36 (1.84)	1.07 (0.16)
0	$Ca(ClO_4)_2$	96.85 (0.96)	93.19 (0.94)	1.55 (0.24)

5.10 REFERENCES

Abu-Omar M. M. (2003) Effective and Catalytic Reduction of Perchlorate by Atom Transfer–Reaction Kinetics and Mechanisms. *Comments Inorg. Chem.* **24**, 15–37. Available at: http://www.tandfonline.com/doi/abs/10.1080/02603590390228326.

Adkins H. and Cramer H. I. (1930) THE USE OF NICKEL AS A CATALYST FOR HYDROGENATION. *J. Am. Chem. Soc.* **52**, 4349–4358. Available at: https://pubs.acs.org/doi/abs/10.1021/ja01374a023.

Alef K., Arp D. J. and Zumft W. G. (1981) Nitrogenase switch-off by ammonia in Rhodopseudomonas palustris: Loss under nitrogen deficiency and independence from the adenylylation state of glutamine synthetase. *Arch. Microbiol.* **130**, 138–142. Available at: http://link.springer.com/10.1007/BF00411066.

Anderson K. L., Apolinario E. E. and Sowers K. R. (2012) Desiccation as a long-term survival mechanism for the archaeon Methanosarcina barkeri. *Appl. Environ. Microbiol.* **78**, 1473–1479.

Armesto X. L., Canle L. M., Fernández M. I., García M. V. and Santaballa J. A. (2000) First steps in the oxidation of sulfur-containing amino acids by hypohalogenation: Very fast generation of intermediate sulfenyl halides and halosulfonium cations. *Tetrahedron*.

Arp D. J. and Zumft W. G. (1983) Overproduction of nitrogenase by nitrogen-limited cultures of Rhodopseudomonas palustris. *J. Bacteriol.* **153**, 1322–1330.

Atreya S. K., Mahaffy P. R. and Wong A. S. (2007) Methane and related trace species on Mars: Origin, loss, implications for life, and habitability. *Planet. Space Sci.*

Bardiya N. and Bae J.-H. (2011) Dissimilatory perchlorate reduction: A review. *Microbiol. Res.* **166**, 237–254. Available at: https://linkinghub.elsevier.com/retrieve/pii/S0944501310001114.

Beaty D., Office M. P., Caltech J. P. L., Buxbaum K., Boynton W., Lma B. C. and Deming J. (2006) Findings of the Mars Special Regions Science Analysis Group. *Astrobiology* **6**, 677–732. Available at: http://www.liebertpub.com/doi/10.1089/ast.2006.6.677.

Bin P., Huang R. and Zhou X. (2017) Oxidation resistance of the sulfur amino acids:

Methionine and cysteine. *Biomed Res. Int.*

Bobik T. (1990) Formyl-methanofuran synthesis in Methanobacterium thermoautotrophicum. *FEMS Microbiol. Lett.* **87**, 323–326. Available at: http://doi.wiley.com/10.1016/0378-1097(90)90473-4.

Brabban, Orcutt and Zinder (1999) Interactions between nitrogen fixation and osmoregulation in the methanogenic archaeon methanosarcina barkeri 227. *Appl. Environ. Microbiol.* **65**, 1222–7. Available at: http://www.ncbi.nlm.nih.gov/pubmed/10049887.

Bryant M. P. and Boone D. R. (1987) Emended Description of Strain MST(DSM 800T), the Type Strain of Methanosarcina barkeri. *Int. J. Syst. Bacteriol.* **37**, 169–170.

Burns A., Watt G. D. and Wang Z. C. (1985) Salt inhibition of nitrogenase catalysis and salt effects on the separate protein components. *Biochemistry* **24**, 3932–3936. Available at: https://pubs.acs.org/doi/abs/10.1021/bi00336a019.

Camacho C., Coulouris G., Avagyan V., Ma N., Papadopoulos J., Bealer K. and Madden T. L. (2009) BLAST+: architecture and applications. *BMC Bioinformatics* **10**, 421. Available at: http://www.biomedcentral.com/1471-2105/10/421.

Casanueva A., Tuffin M., Cary C. and Cowan D. A. (2010) Molecular adaptations to psychrophily: the impact of 'omic' technologies. *Trends Microbiol.* **18**, 374–381. Available at: https://linkinghub.elsevier.com/retrieve/pii/S0966842X10000880.

Chastain B. K. and Kral T. A. (2010) Approaching Mars-like Geochemical Conditions in the Laboratory: Omission of Artificial Buffers and Reductants in a Study of Biogenic Methane Production on a Smectite Clay. *Astrobiology* **10**, 889–897. Available at: http://www.liebertpub.com/doi/10.1089/ast.2010.0480.

Chen S., Zhou Y., Chen Y. and Gu J. (2018) fastp: an ultra-fast all-in-one FASTQ preprocessor. *Bioinformatics* **34**, i884–i890. Available at: https://academic.oup.com/bioinformatics/article/34/17/i884/5093234.

Chevrier V. F., Hanley J. and Altheide T. S. (2009) Stability of perchlorate hydrates and their liquid solutions at the Phoenix landing site, Mars. *Geophys. Res. Lett.* **36**, L10202. Available at: http://doi.wiley.com/10.1029/2009GL037497.

Clark B. C. and Kounaves S. P. (2016) Evidence for the distribution of perchlorates on Mars. *Int. J. Astrobiol.* **15**, 311–318. Available at: https://www.cambridge.org/core/product/identifier/S1473550415000385/type/journal_article.

Coates J. D. and Achenbach L. A. (2004) Microbial perchlorate reduction: rocket-fuelled metabolism. *Nat. Rev. Microbiol.* **2**, 569–580. Available at: http://www.nature.com/articles/nrmicro926.

Conrad R. (2009) The global methane cycle: recent advances in understanding the microbial processes involved. *Environ. Microbiol. Rep.* **1**, 285–292. Available at: http://doi.wiley.com/10.1111/j.1758-2229.2009.00038.x.

COSPAR (2011) COSPAR Planetary Protection Policy. *COSPAR/IAU Work. Planet. Prot.*

Davila A. F., Duport L. G., Melchiorri R., Jänchen J., Valea S., de Los Rios A., Fairén A. G., Möhlmann D., McKay C. P., Ascaso C. and Wierzchos J. (2010) Hygroscopic salts and the potential for life on Mars. *Astrobiology* **10**, 617–628.

Deits T. L. and Howard J. B. (1990) Effect of salts on Azotobacter vinelandii nitrogenase activities. Inhibition of iron chelation and substrate reduction. *J. Biol. Chem.* **265**,

3859–67. Available at: http://www.ncbi.nlm.nih.gov/pubmed/2303482.

Deppenmeier U. (2004) The Membrane-Bound Electron Transport System of Methanosarcina Species. *J. Bioenerg. Biomembr.* **36**, 55–64. Available at: http://link.springer.com/10.1023/B:JOBB.0000019598.64642.97.

Etiope G., Ehlmann B. L. and Schoell M. (2013) Low temperature production and exhalation of methane from serpentinized rocks on Earth: A potential analog for methane production on Mars. *Icarus* **224**, 276–285. Available at: https://linkinghub.elsevier.com/retrieve/pii/S0019103512001832.

Formisano V., Atreya S., Encrenaz T., Ignatiev N. and Giuranna M. (2004) Detection of Methane in the Atmosphere of Mars. *Science* **306**, 1758–1761. Available at: https://www.sciencemag.org/lookup/doi/10.1126/science.1101732.

Francisco D. E., Mah R. A. and Rabin A. C. (1973) Acridine Orange-Epifluorescence Technique for Counting Bacteria in Natural Waters. *Trans. Am. Microsc. Soc.* **92**, 416. Available at: https://www.jstor.org/stable/3225245?origin=crossref.

Fries M., Christou A., Archer D., Conrad P., Cooke W., Eigenbrode J., ten Kate I. L., Matney M., Niles P., Sykes M., Steele A. and Treiman A. (2016) A cometary origin for martian atmospheric methane. *Geochemical Perspect. Lett.* **2**, 10–23. Available at: http://www.geochemicalperspectivesletters.org/article1602.

Geminale A., Formisano V. and Giuranna M. (2008) Methane in Martian atmosphere: Average spatial, diurnal, and seasonal behaviour. *Planet. Space Sci.* **56**, 1194–1203. Available at: https://linkinghub.elsevier.com/retrieve/pii/S0032063308000743.

Glavin D. P., Freissinet C., Miller K. E., Eigenbrode J. L., Brunner A. E., Buch A., Sutter B., Archer P. D., Atreya S. K., Brinckerhoff W. B., Cabane M., Coll P., Conrad P.

G., Coscia D., Dworkin J. P., Franz H. B., Grotzinger J. P., Leshin L. A., Martin M. G., McKay C., Ming D. W., Navarro-González R., Pavlov A., Steele A., Summons R. E., Szopa C., Teinturier S. and Mahaffy P. R. (2013) Evidence for perchlorates and the origin of chlorinated hydrocarbons detected by SAM at the Rocknest aeolian deposit in Gale Crater. *J. Geophys. Res. Planets* **118**, 1955–1973. Available at: http://doi.wiley.com/10.1002/jgre.20144.

Halbleib C. M. and Ludden P. W. (2000) Regulation of Biological Nitrogen Fixation. *J. Nutr.* **130**, 1081–1084. Available at: https://academic.oup.com/jn/article/130/5/1081/4686360.

Harris R. L., Ehlmann B. L., Bhartia R. and Onstott T. C. (2019) Biologically mediated anaerobic methane oxidation – the missing sink of an active martian methane cycle? In *Mars Extant Life: What's Next?*

Hecht M. H., Kounaves S. P., Quinn R. C., West S. J., Young S. M. M., Ming D. W., Catling D. C., Clark B. C., Boynton W. V., Hoffman J., DeFlores L. P., Gospodinova K., Kapit J. and Smith P. H. (2009) Detection of Perchlorate and the Soluble Chemistry of Martian Soil at the Phoenix Lander Site. *Science (80-.).* **325**, 64–67. Available at: http://www.sciencemag.org/lookup/doi/10.1126/science.1172466.

Hippe H., Caspari D., Fiebig K. and Gottschalk G. (1979) Utilization of trimethylamine and other N-methyl compounds for growth and methane formation by Methanosarcina barkeri. *Proc. Natl. Acad. Sci.* **76**, 494–498. Available at: http://www.pnas.org/cgi/doi/10.1073/pnas.76.1.494.

Hoffmann T. and Bremer E. (2017) Guardians in a stressful world: the Opu family of

compatible solute transporters from Bacillus subtilis. *Biol. Chem.* **398**, 193–214. Available at: http://www.degruyter.com/view/j/bchm.2017.398.issue-2/hsz-2016-0265/hsz-2016-0265.xml.

Ide T., Bäumer S. and Deppenmeier U. (1999) Energy Conservation by the H2:Heterodisulfide Oxidoreductase from Methanosarcina mazei Gö1: Identification of Two Proton-Translocating Segments. *J. Bacteriol.* **181**, 4076–4080. Available at: https://jb.asm.org/content/181/13/4076.

Jarrell K. F., Jones G. M., Kandiba L., Nair D. B. and Eichler J. (2010) S-Layer Glycoproteins and Flagellins: Reporters of Archaeal Posttranslational Modifications. *Archaea* **2010**, 1–13. Available at: http://www.hindawi.com/journals/archaea/2010/612948/.

Jones R. M., Goordial J. M. and Orcutt B. N. (2018) Low Energy Subsurface Environments as Extraterrestrial Analogs. *Front. Microbiol.* **9**. Available at: https://www.frontiersin.org/article/10.3389/fmicb.2018.01605/full.

Kempf B. and Bremer E. (1995) OpuA, an Osmotically Regulated Binding Protein-dependent Transport System for the Osmoprotectant Glycine Betaine in Bacillus subtilis. *J. Biol. Chem.* **270**, 16701–16713. Available at: http://www.jbc.org/lookup/doi/10.1074/jbc.270.28.16701.

Kempf B. and Bremer E. (1998) Uptake and synthesis of compatible solutes as microbial stress responses to high-osmolality environments. *Arch. Microbiol.* **170**, 319–330. Available at: http://link.springer.com/10.1007/s002030050649.

Kendrick M. G. and Kral T. A. (2006) Survival of Methanogens During Desiccation: Implications for Life on Mars. *Astrobiology* **6**, 546–551. Available at:

http://www.liebertpub.com/doi/10.1089/ast.2006.6.546.

Keppler F., Vigano I., McLeod A., Ott U., Früchtl M. and Röckmann T. (2012) Ultraviolet-radiation-induced methane emissions from meteorites and the Martian atmosphere. *Nature* **486**, 93–96. Available at: http://www.nature.com/articles/nature11203.

Kessler P. S., Blank C. and Leigh J. A. (1998) The nif gene operon of the methanogenic archaeon Methanococcus maripaludis. *J. Bacteriol.* **180**, 1504–11. Available at: http://www.ncbi.nlm.nih.gov/pubmed/9515920.

Kessler P. S., Daniel C. and Leigh J. A. (2001) Ammonia Switch-Off of Nitrogen Fixation in the Methanogenic Archaeon Methanococcus maripaludis: Mechanistic Features and Requirement for the Novel GlnB Homologues, NifI1 and NifI2. *J. Bacteriol.* **183**, 882–889. Available at: http://jb.asm.org/cgi/doi/10.1128/JB.183.3.882-889.2001.

Kessler P. S. and Leigh J. A. (1999) Genetics of nitrogen regulation in Methanococcus maripaludis. *Genetics* **152**, 1343–51. Available at: http://www.ncbi.nlm.nih.gov/pubmed/10430565.

Korablev O., Vandaele A. C., Montmessin F., Fedorova A. A., Trokhimovskiy A., Forget F., Lefèvre F., Daerden F., Thomas I. R., Trompet L., Erwin J. T., Aoki S., Robert S., Neary L., Viscardy S., Grigoriev A. V., Ignatiev N. I., Shakun A., Patrakeev A., Belyaev D. A., Bertaux J.-L., Olsen K. S., Baggio L., Alday J., Ivanov Y. S., Ristic B., Mason J., Willame Y., Depiesse C., Hetey L., Berkenbosch S., Clairquin R., Queirolo C., Beeckman B., Neefs E., Patel M. R., Bellucci G., López-Moreno J.-J., Wilson C. F., Etiope G., Zelenyi L., Svedhem H. and Vago J. L. (2019) No detection

of methane on Mars from early ExoMars Trace Gas Orbiter observations. *Nature* **568**, 517–520. Available at: http://www.nature.com/articles/s41586-019-1096-4.

Kounaves S. P., Carrier B. L., O'Neil G. D., Stroble S. T. and Claire M. W. (2014a) Evidence of martian perchlorate, chlorate, and nitrate in Mars meteorite EETA79001: Implications for oxidants and organics. *Icarus* **229**, 206–213. Available at: https://linkinghub.elsevier.com/retrieve/pii/S0019103513004752.

Kounaves S. P., Chaniotakis N. A., Chevrier V. F., Carrier B. L., Folds K. E., Hansen V. M., McElhoney K. M., O'Neil G. D. and Weber A. W. (2014b) Identification of the perchlorate parent salts at the Phoenix Mars landing site and possible implications. *Icarus* **232**, 226–231. Available at: https://linkinghub.elsevier.com/retrieve/pii/S0019103514000475.

Kral T. A. and Altheide S. T. (2013) Methanogen survival following exposure to desiccation, low pressure and martian regolith analogs. *Planet. Space Sci.* **89**, 167–171. Available at: https://linkinghub.elsevier.com/retrieve/pii/S0032063313002377.

Kral T. A., Altheide T. S., Lueders A. E. and Schuerger A. C. (2011) Low pressure and desiccation effects on methanogens: Implications for life on Mars. *Planet. Space Sci.* **59**, 264–270. Available at: https://linkinghub.elsevier.com/retrieve/pii/S003206331000214X.

Kral T. A., Goodhart T. H., Harpool J. D., Hearnsberger C. E., McCracken G. L. and McSpadden S. W. (2016) Sensitivity and adaptability of methanogens to perchlorates: Implications for life on Mars. *Planet. Space Sci.* **120**, 87–95. Available at: https://linkinghub.elsevier.com/retrieve/pii/S0032063315003633.

Krasnopolsky V. A., Maillard J. P. and Owen T. C. (2004) Detection of methane in the

martian atmosphere: evidence for life? *Icarus* **172**, 537–547. Available at: https://linkinghub.elsevier.com/retrieve/pii/S0019103504002222.

Kreisl P. and Kandler O. (1986) Chemical structure of the cell wall polymer of methanosarcina. *Syst. Appl. Microbiol.* **7**, 293–299. Available at: https://linkinghub.elsevier.com/retrieve/pii/S0723202086800224.

Kulkarni G., Mand T. D. and Metcalf W. W. (2018) Energy Conservation via Hydrogen Cycling in the Methanogenic Archaeon Methanosarcina barkeri ed. M. W. Ribbe. *MBio* **9**. Available at: http://mbio.asm.org/lookup/doi/10.1128/mBio.01256-18.

Langmead B. and Salzberg S. L. (2012) Fast gapped-read alignment with Bowtie 2. *Nat. Methods* **9**, 357–9. Available at: http://www.ncbi.nlm.nih.gov/pubmed/22388286.

Li H., Handsaker B., Wysoker A., Fennell T., Ruan J., Homer N., Marth G., Abecasis G. and Durbin R. (2009) The Sequence Alignment/Map format and SAMtools. *Bioinformatics* **25**, 2078–2079. Available at: https://academic.oup.com/bioinformatics/article-lookup/doi/10.1093/bioinformatics/btp352.

Liebensteiner M. G., Pinkse M. W. H., Schaap P. J., Stams A. J. M. and Lomans B. P. (2013) Archaeal (Per)Chlorate Reduction at High Temperature: An Interplay of Biotic and Abiotic Reactions. *Science* **340**, 85–87. Available at: http://www.sciencemag.org/lookup/doi/10.1126/science.1233957.

Lobo A. L. and Zinder S. H. (1988) Diazotrophy and Nitrogenase Activity in the Archaebacterium Methanosarcina barkeri 227. *Appl. Environ. Microbiol.* **54**, 1656–61. Available at: http://www.ncbi.nlm.nih.gov/pubmed/16347675.

Lobo A. L. and Zinder S. H. (1992) Nitrogen fixation by methanogenic bacteria. In

Biological Nitrogen Fixation (eds. G. Stacey, R. H. Burris, and H. J. Evans). Chapman and Hall, New York. pp. 191–211.

Lobo A. L. and Zinder S. H. (1990) Nitrogenase in the archaebacterium Methanosarcina barkeri 227. *J. Bacteriol.* **172**, 6789–6796. Available at: https://jb.asm.org/content/172/12/6789.

Logan B. E., Wu J. and Unz R. F. (2001) Biological Perchlorate Reduction in High-Salinity Solutions. *Water Res.* **35**, 3034–3038. Available at: https://linkinghub.elsevier.com/retrieve/pii/S0043135401000136.

Love M., Anders S. and Huber W. (2014) Differential analysis of count data–the DESeq2 package. *Genome Biol.* **15**, 10–1186.

Maeder D. L., Anderson I., Brettin T. S., Bruce D. C., Gilna P., Han C. S., Lapidus A., Metcalf W. W., Saunders E., Tapia R. and Sowers K. R. (2006) The Methanosarcina barkeri Genome: Comparative Analysis with Methanosarcina acetivorans and Methanosarcina mazei Reveals Extensive Rearrangement within Methanosarcinal Genomes. *J. Bacteriol.* **188**, 7922–7931. Available at: http://jb.asm.org/cgi/doi/10.1128/JB.00810-06.

Maestrojuan G. M., Boone J. E., Mah R. A., Menaia J. A. G. F., Sachs M. S. and Boone D. R. (1992) Taxonomy and Halotolerance of Mesophilic Methanosarcina Strains, Assignment of Strains to Species, and Synonymy of Methanosarcina mazei and Methanosarcina frisia. *Int. J. Syst. Bacteriol.* **42**, 561–567. Available at: https://www.microbiologyresearch.org/content/journal/ijsem/10.1099/00207713-42-4-561.

Mand T. D. and Metcalf W. W. (2019) Energy Conservation and Hydrogenase Function

in Methanogenic Archaea, in Particular the Genus Methanosarcina. *Microbiol. Mol. Biol. Rev.* **83**. Available at: http://mmbr.asm.org/lookup/doi/10.1128/MMBR.00020-19.

Marion G. M., Catling D. C., Zahnle K. J. and Claire M. W. (2010) Modeling aqueous perchlorate chemistries with applications to Mars. *Icarus* **207**, 675–685. Available at: https://linkinghub.elsevier.com/retrieve/pii/S0019103509004904.

Meuer J., Kuettner H. C., Zhang J. K., Hedderich R. and Metcalf W. W. (2002) Genetic analysis of the archaeon Methanosarcina barkeri Fusaro reveals a central role for Ech hydrogenase and ferredoxin in methanogenesis and carbon fixation. *Proc. Natl. Acad. Sci.* **99**, 5632–5637. Available at: http://www.pnas.org/cgi/doi/10.1073/pnas.072615499.

Michalski J. R., Onstott T. C., Mojzsis S. J., Mustard J., Chan Q. H. S., Niles P. B. and Johnson S. S. (2018) The Martian subsurface as a potential window into the origin of life. *Nat. Geosci.* **11**, 21–26. Available at: http://www.nature.com/articles/s41561-017-0015-2.

Mickol R. L. and Kral T. A. (2017) Low Pressure Tolerance by Methanogens in an Aqueous Environment: Implications for Subsurface Life on Mars. *Orig. Life Evol. Biosph.* **47**, 511–532. Available at: http://link.springer.com/10.1007/s11084-016-9519-9.

Moores J. E. and Schuerger A. C. (2012) UV degradation of accreted organics on Mars: IDP longevity, surface reservoir of organics, and relevance to the detection of methane in the atmosphere. *J. Geophys. Res. Planets* **117**, n/a-n/a. Available at: http://doi.wiley.com/10.1029/2012JE004060.

Mumma M. J., Villanueva G. L., Novak R. E., Hewagama T., Bonev B. P., DiSanti M. A., Mandell A. M. and Smith M. D. (2009) Strong Release of Methane on Mars in Northern Summer 2003. *Science* **323**, 1041–1045. Available at: https://www.sciencemag.org/lookup/doi/10.1126/science.1165243.

Navarro-González R., Vargas E., de la Rosa J., Raga A. C. and McKay C. P. (2010) Reanalysis of the Viking results suggests perchlorate and organics at midlatitudes on Mars. *J. Geophys. Res.* **115**, E12010. Available at: http://doi.wiley.com/10.1029/2010JE003599.

Nikolakakos G. and Whiteway J. A. (2015) Laboratory investigation of perchlorate deliquescence at the surface of Mars with a Raman scattering lidar. *Geophys. Res. Lett.* **42**, 7899–7906. Available at: https://onlinelibrary.wiley.com/doi/abs/10.1002/2015GL065434.

Oehler D. Z. and Etiope G. (2017) Methane Seepage on Mars: Where to Look and Why. *Astrobiology* **17**, 1233–1264. Available at: http://www.liebertpub.com/doi/10.1089/ast.2017.1657.

Ogata H., Goto S., Sato K., Fujibuchi W., Bono H. and Kanehisa M. (1999) KEGG: Kyoto Encyclopedia of Genes and Genomes. *Nucleic Acids Res.* **27**, 29–34. Available at: https://academic.oup.com/nar/article-lookup/doi/10.1093/nar/27.1.29.

Oren A. (1990) Formation and breakdown of glycine betaine and trimethylamine in hypersaline environments. *Antonie Van Leeuwenhoek* **58**, 291–298. Available at: http://link.springer.com/10.1007/BF00399342.

Oren A., Elevi Bardavid R. and Mana L. (2014) Perchlorate and halophilic prokaryotes: implications for possible halophilic life on Mars. *Extremophiles* **18**, 75–80.

Available at: http://link.springer.com/10.1007/s00792-013-0594-9.

Pestova O. N., Myund L. A., Khripun M. K. and Prigaro A. V (2005) Polythermal Study of the Systems M(ClO4)2-H2O (M2+ = Mg2+, Ca2+, Sr2+, Ba2+). *Russ. J. Appl. Chem.* **78**, 409–413. Available at: http://link.springer.com/10.1007/s11167-005-0306-z.

Quinlan A. R. and Hall I. M. (2010) BEDTools: a flexible suite of utilities for comparing genomic features. *Bioinformatics* **26**, 841–842. Available at: https://academic.oup.com/bioinformatics/article-lookup/doi/10.1093/bioinformatics/btq033.

Rivkina E., Laurinavichius K., McGrath J., Tiedje J., Shcherbakova V. and Gilichinsky D. (2004) Microbial life in permafrost. *Adv. Sp. Res.* **33**, 1215–1221. Available at: https://linkinghub.elsevier.com/retrieve/pii/S0273117703012122.

Rivkina E. M., Laurinavichus K. S., Gilichinsky D. A. and Shcherbakova V. A. (2002) Methane generation in permafrost sediments. *Dokl. Biol. Sci.*, 179–181.

Rivkina E., Shcherbakova V., Laurinavichius K., Petrovskaya L., Krivushin K., Kraev G., Pecheritsina S. and Gilichinsky D. (2007) Biogeochemistry of methane and methanogenic archaea in permafrost. *FEMS Microbiol. Ecol.* **61**, 1–15. Available at: https://academic.oup.com/femsec/article-lookup/doi/10.1111/j.1574-6941.2007.00315.x.

Roessler M., Pfluger K., Flach H., Lienard T., Gottschalk G. and Muller V. (2002) Identification of a Salt-Induced Primary Transporter for Glycine Betaine in the Methanogen Methanosarcina mazei Go1. *Appl. Environ. Microbiol.* **68**, 2133–2139. Available at: http://aem.asm.org/cgi/doi/10.1128/AEM.68.5.2133-2139.2002.

Rummel J. D. (2009) Special regions in Mars exploration: Problems and potential. *Acta Astronaut.* **64**, 1293–1297. Available at: https://linkinghub.elsevier.com/retrieve/pii/S0094576509000046.

Rummel J. D., Beaty D. W., Jones M. A., Bakermans C., Barlow N. G., Boston P. J., Chevrier V. F., Clark B. C., de Vera J.-P. P., Gough R. V., Hallsworth J. E., Head J. W., Hipkin V. J., Kieft T. L., McEwen A. S., Mellon M. T., Mikucki J. A., Nicholson W. L., Omelon C. R., Peterson R., Roden E. E., Sherwood Lollar B., Tanaka K. L., Viola D. and Wray J. J. (2014) A New Analysis of Mars “Special Regions”: Findings of the Second MEPAG Special Regions Science Analysis Group (SR-SAG2). *Astrobiology* **14**, 887–968. Available at: http://www.liebertpub.com/doi/10.1089/ast.2014.1227.

Schuerger A. C., Moores J. E., Clausen C. A., Barlow N. G. and Britt D. T. (2012) Methane from UV-irradiated carbonaceous chondrites under simulated Martian conditions. *J. Geophys. Res. Planets* **117**, n/a-n/a. Available at: http://doi.wiley.com/10.1029/2011JE004023.

Seibel B. A. and Walsh P. J. (2002) Trimethylamine oxide accumulation in marine animals: relationship to acylglycerol storage. *J. Exp. Biol.* **205**, 297–306. Available at: http://www.ncbi.nlm.nih.gov/pubmed/11854367.

Seto M., Noguchi K. and Cappellen P. Van (2019) Potential for Aerobic Methanotrophic Metabolism on Mars. *Astrobiology* **19**, 1187–1195. Available at: https://www.liebertpub.com/doi/10.1089/ast.2018.1943.

Shcherbakova V., Oshurkova V. and Yoshimura Y. (2015) The Effects of Perchlorates on the Permafrost Methanogens: Implication for Autotrophic Life on Mars.

Microorganisms **3**, 518–534. Available at: http://www.mdpi.com/2076-2607/3/3/518.

Shcherbakova V., Rivkina E., Pecheritsyna S., Laurinavichius K., Suzina N. and Gilichinsky D. (2011) Methanobacterium arcticum sp. nov., a methanogenic archaeon from Holocene Arctic permafrost. *Int. J. Syst. Evol. Microbiol.* **61**, 144–147. Available at: https://www.microbiologyresearch.org/content/journal/ijsem/10.1099/ijs.0.021311-0.

Sholes S. F., Krissansen-Totton J. and Catling D. C. (2019) A Maximum Subsurface Biomass on Mars from Untapped Free Energy: CO and H 2 as Potential Antibiosignatures. *Astrobiology* **19**, 655–668. Available at: https://www.liebertpub.com/doi/10.1089/ast.2018.1835.

Sinha N., Nepal S., Kral T. and Kumar P. (2017) Survivability and growth kinetics of methanogenic archaea at various pHs and pressures: Implications for deep subsurface life on Mars. *Planet. Space Sci.* **136**, 15–24. Available at: https://linkinghub.elsevier.com/retrieve/pii/S003206331630441X.

Sohm J. A., Webb E. A. and Capone D. G. (2011) Emerging patterns of marine nitrogen fixation. *Nat. Rev. Microbiol.* **9**, 499–508. Available at: http://www.nature.com/articles/nrmicro2594.

Sorek R. and Cossart P. (2010) Prokaryotic transcriptomics: a new view on regulation, physiology and pathogenicity. *Nat. Rev. Genet.* **11**, 9–16. Available at: http://www.nature.com/articles/nrg2695.

Sowers K. R., Boone J. E. and Gunsalus R. P. (1993) Disaggregation of *Methanosarcina*

spp. and Growth as Single Cells at Elevated Osmolarity. *Appl. Environ. Microbiol.* **59**, 3832–9. Available at: http://www.ncbi.nlm.nih.gov/pubmed/16349092.

Sowers K. R. and Gunsalus R. P. (1988) Adaptation for growth at various saline concentrations by the archaebacterium *Methanosarcina thermophila*. *J. Bacteriol.* **170**, 998–1002. Available at: https://jb.asm.org/content/170/2/998.

Sowers K. R. and Gunsalus R. P. (1995) Halotolerance in *Methanosarcina* spp.: Role of N(sup(epsilon))-Acetyl-(beta)-Lysine, (alpha)-Glutamate, Glycine Betaine, and K(sup+) as Compatible Solutes for Osmotic Adaptation. *Appl. Environ. Microbiol.* **61**, 4382–4388. Available at: https://aem.asm.org/content/61/12/4382.

Srinivasan G. (2002) Pyrrolysine Encoded by UAG in Archaea: Charging of a UAG-Decoding Specialized tRNA. *Science* **296**, 1459–1462. Available at: https://www.sciencemag.org/lookup/doi/10.1126/science.1069588.

Stillman D. E. and Grimm R. E. (2011) Dielectric signatures of adsorbed and salty liquid water at the Phoenix landing site, Mars. *J. Geophys. Res.* **116**, E09005. Available at: http://doi.wiley.com/10.1029/2011JE003838.

Takai K., Nakamura K., Toki T., Tsunogai U., Miyazaki M., Miyazaki J., Hirayama H., Nakagawa S., Nunoura T. and Horikoshi K. (2008) Cell proliferation at 122 degrees C and isotopically heavy CH4 production by a hyperthermophilic methanogen under high-pressure cultivation. *Proc. Natl. Acad. Sci. U. S. A.* **105**, 10949–10954. Available at: papers://0be24a46-325a-4116-a3c6-fd8a3b614472/Paper/p11728.

Thauer R. K., Kaster A.-K., Goenrich M., Schick M., Hiromoto T. and Shima S. (2010) Hydrogenases from Methanogenic Archaea, Nickel, a Novel Cofactor, and H 2 Storage. *Annu. Rev. Biochem.* **79**, 507–536. Available at:

http://www.annualreviews.org/doi/10.1146/annurev.biochem.030508.152103.

Thauer R. K., Kaster A.-K., Seedorf H., Buckel W. and Hedderich R. (2008) Methanogenic archaea: ecologically relevant differences in energy conservation. *Nat. Rev. Microbiol.* **6**, 579–591. Available at: http://www.nature.com/articles/nrmicro1931.

Toner J. D., Catling D. C. and Light B. (2014) The formation of supercooled brines, viscous liquids, and low-temperature perchlorate glasses in aqueous solutions relevant to Mars. *Icarus* **233**, 36–47. Available at: https://linkinghub.elsevier.com/retrieve/pii/S0019103514000499.

Wang D. M., Shah S. I., Chen J. G. and Huang C. P. (2008) Catalytic reduction of perchlorate by H2 gas in dilute aqueous solutions. *Sep. Purif. Technol.* **60**, 14–21. Available at: https://linkinghub.elsevier.com/retrieve/pii/S1383586607003425.

Webster C. R., Mahaffy P. R., Atreya S. K., Flesch G. J., Mischna M. A., Meslin P.-Y., Farley K. A., Conrad P. G., Christensen L. E., Pavlov A. A., Martin-Torres J., Zorzano M.-P., McConnochie T. H., Owen T., Eigenbrode J. L., Glavin D. P., Steele A., Malespin C. A., Archer P. D., Sutter B., Coll P., Freissinet C., McKay C. P., Moores J. E., Schwenzer S. P., Bridges J. C., Navarro-Gonzalez R., Gellert R. and Lemmon M. T. (2015) Mars methane detection and variability at Gale crater. *Science (80-.).* **347**, 415–417. Available at: https://www.sciencemag.org/lookup/doi/10.1126/science.1261713.

Webster C. R., Mahaffy P. R., Atreya S. K., Moores J. E., Flesch G. J., Malespin C., McKay C. P., Martinez G., Smith C. L., Martin-Torres J., Gomez-Elvira J., Zorzano M.-P., Wong M. H., Trainer M. G., Steele A., Archer D., Sutter B., Coll P. J.,

Freissinet C., Meslin P.-Y., Gough R. V., House C. H., Pavlov A., Eigenbrode J. L., Glavin D. P., Pearson J. C., Keymeulen D., Christensen L. E., Schwenzer S. P., Navarro-Gonzalez R., Pla-García J., Rafkin S. C. R., Vicente-Retortillo Á., Kahanpää H., Viudez-Moreiras D., Smith M. D., Harri A.-M., Genzer M., Hassler D. M., Lemmon M., Crisp J., Sander S. P., Zurek R. W. and Vasavada A. R. (2018) Background levels of methane in Mars’ atmosphere show strong seasonal variations. *Science* **360**, 1093–1096. Available at: https://www.sciencemag.org/lookup/doi/10.1126/science.aaq0131.

Weiss B. P., Yung Y. L. and Nealson K. H. (2000) Atmospheric energy for subsurface life on Mars? *Proc. Natl. Acad. Sci. U. S. A.* **97**, 1395–1399.

Widdel F., Kohring G.-W. and Mayer F. (1983) Studies on dissimilatory sulfate-reducing bacteria that decompose fatty acids. *Arch. Microbiol.* **134**, 286–294. Available at: http://link.springer.com/10.1007/BF00407804.

Yu X., Amrhein C., Deshusses M. A. and Matsumoto M. R. (2006) Perchlorate Reduction by Autotrophic Bacteria in the Presence of Zero-Valent Iron. *Environ. Sci. Technol.* **40**, 1328–1334. Available at: https://pubs.acs.org/doi/10.1021/es051682z.

CHAPTER 6

Conclusions

6.1 NEW CONTRIBUTIONS AND MAJOR FINDINGS

Technological advances in high-throughput sequencing, imaging, geochemical instrumentation, and computational power are rapidly changing the fields of microbial ecology and biogeochemistry. As we continue to improve our understanding of the myriad physical and geochemical parameters that influence the habitability of extreme environments, so too are we perpetually surprised by new revelations of the remarkable ways in which microbial life makes the most of available free energy on the biotic fringe. In this dissertation we have investigated the extremes of microbial CH_4 metabolisms, examining both model organisms and complex environmental communities through multi-disciplinary, multi-methodological lenses to expand our understanding of the diversity and metabolic capabilities of methanogens and anaerobic methanotrophs as they relate to the deep subsurface of Earth and Mars.

In Chapter 2 we discussed the development of FISH-TAMB, a novel molecular tool that enables microbial ecologists to fluorescently identify living cells based on the expression of targeted functional genes. We showed the potential widespread applicability of FISH-TAMB by labeling targeted mRNA in both *Archaea* and *Bacteria*, including pure culture isolates of *M. barkeri* and *E. coli*, as well as an enrichment of ANME-2 from BE326 BH2 fracture fluid collected 1.34 km below ground in South Africa. Using confocal microscopy equipped with a Perfect Focus System, we captured what appeared to be real-time fluorescent labeling of mRNA in living cells. Using the inducible *Lac* operon system in *E. coli*, we were able to show via flow cytometry the

sensitivity and specificity of FISH-TAMB to the expression of *Lac*Zα and transformed *Mcr*A. The detection of *Mcr*A mRNA in *E. coli* speaks to FISH-TAMB's potential as a powerful tool to identify the ecophysiological roles novel or poorly characterized lineages, or even taxa which may have obtained functional genes through horizontal gene transfer.

Among potentially novel metabolic players in deep biosphere CH_4 cycling is *Candidatus* "Bathyarchaeota" BE326-BA-RLH, whose genomic potential for AOM coupled to dissimilatory nitrate reduction to ammonia (DNRA) is described in Chapter 3 as the first evidence for evidence for archaeal AOM outside the phylum *Euryarchaeota*. Originally characterized from continental fracture fluid in South Africa, we showed in Chapter 4 that *Ca.* "Bathyarchaeota" BE326-BA-RLH may be pervasive in the deep biosphere based on the detection of 16S rRNA gene sequences from closely related sister lineages from the Nankai Trough. From maximum likelihood estimations of 16S rRNA gene phylogeny, we showed that *Ca.* BE326-BA-RLH belongs to the deeply-branching *Ca.* "Bathyarchaeota" class Subgroup-18, sharing common ancestry with Subgroup-3, known to contain *Ca.* "Bathyarchaeota" methanogens BA1 and BA2 (Evans et al., 2015). The apparent monophyly of methane-metabolizing *Ca.* "Bathyarchaeota" lineages as well as this phylum's divergent *Mcr* genes support the argument that methanogenesis (and now perhaps AOM) evolved in a common ancestor to the *Ca.* "Bathyarchaeota" and the *Euryarchaeota* (Lloyd, 2015).

If the evolutionary history of AOM metabolisms (based on reverse methanogenesis coupled to the reduction of an electron acceptor; i.e., excluding the intra-aerobic pathway unique to *Ca.* "Methylomirabilis oxyfera" (Ettwig et al., 2010)) indeed

predates the evolution of *Euryarchaeota* ANMEs, the apparent scarcity of these clades in environments where biological AOM is ostensibly occurring must mean that either they are biased against detection in sequencing datasets or other uncharacterized groups must be filling the same functional niche. In Chapter 4 we discussed both possibilities when faced with isotopic evidence for AOM at IODP site C0023A in the Nankai Trough. Motivated by suggestive *in situ* $\delta^{13}CH_4$ values at site C0023A and favorable thermodynamic predictions, we performed year-long $^{13}CH_4$ tracer incubations on C0023A sediment slurries at 40 MPa and temperatures between 40˚C and 80˚C to assess the existence of piezophilic and thermophilic ANMEs. Despite concerns surrounding low *in situ* cell counts, we observed statistically significant DIC production within the first 14 days of incubation with corresponding positive $\delta^{13}C_{DIC}$ excursions suggestive of AOM. In addition to 16S rRNA gene-based identification of *Ca.* "Bathyarchaeota" BE326-BA-RLH sister lineages, in metagenomes from 257 and 616 mbsf we were also able to identify evidence of ANME-2d, *Ca.* "Methylomirabilis oxyfera", and *Ca.* "Bathyarchaeota" BA1 and BA2, respectively corresponding to approximate *in situ* temperatures of 37.6˚C and 73.1˚C. Using a combination of FISH-TAMB and 16S rRNA FISH we were able to provide microscopic confirmation of ANME-1 in sulfate-supplemented AOM enrichments from 257 mbsf. Collectively, these data provide evidence for new upper temperature and pressure records for AOM.

Continuing with the theme of exploring new frontiers, in Chapter 5 we performed transcriptomics on the methanogen *M. barkeri* to gain insight into the potential of a microbial origin of CH_4 on modern Mars. Consistent with previous findings, we observed a decrease in CH_4 production when *M. barkeri* was grown at 0˚C and at 30˚C in high

concentrations of perchlorate salts. The combined exposure of *M. barkeri* to perchlorates and 0˚C exposure, however, did not diminish methanogenesis further than at 0˚C alone. From transcriptomic data we infer that the regulatory shifts tied to these observations are likely due to interactions between perchlorates and media components.

Intermittent nitrogen starvation due to interactions between perchlorates and fixed nitrogen was inferred by the simultaneous up-regulation of ammonia transporters, nitrogenases, and their P-II regulatory components. We suggested that an up-regulation of methylamine-based methanogenesis pathways in perchlorate-amended cultures was tied to perchlorate's degradation of the osmoprotectant glycine betaine to trimethylamine (Oren, 1990; Seibel and Walsh, 2002). Based on prior reports of perchlorate reduction in methanogenic media, we proposed that the highly exergonic reaction of H_2-dependent perchlorate reduction could be catalyzed by free Ni in the media, but also perhaps at the Ni active sites of NiFe hydrogenases. Significant down-regulation of the synthesis of redox-sensitive amino acids provided convincing evidence of regulatory shifts in direct response to perchlorate exposure. With respect to what this means for microbial methanogenesis on Mars, we noted that these perchlorates interactions were apparently minimized when *M. barkeri* was grown in their presence at 0˚C. We concluded that the sub-freezing temperatures typical of Mars pose a greater risk to the survival of methanogens than the oxidizing effects of perchlorate salts.

6.2 OPEN QUESTIONS AND OPPORTUNITIES FOR FUTURE RESEARCH

6.2.1 *Divergent* Mcr *proteins and substrate affinities for higher alkanes.* The discovery of the metabolic potential for methanogenesis within the *Ca.* "Bathyarchaeota"

(Evans et al., 2015) has ignited a gold rush to characterize the metabolic capacities of microbial dark matter possessing divergent methyl coenzyme M marker genes that are undetectable by conventional *Mcr* primer sets (e.g., Lloyd, 2015). In addition to our description of *Ca.* "Bathyarchaeota" BE326-BA-RLH in Chapter 3 (Harris et al., 2018), *Mcr* sequences have been recently described in several other dark matter clades, including candidate classes *Ca.* "Hadesarchaea" and *Ca.* "Archaeoglobi" within the *Euryarchaeota* (Laso-Pérez et al., 2016; Wang et al., 2019) and five other candidate archaeal phyla: *Ca.* "Verstraetarchaeota" (Vanwonterghem et al., 2016; Berghuis et al., 2019), *Ca.* "Korarchaeota" (Borrel et al., 2019; McKay et al., 2019; Wang et al., 2019), *Ca.* "Nezhaarchaeota" (Wang et al., 2019), and *Ca.* "Helarchaeota" (Seitz et al., 2019).

Selective enrichments of two candidate euryarchaeal genera, *Ca.* "Argoarchaeum" and *Ca.* "Syntrophoarchaeum", have respectively shown evidence for the anaerobic oxidation of ethane (AOE) and butane (AOB) (Laso-Pérez et al., 2016; Laso-Pérez et al., 2018; Chen et al., 2019). The anaerobic oxidation of propane (AOP) has also been documented in marine sediments (Quistad and Valentine, 2011), but the identity of the responsible organism(s) remains a mystery. These discoveries have led to speculation that clades possessing divergent *Mcr* proteins, such as the *Ca.* "Bathyarchaeota", are actually consumers of higher alkanes rather than CH_4 (e.g., Wang et al., 2019). These claims warrant further investigation. Our results from Chapter 4, while not ruling out the *Ca.* "Bathyarchaeota" as active ANMEs in the Nankai Trough, did not explicitly demonstrate their mediation of AOM, either. Indeed, the characterization of *Ca.* "Bathyarchaeota" BA1 and BA2 as methanogens also requires experimental verification, as their metabolism has only been inferred from metagenomics (Evans et al., 2015). A "smoking

gun" is required to confirm the substrate affinities of *Mcr* proteins belonging to *Ca.* "Bathyarchaeota" and other taxa.

In addition to testing the theory that *Ca.* "Bathyarchaeota" BE326-BA-RLH couples AOM to DNRA, experiments coupling ^{13}C-labeled short-chain alkanes (e.g., methane, ethane, butane, propane) to ^{15}N-labeled nitrate and nitrite in a series of combinatorial selective enrichments can assess for AOM, AOE, AOB, and AOP. Through a combination of SIP, 16S rRNA FISH, and nanoSIMS, ideally, we observations of a stoichiometric balance in the consumption of the supplied electron acceptor and donor, and of FISH-labeled *Ca.* BE326-BA-RLH cells with ^{13}C- and ^{15}N-enriched biomass relative to other cells in the enrichment would support the theory of anaerobic short-chain alkane oxidation by *Ca.* "Bathyarchaeota" species. Unfortunately, this endeavor is much easier said than done. Euryarchaeal ANMEs are thought to have doubling times on the order of weeks to months (Nauhaus et al., 2007; Holler et al., 2011), and the demonstration of butane oxidation in *Ca.* "Syntrophoarchaeum" was the result of 10 years of serial enrichment (Laso-Pérez et al., 2016). Evidence for copiotrophic AOM in our high pressure and high temperature incubations in Chapter 4 offers promising potential for hyperbaric cultivation to further optimize growth conditions of deep biosphere organisms and thus shorten previous doubling time estimates. These efforts would nonetheless require fortunate circumstances such as being able to maintain high pressure chemostats and working with starting materials in which the target organism has high relative *in situ* abundance. Further refinement of FISH-TAMB to separate cells of interest out of complex sedimentary matrices could certainly expedite biomass accumulation, but such fine tuning will be a project unto itself.

6.2.2 ***Next steps in the assessment of potential Martian methanogenesis.*** The discovery of perchlorate salts across the Martian surface is both a blessing and a curse when it comes to the search for life on the Red Planet. On the one hand, perchlorates are highly chaotropic and can disrupt the hydrogen bonds that make up the helical structure of nucleic acids and the secondary structure of proteins. On the other hand, they are excellent potential electron acceptors for microbial redox reactions (Coates and Achenbach, 2004; Yu et al., 2006; Bardiya and Bae, 2011; Liebensteiner et al., 2013). They are also so hygroscopic that they have been observed to deliquescence on the surface of the *Phoenix* lander near Mars' north polar ice cap, where a warm summer day may see temperatures rise to a high of -75˚C (Stillman and Grimm, 2011).

In Chapter 5 we demonstrate the remarkable resiliency and adaptability of *M. barkeri* when it was grown in the presence of perchlorates. But a few lingering questions remain from this work. First is the question of perchlorate reduction. We made assumptions that perchlorate production proceeded in our enrichments based on 1) a puzzling shift in methanogenesis from the use of H_2 to methylamines, and 2) the occurrence of this phenomenon in other methanogen studies (Shcherbakova et al., 2015; Kral et al., 2016). We proposed that H_2 was the reducing agent responsible for the reduction of perchlorate, arguing that the reaction could be abiotically catalyzed by free nickel and perhaps accelerated by nickel active sites in hydrogenases.

The first step in testing this hypothesis requires confirmatory measurements to document the reduction of perchlorate (which can be made using ion chromatography mass spectrometry) and oxidation of H_2 (whose consumption can be monitored using gas chromatography). We can then proceed to assess the potential of nickel as a catalyst by

simply comparing rates of perchlorate reduction in sterile, cell-free methanogenic media with and without supplemented trace nickel. We can also compare these rates to those that are observed in cell cultures to assess whether a biological component is in play. If perchlorate reduction rates indeed increase in the presence of *M. barkeri*, we can then begin to consider isolating and purifying NiFe hydrogenases for substrate binding and affinity assays.

A second unknown resulting from our research is the source of methylamines in the perchlorate-amended cultures. We postulated that the degradation of glycine betaine from complex media components (e.g., yeast extract and casitone) was a likely culprit, as it fit well within our narrative of up-regulated glycine betaine transporters as a means to help maintain osmotic balance. We can quantify both glycine betaine and methylamines using high performance liquid chromatography (HPLC) in the same chronological scheme described above to confirm our inferences and to assess if degradation is primarily abiotic or biologically mediated.

With regards to the next steps in the transcriptomic study of *M. barkeri* under simulated Martian conditions, we are interested in identifying regulatory shifts that are associated with methanogenesis at low pressure. Mars' atmospheric pressure at the surface is ~7-8 mbar (Hess et al., 1980; Withers, 2012), less than 1% that of Earth. The senior thesis work of Jana Suriano ('17) demonstrated that hydrogenotrophic and acetoclastic methanogenesis can proceed at ~30 mbar in the permafrost methanogen *Methanosarcina soligelidi* (*M. soligelidi*) (Suriano, 2017). We intend to follow up on Jana's work and grow *M. barkeri* at 10 mbar in a pressure-, temperature-, and relative humidity-controlled Mars simulation chamber located in Andrew Schuerger's lab at the

University of Florida (Figure 6.1; Schuerger et al., 2008; Schuerger et al., 2011). While Jana grew *M. soligelidi* with two carbon sources to make CH_4 (CO_2 and CH_3COO^-), we plan to grow *M. barkeri* hydrogenotrophically (H_2/CO_2) to assess how decreased pH_2 at Martian atmospheric pressure impacts methanogenesis.

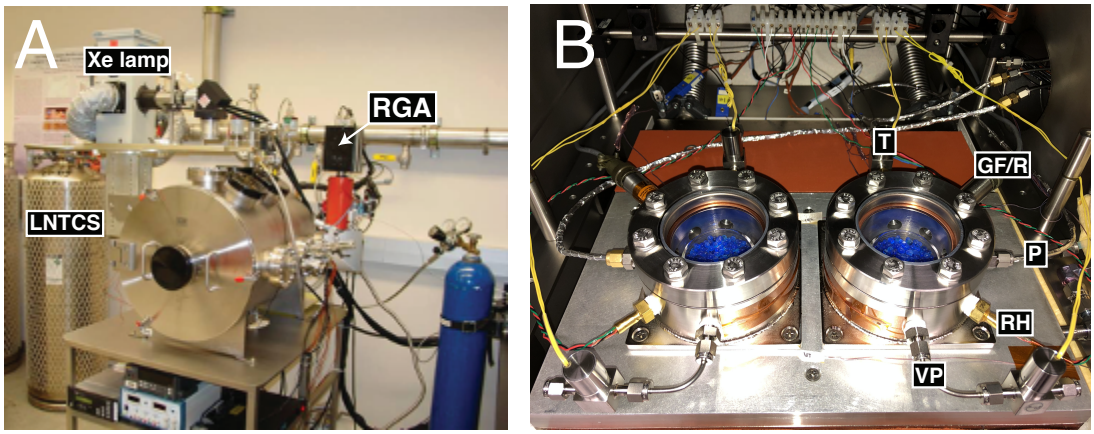

Figure 6.1 The Mars simulation chamber (MSC) in the Schuerger lab at the University of Florida. **(A)** External view, equipped with a liquid nitrogen temperature control system (LNTCS), a xenon-arc lamp equipped for diurnal UV cycling, and a quadrupole mass spectrometer residual gas analyzer (RGA). **(B)** Twin microbial assay chambers (MAC) inside the MSC with connections for real-time measurements of relative humidity (RH), pressure (P) and temperature (T). Headspace composition in each MAC can be measured by evacuating gas through the vacuum pump (VP), which connects to the RGA. A gas flush/resupply (GF/R) line recharges the headspace.

6.3 REFERENCES

Bardiya N. and Bae J.-H. (2011) Dissimilatory perchlorate reduction: A review. *Microbiol. Res.* **166**, 237–254. Available at: https://linkinghub.elsevier.com/retrieve/pii/S0944501310001114.

Berghuis B. A., Yu F. B., Schulz F., Blainey P. C., Woyke T. and Quake S. R. (2019) Hydrogenotrophic methanogenesis in archaeal phylum *Verstraetearchaeota* reveals the shared ancestry of all methanogens. *Proc. Natl. Acad. Sci.* **116**, 5037–5044. Available at: http://www.pnas.org/lookup/doi/10.1073/pnas.1815631116.

Borrel G., Adam P. S., McKay L. J., Chen L.-X., Sierra-García I. N., Sieber C. M. K., Letourneur Q., Ghozlane A., Andersen G. L., Li W.-J., Hallam S. J., Muyzer G., de Oliveira V. M., Inskeep W. P., Banfield J. F. and Gribaldo S. (2019) Wide diversity of methane and short-chain alkane metabolisms in uncultured archaea. *Nat. Microbiol.* **4**, 603–613. Available at: http://www.nature.com/articles/s41564-019-0363-3.

Chen S.-C. C., Musat N., Lechtenfeld O. J., Paschke H., Schmidt M., Said N., Popp D., Calabrese F., Stryhanyuk H., Jaekel U., Zhu Y.-G. G., Joye S. B., Richnow H.-H. H., Widdel F. and Musat F. (2019) Anaerobic oxidation of ethane by archaea from a marine hydrocarbon seep. *Nature* **568**, 108–111. Available at: http://www.nature.com/articles/s41586-019-1063-0.

Coates J. D. and Achenbach L. A. (2004) Microbial perchlorate reduction: rocket-fuelled metabolism. *Nat. Rev. Microbiol.* **2**, 569–580. Available at: http://www.nature.com/articles/nrmicro926.

Ettwig K. F., Butler M. K., Le Paslier D., Pelletier E., Mangenot S., Kuypers M. M. M., Schreiber F., Dutilh B. E., Zedelius J., de Beer D., Gloerich J., Wessels H. J. C. T., van Alen T., Luesken F., Wu M. L., van de Pas-Schoonen K. T., Op den Camp H. J. M., Janssen-Megens E. M., Francoijs K.-J., Stunnenberg H., Weissenbach J., Jetten M. S. M. and Strous M. (2010) Nitrite-driven anaerobic methane oxidation by oxygenic bacteria. *Nature* **464**, 543–548. Available at: http://dx.doi.org/10.1038/nature08883.

Evans P. N., Parks D. H., Chadwick G. L., Robbins S. J., Orphan V. J., Golding S. D. and Tyson G. W. (2015) Methane metabolism in the archaeal phylum *Bathyarchaeota*

revealed by genome-centric metagenomics. *Science* **350**, 434–8. Available at: http://www.sciencemag.org/content/350/6259/434.short.

Harris R. L., Lau M. C. Y., Cadar A., Bartlett D. H., Cason E., van Heerden E. and Onstott T. C. (2018) Draft Genome Sequence of "*Candidatus* Bathyarchaeota" Archaeon BE326-BA-RLH, an Uncultured Denitrifier and Putative Anaerobic Methanotroph from South Africa's Deep Continental Biosphere ed. J. C. Dunning Hotopp. *Microbiol. Resour. Announc.* **7**. Available at: http://mra.asm.org/content/7/20/e01295-18.abstract.

Hess S. L., Ryan J. A., Tillman J. E., Henry R. M. and Leovy C. B. (1980) The annual cycle of pressure on Mars measured by Viking Landers 1 and 2. *Geophys. Res. Lett.* **7**, 197–200. Available at: http://doi.wiley.com/10.1029/GL007i003p00197.

Holler T., Widdel F., Knittel K., Amann R., Kellermann M. Y., Hinrichs K.-U., Teske A., Boetius A. and Wegener G. (2011) Thermophilic anaerobic oxidation of methane by marine microbial consortia. *ISME J.* **5**, 1946–1956. Available at: http://www.nature.com/doifinder/10.1038/ismej.2011.77.

Kral T. A., Goodhart T. H., Harpool J. D., Hearnsberger C. E., McCracken G. L. and McSpadden S. W. (2016) Sensitivity and adaptability of methanogens to perchlorates: Implications for life on Mars. *Planet. Space Sci.* **120**, 87–95. Available at: https://linkinghub.elsevier.com/retrieve/pii/S0032063315003633.

Laso-Pérez R., Wegener G., Knittel K., Widdel F., Harding K. J., Krukenberg V., Meier D. V., Richter M., Tegetmeyer H. E., Riedel D., Richnow H.-H., Adrian L., Reemtsma T., Lechtenfeld O. J. and Musat F. (2016) Thermophilic archaea activate butane via alkyl-coenzyme M formation. *Nature* **539**, 396–401. Available at:

http://www.nature.com/articles/nature20152.

Laso-Pérez R., Krukenberg V., Musat F. and Wegener G. (2018) Establishing anaerobic hydrocarbon-degrading enrichment cultures of microorganisms under strictly anoxic conditions. *Nat. Protoc.* **13**, 1310–1330. Available at: http://www.nature.com/articles/nprot.2018.030.

Liebensteiner M. G., Pinkse M. W. H., Schaap P. J., Stams A. J. M. and Lomans B. P. (2013) Archaeal (Per)Chlorate Reduction at High Temperature: An Interplay of Biotic and Abiotic Reactions. *Science* **340**, 85–87. Available at: http://www.sciencemag.org/lookup/doi/10.1126/science.1233957.

Lloyd K. (2015) Beyond known methanogens. *Science* **350**, 384–384. Available at: https://www.sciencemag.org/lookup/doi/10.1126/science.aad4066.

McKay L. J., Dlakić M., Fields M. W., Delmont T. O., Eren A. M., Jay Z. J., Klingelsmith K. B., Rusch D. B. and Inskeep W. P. (2019) Co-occurring genomic capacity for anaerobic methane and dissimilatory sulfur metabolisms discovered in the *Korarchaeota*. *Nat. Microbiol.* **4**, 614–622. Available at: http://www.nature.com/articles/s41564-019-0362-4.

Nauhaus K., Albrecht M., Elvert M., Boetius A. and Widdel F. (2007) In vitro cell growth of marine archaeal-bacterial consortia during anaerobic oxidation of methane with sulfate. *Environ. Microbiol.* **9**, 187–196. Available at: http://doi.wiley.com/10.1111/j.1462-2920.2006.01127.x.

Oren A. (1990) Formation and breakdown of glycine betaine and trimethylamine in hypersaline environments. *Antonie Van Leeuwenhoek* **58**, 291–298. Available at: http://link.springer.com/10.1007/BF00399342.

Quistad S. D. and Valentine D. L. (2011) Anaerobic propane oxidation in marine hydrocarbon seep sediments. *Geochim. Cosmochim. Acta* **75**, 2159–2169. Available at: https://linkinghub.elsevier.com/retrieve/pii/S0016703711000706.

Schuerger A. C., Clausen C. and Britt D. (2011) Methane evolution from UV-irradiated spacecraft materials under simulated martian conditions: Implications for the Mars Science Laboratory (MSL) mission. *Icarus* **213**, 393–403. Available at: https://linkinghub.elsevier.com/retrieve/pii/S0019103511000753.

Schuerger A. C., Trigwell S. and Calle C. I. (2008) Use of non-thermal atmospheric plasmas to reduce the viability of Bacillus subtilis on spacecraft surfaces. *Int. J. Astrobiol.* **7**, 47–57. Available at: https://www.cambridge.org/core/product/identifier/S1473550407004016/type/journal_article.

Seibel B. A. and Walsh P. J. (2002) Trimethylamine oxide accumulation in marine animals: relationship to acylglycerol storage. *J. Exp. Biol.* **205**, 297–306. Available at: http://www.ncbi.nlm.nih.gov/pubmed/11854367.

Seitz K. W., Dombrowski N., Eme L., Spang A., Lombard J., Sieber J. R., Teske A. P., Ettema T. J. G. and Baker B. J. (2019) Asgard archaea capable of anaerobic hydrocarbon cycling. *Nat. Commun.* **10**, 1822. Available at: http://www.nature.com/articles/s41467-019-09364-x.

Shcherbakova V., Oshurkova V. and Yoshimura Y. (2015) The Effects of Perchlorates on the Permafrost Methanogens: Implication for Autotrophic Life on Mars. *Microorganisms* **3**, 518–534. Available at: http://www.mdpi.com/2076-2607/3/3/518.

Stillman D. E. and Grimm R. E. (2011) Dielectric signatures of adsorbed and salty liquid water at the Phoenix landing site, Mars. *J. Geophys. Res.* **116**, E09005. Available at: http://doi.wiley.com/10.1029/2011JE003838.

Suriano J. (2017) Survival and metabolism of *Methanosarcina soligelidi* under simulated Martian subsurface conditions. Princeton University. Available at: http://arks.princeton.edu/ark:/88435/dsp01tm70mx813.

Vanwonterghem I., Evans P. N., Parks D. H., Jensen P. D., Woodcroft B. J., Hugenholtz P. and Tyson G. W. (2016) Methylotrophic methanogenesis discovered in the archaeal phylum *Verstraetearchaeota*. *Nat. Microbiol.* **1**, 16170. Available at: http://dx.doi.org/10.1038/nmicrobiol.2016.170%5Cnhttp://www.ncbi.nlm.nih.gov/pubmed/27694807.

Wang Y., Wegener G., Hou J., Wang F. and Xiao X. (2019) Expanding anaerobic alkane metabolism in the domain of *Archaea*. *Nat. Microbiol.* **4**, 595–602. Available at: http://www.nature.com/articles/s41564-019-0364-2.

Withers P. (2012) Empirical Estimates of Martian Surface Pressure in Support of the Landing of Mars Science Laboratory. *Space Sci. Rev.* **170**, 837–860. Available at: http://link.springer.com/10.1007/s11214-012-9876-2.

Yu X., Amrhein C., Deshusses M. A. and Matsumoto M. R. (2006) Perchlorate Reduction by Autotrophic *Bacteria* in the Presence of Zero-Valent Iron. *Environ. Sci. Technol.* **40**, 1328–1334. Available at: https://pubs.acs.org/doi/10.1021/es051682z.

Appendix A

Supplementary Tables

Table A.1 Gene abbreviations of proteins visualized in Figure 3.3.

Encoded Protein	Nomenclature
Formate dehydrogenase	*Fdh*
Carbon monoxide dehydrogenase	*Coo*S
Tungsten-containing formylmethanofuran dehydrogenase	*Fwd*
Formylmethanofuran:tetrahydromethanopterin (H_4MPT) formyltransfersase	*Ftr*
Methenyl-H_4MPT cyclohydrolase	*Mch*
F420-reducing hydrogenase	*Frh*
F420-H_2-dependent quinone reductase	*Fqo*
F420-reducing methylene-H_4MPT dehydrogenase	*Mtd*
F420-H_2-dependent methylene-H_4MPT reductase	*Mer*
Na^+ transporting methyl-H_4MPT:coenzyme M methyltransferase	*Mtr*
Methyl-coenzyme M reductase	*Mcr*
Methylamine-specific methylcobalamin:coenzyme M methyltransferase	*Mtb*A
Trimethylamine methyltransferase corrinoid protein	*mtt*C
Heterodisulfide reductase	*Hdr*
Methyl viologen reducing hydrogenase	*Mvh*
Carbon monoxide dehydrogenase	*Cdh*
Acetyl-CoA synthetase	*Acd*
Phosphate acetyltransferase	*Pta*
Acetate kinase	*Ack*
Pyruvate ferredoxin oxidoreductase	*Por*A
Phosphoenolpyruvate synthase	*Pps*A
Phosphoenolpyruvate carboxylase	*Ppc*A
Malate dehydrogenase	*Mdh*
Fumarate hydratase	*Fum*
Succinate dehydrogenase	*Sdh*
Succinate-CoA ligase	*Suc*D
2-oxoglutarate synthase	*Kor*
Isocitrate dehydrogenase	*Idh*
Aconitate hydratase	*Acn*
ATP-citrate lyase	*Acl*
Archaeal flagellin	*Fla*I
Methyl-accepting chemotaxis protein	*MCP*
Cytoplasmic chemotaxis proteins	*Che*
Ion-transporting ATP synthase	*ATPase*
Periplasmic nitrate oxidoreductase	*Nar*
Ammonium-forming periplasmic nitrite reductase	*Nrf*

Table A.2 Gene abbreviations of proteins visualized in Figures 5.4 – 5.7

Encoded Protein	Nomenclature
Methylamine-specific methylcobalamin:coenzyme M methyltransferase	*Mtb*A
Dimethylamine:corrindoid methyltransferase	*Mtb*B
Dimethylamine methyltransferase corrinoid protein	*Mtb*C
Dimethylamine permease	*Mtb*P
Monomethylamine:corrinoid protein	*Mtm*B
Monomethylamine methyltransferase corrinoid protein	*Mtm*C
Monomethylamine permease	*Mtm*P
Trimethylamine:corrinoid methyltransferase	*Mtt*B
Trimethylamine methyltransferase corrinoid protein	*Mtt*C
Methyl-coenzyme M reductase subunit	*Mcr*
CoB--CoM heterodisulfide reductase subunit	*Hdr*
Methanol:corrinoid methyltransferase	*Mta*B
Methanol methyltransferase corrinoid protein	*Mta*C
Methanol-specific methylcobalamin:coenzyme M methyltransferase	*Mta*A
CoB--CoM heterodisulfide reductase 2	*Hdr*
Methanophenazine hydrogenase large subunit	*Vht*A
Methanophenazine hydrogenase cytochrome b subunit	*Vht*C
Methanophenazine hydrogenase small subunit	*Vht*G
Na^+ transporting methyl-H_4MPT:coenzyme M methyltransferase	*Mtr*
F420-H_2-dependent methylene-H_4MPT reductase	*Mer*
Methenyl-tetrahydrosarcinopterin (H_4SPT) cyclohydrolase	*Mch*
Formylmethanofuran-H_4SPT formyltransferase	*Ftr*
F_{420}-reducing hydrogenase	*Frh*
Mo-containing formylmethanofuran dehydrogenase	*Fmd*
Energy-conserving hydrogenase (ferredoxin)	*Ech*
$F_{420}H_2$ dehydrogenase	*Fpo*
Carbon monoxide dehydrogenase/Acetyl-CoA synthase complex	*Cdh*/*Coo*

Table A.3 Abbreviated metabolites visualized in Figures 5.4 – 5.7

Metabolite	Nomenclature
Coenzyme M	CoM-SH
Methyl-coenzyme M	CH_3-S-CoM
Coenzyme B	CoB-SH
Coenzyme $F_{420}H_2$	$F420_{red}$
Coenzyme F_{420}	$F420_{ox}$
Reduced ferredoxin	Fd_{red}
Oxidized ferredoxin	Fd_{ox}
Methanophenazine-H_2	MP_{red}
Methanophenazine	MP_{ox}
Tetrahydrosarcinopterin	H_4MPT
Acetyl-Coenzyme A	Acetyl-CoA
Methanofuran	MFR

Table A.4 Gene abbreviations of proteins visualized in Figure 5.8

Encoded Protein	Nomenclature
Methylamine-specific methylcobalamin:coenzyme M methyltransferase	*Mtb*A
Dimethylamine:corrindoid methyltransferase	*Mtb*B
Dimethylamine methyltransferase corrinoid protein	*Mtb*C
Dimethylamine permease	*Mtb*P
Monomethylamine:corrinoid protein	*Mtm*B
Monomethylamine methyltransferase corrinoid protein	*Mtm*C
Monomethylamine permease	*Mtm*P
Trimethylamine:corrinoid methyltransferase	*Mtt*B
Trimethylamine methyltransferase corrinoid protein	*Mtt*C

Table A.5 Gene abbreviations of proteins visualized in Figure 5.9.

Encoded Protein	Nomenclature
Nitrogenase FeS scaffold assembly protein	*Nif*B
Nitrogenase FeMo protein alpha chain	*Nif*D
Nitrogenase FeMo biosynthesis protein	*Nif*E
Nitrogenase FeMo reductase and maturase protein	*Nif*H
Nitrogenase regulatory protein P-II	*Nif*I
Nitrogenase FeMo protein beta chain	*Nif*K
Nitrogenase FeMo-cofactor scaffold and assembly protein	*Nif*N
Nitrogenase vanadium cofactor synthesis protein	*Vnf*E
Nitrogenase vanadium-iron protein beta chain	*Vnf*K

Table A.6 Gene abbreviations of proteins visualized in Figure 5.10

Encoded Protein	Nomenclature
Tryptophan beta chain	*Trp*B
Threonine synthetase	*Thr*C
Serine—glyoxylate aminotransferase	*SGAT*
Phosphoserine phosphatase	*Ser*B
Aspartate carbamoyltransferase	*Pyr*B
Pyrrolysine synthetase	*Pyl*C
Phosphoribosylformylglycinamidine synthase, glutamine amidotransferase subunit	*Pyr*Q
Pyrroline-5-carboxylate reductase	*Pro*C
Prephenate dehydratase	*Phe*A2
Methionine gamma-lyase	*Mgl*
5-methyltetrahydropteroyltriglutamate—homocysteine methyltransferase	*Met*E
Diaminopimelate decarboxylase	*Lys*A
Branched-chain amino acid aminotransferase	*Ilv*E
Histidinol dehydrogenase	*His*D
Aspartate aminotransferase / Histidinol-phosphate aminotransferase	*His*C
Serine hydroxymethyltransferase / L-threonine aldolase / L-allo threonine aldolase	*Gly*A

Glutamate synthase (NADPH) small chain	*Glt*D
Glutamine synthetase type I	*Gln*A
Glutamate dehydrogenase 2	*Gdh*A
Cysteine synthase	*Cys*K
Serine acetyltransferase	*Cys*E
Biosynthetic aromatic amino acid aminotransferase alpha / Aspartate aminotransferase	*Asp*B
Asparagine synthetase (glutamine hydrolyzing)	*Asn*B
Argininosuccinate synthase	*Arg*G
Arginine deaminase	*Arc*A
Ornithine cyclodeaminase	*Ala*
Phosphoserine aminotransferase	*Ser*C
D-3-phosphoglycerate dehydrogenase	*Ser*A
5'-methylthioadenosine phosphorylase	*Mtn*N
Methylthioribose-1-phosphate isomerase	*Mtn*A
S-adenosylhomocysteine deaminase	*Mta*D
Homoserine O-acetyltransferase	*Met*X
Archaeal S-adenosylmethionine synthetase	*Met*K
O-acetylhomoserine sulfhydralase	*Met*C
Malade dehydrogenase	*Mdh*
Aspartokinase	*Lys*C
Homoserine dehydrogenase	*Hsd*
Ferredoxin	*Fdx*
Aspartate aminotransferase	*Asp*C
Aspartate-semialdehyde dehydrogenase	*Asd*
Adenosylhomocysteinase	*Ach*Y

Table A.7 Amino acid abbreviations reported from Figure 5.10.

Amino Acid	**Nomenclature**
Alanine	A
Arginine	R
Asparagine	N
Aspartate	D
Cysteine	C
Glutamine	Q
Glutamate	E
Glycine	G
Histidine	H
Isoleucine	I
Lysine	K
Methionine	M
Phenylalanine	F
Proline	P
Pyrrolysine[a]	O
Serine	S

Threonine	T
Tryptophan	W
Tyrosine	Y
Valine	V

[a]Pyrrolysine is a lysine derivative encoded by the UAG codon in *Methanosarcina barkeri* (Srinivasan et al., 2002).

Tables A.8 – A.14 are available to view and download at https://tinyurl.com/rjlu2gb.

REFERENCES

Srinivasan G., James C. M. and Krzycki J. A. (2002) Pyrrolysine encoded by UAG in archaea: Charging of a UAG-decoding specialized tRNA. *Science* **296**, 1459 - 1462.

Appendix B

Supplementary Figures

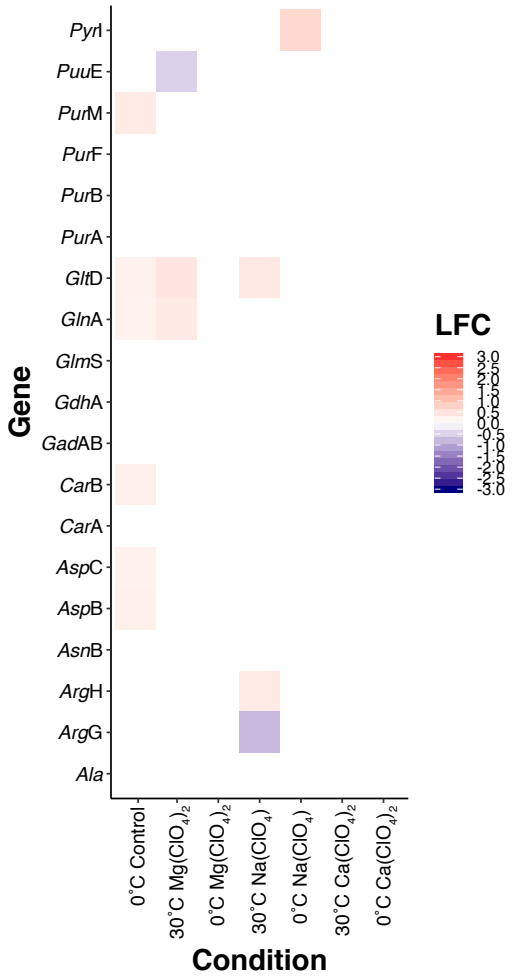

Figure B.1. Differential expression (Log_2-fold change, LFC) of genes involved in alanine, aspartate, and glutamate metabolisms in *M. barkeri*. Perchlorate-amended 30˚C and 0˚C perchlorate-free control cultures are relative to 30˚C perchlorate-free control. 0˚C perchlorate-amended cultures are relative to 0˚C perchlorate-free control. Significant differential expression was identified via Wald test ($P < 0.05$). Gene abbreviations: *Puu*E, 4-aminobutyrate aminotransferase; *Pur*B, Adenylosuccinate lyase; *Pur*A, Adenylosuccinate synthase; *Pur*F, Amidophosphoribosyltransferase; *Arg*H, Arginosuccinate lyase; *Arg*G, Argininosuccinate synthase; *Asn*B, Asparagine synthetase; *Asp*C, Aspartate aminotransferase; *Pyr*I, Aspartate carbamoyltransferase regulatory subunit; *Asp*B, Biosynthetic aromatic amino acid aminotransferase alpha; *Car*B, Carbamoyl-phosphate synthase large chain; *Car*A, Carbamoyl-phosphate synthase small subunit; *Glm*S, Glucosamine—fructose-6-phosphate aminotransferase; *Gad*AB, Glutamate decarboxylase; *Gdh*A, Glutamate dehydrogenase; *Glt*D, Glutamate synthase [NADPH] large chain; *Gln*A, Glutamine synthetase type I, *Ala*, Ornithine cyclodeaminase; *Pur*M, Phosphoribosylformylglycinamidine cyclo-ligase; *Gab*D, Succinate-semialdehyde dehydrogenase.

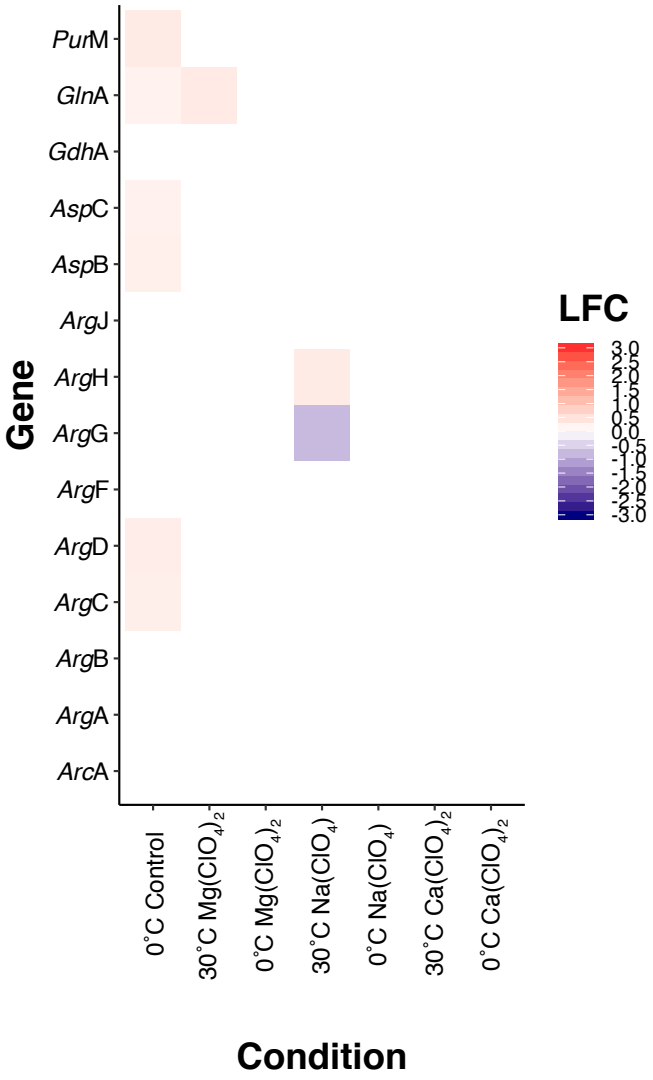

Figure B.2. Differential expression (Log_2-fold change, LFC) of genes involved in arginine biosynthesis in *M. barkeri*. Perchlorate-amended 30˚C and 0˚C perchlorate-free control cultures are relative to 30˚C perchlorate-free control. 0˚C perchlorate-amended cultures are relative to 0˚C perchlorate-free control. Significant differential expression was identified via Wald test ($P < 0.05$). Gene abbreviations: *Arg*B, Acetylglutamate kinase; *Arg*D, Acetylornithine aminotransferase; *Arc*A, Arginine deaminase; *Arg*H, Arginosuccinate lyase; *Arg*G, Arginosuccinate synthase; *Asp*C, Aspartate aminotransferase; *Asp*B, Biosynthetic aromatic amino acid aminotransferase alpha; *Arg*A, GCN5-related N-acetyltransferase; *Gdh*A, Glutamate dehydrogenase; *Gln*A, Glutamine synthetase type I; *Arg*J, Glutamate N-acetyltransferase; *Arg*C, N-acetyl-gamma-glutamyl-phosphate reductase; *Arg*F, Ornithine carbamoyltransferase; *Pur*Q, Phosphoribosylformylglycinamidine synthase, glutamine amidotransferase subunit.

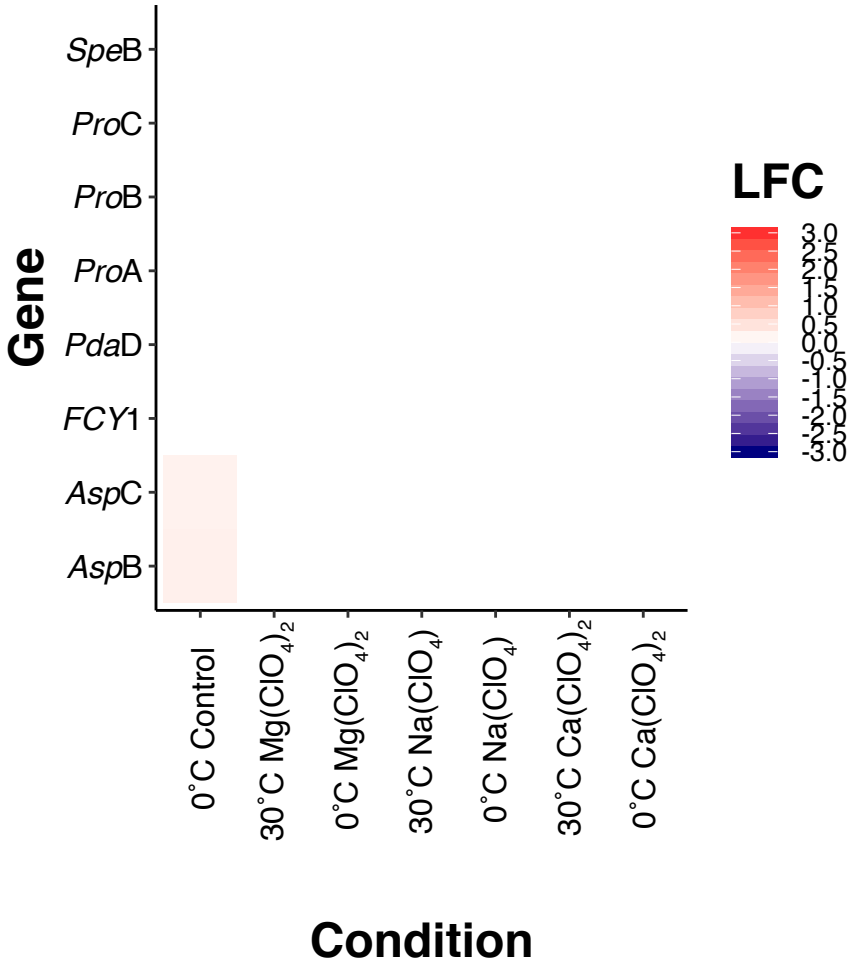

Figure B.3. Differential expression (Log_2-fold change, LFC) of genes involved in arginine and proline metabolisms in *M. barkeri*. Perchlorate-amended 30˚C and 0˚C perchlorate-free control cultures are relative to 30˚C perchlorate-free control. 0˚C perchlorate-amended cultures are relative to 0˚C perchlorate-free control. Significant differential expression was identified via Wald test ($P < 0.05$). Gene abbreviations: *Spe*B, Agmatinase; *Asp*C, Aspartate aminotransferase; *Asp*B, Biosynthetic aromatic amino acid aminotransferase alpha; *FCY*1, Cytosine deaminase; *Pro*A, Gamma-glutamyl phosphate reductase; *Pro*B, Glutamate 5-kinase; *Pro*C, Pyrroline 5-carboxylate reductase; *Pda*D, Pyruvoyl-dependent arginine decarboxylase.

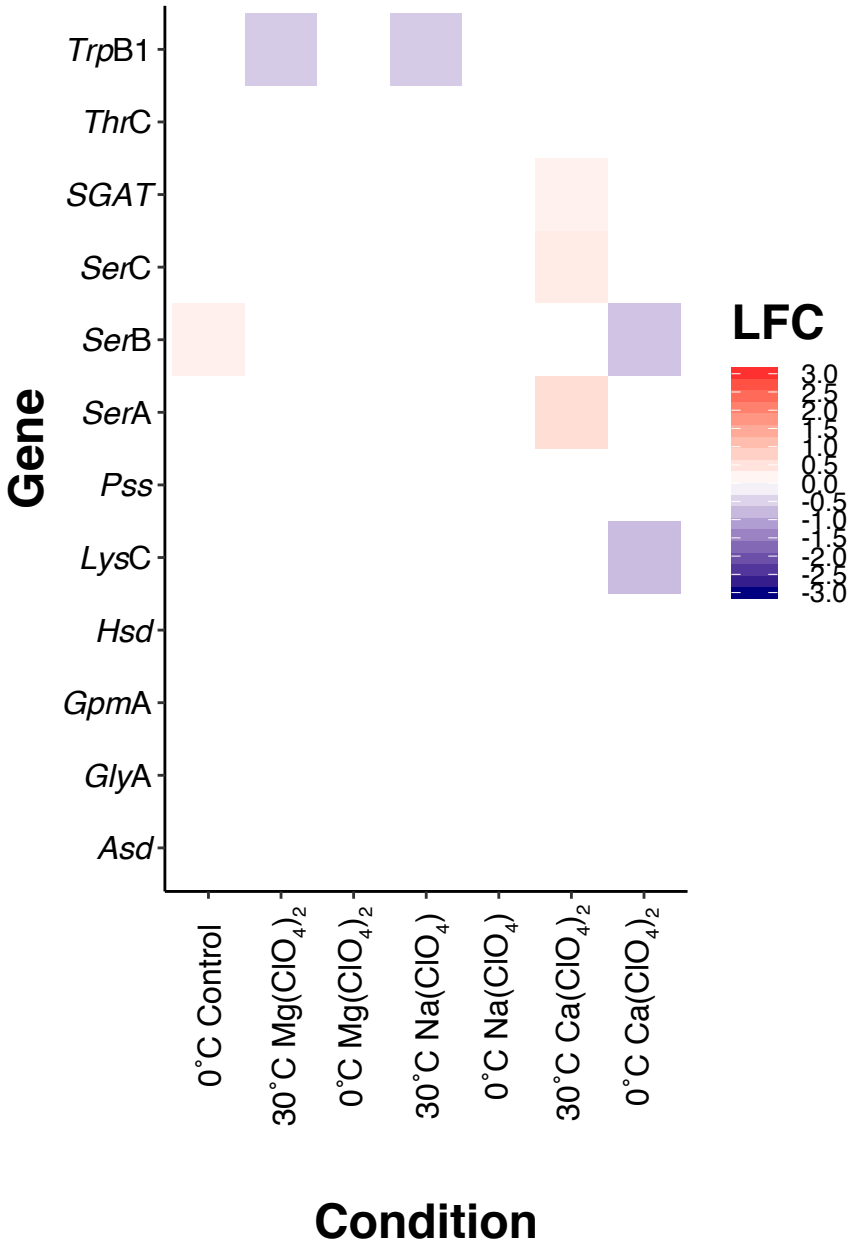

Figure B.4. Differential expression (Log_2-fold change, LFC) of genes involved in glycine, serine, and threonine metabolisms in *M. barkeri*. Perchlorate-amended 30˚C and 0˚C perchlorate-free control cultures are relative to 30˚C perchlorate-free control. 0˚C perchlorate-amended cultures are relative to 0˚C perchlorate-free control. Significant differential expression was identified via Wald test ($P < 0.05$). Gene abbreviations: *Asd*, Aspartate-semialdehyde dehydrogenase; *Lys*C, Aspartokinase; *Pss*, CDP-diaglycerol--serine O-phosphatidyltransferase; *Ser*A, D-3-phosphoglycerate dehydrogenase; *Hsd*, Homoserine dehydrogenase; *Gpm*A, Phosphoglycerate mutase; *Ser*C, Phosphoserine aminotransferase; *Ser*B, Phosphoserine phosphatase, *Gly*A, Serine hydroxymethyltransferase/L-threonine aldolase; *SGAT*, Serine--glyoxylate aminotransferase; *Thr*C, Threonine synthase; *Trp*B, Tryptophan synthase beta chain.

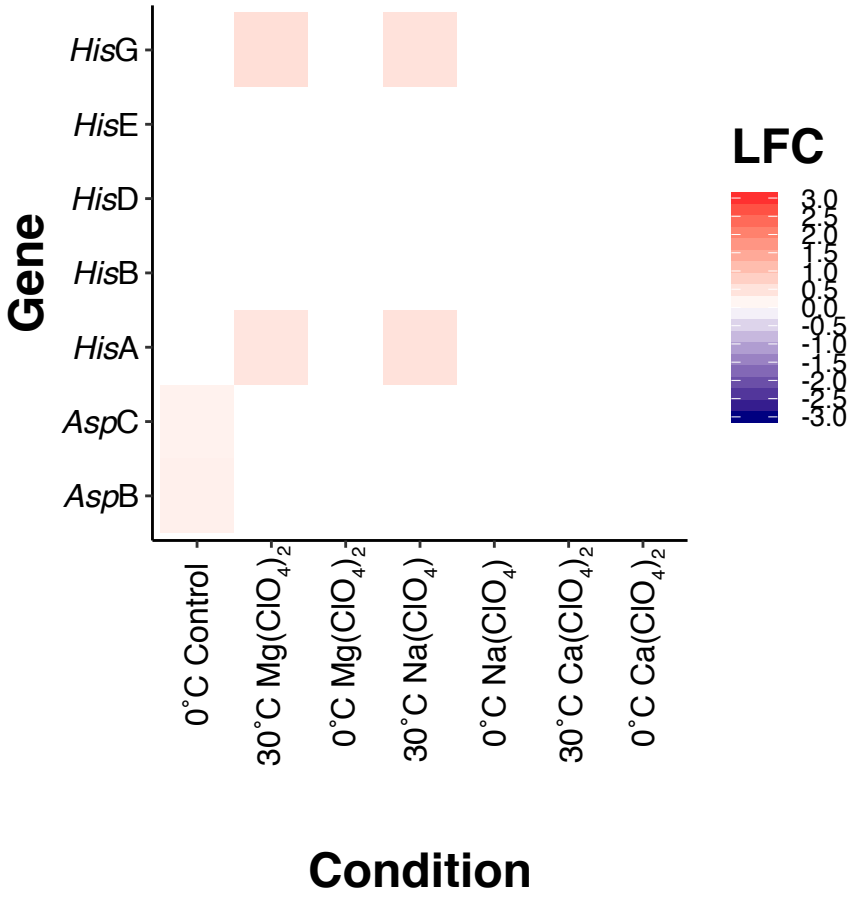

Figure B.5. Differential expression (Log_2-fold change, LFC) of genes involved in histidine metabolism in *M. barkeri*. Perchlorate-amended 30˚C and 0˚C perchlorate-free control cultures are relative to 30˚C perchlorate-free control. 0˚C perchlorate-amended cultures are relative to 0˚C perchlorate-free control. Significant differential expression was identified via Wald test ($P < 0.05$). Gene abbreviations: *Asp*C, Aspartate aminotransferase; *His*G, ATP phosphoribosyltransferase; *Asp*B, Biosynthetic aromatic amino acid aminotransferase alpha; *His*D, Histidinol dehydrogenase; *His*B, Imidazoleglycerol-phosphate dehydratase; *His*E, Phosphoribosyl-ATP pyrophosphatase; *His*A, Phosphoribosylformimino-5-aminoimidazole carboxamide ribotide isomerase.

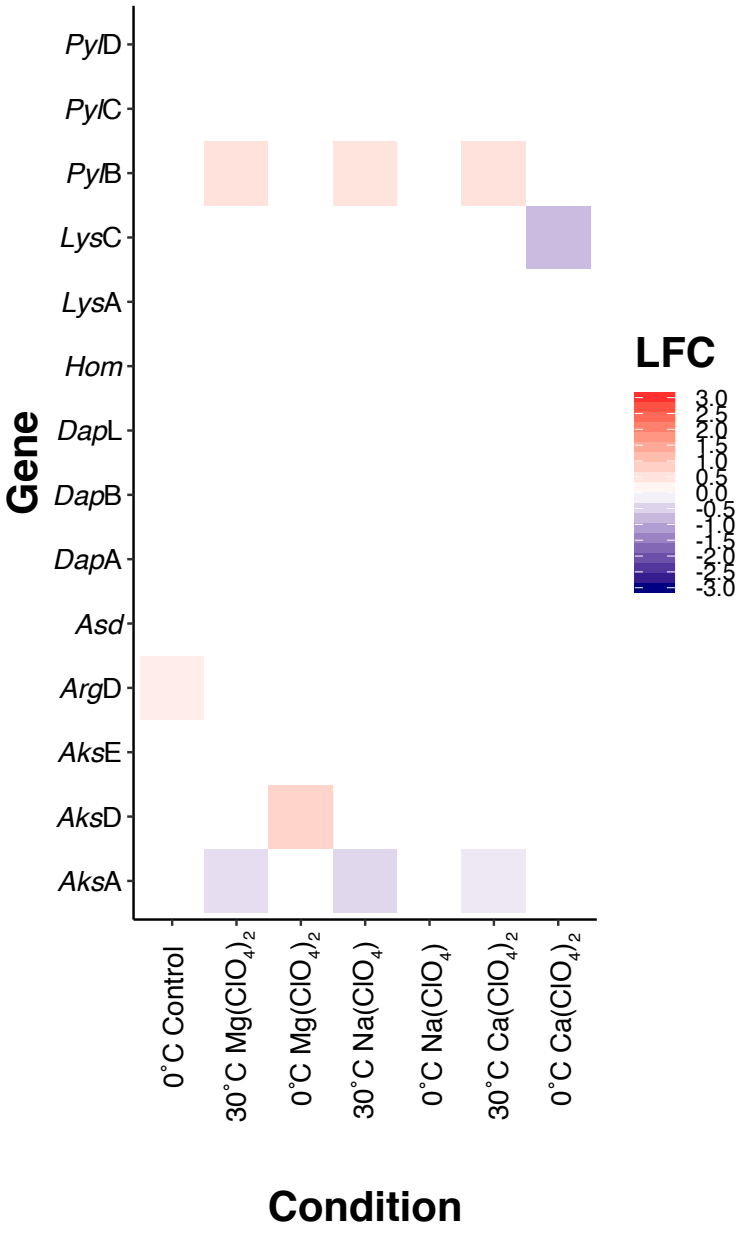

Figure B.6. Differential expression (Log_2-fold change, LFC) of genes involved in lysine and pyrrolysine biosynthesis in *M. barkeri*. Perchlorate-amended 30˚C and 0˚C perchlorate-free control cultures are relative to 30˚C perchlorate-free control. 0˚C perchlorate-amended cultures are relative to 0˚C perchlorate-free control. Significant differential expression was identified via Wald test ($P < 0.05$). Gene abbreviations: *Arg*D, Acetylornithine aminotransferase; *Asd*, Aspartate-semialdehyde dehydrogenase; *Lys*C, Aspartokinase; *Aks*A, Coenzyme B synthesis from 2-oxoglutarate: steps 1, 6, and 10; *Aks*D, Coenzyme B synthesis from 2-oxoglutarate: steps 4, 7, 8, 11, and 12 (large subunit); *Aks*E, Coeznyme B synthesis from 2-oxoglutarate: steps 4, 7, 8, 11, and 12 (small subunit); *Lys*A, Diaminopimelate decarboxylase; *Dap*B, Dihydrodipicolinate reductase; *Dap*A, Dihydrodipicolinate synthase; *Hom*; Homoserine dehydrogenase; *Dap*L, LL-diaminopimelate aminotransferase; *Pyl*B, Proline 2-methylase for pyrrolysine biosynthesis; *Pyl*D, Proline reductase for pyrrolysine biosynthesis; *Pyl*C, Pyrrolysine synthetase.

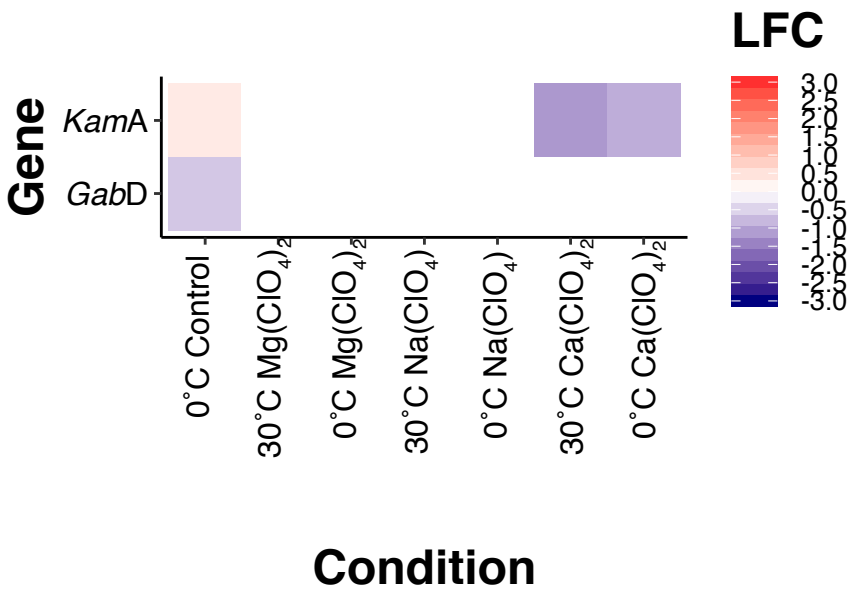

Figure B.7. Differential expression (Log_2-fold change, LFC) of genes involved in **l**ysine degradation in *M. barkeri*. Perchlorate-amended 30˚C and 0˚C perchlorate-free control cultures are relative to 30˚C perchlorate-free control. 0˚C perchlorate-amended cultures are relative to 0˚C perchlorate-free control. Significant differential expression was identified via Wald test ($P < 0.05$). Gene abbreviations: *Kam*A, Lysine 2,3-aminomutase; *Gab*D, Succinate-semialdehyde dehydrogenase [NAD].

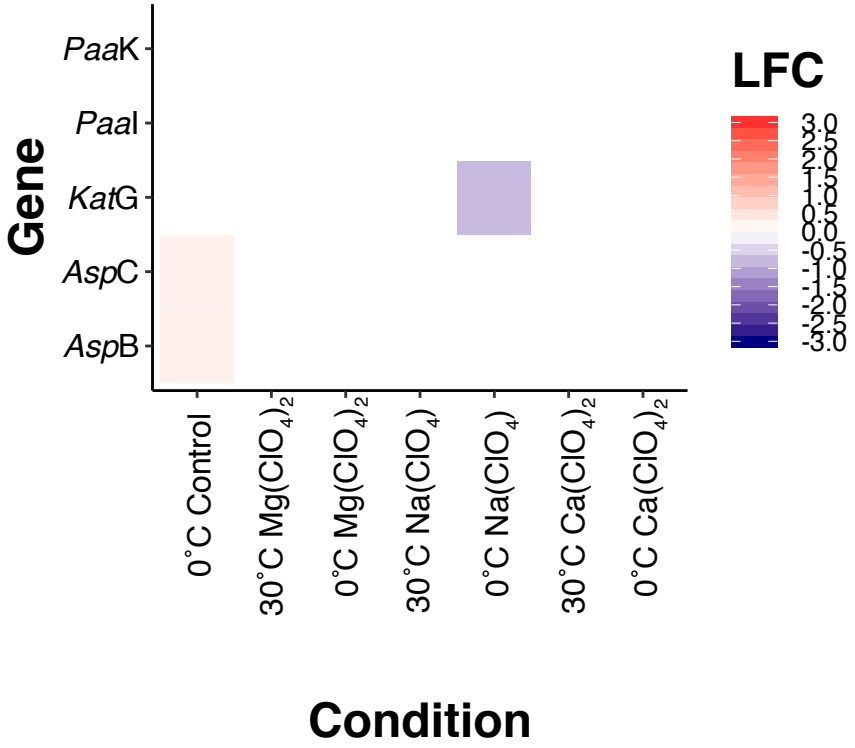

Figure B.8. Differential expression (Log_2-fold change, LFC) of genes involved in phenylalanine metabolism in *M. barkeri*. Perchlorate-amended 30˚C and 0˚C perchlorate-free control cultures are relative to 30˚C perchlorate-free control. 0˚C perchlorate-amended cultures are relative to 0˚C perchlorate-free control. Significant differential expression was identified via Wald test ($P < 0.05$). Gene abbreviations: *Asp*C, Aspartate aminotransferase; *Asp*B, Biosynthetic aromatic amino acid aminotransferase alpha; *Kat*G, Catalase; *Paa*I, Phenylacetic acid degradation protein; *Paa*K, Phenylacetate-CoA ligase.

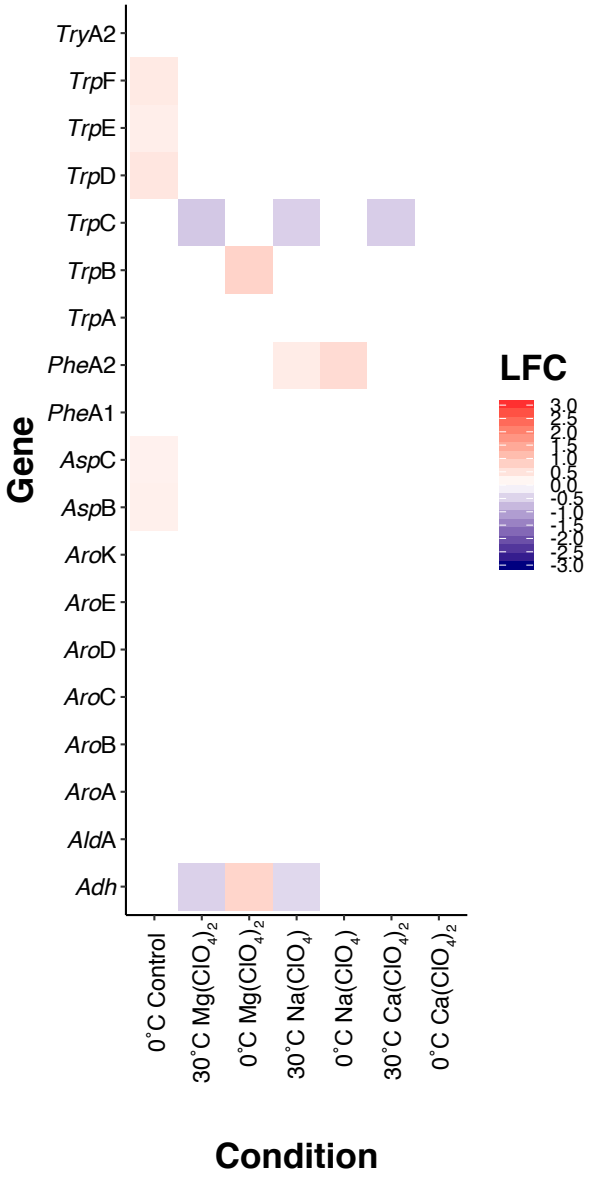

Figure B.9. Differential expression (Log_2-fold change, LFC) of genes involved in phenylalanine, tyrosine, and tryptophan metabolism in *M. barkeri*. Perchlorate-amended 30˚C and 0˚C perchlorate-free control cultures are relative to 30˚C perchlorate-free control. 0˚C perchlorate-amended cultures are relative to 0˚C perchlorate-free control. Significant differential expression was identified via Wald test ($P < 0.05$). Gene abbreviations: *Adh*, 2-amino-3,7 dideoxy-D-threo-hept-6-ulosonate synthase; *Aro*D, 3-dehydroquinate dehydratase I; *Aro*B, 3,7-dideoxy-D-threo-hepto-2,6-diulosonate synthase; *Aro*A, 5-Enolpyruvylshikimate-3-phosphate synthase; *Trp*D, Anthranilate phosphoribosyltransferase; *Trp*E, Anthranilate synthase, aminase component; *Asp*C, Aspartate aminotransferase; *Asp*B, Biosynthetic aromatic amino acid aminotransferase alpha; *Phe*A1, Chorismate mutase I; *Aro*C, Chorismate synthase; *Ald*A, Fructose-bisphosphate aldolase; *Trp*C, Indole-3-glycerol phosphate synthase; *Trp*F, Phosphoribosylanthranilate isomerase; *Try*A2, Prephenate and/or arogenate dehydrogenase; *Phe*A2, Prephenate dehydratase; *Aro*E, Shikimate 5-dehydrogenase I alpha; *Aro*K, Shikimate kinase II; *Trp*A, Tryptophan synthase alpha chain; *Trp*B, Tryptophan synthase beta chain.

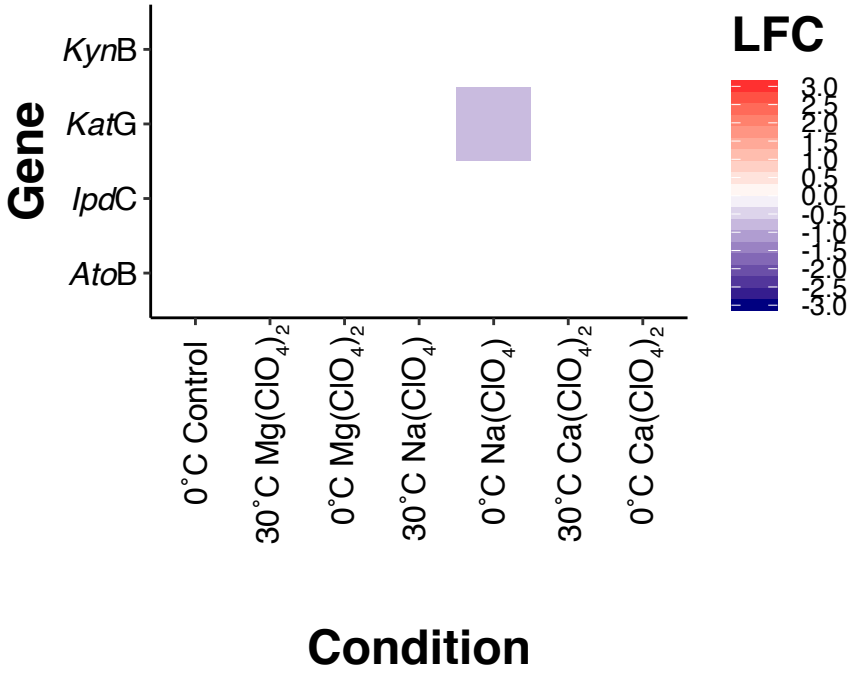

Figure B.10. Differential expression (Log_2-fold change, LFC) of genes involved in tryptophan metabolism in *M. barkeri*. Perchlorate-amended 30˚C and 0˚C perchlorate-free control cultures are relative to 30˚C perchlorate-free control. 0˚C perchlorate-amended cultures are relative to 0˚C perchlorate-free control. Significant differential expression was identified via Wald test ($P < 0.05$). Gene abbreviations: *Ato*B, Beta-ketoacyl synthase/thiolase; *Kat*G, Catalase; *Kyn*B, Metal-dependent hydrolase; *Ipd*C, Pyruvate decarboxylase.

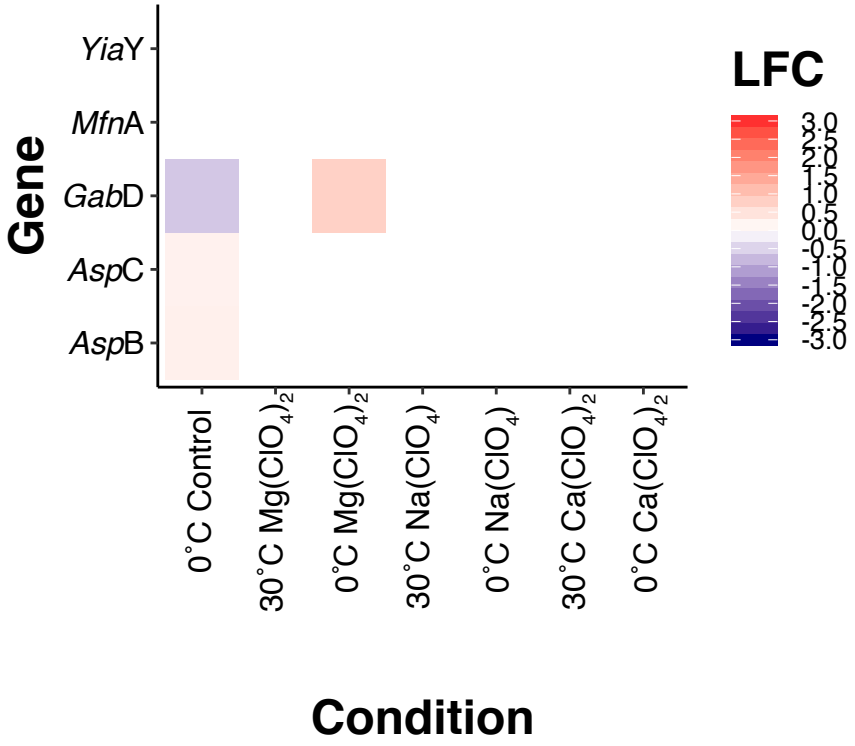

Figure B.11. Differential expression (Log_2-fold change, LFC) of genes involved in tyrosine metabolism in *M. barkeri*. Perchlorate-amended 30˚C and 0˚C perchlorate-free control cultures are relative to 30˚C perchlorate-free control. 0˚C perchlorate-amended cultures are relative to 0˚C perchlorate-free control. Significant differential expression was identified via Wald test ($P < 0.05$). Gene abbreviations: *Yia*Y, Alcohol dehydrogenase; *Asp*C, Aspartate aminotransferase; *Asp*B, Biosynthetic aromatic amino acid aminotransferase alpha; *Mfn*A, L-tyrosine decarboxylase; *Gab*D, Succinate-semialdehyde dehydrogenase [NAD].

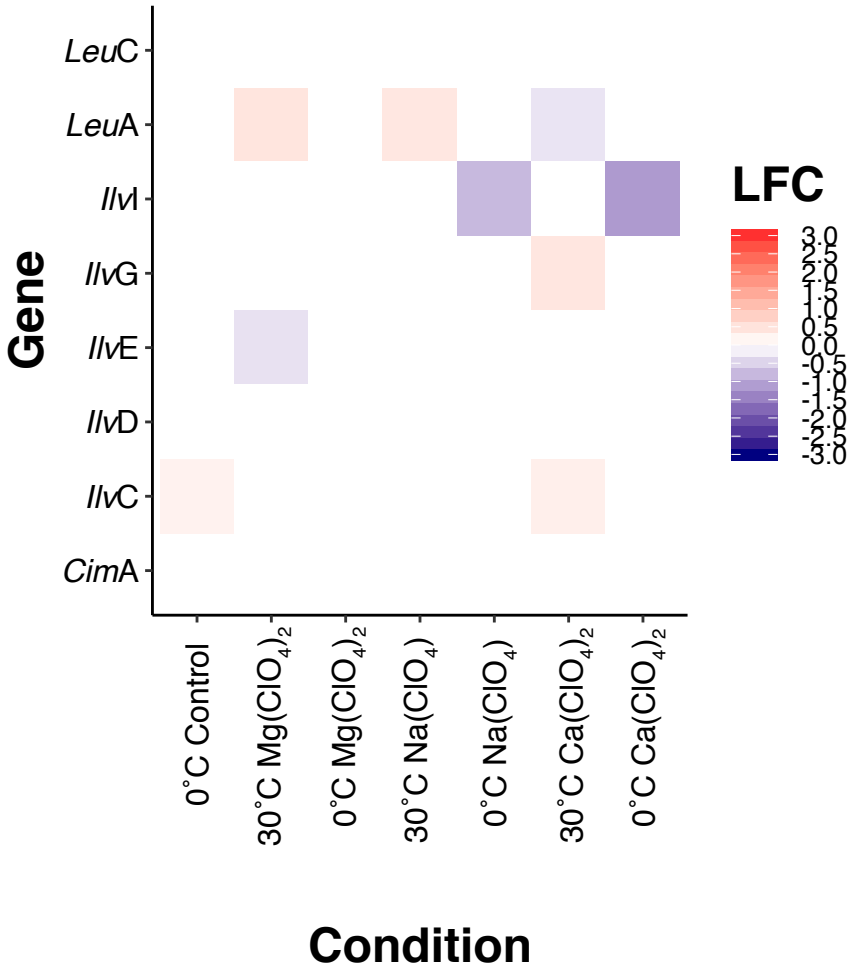

Figure B.12. Differential expression (Log_2-fold change, LFC) of genes involved in valine, leucine, and isoleucine biosynthesis in *M. barkeri*. Perchlorate-amended 30˚C and 0˚C perchlorate-free control cultures are relative to 30˚C perchlorate-free control. 0˚C perchlorate-amended cultures are relative to 0˚C perchlorate-free control. Significant differential expression was identified via Wald test ($P < 0.05$). Gene abbreviations: *Cim*A, (R)-citramalate synthase; *Leu*A, 2-isopropylmalate synthase; *Leu*C, 3-isopropylmalate dehydratase; *Ilv*I, Acetolactate synthase large subunit; *Ilv*G, Acetolactate synthase small subunit; *Ilv*E, Branched-chain amino acid aminotransferase alpha; *Ilv*D, Dihydroxy-acid dehydratase; *Ilv*C, Ketol-acid reductoisomerase.

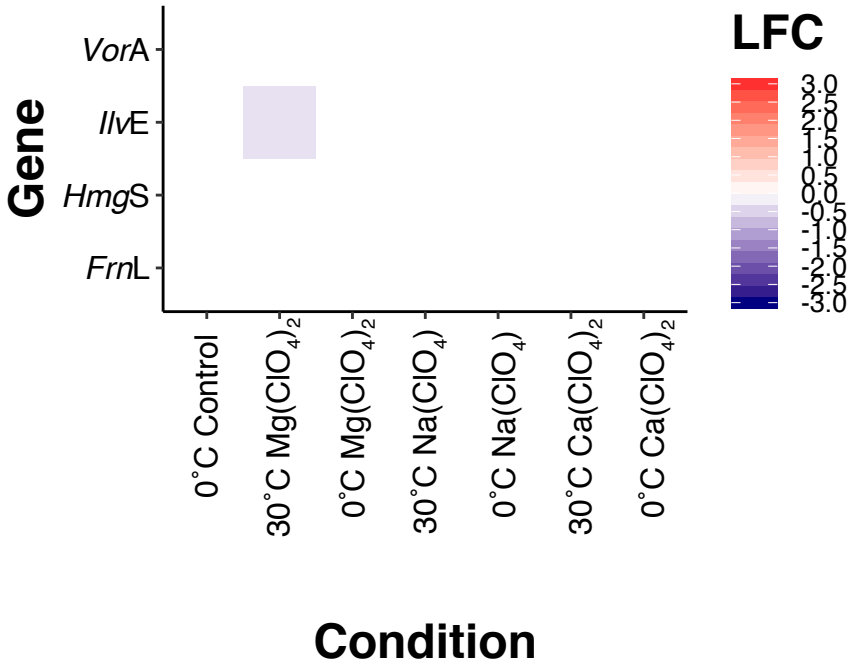

Figure B.13. Differential expression (Log_2-fold change, LFC) of genes involved in valine, leucine, and isoleucine degradation in *M. barkeri*. Perchlorate-amended 30˚C and 0˚C perchlorate-free control cultures are relative to 30˚C perchlorate-free control. 0˚C perchlorate-amended cultures are relative to 0˚C perchlorate-free control. Significant differential expression was identified via Wald test ($P < 0.05$). Gene abbreviations: *Frn*L, Beta-ketoacyl synthase/thiolase; *Ilv*E, Branched-chain amino acid aminotransferase; *Hmg*S, Hydroxymethylglutaryl-CoA synthase; *Vor*A, Ketoisovalerate oxidoreductase.

Appendix C

Supplementary Files

File_3C.1.fasta: https://tinyurl.com/u23bqg6

File_3C.2.fasta: https://tinyurl.com/vmytlyl

File_4C.1.html: https://tinyurl.com/tgsxnzc

File_4C.2.html: https://tinyurl.com/v8ooojs